# Surfactants, Ionic liquids and Ionosilicas : functional ionic systems for supramolecular chemistry and elaboration of materials by design (ion exchange and vectorization)

Roza Bouchal

Collège Doctoral du Languedoc-Roussillon

# THÈSE

Pour obtenir le grade de

Docteur

Délivré par **l'Université de Montpellier**

Préparée au sein de l'école doctorale **Sciences Chimiques Balard**

Et de l'unité de recherche

**Chimie Moléculaire et Organisation du Solide** (ICGM)

Spécialité : **Chimie et Physicochimie des Matériaux**

Présentée par **Roza Bouchal**

## Surfactants, Ionic liquids and Ionosilicas: Functional ionic systems for supramolecular chemistry and elaboration of materials by design (ion exchange and vectorization)

Soutenue le 19 Octobre 2016 devant le jury composé de

| | |
|---|---|
| Mme Marie-Helène DELVILLE, DR, Université de Bordeaux | Rapporteur |
| M. Giang VO THANH, Professeur, Université Paris Paris-Sud 11 | Rapporteur |
| M. Jean-Olivier DURAND, DR, Université de Montpellier | Président du jury |
| M. Hocine DJIDJELLI, Professeur, Université de Béjaia | Examinateur |
| M. Peter HESEMANN, DR, Université de Montpellier | Directeur de thèse |

# Remerciements

La préparation de ma thèse n'a pas été un travail individuel mais plutôt un travail collectif qui a rassemblé un certain nombre de personnes venues d'horizons divers mais qui ont su mettre au profit du groupe, avec beaucoup de générosité, leur expérience et savoir-faire respectifs. Pour cela, elle ne peut s'achever sans remercier tous ceux qui, tout le long des trois années passées avec eux, n'ont jamais cessé de me soutenir par leur présence à mes côtés, m'encourager par la pertinence de leurs conseils, leur intérêt jamais démenti pour ma recherche, leur écoute et leur disponibilité à chaque fois renouvelées.

En premier lieu, je tiens à remercier Marie-Helène Delville directeur de recherche à l'institut de Chimie de la Matière Condensée de Bordeaux et Giang Vo Thanh professeur à l'université Paris 11 de me faire l'honneur d'être les rapporteurs de cette thèse.

J'exprime également toute ma gratitude au Professeur Hocine Djidjelli de l'université de Béjaia et au Directeur de recherche Jean-Olivier Durand de l'institut Charles Gerhardt de Montpellier d'avoir accepté d'être examinateurs au sein de ce jury.

Je tiens à remercier, monsieur Peter Hesemann, directeur de recherche à l'institut Charles Gerhardt de Montpellier et directeur de la présente thèse, pour m'avoir fait confiance puis pour m'avoir guidé, encouragé, conseillé tout en me laissant une grande liberté.

J'exprime aussi toute ma gratitude à monsieur Jerzy Zajac, professeur à l'université de Montpellier et Bénédict Prelot, directeur de recherche à l'institut Charles Gerhardt de Montpellier pour leur contribution dans la réalisation des caractérisations physico-chimiques des tensio-actifs guanidinium.

Je remercie madame Gloria Berlier, directeur de recherche de l'université de Turin en Italie ainsi que Ivana Milletto pour m'avoir chaleureusement accueillie au sein de leur laboratoire, leur précieuse aide et les conseils stimulants que j'ai eu l'honneur de recevoir de leur part.

Par la même, je remercie le réseau European COST Action MP1202 'Rational design of hybridorganicinorganic interfaces: 'the next step towards advanced functional materials' d'avoir financé mon séjour en Italie et de m'avoir permis de m'enrichir.

Tous mes remerciements vont également à monsieur Rénal Backov, professeur à l'université de Bordeaux pour son accueil chaleureux, son entrain et son savoir-faire dans le domaine la synthèse des monolithes qu'il n'a pas hésité à partager avec moi avec beaucoup de générosité et de modestie.

Je tiens à remercier Jean-Olivier Durand et Clarence Charnay, respectivement directeur de recherche à l'institut Charles Gerhardt de Montpellier et maitre de conférences à l'université de Montpellier, pour leur aide précieuse et leurs conseils avisés sur la partie nanoparticules, prodigués en toute simplicité et avec beaucoup d'amabilité chaque fois que sollicités.

Mes sincères remerciements vont à madame Magalie Gary-Bobo, directeur de recherche à l'institut de Biomolécules Max Mousseron de Montpellier et à son étudiante en Master, Morgane Daurat, pour leur bonne humeur et surprenante réactivité ainsi que pour toutes les expériences effectuées sur les nanoparticules au niveau biologique avec enthousiasme et sérieux. Les résultats de leurs travaux ont été d'un apport considérable pour ma thèse.

Je remercie le ministère de l'enseignement supérieur et de la recherche scientifique du gouvernement algérien de m'avoir octroyé cette bourse d'étude qui m'a permis d'entrer dans le monde de la recherche.

Je remercie tous ceux sans qui cette thèse ne serait pas ce qu'elle est : aussi bien par les discussions que j'ai eu la chance d'avoir avec eux, leurs suggestions ou contributions.

Au terme de ce parcours, je remercie enfin toute ma famille qui a plus particulièrement assuré le soutien affectif de ce travail doctoral. Je suis redevable à mes parents pour leur soutien moral et matériel et leur confiance indéfectible dans mes choix.

*« La plus belle chose que nous puissions éprouver, c'est le côté mystérieux de la vie. C'est le sentiment profond qui se trouve au berceau de l'art et de la science véritable ».*

*Albert Einstein*

# Abbreviations

| | |
|---|---|
| **ALT** | **Alanine amino transferase** |
| **CMC** | **Critical micellar concentration** |
| **CSDA** | **Co-structure directing agent** |
| **CTM** | **Cooperative templating mechanism** |
| **DCF** | **Diclofenac** |
| **DCFDA** | **Dichlorofluorescin diacetate** |
| **$\Delta_{mic}H°$** | **Enthalpy of micelle formation per mole** |
| **F127** | **Triblock copolymer** |
| **FITC** | **Fluorescein isothiocyanate** |
| **LCT** | **True liquid-crystal template mechanism** |
| **LPS** | **Lipopolysaccharides** |
| **$NP_{is}$** | **Ionosilica nanoparticle** |
| **PEG** | **Polyethylene glycol** |
| **PMO** | **Periodic mesoporous organosilicas** |
| **RAW 264.7** | **Murine macrophage 264.7 cells** |
| **ROS** | **Reactive oxygen species** |
| **SDS** | **Sodium dodecyl sulfate** |
| **SHS** | **Sodium hexadecyl sulfate** |
| **SUL** | **Sulindac** |
| **TEOS** | **Tetraethoxyorthosilicate** |
| **$T_k$** | **Krafft temperature** |
| **TTAB** | **Tetradecyltrimethylammnoium bromide** |

**List of molecules synthesized in the thesis**

| | |
|---|---|
| **Guanidinium surfactants**<br>• Decylguanidinium chloride (DGC)<br>• Dodecylguanidinium chloride (DDGC)<br>• Tetradecylguanidinium chloride (TDGC)<br>• Cetylguanidinium chloride (CGC) | 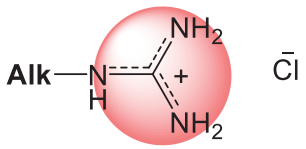 <br>Alk= n-$C_{10}H_{21}$, n-$C_{12}H_{25}$, n-$C_{14}H_{29}$, n-$C_{16}H_{33}$. |
| **Guanidinium ionic liquids**<br>• Hexylguanidinium bis-trifluoromethane sulfonimides ($C_6$Gua $NTf_2$).<br>• Octylguanidinium bis-trifluoromethane sulfonimides ($C_8$Gua $NTf_2$).<br>• Decylguanidinium bis-trifluoromethane sulfonimides ($C_{10}$Gua $NTf_2$). | 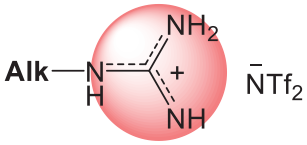 <br>Alk= n-$C_6H_{13}$, n-$C_8H_{17}$, n-$C_{10}H_{21}$. |
| Tris(3-(trimethoxysilyl)propyl)amine (TrisN). | 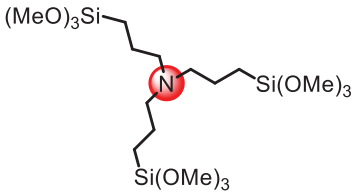 |
| Methyl-(tris(3-trimethoxysilyl)propyl) ammonium iodide (MeTrisN). | 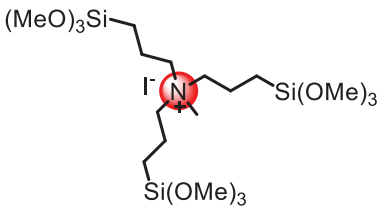 |

# Summary

# General introduction

One of the major lines of development of chemical science resides in the ever clearer perception, deeper analysis, and more deliberate application of the information paradigm in the elaboration and transformation of matter, thus tracing the path from merely condensed matter to more and more highly organized matter toward systems of increasing complexity.[1]

The properties of a material depend both on the nature of its constituents and the interactions between them. Supramolecular chemistry may thus be expected to have a strong impact on materials science by means of the explicit manipulation of the noncovalent forces that hold the constituents together. These interactions allow the design of materials and the control of their construction from suitable units by self-organization. [1]
Supramolecular chemistry is by nature a dynamic chemistry in view of the lability of the interactions connecting the molecular components of a supramolecular entity. The reversibility of the association allows a continuous change in constitution, which may be either internal, by rearrangement of the components with modification of the connectivity between them, or external, by exchange, incorporation, or extrusion of components, therefore conferring constitutional flexibility to the system.

Surfactants and sol-gel materials are good examples of supramolecular self-organization. Moreover, due to the electrostatic interactions present in ionic liquids and their unusual self-aggregation properties, they are also referred as ‘supramolecular solvents’ which are also opened new routes in materials science.

This thesis deals with different aspect as illustrated in Figure 1: self-assembly behavior, material shaping, ion exchange reaction, separation process and drug vectorization. For this purpose, three functional ionic systems were studied: surfactant, ionic liquid and ionosilica materials. Each functional system contains cationic entities particularly guanidinium and ammonium groups.

Regarding these cationic entities, we divided our functional systems in two families compounds: guanidinium salts and ionosilica materials.

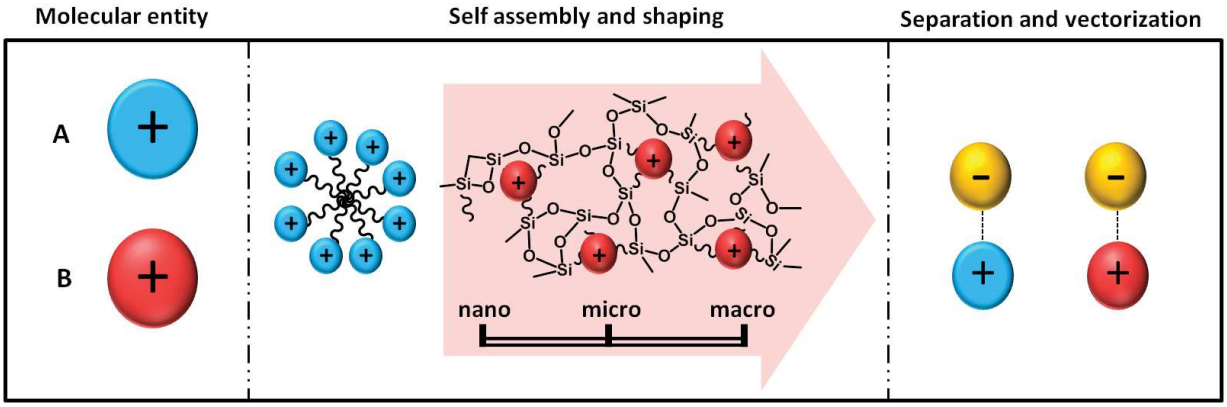


**Figure 1: Schematic representation of different ionic functional systems and applications studied.** Molecular entity: A) guanidinium and B) ammonium, surfactant self-assembly behavior and ionosilica material design at different scale. Finally different applications performed on ionic liquid and ionosilica material by ion exchange reaction.

Concerning guanidinium salts, we synthesized monoalkyl guanidinium surfactant and ionic liquid. Firstly, a fundamental study was conducted on chloride guanidinium surfactant. Different guanidinium surfactants with alkyl chain lengths from $C_{10}$ to $C_{16}$ were synthesized and characterized. Thereafter, a physicochemical study of the self-assembly behavior was performed using different measurement techniques: ionic conductivity, surface tension and calorimetry. The results were then compared with conventional ammonium surfactants.

Secondly, we synthesized mono-alkylguanidinium bis-trifluoromethane sulfonimides with a short chain length as a new class of functional ionic liquids. These ionic liquids were used for the extraction of anionic compounds. The extraction was performed against an organic dye (Methyl orange), anionic drug (Diclofenac) and a metallic anion (Chromate). In order to evaluate the potential of guanidinium ionic liquid we compared our results with those of a conventional imidazolium based ionic liquid.

Finally regarding ionosilica materials, we performed the synthesis of materials displaying three different shapes: ionosilica powder, nanoparticles and monoliths.

In order to investigate the potential of ionosilica for waste water treatment, adsorption of active ingredients from aqueous solution was performed on powder ionosilica material. Different molecules were used such as sodium diclofenac and sulindac in neutral and ionic forms. In this part we studied the selectivity of ionosilica materials and the driving forces of their adsorption potential.

The formation of ionosilica nanoparticles allows the extension of ionosilica applications in the field of nanomedicine. Thus during this thesis, nanoparticles containing ionic substructures essentially ammonium were investigated. Using in vitro and in vivo investigations of these nanoparticles, the non-toxicity and biocompatibility were then verified. The nanoparticles were synthesized in order to use them as nano-carriers for the vehiculation of drugs. For this purpose an anti-inflammatory drug sodium diclofenac was used as model compound.

Finally, with the aim of ionic extraction in continuous flow, materials containing ionic functions were synthesized in monolithic shape. Hybrid monoliths containing ammonium substructures were synthesized using co-condensation process from TEOS with amine or ammonium silylated precursors. PMO monoliths bearing ammonium substructures were also synthesized starting exclusively from ionic silylated precursors. In this study different parameters were optimized in order to synthesize well defined monoliths with hierarchical porosity.

The work of this thesis is presented in three chapters. The first chapter gives a general introduction to each functional system together with some examples. The second concerns guanidiniums salts (surfactant and ionic liquid). Finally, the third chapter presents ionosilicas materials in different shapes: powders, nanoparticles and monoliths as well as their applications in the field of separation and vectorization.

1. Lehn, J. M., Toward complex matter: Supramolecular chemistry and self-organization. *Proceedings of the National Academy of Sciences of the United States of America* **2002,** 99, (8), 4763-4768.

# Chapter I

## Introduction

# Summary

## **Chapter I:** Introduction

*Oh small molecule*
*Friend or foe*
*To love or hate*
*To understand you better*
*Before it's too late!*
***Geoffrey A Ozin, April 2012***

During the last few decades, chemists have extended their investigations beyond atomic and molecular chemistry into the realm of supramolecular chemistry.

> "*Supramolecular chemistry is the chemistry of the intermolecular bond, covering the structures and functions of the entities formed by association of two or more chemical species*" Jean-Marie Lehn, Nobel lecture, 1987[1]

Terms such as molecular self-assembly, hierarchical order, and nano-science are often associated with this area of research. The desire to design new materials is still present in the scientific community, functional small-molecule building blocks are often used to design new synthetic materials that feature even more useful properties emanating directly from nanoscale and microscale ordering.[2]

The state of the art exposed in this introduction will focus on three functional ionic systems: 1) surfactant self-assembly, 2) ionic liquids for green chemistry and 3) mesoporous organic-inorganic silica bearing ionic substructures. In this introduction we review succinctly these three systems. In the first section we will give the surfactant definition with some properties focusing on their self assembly behavior. In the second section, a succinct presentation of ionic liquids and their properties will be done followed by their applications as pollutant extractant. Finally, we will describe the synthesis of mesoporous materials, sol gel art and different approaches to the silica functionalization, concluding with strategies for materials' design.

# 1 Surfactants

## 1.1 Introduction

Sustained interest in amphiphilic systems is due to their wide range of real life applications such as oil recovery, surfactant enhanced carbon regeneration for waste water treatment, herbicide dispersions, filtration of ultrafine particles, stabilization of particulate suspensions, and as cleaning detergents. In addition to these known applications, there are also numerous exploratory usages of amphiphiles in modern high technology industries. From a fundamental viewpoint, this field remains an important source of inspiration for researchers from many different scientific disciplines.[3, 4]

The name amphiphile is sometimes used synonymously with surfactant. The word amphiphile was introduced by Hartley in 1936 being derived from the Greek word amphi (both) and relating to the fact that all surfactant molecules consist of at least two parts, one which is soluble in a specific fluid (the lyophilic part) and one which is insoluble (the lyophobic part). When the fluid is water, usually talks about the hydrophilic and hydrophobic parts, respectively. The hydrophilic part is referred to as the head group and hydrophobic part as the tail.[5] Surfactants are classified on the basis of the charge of the hydrophilic group and they can be either ionic (anionic / cationic) or nonionic. Carboxylate, sulfate, sulphonate, and phosphate are commonly used polar groups in anionic surfactants. Most of the cationic surfactants are based on quaternary nitrogen-containing compound with positive charges. Sodium dodecyl sulphate (SDS) and cetyltrimethylammonium bromide (CTAB) are the most commonly used anionic and cationic surfactants, respectively. Nonionic surfactants contain either polyether or polyhydroxyl units as the hydrophilic group.[5]
This dual nature endows the surfactants with their unique solution and interfacial characteristics. Among these, the most noteworthy is the behavior in dilute aqueous solutions, where the surfactant molecules self assemble to form aggregates so as to achieve segregation of their hydrophobic parts from water.
The study of the self-assembly of amphiphilic molecules such as lipids, surfactants or block copolymers has been a center of interest for colloid, polymer, and materials scientists for several years, and continues to attract attention due to its fundamental importance for day-to-day

applications in diverse fields including pharmaceutical, food and cosmetic formulations, catalysis and controlled synthesis of nanostructured materials.[3]

## 1.2 Micellization: the concept of CMC

The physical properties of surfactants called also surface active agents differ from those of smaller or non-amphiphilic molecules in one major aspect. At lower surfactant concentration, most physicochemical properties do not vary significantly. However, at a certain concentration of surfactant, an abrupt change in these properties takes place. The concentration of surfactant at which this change occurs is known as the Critical Micellar Concentration (CMC).[6] Below the CMC, surfactant molecules are present in the form of individual molecules, whilst above the CMC, surfactant molecules are present in the form of aggregates. These aggregates are known as micelles and the process of their formation is called micellization. A low CMC value indicates that micelle formation occurs at low surfactant concentration.[7]

Amphiphilicity is one of the main driving forces for this self-assembly of surfactants. The thermodynamic properties of amphiphiles in solution are controlled by the strong tendency of hydrophobic tails to avoid direct contact with water (*i.e.* hydrophobicity). This unfavorable interaction can be minimized by aggregation of surfactant molecules into micelles (*i.e.* self-assembly) in which the hydrophilic domains become exposed to water and the hydrophobic parts are shielded.[4] This micellization process can also be explained in terms of entropy.[8] The entropic contribution arises from the local structure of water due to hydrogen bonding. The segregated hydrocarbon chains of surfactants interrupt hydrogen bonding between water molecules causing a locally more ordered structure, which is entropically unfavorable. Therefore, entropically more favorable aggregated structures (micelles) are formed to avoid disruption of the water structure. Micellization can also be considered as an alternative mechanism to adsorption at interfaces for avoiding direct contact of hydrophobic groups with water, thereby reducing the free energy of the system. Micelles are thermodynamically stable species that are in equilibrium with the free ‘monomers’ (unassociated surfactant molecules). It should be noted that the surfactant molecules behave very differently when present as free monomers in solution compared to micelles.[3]

The value of the CMC can be determined by the change of the physicochemical properties of the surfactant solution as the concentration of the surfactant is increased as shown in Figure 1. The most common is the break in electrical conductivity, surface tension or light scattering–concentration curve.

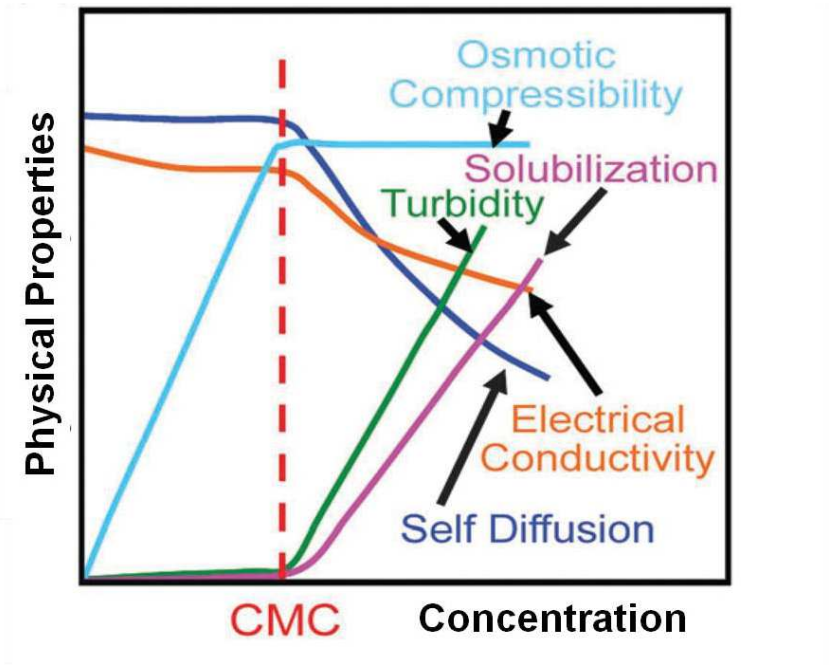


**Figure 1: Changes in physical properties at critical micelle concentration (CMC).**[3]

The existence of surfactant micelles was established in the beginning of the twentieth century by W. B. Hardy, J. W. McBain[9] and coworkers in their studies on electrolytic conductivity of carboxylate solutions. They found that both solutions of sodium laurate and myristate contain both electrolytic and colloidal constituents (dissociated surfactant monomers and surfactant aggregates).[10]

For example, when the equivalent conductivity (specific conductance per gram-equivalent of solute) of an ionic surfactant in water is plotted against the square root of the normality of the solution, the obtained curve, instead of being the smoothly decreasing curve characteristic of ionic electrolytes of this type, displays a sharp break at low concentrations. As demonstrated in Figure 1 (orange curve), this break in the curve, with its sharp reduction in the conductivity of the

solution, indicating a sharp increase in the mass per unit charge of the surfactant in solution, is interpreted as evidence of the formation at that point of micelles from the unassociated molecules of surfactant.[11-13]

## 1.3 Solubility of surfactants

Some surfactants have such low solubilities that, at a given temperature, the CMC value may be higher than the solubility of the surfactant. If the temperature is raised, the solubility will increase and, at some temperature, will reach the CMC value (Figure 2). The temperature where the solubility of the surfactant becomes equal to the CMC value is known as the Krafft point.[5]

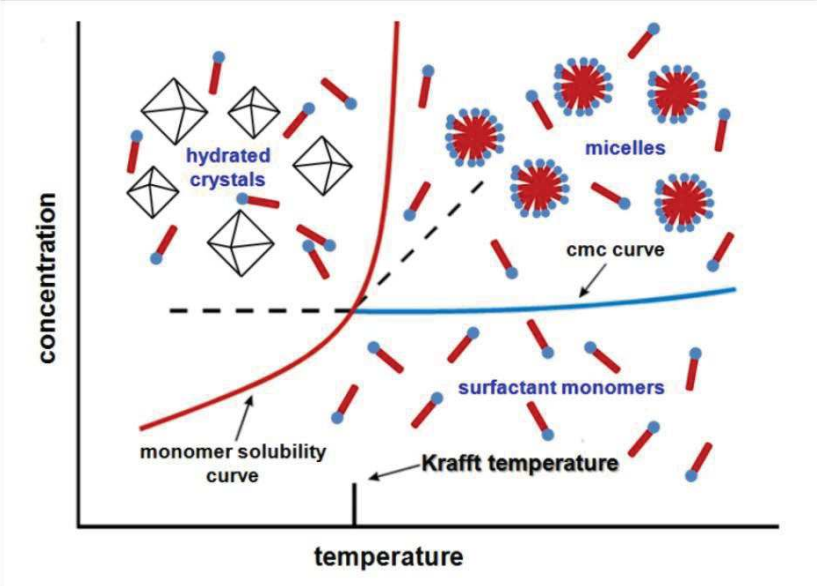


**Figure 2. Schematical representation of the solubility curve for the ionic surfactants.**[14] The Krafft temperature ($T_K$) is the temperature at which surfactant solubility equals the CMC. Above $T_K$ surfactant molecules form a dispersed phase; below $T_K$ hydrated crystals are formed.

The Kraft temperature varies with alkyl chain length and structure, as well as with the counterion. A decrease of the Krafft temperature can be achieved by introducing chain branching. The Krafft temperature is usually determined either by measuring the change of electrical conductivity with temperature for the ionic surfactant or visually via the observation of the change of turbidity of supersaturated surfactant solution (usually 1 wt %).

Knowledge of the Krafft temperature is crucial in many applications since below $T_K$, the surfactant will clearly not perform efficiently. Hence, typical characteristics such as maximum surface tension lowering and micelle formation cannot be investigated.[15]

## 1.4 Surface activity

A key characteristic of surfactants is their ability to lower the surface tension at an air–water interface. The word surfactant originates from its use to describe surface-active agents which can adsorb at surfaces or interfaces and markedly modify the surface or interfacial free energy. The term 'interface' indicates a boundary between any two immiscible phases while the term 'surface' denotes an interface where one phase is usually a gas or air. Amphiphilic molecules tend to adsorb at an air–water interface and consequently reduce the surface tension of water.
Amphiphiles are usually characterized by their tendency to adsorb at surfaces or interfaces. When amphiphilic molecules are added to water, their hydrophobic groups distort the water structure thus decreasing the entropy of the system with the result that some of the molecules are expelled from the bulk of the solvent being then adsorbed at the interface (*i.e.* an air–water interface). In that case, hydrophilic headgroups remain in solution while the hydrophobic tail avoids direct contact with water. This is because the adsorbed molecules at the interface have to be arranged with hydrophilic portions in contact with the water phase and hydrophobic portions oriented to the air phase (Figure 3). This orientation at the interface is an important factor in determining the change in properties of the interface induced by the presence of the surfactant. The properties of an interface having adsorbed molecules may vary greatly depending on the orientation of these molecules.[3, 8]

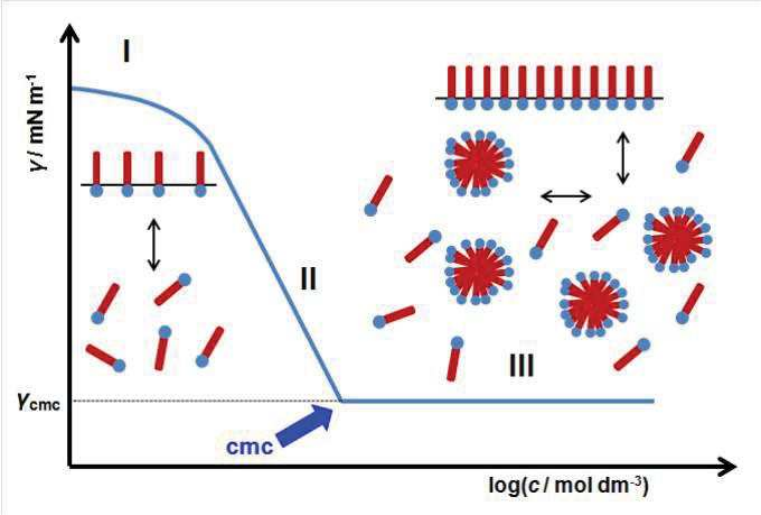


**Figure 3. Plot of surface tension versus log of the bulk phase concentration for an aqueous solution of a surfactant.**[14]

The curve represents three distinctive parts.

I. At low surfactant concentrations surfactant monomers are forming monolayer at the air/water interface. Surface tension is decreasing with the surfactant bulk concentration due to the increasing surfactant surface concentration at the air/water interface.

II. At concentrations below, but close to CMC slope of the curve is constant because surface concentration reached its maximum value.

III. At concentrations above CMC, surface tension remains almost constant, due to constant monomer concentration

## 1.5 Formation of liquid crystals and vesicles

When there is a sufficient number of micelles in the solution phase, they start to pack together in a number of geometric arrangements, depending on the shape of the individual micelles. These packing arrangements are known as liquid crystals.

Liquid crystals have the ordered molecular arrangement of solid crystals but with the mobility of liquids. Because of this ordered arrangement of the molecules, they increase the viscosity of the solution phase, sometimes very considerably. Spherical micelles pack together into cubic liquid crystals, cylindrical micelles pack to form hexagonal liquid crystals, and lamellar micelles form lamellar liquid crystals (Figure 4). It is easier to pack surfactant molecules having a bulky head group into hexagonal phases, while surfactants having two alkyl groups pack better into a

lamellar phase. Because some types of micelles change their structure from spherical to cylindrical to lamellar with increase in surfactant concentration, hexagonal phases are usually encountered at lower surfactant concentrations than lamellar phases.[12, 16]

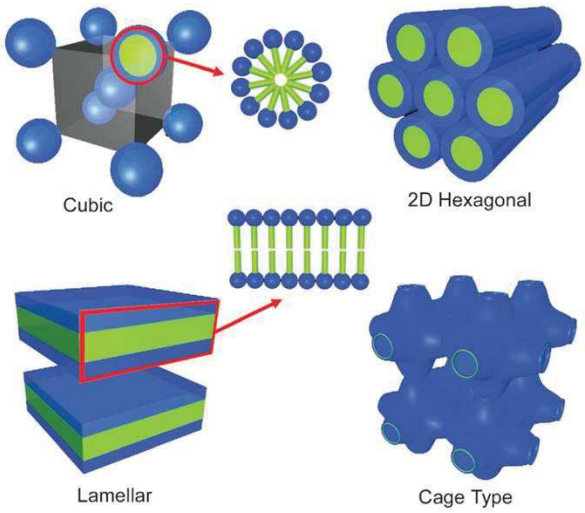


**Figure 4. A few examples of surfactant self-assembled structures of amphiphilic molecules in the bulk phase.[3]**

## 1.6 Surfactant assemblies for/in mesoporous materials

The role of surfactant self-assembly in developing a wide range of high quality mesoporous materials is essential. Surfactant-templated synthesis of mesoporous inorganic materials is a good example of how the efforts aimed at surfactant development and characterization have guided the progress achieved in the synthesis of advanced materials with tunable porous architecture, particle size and morphology. The typical mesoporous silica materials can be prepared by silica formation in the presence of surfactant template, acting as liquid crystal phase, followed by removal of the template by appropriate methods such as calcination or washing. These advanced structures all essentially originate from amphiphile assembly.[3] A detailed description of typical mesoporous materials will be given in section three.

# 2 Ionic Liquids

## 2.1 Introduction

The story of ionic liquids is generally regarded as beginning with the first report of the preparation of ethyl-ammonium nitrate in 1914 by Paul Walden (see Figure 5). This species $[C_2H_5NH_3]^+[NO_3]^-$ was formed by the addition of concentrated nitric acid to ethylamine, after which water was removed by distillation to give the pure salt, which was liquid at room temperature with a melting point 12°C.[17, 18] Before, it was never suspected that ions could form a liquid at room temperature unless diluted in a molecular solvent.[19]


**Figure 5. Paul Walden, the discoverer of ionic liquids (and the Walden inversion).**[17]

Ionic liquids are a class of molten salts composed entirely of ions, whose melting temperature is lower than 100 °C. The main advantage of an ionic liquid is the high ionic mobility, a broad range of room-temperature liquid compositions, negligible vapor pressure, and excellent chemical and thermal stabilities.[20, 21]

"*Ionic liquids are most commonly defined as materials that are composed of cations and anions which melt at or below 100 °C. This temperature does not have any chemical or physical significance, but has persisted until the present day; it is only now that it is being queried*" Kenneth R. Seddon, 2008[17]

The novelty of the new non-molecular class of IL solvents is the low melting temperature of these salts. To be part of the IL family, a given salt must have a melting point arbitrarily fixed at or below 100 °C.[22] Ionic liquids with melting point below room temperature (~25 °C) are called room-temperature ionic liquids (RTIL). The term ionic liquid covers inorganic as well as organic molten salts. However, the recent literature deals with RTILs made of large dissymmetrical organic cations such as alkyl-imidazolium, pyridinium or pyrrolidinium, ammonium, phosphonium or guanidinium cations, and a variety of organic counter anions such as, triflate, dicyanamide, acetate, trifluoroacetate, or inorganic, bromide, chloride, nitrate, perchlorate, chloroaluminate, tetrafluoroborate, or hexafluorophosphate.[17, 22, 23] Some cations and anions of ionic liquids, and their common abbreviations, are shown in Figure 6. However, it should be remembered that, in principle, any singly charged cation or anion can be used.[17, 24]

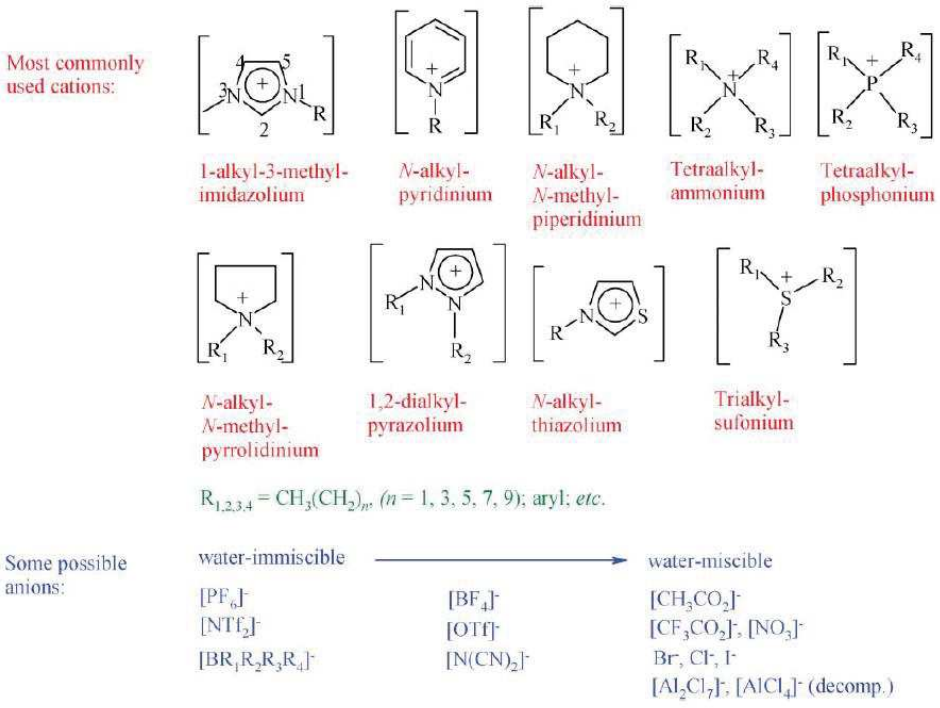


**Figure 6. Most commonly used cation structures and possible anion types.**[17]

## 2.2 Designer solvents

Initial research on the properties of pure RTILs has focused on developing and understanding the relationship between the nature and structure of the cation and anion and their physical properties.[23]

The main factors that influence the melting point are the charge distribution on the ions, H-bonding ability, the symmetry of the ions and the van der Waals interactions. On comparing the melting points of ILs with those for inorganic salts (for instance, 803 °C for NaCl and 60 °C for 1-propyl-3-methylimidazolium chloride) it is clear that the most of the reduction in melting temperature is caused by replacing the small inorganic cations by bulky asymmetric organic cations.[23] Selected properties, such as thermal stability and miscibility, mainly depend on the anion, while others, such as viscosity, surface tension and density, depend on the length of the alkyl chain in the cation and/or shape or symmetry.[25]

The novel feature of ILs as solvents is the possibility to design ILs with the necessary properties for a specific application, hence the term "*designer solvents*". The fine tuning of properties is possible by the combination of different anions and cations and also the variation of the length and branching of the alkyl groups incorporated into the cation. As an example, for 1-alkyl-3-alkylimadazolium cation replacing the ($PF_6^-$) anion by ($BF_4^-$) dramatically increases the solubility of the ionic liquid in water while replacement with the ($Tf_2N^-$) ion decreases the water solubility. The change in length of the alkyl chain from 1 to 9 on 1-alkyl-3-methyl imidazolium hexafluorophosphate [$C_n$mim][$PF_6$] can turn the liquid from being soluble in water to immiscible.[25]

"*For the first time it is possible to design a solvent to optimize a reaction rather than let the solvent dictate the course of the reaction*" Kenneth R. Seddon, 2000

## 2.3 Applications of Ionic liquids

ILs have been known for a long time, but their extensive use as solvents in chemical processes for synthesis and catalysis has only recently become significant.[24]

The main advantage for other applications of ionic liquids in analytical chemistry lies in their low volatility which makes them useful as solvents for working in both high-temperature (gas chromatography (GC) stationary phases) and high-vacuum (MALDI matrixes) environments.

Ionic liquids have been proposed for uses in catalytic and biocatalytic processes and organic synthesis. Another field of application of ionic liquids as solvent is separation. The advantage of non-volatility promote the use of ILs in a large scale processes, and RTILs thus may be suitable candidates for replacement of volatile organic solvents in liquid-liquid extraction processes.

ILs can be easily prepared from relatively inexpensive materials and their properties can be tuned by combination of different anions and cations, preparing by this way liquids for task-specific extraction of analytes from various solvent media and create new liquid-liquid extraction systems in order to achieve high efficiencies and selectivities of separation.

## 2.4 Liquid-liquid extraction

In most chemical applications, liquid-liquid extraction is used for separation since it is an energy efficient technique. Generally, extraction consists of two immiscible phases such as an organic phase and an aqueous phase.[24] Typically, organic solvents have been used in liquid–liquid extraction because of their immiscibility in water. There are, however, considerable problems associated with the safe handling of these solvents because of their toxicity and flammability. Room-temperature ionic liquids, especially those that are only partially miscible with water, are receiving wide attention as substitutes for organic solvents. They are non-flammable and is possible to recycle and repeatedly reuse them. It is more convenient to work with ILs in the laboratory since the non-evaporating properties of ILs limit the hazardous exposure and air pollution problems.[17, 24]

### 2.4.1 Extraction of organic compounds from aqueous phase

Extensive studies have been conducted for the extraction of organic compounds from aqueous phase with ILs, depending on the affinity between hydrophobic ILs and organic solutes.

The first utilization of RTILs for extraction purposes was reported by Rogers et al. in 1998.[26] This group studied the partitioning of substituted benzene derivatives between water and $C_4mimPF_6$. In 2000, the Rogers' group investigated the effect of aqueous phase pH on the partitioning of an indicator dye thymol blue, A remarkable dependence of distribution ratio between $[C_nmim]PF_6$ and water on the pH value was revealed, suggesting a possible approach of separating ILs and extract after extraction see Figure 7.[27]

"*Ionic liquids may in themselves be suitable, and indeed favorable, media for the design of novel liquid-liquid extraction systems*" Robin D. Rogers, 1998

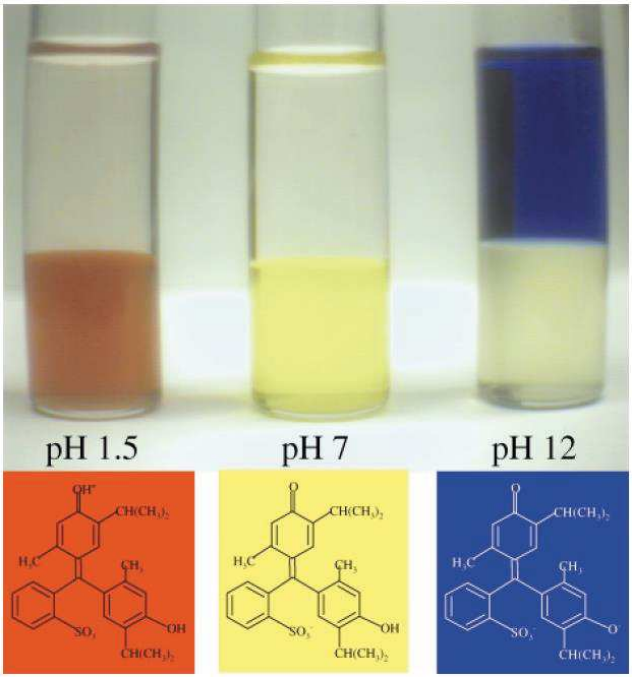


**Figure 7. Distribution of an indicator dye thymol blue in $[C_4mim][PF_6]$-water biphasic system at different pH** (R.D.Rogers et al, 2000).[27]

The extraction of phenolic compounds from aqueous solution using a imidazolium based ionic liquid $C_4mim\ PF_6$ was also reported by Khachatryan et al[28] demonstrating a relatively large distribution coefficient of phenolate anions which indicates ion exchange mechanism between the

extracted phenolate anions and the hexafluorophosphate anion of ionic liquid. This mechanism was also suggested by Li et al., by using the same ionic liquid to remove acid dyes from aqueous solution.[29]

Ionic liquids are also used for the extraction of biological target products, for example, several ionic liquids such as imidazolium based ionic liquid were reported for liquid-liquid extraction system to separate antibiotics, hemoglobin and proteins from aqueous solutions[30-32]

Fan et al. studied the removal of anionic dyes such as methyl orange, eosin yellow, and orange G from aqueous solutions using imidazolium based ionic liquids.[33] The extraction efficiencies of dyes were strongly affected by the pH of the aqueous phase and for a given dye the extraction was also affected by the temperature and the alkyl chain length of cation of the ionic liquids. It was reported that the extraction process was driven by hydrophobic interaction of the anionic dyes and the ionic liquids.

Aqueous two phase systems composed of ionic liquids and aqueous phase containing salt were also used in the extraction of certain organic compounds. Functional guanidinium ionic liquids were also used with $KH_2PO_4$ salt to form an aqueous two phase system in order to purify proteins.[34]

### 2.4.2 Recovery and extraction of metals from aqueous phase

In recent years, there is a growing interest in using ionic liquids (ILs) for metal extraction from aqueous solutions, since they can replace volatile organic solvents that have been widely used for this purpose. However, a major limitation has been the low solubility of metals in ILs. To improve the extraction of the metal ion from aqueous solution, organic ligands were added in biphasic solutions (for example, crown ethers[35]) in order to increase the metal solubility in the IL.

Another strategy is the synthesis of task-specific ionic liquids (TSIL), defined as ionic liquids in which reactive functionality covalently linked to the cation or anion part (or both). This function confers additional properties (chemical, optical, magnetic, physical or biological) which can then be employed to perform a specific task.[36]

Rogers et al. reported for the first time TSILs for the selective liquid/liquid extraction of heavy metals from aqueous systems, [37] and this by introducing specific functional groups on the IL cation (namely thiother, urea and thiourea) with the aim to favor $Hg^{2+}$ and $Cd^{2+}$ ion adsorption

(Figure 8). They demonstrate that both the appended functional group and the alkyl group of the IL affect the extraction of targeted metal ions.

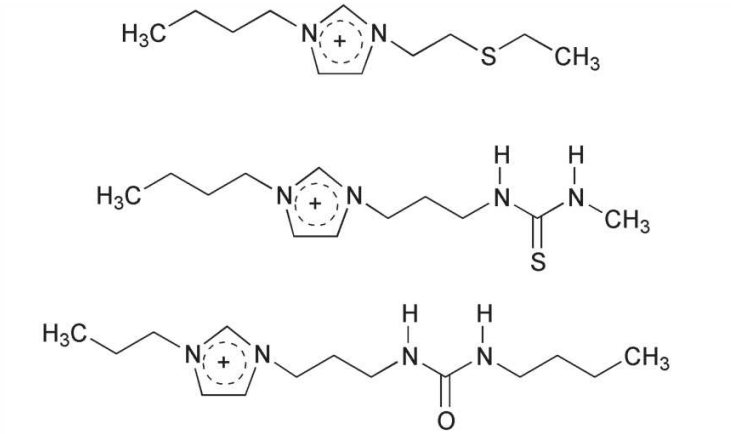

**Figure 8. From top to bottom: Thiother, thiourea and urea derivatized ionic liquids with $PF_6^-$ as anion.**[37]

However, the use of ionic liquids for the extraction of metals has until now only partially answered the high expectations of it. Several problems are related to the hydrophobic nature of the ionic liquids, also to the transfer of cations ILs or anions in water which caused generally aqueous phase contamination. For this, the extraction mechanisms must be overcome and improved in order to increase the efficiency of the processes.[39]

## 2.5 Conclusion

ILs are regarded as "green" alternatives to common organic solvents and they are receiving a particular attention for the application in a wide range of fields such as liquid-liquid extraction. The substitution of conventional organic solvent by ILs is supported by their exceptional physico-chemical properties; their negligible volatility can reduce the air pollution and facilitate the regeneration from volatile components. In addition, the ILs properties can be adjusted for the uses in specific application. Overall, favorable distribution coefficient and separation selectivity, together with less energy consumption and less volatile pollution, may be achieved in liquid-liquid extraction using IL as extracting medium.

# 3 Porous Materials

## 3.1 Introduction

The synthesis, characterization, and application of novel porous materials have been driven by their wide range of applications in adsorption, separation, catalysis, and sensing. The design, synthesis, and modification of porous materials are in some aspects more challenging than the synthesis of dense materials. Therefore, the development of new strategies and techniques are still a challenge for synthesis and structure-tailoring of mesoporous materials.[40, 41]

Porous materials created by nature or by synthetic design have found great utility in all aspects of human activities. Porous materials with small pore diameters (0.3 nm to 10 μm) are being studied for their molecular sieving properties. The pore shape can be roughly approximated by any of the following three basic pore models, (a) cylindrical (b) ink-bottled and (c) slit-shaped pores.[42, 43]

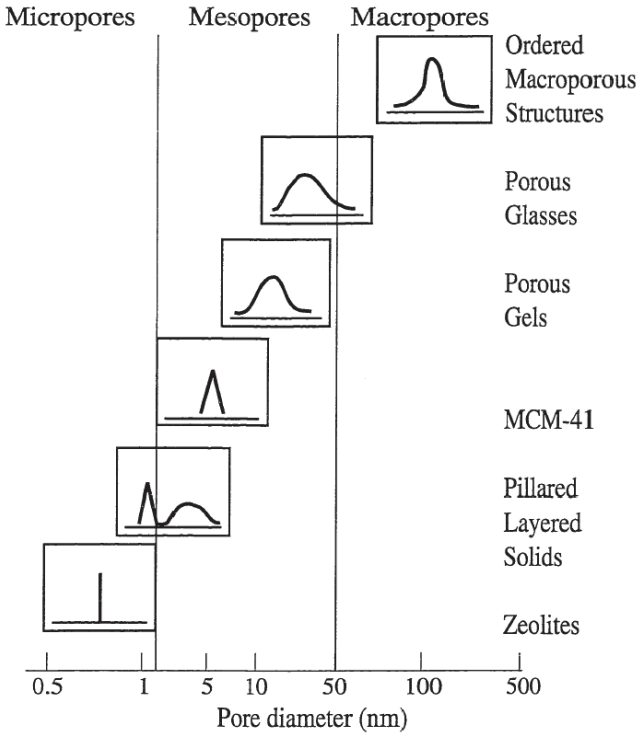


**Figure 9. Schematic illustrating pore size distribution of some porous materials.[43]**

Depending on the predominant pore sizes, porous solid materials are classified by IUPAC: firstly, microporous materials, in which the pore diameter is less than 2 nm; secondly, mesoporous

materials, in which pores size are between 2 nm and 50 nm; and, thirdly, macroporous materials with pore diameter exceeding 50 nm (Figure 9).[44]

## 3.2 An overview on sol gel chemistry

Sol-gel chemistry has been investigated extensively since the 1970's, when sol-gel reactions were shown to produce a variety of inorganic networks. Sol-gel reactions are those which convert an aqueous metal alkoxide [Mn+(OR)n] solution into an inorganic network. [45]

The sol-gel method is also capable of producing homogeneous, high purity inorganic oxide glasses at room temperature,[46] much lower than the high temperatures required by the conventional glass manufacturing process. For example, silica can be obtained from melt processing glass, but the sol-gel method is more effective for the production of amorphous silica. Another advantage of the sol-gel procedure is its ability to produce silica in different forms such as molded gels,[46] spun fibers, thin films, molecular cages, aerogels, xerogels, and mesoporous materials for a variety of applications such as gas, and liquid separations, optical coatings, protective films, membranes, and catalysis. Therefore, changing the conditions of sol-gel polymerization and processing is helpful for controlling the bulk properties of silica. The sol-gel process involves transformation of a sol to a gel.[45] A sol is defined as a colloid of small particles that are dispersed into a liquid. A gel, on the other hand, is a rigid non-fluid mass and is usually a substance made up of a continuous network including a continuous liquid phase.[46] Therefore, sol-gel reactions involve hydrolysis and condensation reactions of inorganic alkoxide monomers in order to develop colloidal particles (sol) and consequently convert them into a network (gel). Metal alkoxides are the reagents most used for this purpose due to their ease of hydrolysis in the presence of water. Alkoxysilanes, such as tetramethoxysilane (TMOS) and tetraethoxysilane (TEOS), are extensively used for the production of silica gels. Figure 10 displays the involved hydrolysis and condensation reactions of TEOS. The hydrolysis step takes place by the addition of water to the TEOS solution under neutral, acidic, or basic conditions.[42]

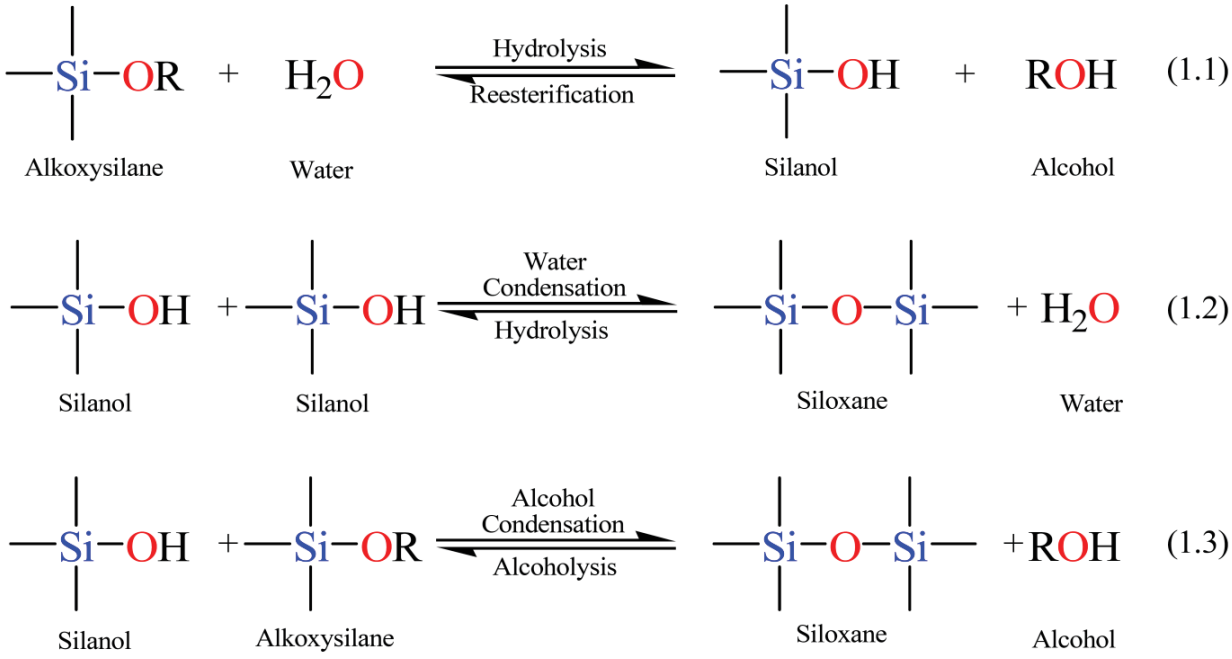


**Figure 10. Sol-gel general reaction scheme.**[42]

### 3.3 Soft templating synthesis of mesoporous $SiO_2$

In 1992, researchers at Mobil Corporation discovered a new family of mesoporous silicate/aluminosilicate materials designated M41S mesoporous molecular sieves with exceptionally large uniform pore structures, which resulted in a worldwide resurgence in this area.[40, 41, 47] These materials superseded zeolite molecular sieves, which were restricted to a pore size of around 15 Å. Like the microporous crystalline zeolites, this class of materials is characterized by very large specific surface areas, ordered pore systems, and narrow pore size distributions [48], thus offering new opportunities for applications in catalysis,[43] chemical separation, adsorption, and for the synthesis of advanced composite materials. The synthesis of this family of mesoporous materials is based on the combination of two major scientific domains, sol-gel science and surfactant (templating) science.[42] Three different mesophases in this family include the silica solids have been identified, *i.e.*, hexagonal (MCM-41) (Beck et al., 1992)[47], lamellar (MCM-50) by Dubois et al in 1993,[49] and cubic (MCM-48) phases (Vartuli et al., 1994).[50] The Figure 11 illustrates these different mesophases. The 2d hexagonal mesophase, denoted as MCM-41, possesses highly regular arrays of uniform-sized channels whose diameters are in the range of 15–100 Å and is obtained using a supramolecular aggregate of ionic

surfactants (long-chain alkyltrimethylammonium halides) as structure-directing agents (SDAs) during the synthesis under basic conditions.[40, 43, 47] The mesoporous materials are obtained by subsequent removal of the surfactant by extraction or calcination. MCM-41 exhibits several remarkable features: i) well defined pore sizes and shape, as compared to other mesoporous materials; ii) fine adjustability of the pore size; iii) high thermal and hydrolytic stability if properly prepared; and iv) a high degree of pore ordering over micron length scales. These important and unusual properties are a direct result of the interplay between organized arrays of the surfactant molecules and silicate species in the aqueous phase during hydrolysis polycondensation process.[41, 47]

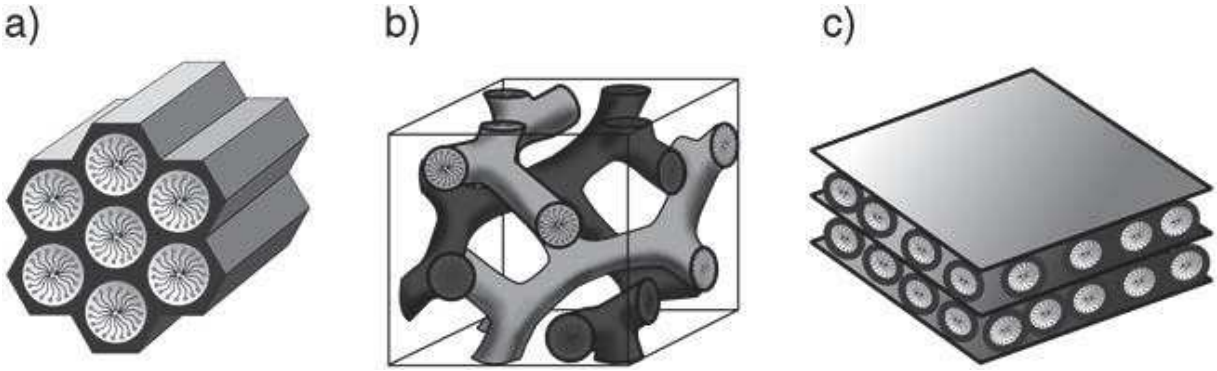


**Figure 11. Structures of mesoporous M41S materials:** a) MCM-41 (2D hexagonal), b) MCM-48 (cubic) and c) MCM-50 (lamellar).[48]

In 1998, prominent research produced another material type of hexagonal array of pores namely Santa Barbara Amorphous-15 (SBA-15). The synthesis was performed in the presence of a nonionic triblock copolymer surfactant under acidic conditions. SBA-15 showed larger pore size from 46 to 300 Å. The discovery of this type of material was a research breakthrough in the field of mesoporous material development.[51] This SBA-15 mesoporous material has not only larger pores, but also enhanced thermal, mechanical and chemical resistance properties compared to MCM-41.[42]

### 3.4 Liquid Crystal Templating Mechanism

In M41S family, a liquid crystal templating (LCT) mechanism was proposed by the Mobil scientists in which supramolecular assemblies of surfactant micelles (*e.g.*, alkyltrimethylammonium surfactants) act as structure directors for the formation of the mesophase (Figure 6). Accordingly, the final product is a silicate skeleton which contains voids that originate from these mesophases after surfactant elimination. The silicate condensation is not the dominant factor in the formation of the mesoporous structure. The whole process may take place *via* two possible mechanistic pathways as schematically shown in Figure 12:

- **True liquid-crystal template mechanism (LCT):** is based on true or semi-liquid-crystal mesophase micelles produced by high-concentration surfactants as templates. The condensation of inorganic precursors is improved owing to the confined growth around surfactants, forming ceramic-like frameworks. After condensation, the organic templates can be removed. The inorganic materials "nanocast" the mesostructures, pore sizes, and symmetries from the liquid-crystal scaffolds.
- **Cooperative Templating Mechanism (CTM):** In this case the mesophase is formed even at lower concentrations of surfactant molecules below CMC, inorganic species interact with surfactants driven by Coulomb force, covalent bond or hydrogen bonding. The inorganic species at the interface polymerize and cross-link, and thus cooperatively assemble with surfactants. Upon the reaction, the cooperative arrangements of surfactants and the charge density between inorganic and organic species influence each other. Hence the compositions of inorganic–organic hybrids differ to some extent. The matching of charge density at the surfactant/inorganic interfaces governs the assembly process, thus resulting in phase separation and reorganization, finally leading to the formation of ordered 3-d arrangement with the lowest energy.[52]

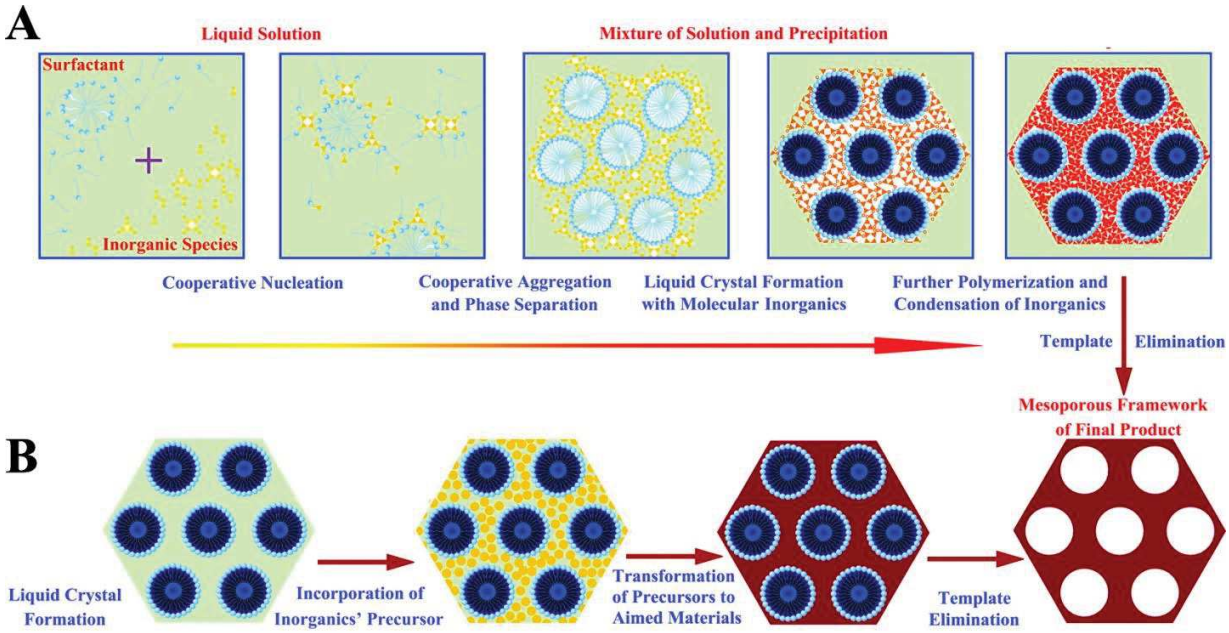


**Figure 12. Two synthetic strategies of mesoporous materials:** (A) cooperative self-assembly; (B) "true" liquid-crystal templating process.[53]

Using this soft-templating method, numerous novel ordered mesoporous materials composed of inorganic, organic, and inorganic–organic composite frameworks have been prepared via various synthetic methods such as aqueous process, nonaqueous approach,[54] hydrothermal method, etc. Plenty of soft templates, including cationic, anionic and non-ionic surfactants, and mixed surfactant systems, have been utilized to synthesize ordered mesoporous materials with controllable structures and tunable pore architecture.[52]

## 3.5 Organically Functionalized Mesoporous Silica Phases

In order to enhance the functionalities of mesoporous silica materials, many efforts have been made for modification and functionalization of silica framework.

The combination of the properties of organic and inorganic building blocks within a single material is particularly attractive from the viewpoint of materials scientists because of the possibility to combine the enormous functional variation of organic chemistry with the advantages of a thermally stable and robust inorganic matrix.[48] Adjustment of the polarity of the pore surfaces of an inorganic matrix by the addition of organic building blocks extends

considerably the range of materials, such as optical materials and sensors, low-k materials, solid catalysts, adsorbents, and biological drug delivery systems and controlled release materials.

For the synthesis of porous hybrid materials based on organosilica units, three pathways are available:

1. The subsequent modification of the pore surface of a purely inorganic silica material ("post-synthesis - grafting"),
2. The simultaneous condensation of corresponding silica and organosilica precursors ("co-condensation"),
3. The incorporation of organic groups as bridging components directly and specifically into the pore walls by the use of bis- or oligo-silylated single-source organosilica precursors ("Periodic Mesoporous Organosilicas (PMO)").

- **Postsynthetic Functionalization of Silicas ("Grafting")**

Grafting refers to the subsequent modification of the inner surfaces of mesostructured silica phases with organic groups. This process is carried out primarily by reaction of organosilanes of the type $(R'O)_3SiR$, or less frequently chlorosilanes $ClSiR_3$ or silazanes $HN(SiR_3)_3$, with the free silanol groups of the pore surfaces (Figure 13). In principle, functionalization with a variety of organic groups can be performed in this way by variation of the organic group R.

- **Co-Condensation (Direct Synthesis)**

An alternative method to synthesize organically functionalized mesoporous silica phases is the co-condensation method (one-pot synthesis) which is associated with the co-assembling of TEOS with an organosiloxane of the type$(R[Si(OR')_3]_n)$ (R stands for organic group and R' stands for methoxy or ethoxy group in general) in the presence of surfactant under acid or basic conditions (Figure 13). If the organic hybrid precursor is monosilylated (n = 1) the reaction leads to materials with organic residues anchored covalently to the pore walls, the organic functionalities are direct components of the silica matrix. Furthermore, the organic units are generally more homogeneously distributed than in materials synthesized with the grafting process. When the

hybrid precursor is bis- or oligo-silylated more n ≥ 2 the organic functional groups in this case are usually incorporated onto the silica framework through covalent bonds.[48, 55]

However, both methods suffer from inhomogeneous distribution of organic groups inside the pores and silica network. Finally, when a higher amount of silsesquioxane materials is co-condensed with TEOS totally disordered/amorphous structures are obtained. As a result to control the efficient mesoporous functionalization and to ensure the pores structure, the amount of functional groups should be in the concentration range of 5–15 mol%.[56]

- **Periodic Mesoporous Organosilicas (PMOs)**

Periodic mesoporous organosilicas (PMOs) prepared by surfactant-directed polycondensation of bridged organosilane precursors are promising for a variety of next-generation functional materials.[55] This class of materials was synthesized independently for the first time in the year 1999 by three different research groups Inagaki, Ozin and Stein.[57-59] The materials were obtained by sol gel process from organo-bridged alkoxysilanes using structure directing agents in the absence of silica source (*e.g.* tetraethoxysilane). A large diversity of bulk PMO materials were then synthesized from a wide variety of organosilica precursor.[48]

In contrast to the organically functionalized silica phases, which are obtained by post synthetic or direct synthesis, the organic units are in this case incorporated in the three-dimensional network structure of the silica matrix through covalent bonds and thus distributed totally homogeneously in the pore walls.[48]

The synthesis of PMOs is rather straightforward and the corresponding mechanism is similar to that of mesoporous silica materials (see Figure 13), which is also based on sol–gel chemistry via the self-assembly of hydrolyzed/ condensed bi- or multi-silylated organosilica precursor with mesopore structural-directing agents (SDAs) (*e.g.* surfactants or block copolymers).[60] In this case two or even three different kinds of organic moieties can be incorporated into the PMOs' framework simply by choosing multiple bis-silylated organosilica precursors.[55]

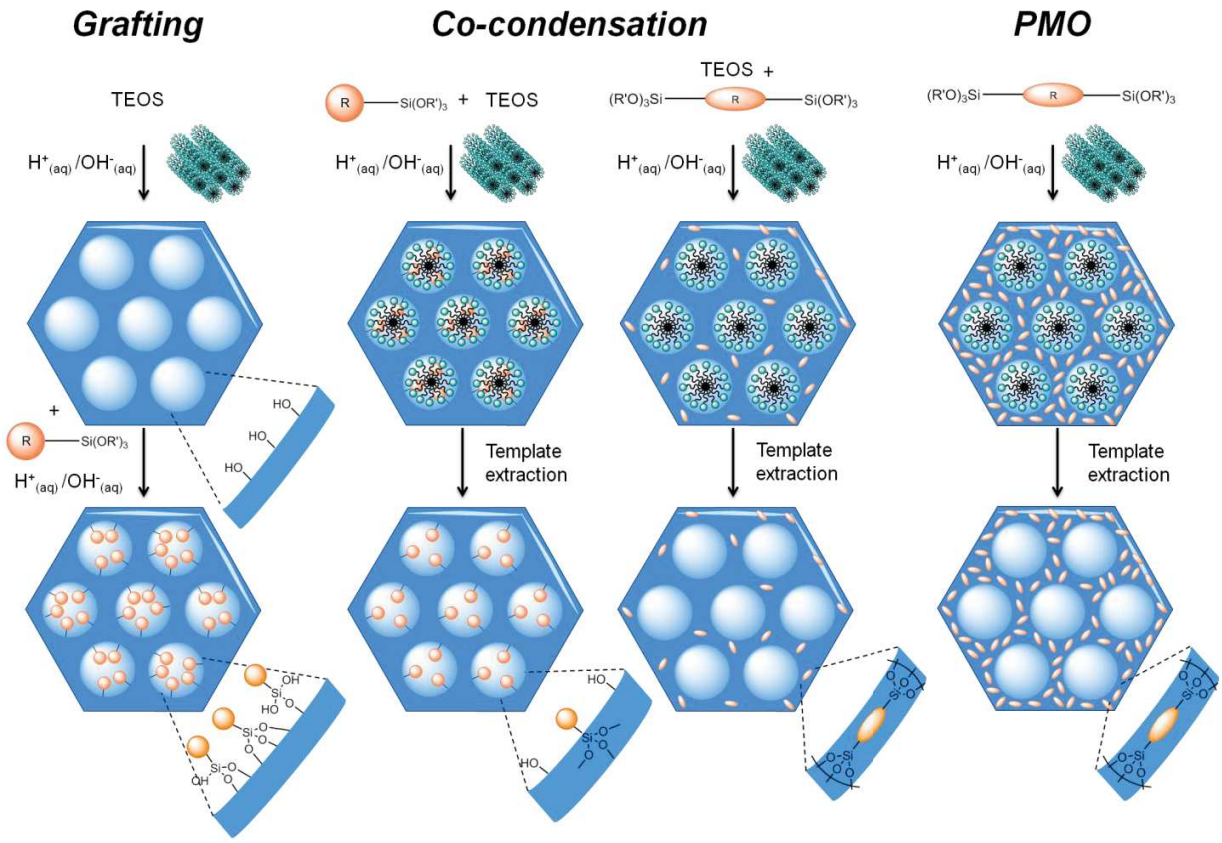


**Figure 13. Different pathways for the organic funtionalization of mesoporous silica phases: grafting, co-condensation and PMO;** R: organic bridging group, R': methyl or ethyl). Such mesoporous hybrids prepared from bridged organosilane precursors ($R[Si(OR')_3]_n$; $n \geq 2$) have been classified as periodic mesoporous organosilica (PMO)

In this introduction we are particularly interested on the functionalization of silica materials with ionic organic groups. For this reason, we discuss here in particular the co-structure-directing method where ionic precursor acts as co-structure directing agent. Moreover, our interest is especially on PMO type materials called ionosilica which are synthesized exclusively from ionic precursors.

### 3.6 Co-structure directing agent

The synthesis of mesoporous silica using an anionic surfactant has been unsuccessful for a long time. The use of anionic surfactants as SDA is highly desirable due to several advantages compared with cationic and nonionic surfactants. Anionic surfactants used in greater volume than any other surfactants have biodegradability properties and low cytotoxicity. For this reason, a co-structure-directing method was developed to synthesize anionic-surfactant-templated mesoporous silicas, AMSs. This method is conducted via co-condensation reaction from monosilylated ionic precursors and silica precursors (TEOS or TMOS). In this case the organic precursor plays the role of co-structure directing agents (CSDAs), amino silane (APS) and quaternary ammonium silanes (TMAPS) are commonly used in the synthesis of AMS. The CSDA interacts electrostatically with the negatively-charged head group of an anionic surfactant, while the alkoxysilane site co-condenses with the silica source to form a silica framework as demonstrated in Figure 154, b, c. This method is also used in the presence of cationic surfactant with a anionic organic monosilylated precursor and even in the presence of mixed cationic/anionic precursors and cationic/anionic surfactants schematized in the Figure 14,d and c respectively.[61, 62]

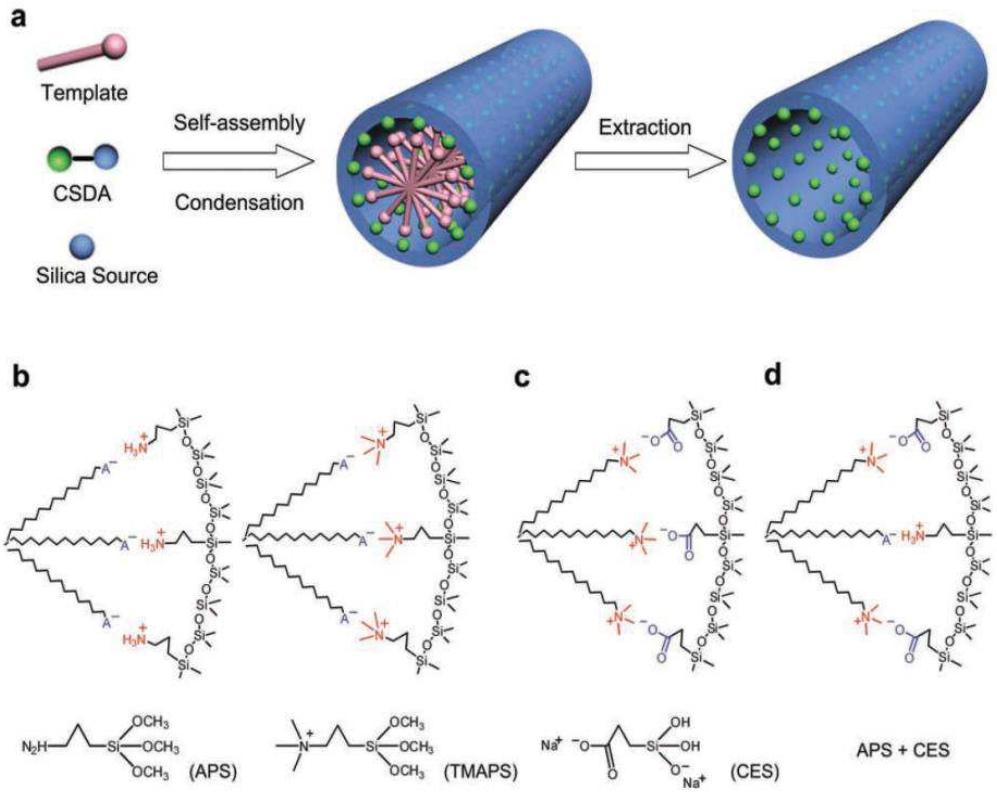


**Figure 14. Synthesis of mesoporous silica by co-structure directing method:** a) Schematic illustration of the interactions between CSDA and headgroup of surfactant in the co structure-directing synthesis of mesoporous silicas. b,c) For synthesis systems of mesoporous silica using anionic or cationic surfactants as the template, cationic CSDA (e.g., APS and TMAPS) and anionic CSDA (e.g., CES) could be employed respectively to provide the organic/inorganic interactions and give rise to highly ordered mesostructures. d) Synthesis of acid/base bifunctional mesoporous silica using mixture of anionic/cationic surfactants and cationic/anionic CSDAs.[62]

## 3.7 Ionosilica hybrid materials

The co-structure directing method as described above beautifully illustrates the templating involving surfactant/precursor ion pairs which allows accessing highly structured functionalized silica materials.

In our group, we are interested in the synthesis of silica based materials bearing covalently attached ionic groups. These PMO type materials, so-called Ionosilicas, are defined as mesoporous silica materials containing covalently incorporated ionic groups. These materials are situated at the interface of structured silica mesophases and ionic liquids.[63-65] They are obtained by template directed hydrolysis-polycondensation from oligosilylated ionic precursors.[64] This

approach is particularly attractive since the organo-ionic group of the silylated precursor promotes the structuration process during the template directed hydrolysis-polycondensation reaction.[66, 67]

S. Dai *et al* reported for the first time PMO material containing ionic organic group within the silica network from ionorganic silylated precursor, named PMO anions exchange resins for the separation of perrhenate ions. These materials containing imidazolium substructures were obtained through hydrolysis polycondensation of the imidazolium precursor in the presence of cationic surfactant and without silica source (Figure 15). [65] Similarly, Inagaki *et al*. reported the synthesis of PMO material with cationic methylacridinium substructures using a nonionic surfactant under acidic condition.[55]

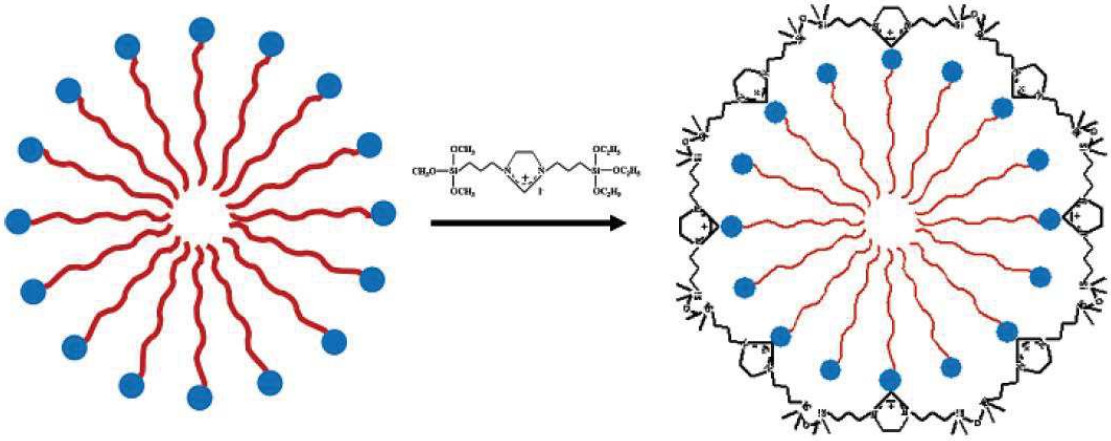

**Figure 15. Synthetic Procedure for the Preparation of PMO Anion Exchange Resins containing imidazolium.**[65]

Our group recently showed that the preparation of nanostructured PMO materials can also be achieved from well-defined SDA-precursor ion pairs. [66, 67] In this case, the ionic silylated precursor plays two roles at the same time; it acts as CSDA for the formation of surface functionalized silica, and as molecular brick for solid phase formation. A large variety of ionic compounds bearing ammonium and imidazolium substructures was used for the formation of the hybrid ionosilica materials, the Figure 16 illustrates the different precursors used for the synthesis of ionosilica PMO materials.

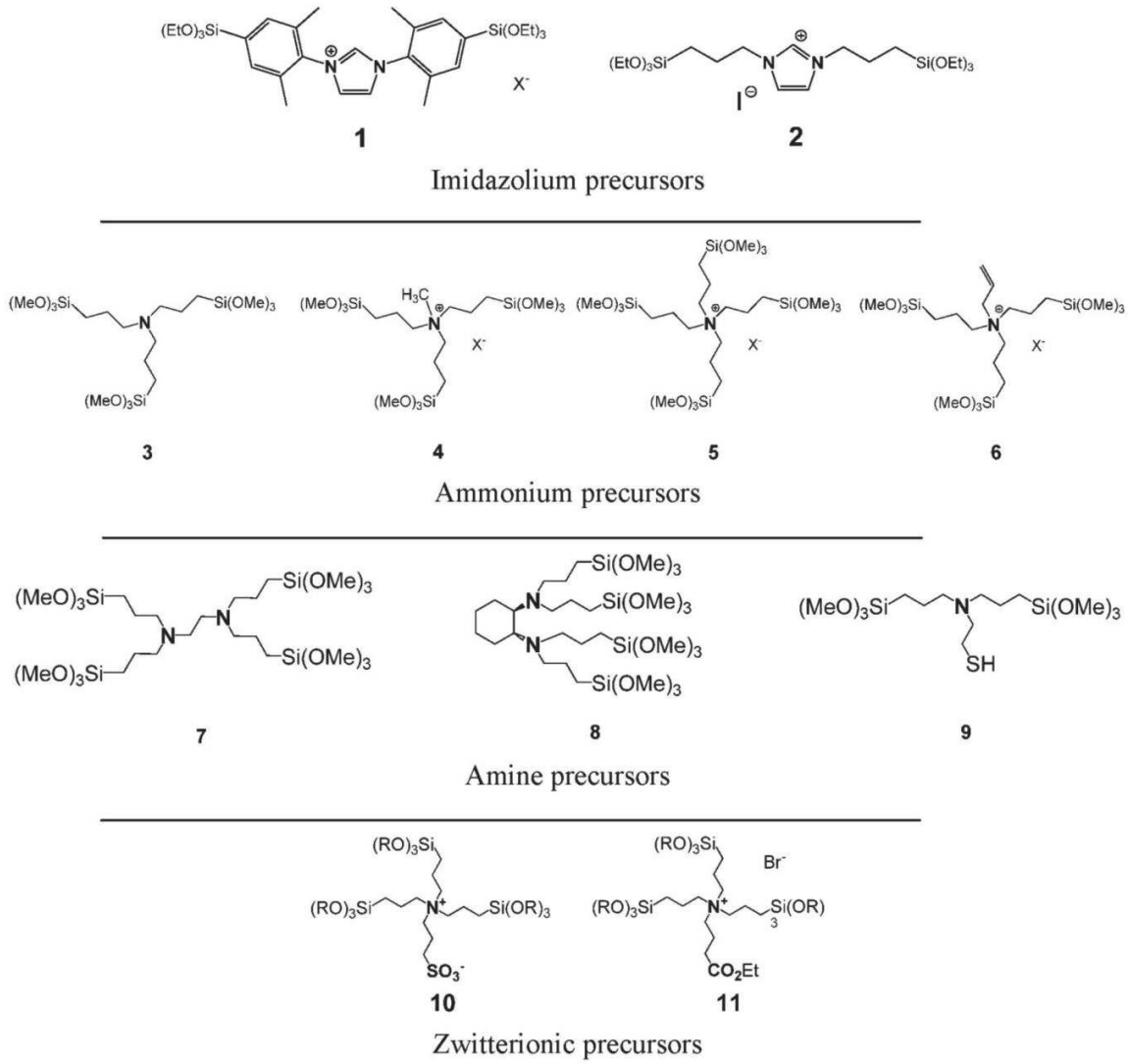


**Figure 16. Families of ionosilica precursors studied in template directed hydrolysis-polycondensation reactions: from upper to lower: diaryl- and dialkyl-imidazolium precursors 1 and 2; ammonium precursors 3–6; functional amine precursors 7–9; zwitterionic precursors 10 and 11.**[67]

Nguyen *et al.*[66]reported a study on the use of di-alkyl-imidazolium precursor in template directed by hydrolysis-polycondensation. The materials were prepared in the presence of three different surfactants; cationic, nonionic and anionic. Remarkably the formation of nanostructured materials with 2d-hexagonal architecture was observed only in the presence of anionic surfactant. In contrast, the use of cationic and nonionic surfactant led to the formation of non-porous but non structured materials. These results demonstrate clearly that the formation of materials displaying

2 d-hexagonal phases involves ionic precursor/surfactant ion pairs. It is to note that Nguyen *et al*. were not able to reproduce S. Dai's results.

In the following, the anionic templating strategy was applied to other types of organo-cationic precursors, in particular to the silylated ammonium salts. As described above, these ammonium precursors also involve the formation of precursor/ surfactant ion pairs during the hydrolysis polycondensation reaction. Similarly, the formation of structured materials from ammonium precursors gave rise only in the presence of anionic surfactants. The use of non-ionic or cationic surfactants led to porous but non-structured materials. Once more, this result can be attributed to ionic interactions between the cationic centre of the ammonium precursor and the anionic head-group of the SDA (Figure 17).

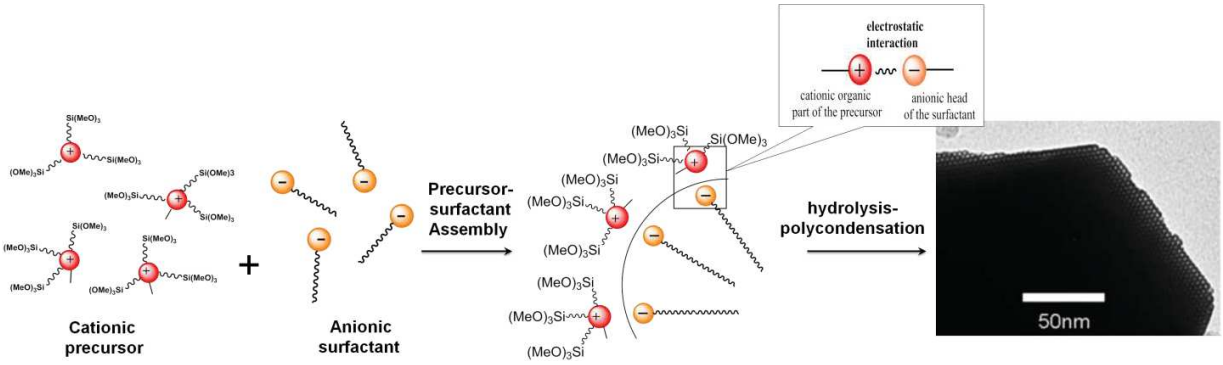


**Figure 17. Synthesis of nanostructured ionosilica mesophases by anionic templating from cationic ammonium precursors.**

### 3.7.1 Some applications of ionosilica

These ionosilica materials, constituted of ionic species homogeneously distributed over the whole silica material[68] with a high porosity and narrow pore size distribution, have large potential for applications in catalysis[63] and separation via ion exchange reaction[69]. Furthermore ionosilica exhibits particularly hydrophilic properties, displaying high affinity for water, leading to enhanced mass transfer and, in fine, to a high accessibility of ionic sites. For this purpose, ionosilicas appear as interesting anion adsorbing materials for metallic anions such as chromate, perrhenate and pertechnatate.[65, 70, 71] We recently demonstrated that ionosilica are efficiently and selectively adsorbing anionic drugs as well (*see* chapter III, part I).[72]

## 3.8 Morphology control of PMO type material

Morphology control of PMOs has been further developed on the molecular to macroscopic scale. The one significant advantage of these materials is the controllability of their particle morphology, shape and size (*e.g.* powder, film and nanoparticle). Selection of the reaction conditions for PMO syntheses and post-processing of the resulting hybrids can optimize the morphology at the macroscopic to nano-scale for specific applications ranging from adsorbents, catalysts, optical materials to nanocatalyis, nanoreactors and nanomedecine.

Precipitation of organosilica hybrids in the aqueous phase usually yields powders suitable for porous supports and recyclable solid catalysts. An entire series of different morphologies, such as rods, spheres and platelets, has been reported for PMO powders prepared under various hydrolytic reactions and aging conditions. Hole-transport organosilica containing transparent PMO films have also been reported for optical and coating applications by sol–gel polycondensation on solid substrates in the presence of evaporable organic solvents, which is referred to as evaporation-induced self-assembly.[55, 56]

In this section we will present some examples of processing PMO materials into monoliths and nanoparticles. It should be noted that examples of PMO materials synthesized in these shapes are scarce, as it is well known that modulation of the PMO type materials is often difficult to reach and depend on the organic moieties of the hybrid precursor.

### 3.8.1 PMO Monoliths

The ability to mold porous materials into any desired shape and size increases significantly their range of application. In particular, the synthesis of monolithic materials with hierarchical pore structures is an extensive field of investigation, as the combination of different pore-size regimes within one material leads to multiple benefits arising from each regime; for example, micro- and mesopores act in a size- or shape-selective manner, and macropores reduce diffusion limitations to the active sites. These features are of interest for a wide range of application fields such as separation science, catalysis or biocatalyst supports, and sensing. The first organosilica materials in monolithic form were reported by Nakanishi and co-workers. This group used ethane bridge organosilica precursor and a triblock copolymer for templating. They obtained macro-

mesoporous ethane-silica monoliths containing co-continuous macropores and mesopores within a glass tube.[73, 74] Huesing *et al*. reported the synthesis of methyl-, phenyl-, ethylene- bridged and phenylene-bridged silica monoliths with a hierarchical buildup on at least four levels:

a) Deliberate macroscopic shape,
b) Uniform macropores,
c) Highly ordered mesopores (plus micropores),
d) Molecular periodicity of the phenylene moieties within the pore walls.

Figure 18 shows the monolith with phenylene-bridged group.[73, 75]

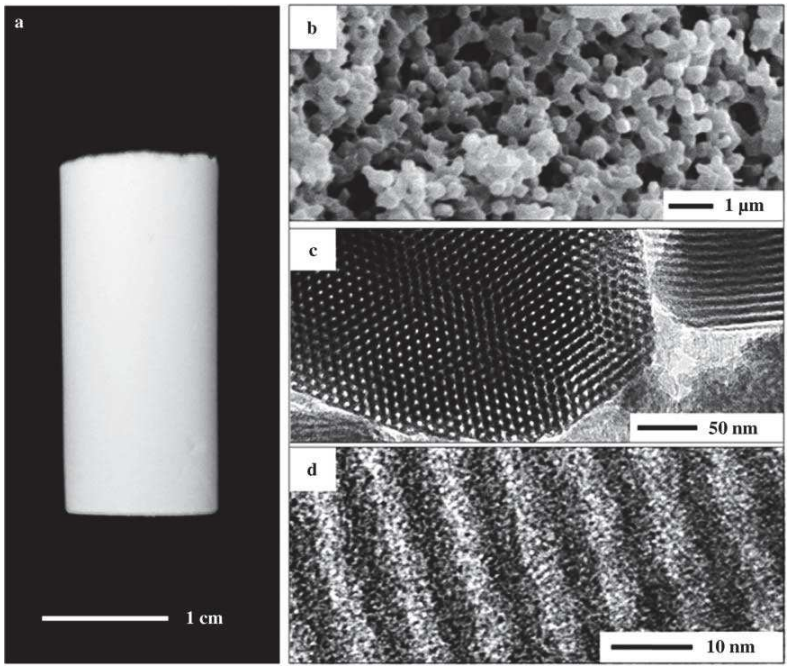


**Figure 18. Phenylene-bridged silica monolith:** Hierarchy on four levels: a) photograph, b) SEM image, and c, d) TEM images of the dried phenylene- bridged silica monolith, which show its hierarchical buildup.[73]

A novel PMO monolith based on an ethylene bridged alkoxysilane precursor was reported by Wu *et al.* This material showed large surface area, great rigidity, and an abundance of vinyl groups within the framework (Figure 19). Using the highly efficient thiol−ene "click" chemistry, the monolith was functionalized with C18 groups, and applied as an excellent reversed stationary phase for highly efficient nanoRPLC separation of not only small molecules but also complex protein samples.[76]

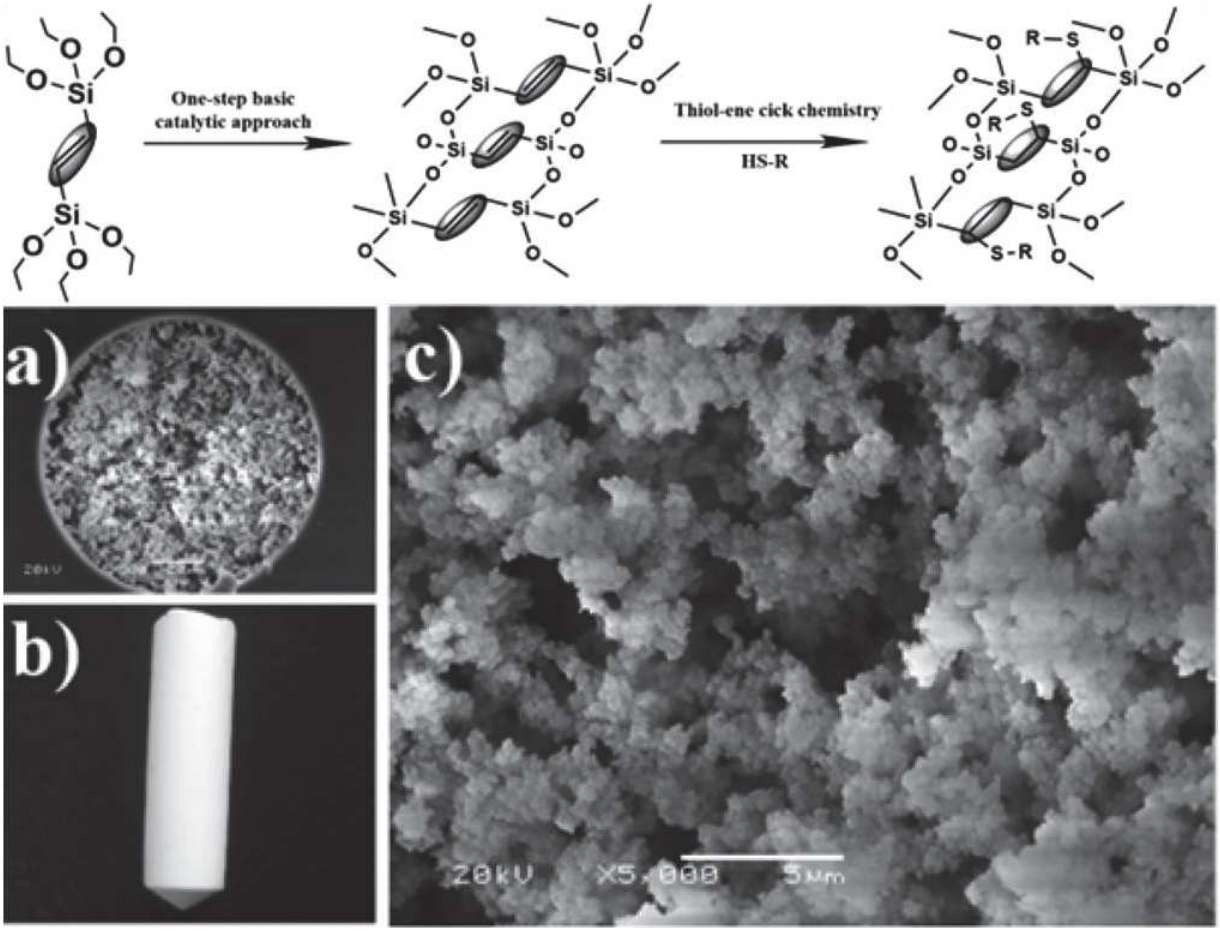


**Figure 19. Ethylene bridged silica monolith,** Upper: synthesis and Functionalization via Thiol−ene Click Chemistry, Lower. **(a)** SEM image of the ethylene bridged silica monolith in a capillary (i.d. 100 μm) 900×, **(b)** photograph of the bulk ethylene bridged silica monolith, **(c)** SEM image of the ethylene bridged silica monolith 5000×.[76]

### 3.8.2 PMO nanoparticles

Reaching the nanoscale with PMO materials is still a major challenge.[77, 78] However, examples of PMO nanoparticles are scarce. In 2006, Lu *et al.* reported for the first time hollow PMO ethane bridged silica nanospheres (HMONs) with 100-400 nm of diameter, these nanospheres display relatively uniform spherical geometry. [79] These nanoparticles were synthesized by a liquid-crystal "dual-templating" method. Cetyltrimethylammonium bromide (CTAB) and fluorocarbon surfactant (FC4) were used as SDAs and 1,2-bis(trimethoxysilyl)ethane (BTME) (R = ethane) was employed as a bis-silylated organosilica precursor. In a first step vesicles were formed by

self assembly of FC4 followed by a liquid-crystal-templating procedure by CTAB and hydrolyzed/condensed BTME.

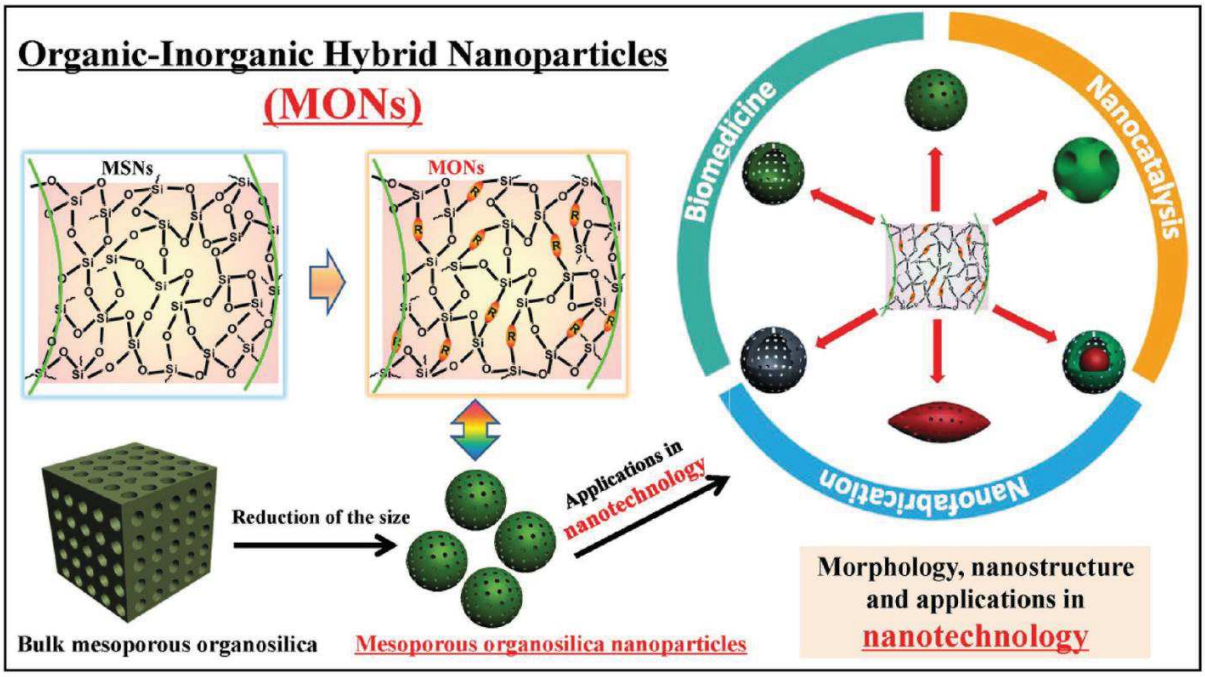


**Figure 20. Schematic illustration of the framework-composition alteration from traditional inorganic –Si–O–Si– (mesoporous Silica Nanoparticles MSNs) to organic–inorganic hybrid –Si–R–Si– (Mesoporous Organosilica Nanoparticles MONs),** transformation of bulk mesoporous organosilica (e.g., PMOs) into MONs, and their representative morphologies, nanostructures and applications in nanotechnology.[60]

However, these HMONs featured a highly ordered mesoporous shell but low dispersity and irregular morphology. These properties limit applications in nanotechnology, especially in nanomedicine, where particle monodispersity and uniform size distribution are necessary.[60]

Phenylene-bridged PMO nanospheres were then reported in 2009. These nano-objetcs display a diameter ranging from 50 to 1000 nm, and a worm-like porosity.[80] The procedure was based on co-templating by a triblock copolymer P123 and fluorocarbon surfactant (FC4) in water/ethanol under acidic conditions. Interestingly, the nanospheres show a core–shell structure, the shell being templated by FC-4 and the core by the poly-lactic acid based polymer P123. Using the well known P123 block co-polymer, but without FC-4, ethylene- or phenylene-bridged hollow organosilica nanospheres of 12 to 25 nm of diameter were obtained.

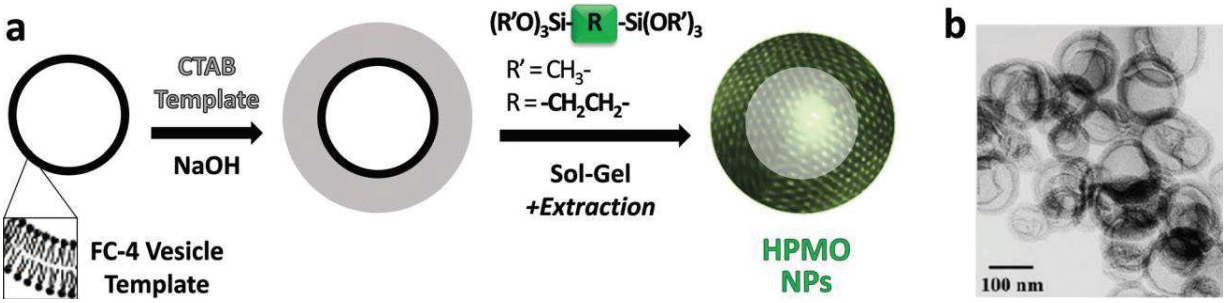


**Figure 21. Schematic representation of the FC-4 vesicle and CTAB dual templating strategy for the preparation of HPMO NPs** (a), and a Transmission Electron Microscopy (TEM) image of a resulting nanomaterial (b).[79]

The preparation of an aqueous colloidal mesoporous nanoparticle was only reported in 2011 by the Kuroda group.[81] The colloidal solution of monodisperse PMO nanospheres of 20 nm in diameter for simple organic bridges such as methylene, ethylene and ethenylene, but not for the larger phenylene linker. These nanoparticles, which feature a worm-like architecture, were obtained from a basic aqueous mixture of CTAB and triethanolamine.[77]

In 2012, Guan *et al.* reported the first ordered and monodisperse PMO nanoparticles with caged or cylindrical mesostructures.[78] These monodispersed PMO nanoparticles synthesized from containing methylene-, ethylene-, ethenylene-, and phenylene-bridged precursors, showed a highly ordered pore structures and typical NP diameters of 100 to 200 nm (Figure 22). The nanoparticles were synthesized using a cationic surfactant cetyltrimethylammonium bromide (CTAB) with an organo-silylilated precursor in the presence of ammonia as a catalyzer. The pore structures of the as-made particles with three-dimensional hexagonal (P63/mmc), cubic (Pm3n), two-dimensional hexagonal (P6mm), and wormlike structure were evidenced by powder X-ray diffraction analysis (XRD). The size of the nanoparticles can be adjusted from 30 nm to 500 nm by variation of the ammonia concentration or the co-solvent content of the reaction medium.

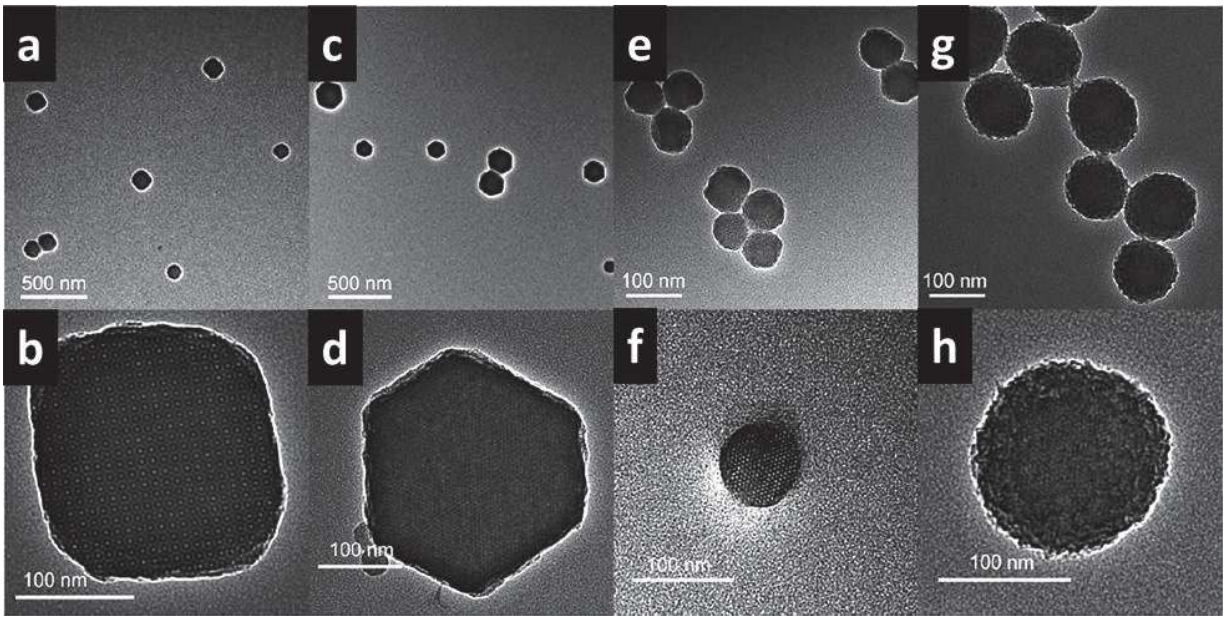


**Figure 22. TEM images of ethylene- (a, b), methylene- (c, d), ethenylene-(e, f ), and phenylene-bridged PMO NPs (g, h) at low and high magnification.**[78]

In these new materials, the organic groups are homogeneously distributed over the whole materials' framework. The approach of combining a homogeneous dispersion of the organic groups within nanoparticles of controlled size and shape offers the possibility to control the interfacial, chemical and physico-chemical properties of these objects. For this reason, PMO-type nanoparticles appear as original and tunable nanoobjects[77, 82] which offer new perspectives such as in catalysis[83] and nanomedecine.[77, 82, 84]

## 3.9 Conclusion

Further development of functional PMOs is strongly expected by expansion of the functional organic bridges, control of meso-scale symmetry and porosity, optimization of morphology, and the construction of well-designed multicomponent systems. PMOs have a great future for various applications, such as efficient and recyclable solid catalysts, highly-sensitive sensors, photovoltaic materials and artificial photosynthetic systems.

In this thesis, we investigated three functional ionic systems. Alkylguanidinium surfactant self assembly behavior, Alkylguanidinium based ionic liquid for liquid-liquid extaction and ionosilica material for the drug adsorption including shaping on nanoparticles and monoliths.
The results are presented in two chapters; the first one encompasses alkylguanidinium based surfactants and ionic liquids and the second concerns ionosilica materials.

The chapter two presents a study of both surfactants and ionic liquids containing the guanidinium substructure. The work is presented separately in two parts.

The part one is about the synthesis of mono-alkylguanidinium chlorides with variable chain length ($C_{10}$-$C_{16}$), followed by different characterization techniques in order to improve their purity. Then, the micelle formation and surface activity of these compounds were determined using the conductivity, surface tension and isothermal titration calorimetry measurements. Our results show a clear relationship between alkyl chain length and self-aggregation behavior. Compared to alkyltrimethylammonium chlorides, alkylguanidinium surfactants display different surface activity and micelle formation is much more exothermic. These differences can be attributed to the hydrogen-bonding capacity and the different shape of guanidinium head-group.

In the second part, we synthesized mono-alkylguanidium bis-trifluoromethane sulfonimides with a short chain length as a new class of functional ionic liquids for the extraction of anionic compounds. The extraction was performed against an organic dye (Methyl orange), anionic drug (Diclofenac) and a metallic anion (Chromate).
These new compounds show significantly enhanced extraction efficiency compared to conventional imidazolium based ionic liquids. These results were achieved via ion exchange reaction through the hydrogen bonding properties of the guanidinium group. This guanidinium substructure displays high affinity towards anionic sulfonate and carboxylate groups, contrarily to conventional ionic liquids where the extraction process is generally driven by hydrophobic interaction.

The chapter three concerns ionosilicas materials. The study focuses on three different shapes materials: powders, nanoparticles and monoliths. For this, the chapter is divided on three parts.

In the first part, the potential of porous ammonium containing ionosilica for the removal of different drug molecules from water solutions was evaluated; this material is in a powder form. The adsorption was performed on neutral and anionic drug (sulindac, sodium diclofenac and sodium sulindac). The study show that ionosilica materials are selective adsorbent for anionic drugs, high amounts of the anionic drugs diclofenac and sulindac are irreversibly trapped within the material whereas neutral species are hardly adsorbed.
Our study concerned the adsorption process driven via electrostatic interaction between the drug and the positively charged ionosilicas. The material was characterized with regard to their adsorption/release performances, in order to investigate its potential for waste water treatment. The physico-chemical properties of the loaded materials were investigated employing Fourier Transform infrared spectroscopy, with particular attention to the drug-ionosilica interactions.

The use of ionosilica materials for biomedical purposes is highly desired. For this reason, in the second part periodic mesoporous ionosilica nanoparticles with ammonium walls were synthesized from a trisilylated ammonium precursor. The formation of these nanoparticles was achieved following Stöber method. The nanoparticles were stabilized via surface recovery using a binary surfactant system composed of an anionic/non-ionic surfactant mixture. The formation of porous nanoparticles was based on the balance between the ordered assembly of cationic organic bridged precursor/anionic surfactant ion pairs and the inhibition of grain agglomeration involving the nonionic surfactant.
The nanoparticles display uniform particle size together with ordered hexagonal pore architecture and high specific surface area.
*In vitro* and *in vivo* investigation show that ionosilica nanoparticles are completely biocompatible and are efficiently endocytosed by macrophages. Diclofenac delivery was studied and the loaded nanoparticles are efficient in inhibiting lipopolysaccharides (LPS) induced inflammation.

Finally, the third part concerns the synthesis of silica hybrid monoliths containing amine and ammonium substructures, the as synthesized monolith display trimodal hierarchical porous structure (micro, meso, and macroporosity). These materials were obtained via high internal phase emulsion (HIPE) process and lyotropic mesophases.

The incorporation of organic functionalities (ammonium) has been achieved in two pathways: by simultaneous reaction of TEOS and silylated organic precursor (co-codensation) and by the using only ammonium precursors that lead to periodic mesoporous organosilcas (PMOs). The resulting materials have been characterized by several techniques such as: Scanning electron microscopy, mercury porosimetry, nitrogen sorption and solid state NMR spectroscopy.

Ionosilica monoliths are particularly interesting in the field of separation and adsorption of molecules supported by the high concentration of ionic organic group located in the materials' framework, thus enabling immobilization of ionic molecules via ion exchange reactions.

## References


1. Lehn, J. M., SUPRAMOLECULAR CHEMISTRY - SCOPE AND PERSPECTIVES MOLECULES, SUPERMOLECULES, AND MOLECULAR DEVICES. *Angewandte Chemie-International Edition in English* 1988, 27, (1), 89-112.
2. Nguyen, S. B. T.; Gin, D. L.; Hupp, J. T.; Zhang, X., Supramolecular chemistry: Functional structures on the mesoscale. *Proceedings of the National Academy of Sciences of the United States of America* 2001, 98, (21), 11849-11850.
3. Ramanathan, M.; Shrestha, L. K.; Mori, T.; Ji, Q.; Hill, J. P.; Ariga, K., Amphiphile nanoarchitectonics: from basic physical chemistry to advanced applications. *Physical Chemistry Chemical Physics* 2013, 15, (26), 10580-10611.
4. Khiterer, M.; Shea, K. J., Spherical, monodisperse, functional bridged polysilsesquioxane nanoparticles. *Nano Letters* 2007, 7, (9), 2684-2687.
5. Swarup, S.; Schoff, C. K., A SURVEY OF SURFACTANTS IN COATINGS TECHNOLOGY. *Progress in Organic Coatings* 1993, 23, (1), 1-22.
6. Krister Holmberg, B. J., Bengt Kronberg, Björn Lindman, *Surfactants and Polymers in Aqueous Solution, second eddition*. John Wiley & Sons, Ltd: Lund, 2003.
7. Nagarajan, R.; Ruckenstein, E., THEORY OF SURFACTANT SELF-ASSEMBLY - A PREDICTIVE MOLECULAR THERMODYNAMIC APPROACH. *Langmuir* 1991, 7, (12), 2934-2969.
8. Hill, J. P.; Shrestha, L. K.; Ishihara, S.; Ji, Q.; Ariga, K., Self-Assembly: From Amphiphiles to Chromophores and Beyond. *Molecules* 2014, 19, (6), 8589-8609.
9. McBain, T. W.; Cornish, E. C. V.; Bowden, R. C., Studies of the constitution of soap in solution sodium myristate and sodium laurate. *Journal of the Chemical Society* 1912, 101, 2042-2056.
10. Danov, K. D.; Kralchevsky, P. A.; Ananthapadmanabhan, K. P., Micelle-monomer equilibria in solutions of ionic surfactants and in ionic-nonionic mixtures: A generalized phase separation model. *Advances in Colloid and Interface Science* 2014, 206, 17-45.
11. Williams, R. J.; Phillips, J. N.; Mysels, K. J., THE CRITICAL MICELLE CONCENTRATION OF SODIUM LAURYL SULPHATE AT 25-DEGREES-C. *Transactions of the Faraday Society* 1955, 51, (5), 728-737.

12. Rosen, M. J., *Surfactants and Interfacial Phenomena, Third Edition*. John Wiley & Sons: New York, 2004

13. Evans, H. C., ALKYL SULPHATES .1. CRITICAL MICELLE CONCENTRATIONS OF THE SODIUM SALTS. *Journal of the Chemical Society* 1956, (MAR), 579-586.

14. Jurašin, D.; Sikirić, M. D., Higher Oligomeric Surfactants - From Fundamentals to Applications. In *Oligomerization of Chemical and Biological Compounds*, InTech: 2014.

15. Manojlović, J. Ž., The Krafft Temperature of Surfactant Solutions. *Thermal Science* 2012, 16, S631-S640.

16. Tadros, T. F., Front Matter. In *Applied Surfactants*, Wiley-VCH Verlag GmbH & Co. KGaA: 2005.

17. Plechkova, N. V.; Seddon, K. R., Applications of ionic liquids in the chemical industry. *Chemical Society Reviews* 2008, 37, (1), 123-150.

18. Wilkes, J. S., A short history of ionic liquids - from molten salts to neoteric solvents. *Green Chemistry* 2002, 4, (2), 73-80.

19. Hayes, R.; Warr, G. G.; Atkin, R., Structure and Nanostructure in Ionic Liquids. *Chemical Reviews* 2015, 115, (13), 6357-6426.

20. Wilkes, J. S.; Levisky, J. A.; Wilson, R. A.; Hussey, C. L., DIALKYLIMIDAZOLIUM CHLOROALUMINATE MELTS - A NEW CLASS OF ROOM-TEMPERATURE IONIC LIQUIDS FOR ELECTROCHEMISTRY, SPECTROSCOPY, AND SYNTHESIS. *Inorganic Chemistry* 1982, 21, (3), 1263-1264.

21. Dupont, J.; de Souza, R. F.; Suarez, P. A. Z., Ionic Liquid (Molten Salt) Phase Organometallic Catalysis. *Chemical Reviews* 2002, 102, (10), 3667-3692.

22. Berthod, A.; Ruiz-Angel, M.; Carda-Broch, S., Ionic liquids in separation techniques. *Journal of Chromatography A* 2008, 1184, (1-2), 6-18.

23. Marsh, K. N.; Boxall, J. A.; Lichtenthaler, R., Room temperature ionic liquids and their mixtures - a review. *Fluid Phase Equilibria* 2004, 219, (1), 93-98.

24. Keskin, S.; Kayrak-Talay, D.; Akman, U.; Hortacsu, O., A review of ionic liquids towards supercritical fluid applications. *Journal of Supercritical Fluids* 2007, 43, (1), 150-180.

25. Huddleston, J. G.; Visser, A. E.; Reichert, W. M.; Willauer, H. D.; Broker, G. A.; Rogers, R. D., Characterization and comparison of hydrophilic and hydrophobic room temperature ionic liquids incorporating the imidazolium cation. *Green Chemistry* 2001, 3, (4), 156-164.

26. Huddleston, J. G.; Willauer, H. D.; Swatloski, R. P.; Visser, A. E.; Rogers, R. D., Room temperature ionic liquids as novel media for 'clean' liquid-liquid extraction. *Chemical Communications* 1998, (16), 1765-1766.

27. Visser, A. E.; Swatloski, R. P.; Rogers, R. D., pH-dependent partitioning in room temperature ionic liquids provides a link to traditional solvent extraction behavior. *Green Chemistry* 2000, 2, (1), 1-4.

28. Khachatryan, K. S.; Smirnova, S. V.; Torocheshnikova, II; Shvedene, N. V.; Formanovsky, A. A.; Pletnev, I. V., Solvent extraction and extraction-voltammetric determination of phenols using room temperature ionic liquid. *Analytical and Bioanalytical Chemistry* 2005, 381, (2), 464-470.

29. Li, C.; Xin, B.; Xu, W.; Zhang, Q., Study on the extraction of dyes into a room-temperature ionic liquid and their mechanisms. *Journal of Chemical Technology and Biotechnology* 2007, 82, (2), 196-204.

30. Cheng, D.-H.; Chen, X.-W.; Shu, Y.; Wang, J.-H., Selective extraction/isolation of hemoglobin with ionic liquid 1-butyl-3-trimethylsilylimidazolium hexafluorophosphate (BtmsimPF6). *Talanta* 2008, 75, (5), 1270-1278.

31. Tzeng, Y.-P.; Shen, C.-W.; Yu, T., Liquidâ€“liquid extraction of lysozyme using a dye-modified ionic liquid. *Journal of Chromatography A* 2008, 1193, (1â€“2), 1-6.

32. Cull, S. G.; Holbrey, J. D.; Vargas-Mora, V.; Seddon, K. R.; Lye, G. J., Room-temperature ionic liquids as replacements for organic solvents in multiphase bioprocess operations. *Biotechnology and Bioengineering* 2000, 69, (2), 227-233.

33. Pei, Y. C.; Wang, J. J.; Xuan, X. P.; Fan, J.; Fan, M., Factors affecting ionic liquids based removal of anionic dyes from water. *Environmental Science & Technology* 2007, 41, (14), 5090-5095.

34. Ding, X.; Wang, Y.; Zeng, Q.; Chen, J.; Huang, Y.; Xu, K., Design of functional guanidinium ionic liquid aqueous two-phase systems for the efficient purification of protein. *Analytica Chimica Acta* 2014, 815, 22-32.

35. Chun, S.; Dzyuba, S. V.; Bartsch, R. A., Influence of structural variation in room-temperature ionic liquids on the selectivity and efficiency of competitive alkali metal salt extraction by a crown ether. *Analytical Chemistry* 2001, 73, (15), 3737-3741.

36. Pucheault, M.; Vaultier, M., Task Specific Ionic Liquids and Task Specific Onium Salts. In *Ionic Liquids*, Kirchner, B., Ed. Springer-Verlag Berlin: Berlin, 2009; Vol. 290, pp 83-126.
37. Visser, A. E.; Swatloski, R. P.; Reichert, W. M.; Mayton, R.; Sheff, S.; Wierzbicki, A.; Davis, J. H.; Rogers, R. D., Task-specific ionic liquids for the extraction of metal ions from aqueous solutions. *Chemical Communications* 2001, (01), 135-136.
38. Goncalves, R. M.; Leite Pereira, A. C.; Pereira, I. O.; Oliveira, M. J.; Barbosa, M. A., Macrophage response to chitosan/poly-(gamma-glutamic acid) nanoparticles carrying an anti-inflammatory drug. *Journal of Materials Science-Materials in Medicine* 2015, 26, (4).
39. Cevasco, G.; Chiappe, C., Are ionic liquids a proper solution to current environmental challenges? *Green Chemistry* 2014
16, (5), 2375-2385.
40. Kresge, C. T.; Leonowicz, M. E.; Roth, W. J.; Vartuli, J. C.; Beck, J. S., ORDERED MESOPOROUS MOLECULAR-SIEVES SYNTHESIZED BY A LIQUID-CRYSTAL TEMPLATE MECHANISM. *Nature* 1992, 359, (6397), 710-712.
41. Monnier, A.; Schuth, F.; Huo, Q.; Kumar, D.; Margolese, D.; Maxwell, R. S.; Stucky, G. D.; Krishnamurty, M.; Petroff, P.; Firouzi, A.; Janicke, M.; Chmelka, B. F., COOPERATIVE FORMATION OF INORGANIC-ORGANIC INTERFACES IN THE SYNTHESIS OF SILICATE MESOSTRUCTURES. *Science* 1993, 261, (5126), 1299-1303.
42. Alothman, Z. A., A Review: Fundamental Aspects of Silicate Mesoporous Materials. *Materials* 2012, 5, (12), 2874-2902.
43. Zhao, X. S.; Lu, G. Q. M.; Millar, G. J., Advances in mesoporous molecular sieve MCM-41. *Ind. Eng. Chem. Res.* 1996, 35, (7), 2075-2090.
44. Brinker, C. J., Porous inorganic materials. *Current Opinion in Solid State & Materials Science* 1996, 1, (6), 798-805.
45. Brinker, C. J.; Scherer, G. W., *SOL-GEL SCIENCE, the physics and chemistry of sol-gel processing*. Academic press, INC: San Diego, 1990.
46. Wen, J. Y.; Wilkes, G. L., Organic/inorganic hybrid network materials by the sol-gel approach. *Chemistry of Materials* 1996, 8, (8), 1667-1681.
47. Beck, J. S.; Vartuli, J. C.; Roth, W. J.; Leonowicz, M. E.; Kresge, C. T.; Schmitt, K. D.; Chu, C. T. W.; Olson, D. H.; Sheppard, E. W.; McCullen, S. B.; Higgins, J. B.; Schlenker, J. L., A NEW FAMILY OF MESOPOROUS MOLECULAR-SIEVES PREPARED WITH LIQUID-

CRYSTAL TEMPLATES. *Journal of the American Chemical Society* 1992, 114, (27), 10834-10843.

48. Hoffmann, F.; Cornelius, M.; Morell, J.; Froba, M., Silica-based mesoporous organic-inorganic hybrid materials. *Angew. Chem.-Int. Edit.* 2006, 45, (20), 3216-3251.

49. Dubois, M.; Gulikkrzywicki, T.; Cabane, B., GROWTH OF SILICA POLYMERS IN A LAMELLAR MESOPHASE. *Langmuir* 1993, 9, (3), 673-680.

50. Vartuli, J. C.; Schmitt, K. D.; Kresge, C. T.; Roth, W. J.; Leonowicz, M. E.; McCullen, S. B.; Hellring, S. D.; Beck, J. S.; Schlenker, J. L., Effect of Surfactant/Silica Molar Ratios on the Formation of Mesoporous Molecular Sieves: Inorganic Mimicry of Surfactant Liquid-Crystal Phases and Mechanistic Implications. *Chemistry of Materials* 1994, 6, (12), 2317-2326.

51. Zhao, D. Y.; Huo, Q. S.; Feng, J. L.; Chmelka, B. F.; Stucky, G. D., Nonionic triblock and star diblock copolymer and oligomeric surfactant syntheses of highly ordered, hydrothermally stable, mesoporous silica structures. *Journal of the American Chemical Society* 1998, 120, (24), 6024-6036.

52. Li, W.; Zhao, D. Y., An overview of the synthesis of ordered mesoporous materials. *Chemical Communications* 2012, 49, (10), 943-946.

53. Wan, Y.; Zhao, D. Y., On the controllable soft-templating approach to mesoporous silicates. *Chemical Reviews* 2007, 107, (7), 2821-2860.

54. Nicole, L.; Boissiere, C.; Grosso, D.; Quach, A.; Sanchez, C., Mesostructured hybrid organic-inorganic thin films. *Journal of Materials Chemistry* 2005, 15, (35-36), 3598-3627.

55. Mizoshita, N.; Tani, T.; Inagaki, S., Syntheses, properties and applications of periodic mesoporous organosilicas prepared from bridged organosilane precursors. *Chemical Society Reviews* 2011, 40, (2), 789-800.

56. Wahab, M. A.; Beltramini, J. N., Recent advances in hybrid periodic mesostructured organosilica materials: opportunities from fundamental to biomedical applications. *RSC Adv.* 2015, 5, (96), 79129-79151.

57. Inagaki, S.; Guan, S.; Fukushima, Y.; Ohsuna, T.; Terasaki, O., Novel mesoporous materials with a uniform distribution of organic groups and inorganic oxide in their frameworks. *Journal of the American Chemical Society* 1999, 121, (41), 9611-9614.

58. Asefa, T.; MacLachlan, M. J.; Coombs, N.; Ozin, G. A., Periodic mesoporous organosilicas with organic groups inside the channel walls. *Nature* 1999, 402, (6764), 867-871.

59. Melde, B. J.; Holland, B. T.; Blanford, C. F.; Stein, A., Mesoporous sieves with unified hybrid inorganic/organic frameworks. *Chemistry of Materials* 1999, 11, (11), 3302-3308.
60. Chen, Y.; Shi, J., Chemistry of Mesoporous Organosilica in Nanotechnology: Molecularly Organic–Inorganic Hybridization into Frameworks. *Advanced Materials* 2015, n/a-n/a.
61. Yokoi, T.; Yoshitake, H.; Yamada, T.; Kubota, Y.; Tatsumi, T., Amino-functionalized mesoporous silica synthesized by an anionic surfactant templating route. *Journal of Materials Chemistry* 2006, 16, (12), 1125-1135.
62. Gao, C. B.; Che, S. A., Organically Functionalized Mesoporous Silica by Co-structure-Directing Route. *Advanced Functional Materials* 2010, 20, (17), 2750-2768.
63. El Hankari, S.; Motos-Perez, B.; Hesemann, P.; Bouhaouss, A.; Moreau, J. J. E., Pore size control and organocatalytic properties of nanostructured silica hybrid materials containing amino and ammonium groups. *Journal of Materials Chemistry* 2011, 21, (19), 6948-6955.
64. Nguyen, T. P.; Hesemann, P.; Tran, T. M. L.; Moreau, J. J. E., Nanostructured polysilsesquioxanes bearing amine and ammonium groups by micelle templating using anionic surfactants. *Journal of Materials Chemistry* 2010, 20, (19), 3910-3917.
65. Lee, B.; Im, H. J.; Luo, H. M.; Hagaman, E. W.; Dai, S., Synthesis and characterization of periodic mesoporous organosilicas as anion exchange resins for perrhenate adsorption. *Langmuir* 2005, 21, (12), 5372-5376.
66. Nguyen, T. P.; Hesemann, P.; Moreau, J. l. J. E., i-Silica: Nanostructured silica hybrid materials containing imidazolium groups by hydrolysis-polycondensation of disilylated bis-N,Nâ€²-alkyl-imidazolium halides. *Microporous and Mesoporous Materials* 2011, 142, (1), 292-300.
67. Hesemann, P.; Nguyen, T. P.; El Hankari, S., Precursor Mediated Synthesis of Nanostructured Silicas: From Precursor-Surfactant Ion Pairs to Structured Materials. *Materials* 2014, 7, (4), 2978-3001.
68. Nguyen, T. P.; Hesemann, P.; Gaveau, P.; Moreau, J. J. E., Periodic mesoporous organosilica containing ionic bis-aryl-imidazolium entities: Heterogeneous precursors for silica-hybrid-supported NHC complexes. *Journal of Materials Chemistry* 2009, 19, (24), 4164-4171.
69. Ju, Y. H.; Webb, O. F.; Dai, S.; Lin, J. S.; Barnes, C. E., Synthesis and characterization of ordered mesoporous anion-exchange inorganic/organic hybrid resins for radionuclide separation. *Ind. Eng. Chem. Res.* 2000, 39, (2), 550-553.

70. Zhu, L.; Zhang, C.; Liu, Y.; Wang, D.; Chen, J., Direct synthesis of ordered N-methylimidazolium functionalized mesoporous silica as highly efficient anion exchanger of Cr(vi). *Journal of Materials Chemistry* 2009, 20, (8), 1553-1559.

71. Petrova, M.; Guigue, M.; Venault, L.; Moisy, P.; Hesemann, P., Anion selectivity in ion exchange reactions with surface functionalized ionosilicas. *Physical Chemistry Chemical Physics* 2015, 17, (15), 10182-10188.

72. Bouchal, R.; Miletto, I.; Thach, U. d.; Prelot, B.; Berlier, G.; Hesemann, P., Ionosilicas for drug removal from wastwater. *submitted* 2016.

73. Brandhuber, D.; Peterlik, H.; Huesing, N., Facile self-assembly processes to phenylene-bridged silica monoliths with four levels of hierarchy. *Small* 2006, 2, (4), 503-506.

74. Park, S. S.; An, B.; Ha, C. S., High-quality, oriented and mesostructured organosilica monolith as a potential UV sensor. *Microporous and Mesoporous Materials* 2008, 111, (1-3), 367-378.

75. Husing, N.; Brandhuber, D.; Kaiser, P., Glycol-modified organosilanes in the synthesis of inorganic-organic silsesquioxane and silica monoliths. *Journal of Sol-Gel Science and Technology* 2006, 40, (2-3), 131-139.

76. Wu, C.; Liang, Y.; Yang, K. G.; Min, Y.; Liang, Z.; Zhang, L. H.; Zhang, Y. K., Clickable Periodic Mesoporous Organosilica Monolith for Highly Efficient Capillary Chromatographic Separation. *Analytical Chemistry* 2016, 88, (3), 1521-1525.

77. Croissant, J. G.; Cattoen, X.; Man, M. W. C.; Durand, J. O.; Khashab, N. M., Syntheses and applications of periodic mesoporous organosilica nanoparticles. *Nanoscale* 2015, 7, (48), 20318-20334.

78. Guan, B. Y.; Cui, Y.; Ren, Z. Y.; Qiao, Z. A.; Wang, L.; Liu, Y. L.; Huo, Q. S., Highly ordered periodic mesoporous organosilica nanoparticles with controllable pore structures. *Nanoscale* 2012, 4, (20), 6588-6596.

79. Djojoputro, H.; Zhou, X. F.; Qiao, S. Z.; Wang, L. Z.; Yu, C. Z.; Lu, G. Q., Periodic mesoporous organosilica hollow spheres with tunable wall thickness. *Journal of the American Chemical Society* 2006, 128, (19), 6320-6321.

80. Cho, E.-B.; Kim, D.; Jaroniec, M., Preparation of mesoporous benzene-silica nanoparticles. *Microporous and Mesoporous Materials* 2009, 120, (3), 252-256.

81. Urata, C.; Yamada, H.; Wakabayashi, R.; Aoyama, Y.; Hirosawa, S.; Arai, S.; Takeoka, S.; Yamauchi, Y.; Kuroda, K., Aqueous Colloidal Mesoporous Nanoparticles with Ethenylene-Bridged Silsesquioxane Frameworks. *Journal of the American Chemical Society* 2011, 133, (21), 8102-8105.

82. Wei, Y.; Li, X. M.; Zhang, R. Y.; Liu, Y.; Wang, W. X.; Ling, Y.; El-Toni, A. M.; Zhao, D. Y., Periodic Mesoporous Organosilica Nanocubes with Ultrahigh Surface Areas for Efficient CO2 Adsorption. *Sci Rep* 2016, 6, 11.

83. Liu, J.; Yang, H. Q.; Kleitz, F.; Chen, Z. G.; Yang, T.; Strounina, E.; Lu, G. Q.; Qiao, S. Z., Yolk–Shell Hybrid Materials with a Periodic Mesoporous Organosilica Shell: Ideal Nanoreactors for Selective Alcohol Oxidation. *Advanced Functional Materials* 2012, 22, (3), 591-599.

84. Lu, N.; Tian, Y.; Tian, W.; Huang, P.; Liu, Y.; Tang, Y. X.; Wang, C. Y.; Wang, S. J.; Su, Y. Y.; Zhang, Y. L.; Pan, J.; Teng, Z. G.; Lu, G. M., Smart Cancer Cell Targeting Imaging and Drug Delivery System by Systematically Engineering Periodic Mesoporous Organosilica Nanoparticles. *ACS Appl. Mater. Interfaces* 2016, 8, (5), 2985-2993.

85. Miyake, M.; Yamada, K.; Oyama, N., Self-assembling of guanidine-type surfactant. *Langmuir* 2008, 24, (16), 8527-8532.

86. Ward, M. D., Design of Crystalline Molecular Networks with Charge-Assisted Hydrogen Bonds. *Chemical Communications* 2005, (47), 5838-5842.

# Chapter II

## Alkylguanidinium Based Surfactants & Ionic Liquids: Micellization behavior and adsorption properties

The Guanidine/Guanidinium substructure is a relevant functional group which is widely present in nature, for example in proteins via the essential amino acid arginine and in a variety of natural products. Guanidine is a strong base and behaves as a cation in a wide pH range. The guanidinium group is the basis of a rich supramolecular chemistry due to its ability to interact with various substances via ionic interaction and hydrogen bonding.
This chapter is about the synthesis and characterization of components containing guanidinium substructure including their potential application. This work highlights guanidinium surfactants and ionic liquids that will be presented separately in two parts.

*i)* Part I: As described above in chapter I, surfactant have a self-assembly behavior in aqueous phase forming, thereby, aggregates with different shapes depending on the concentration. The second characteristic is the lowering of the surface tension between two liquids or between a liquid and a solid. In this thesis, we studied these two behaviors of a mono-alkyl guanidinium based surfactant. We synthesized mono-alkyl guanidinium chlorides with variable chain alkyl length ($C_{10}$-$C_{16}$). Micelle formation and surface activity of these compounds were determined by means of conductivity, surface tension and isothermal titration calorimetry measurements. This work was in the collaboration with Prof. Jerzy Zajak and Dr. Bénédicte Prelot at ICGM institute of Montpellier. The isothermal titration calorimetry measurements were performed by Dr. Bénédicte Prelot. This work was published in *International Journal of Molecular sciences* and is presented here in the form of scientific publication. DOI: 10.3390/ijms17020223

*ii)* Part II: Monoalkylguanidinium bis-trifluoromethane sulfonimides are water immiscible functional ionic liquids which appear as highly efficient phases for the sequestration of anionic pollutants from aqueous solutions. These new compounds show significantly enhanced extraction efficiency compared to conventional imidazolium based ionic liquids. In this part, we focused in particular on the sequestration of an organic dye (methyl orange), an anionic drug (diclofenac) and a metallic anion (chromate). Our work highlights the particular properties of guanidinium based ionic liquids towards the extraction of anionic molecules from aqueous solution through ion exchange reaction. The results obtained in this part were published in *RSC advances*. For seek of clarity, we assembled together the main article and the supporting information. DOI: 10.1039/C6RA03607D

# Part I

## Micellization behavior of long-chain substituted alkylguanidinium surfactants

## Summary

# Micellization Behavior of Long-Chain Substituted Alkylguanidinium Surfactants

A paper published in ***International Journal of Molecular sciences*, 2016**, 17, in the press.

Roza Bouchal , Abdellah Hamel, Peter Hesemann, Martin In, Bénédicte Prelot and Jerzy Zajac

## 1 Abstract

Surface activity and micelle formation of alkylguanidinium chlorides containing 10, 12, 14 and 16 carbon atoms in the hydrophobic tail were studied by combining conductivity and surface tension measurements with isothermal titration calorimetry. The purity of the resulting surfactants, their temperatures of Cr→LC and LC→I transitions, as well as their propensity of forming birefringent phases, were assessed based on the results of $^{1}$H and $^{13}$C NMR, differential scanning calorimetry (DSC), and polarizing microscopy studies. Whenever possible, the resulting values of Krafft temperature ($T_K$), critical micelle concentration (CMC), minimum surface tension above the CMC, chloride counter-ion binding to the micelle, and the standard enthalpy of micelle formation per mole of surfactant ($\Delta_{mic}H°$) were compared to those characterizing alkyltrimethylammonium chlorides or bromides with the same tail lengths. The value of $T_K$ ranged between 292 and 314 K and increased strongly with the increase in the chain length of the hydrophobic tail. Micellization was described as both entropy and enthalpy-driven. Based on the direct calorimetry measurements, the general trends in the CMC with the temperature, hydrophobic tail length, and NaCl addition were found to be similar to those of other types of cationic surfactants. The particularly exothermic character of micellization was ascribed to the hydrogen-binding capacity of the guanidinium head-group.

# 2 Article

## 2.1 Introduction

The self-aggregation of amphiphilic molecules and ions into such supramolecular objects as micelles, vesicles, and membranes[1] plays an important role in many fields like biology, pharmacy, and materials science.[2, 3] The diversity of such uses has been a powerful driving force behind the design and preparation of new families of surface-active agents over the last several decades.[2, 4-8] Surfactant-templated synthesis of mesoporous inorganic materials is a good example of how the efforts aimed at surfactant development and characterization have guided the progress in conception, design and synthesis of advanced materials with tunable porous architecture, particle size and morphology.[9-11] The present paper is primarily concerned with a special case of the synthesis of nanostructured silica phases using soft templating approaches. Together with the structure of silylated precursors, the use of tailor made surfactants can be an important parameter to access structured materials. In this context, long-chain substituted guanidinium halides were recently considered as a promising alternative to alkyltrimethylammonium bromides in the preparation of silica hybrid materials displaying a regular architecture on a mesoscopic scale length [12]. The guanidinium group is the basis of a rich supramolecular chemistry due to its ability to interact with various substances via ionic bonds and hydrogen bonding. In combination with sulfonate, carboxylate or phosphonate groups, it can produce a large variety of hydrogen-bonded supramolecular structures.[13-15] Moreover, it facilitates surface etching of MOF crystals of the HKUST-1 type.[16] Guanidinium salts are also strong denaturating agents for proteins, and the denaturation mechanism is due to the action of hydrogen bonding.[17, 18] Therefore, in order to get a deeper understanding of the observed differences in the templating mechanism, a detailed study of the self-aggregation behavior of guanidinium salts against that of alkyltrimethylammonium homologues seems indispensable.

The self-assembly and surface-activity of long-chain guanidinium surfactants have rarely been studied in the literature.[7, 19] Miyake *et al.* reported an intensive study on the self-assembling characteristics of dodecylguanidine hydrochloride based on the experimental results on the phase diagram, area occupied per surfactant unit at the aqueous solution-air interface, micellar aggregation number, as well as thermodynamic functions of micelle formation.[7] It was argued

that the increased assembly formability, compared to the dodecyltrimethylammonium (DTAC) homologue, was caused mostly by hydrogen bonding among guanidinium groups via water molecules, thereby overcoming the repulsive force between the cationic charges. The guanidinium head-groups were postulated to be closely packed both at the solution–air and micelle–solution interface in the absence of added background electrolyte, and the addition of even a small amount of NaCl was responsible for the observed shape change of the micelle growing to form the string-like structure. The micellization was demonstrated to be an exothermic and entropy-driven phenomenon. The Krafft temperature of the surfactant was determined to be about 293 K, much higher than that of DTAC. Song *et al.* carried out the surface tension and conductivity measurements at 298 K for two series of guanidinium-type surfactants, mono-alkylguanidinium and *N*,*N*,*N*′-dimethylalkylguanidinium chlorides containing 8, 10 and 12 carbon atoms in the alkyl chain. These cationic surfactants showed antimicrobial activity, and their efficiency as antimicrobial agents increased as the length of the hydrophobic tail was increased. The *N*,*N*,*N*′-dimethylalkylguanidinium surfactants reduced the surface tension of water to about 30–33 $mN \cdot m^{-1}$, whereas the minimum surface tensions ranging between 23 and 25 $mN \cdot m^{-1}$ were observed with the mono-alkylguanidinium counterparts. The values of the critical micelle concentration, CMC, and chloride counter-ion binding to the micelle, β, were found to be chain-length dependent, in accordance with the general trends documented for numerous ionic surfactants.[2] In the above-mentioned two papers,[7, 19] a very small degree of micelle dissociation was deduced from the β values being close to unity.

The aim of the present paper is to report the results of a systematic study of surface activity and self-assembling behavior for a series of mono-alkylguanidinium chlorides containing 10, 12, 14 and 16 carbon atoms in the alkyl chain. The main characteristics were inferred from the appropriate conductivity, surface tension and calorimetry measurements. The possible increase in the Krafft temperature ($T_K$) above room temperature upon increasing the alkyl chain length was corroborated by the determination of the $T_K$ values for the four cationic surfactants studied here. Since only isothermal titration calorimetry guaranteed a leak-proof and temperature-controlled measuring system, this was the principal technique used to investigate the effect of the alkyl chain length, temperature and salt addition on the micelle formation. It is a commonly accepted premise[2, 3] that the behavior of ionic surfactants in aqueous solutions and at interfaces is an intricate outcome of various kinds of interactions involving surfactant hydrophobic tails, ionized

head-groups, and counter-ions, as well as water molecules able to form hydrogen bonds among themselves and with other dissolved species. In this context, direct calorimetry studies of such interactions may provide greater insight into the mechanism of surfactant-assisted synthesis of porous materials via soft templating approaches, in which cationic surfactants are suitable structure directing agents.

In comparison with the paper by Miyake *et al.*, the $C_{10}$, $C_{14}$ and $C_{16}$-members of the guanidinium series were additionally characterized based on the research strategy adopted here. To complete the work by Song *et al.*, more information was provided on the self-assembly behavior of $C_{10}$ and $C_{12}$-guanidinium chlorides, representing the common part of the two studies. Therefore,a more specific goal here was to focus on the micellization performance of such long-chain guanidinium-type cationic surfactants, based on which their adequacy and relevance as potential structure-directing agents in preparation of nanostructured silica materials can be judged.

## 2.2 Results and Discussion

Several methods have been reported in the literature for the synthesis of guanidinium salts,[20] including desulfurization-addition sequences, the addition of amines to electrophiles such as carbodiimides, cyanamides or chloramidinium salts,[21, 22] and the utilization of guanylation reagents.[23] The synthesis route employed here made use of 1*H*-Pyrazol-1-carboxamidine hydrochloride as guanylating reagent.[24] This method allowed a nearly quantitative transformation of the starting material to the desired product under mild reaction conditions and afforded guanidinium salts in high purities and high yields.[25]

The phase transition temperatures of the resulting guanidinium chlorides, as inferred from appropriate DSC measurements, are given in Table 1. It is necessary to emphasize that the DSC thermograms (not shown here) indicate the crystalline character of the guanidinium compounds; DGC directly forms an isotropic melt, whereas DDGC, TDGC and CGC exist in the form of liquid-crystalline mesophases. The phase transition temperatures have been taken from the first heating and cooling cycle, as the salts did not crystallize once molten. It can be seen that increasing the length of the alkyl tail results in a significant increase in the phase transition temperature.

**Table 1.** Phases transition temperatures and enthalpies, as taken from the first heating and cooling cycle.

| Compound | *T* (°C) Cr→LC<br>Δ*H* (kJ·mol$^{-1}$) | *T* (°C) LC→I<br>Δ*H* (kJ·mol$^{-1}$) |
|---|---|---|
| DCG | Heating: 54.1 °C; −28.3 kJ·mol$^{-1}$ | – |
| DDGC | Heating: 65.2 °C; −34.7 kJ·mol$^{-1}$ | Heating: 113.5 °C; −0.78 kJ·mol$^{-1}$<br>Cooling: 112.3 °C; 0.79 kJ·mol$^{-1}$ |
| TDGC | Heating: 72.2 °C; −22.9 kJ·mol$^{-1}$ | Heating: 169.2 °C; −0.37 kJ·mol$^{-1}$<br>Cooling: 160.5 °C; 0.36 kJ·mol$^{-1}$ |
| CGC | Heating: 76.8 °C; −38.2 kJ·mol$^{-1}$ | Heating: 189.9 °C; −0.62 kJ·mol$^{-1}$<br>Cooling: 185.2 °C; 0.47 kJ·mol$^{-1}$ |

The synthesized guanidinium chlorides are capable of forming birefringent phases in water, as can be seen in Figure 1. This behavior, although only evaluated qualitatively, indicates that guanidinium halides form anisotropic lyotropic phases. Additionally, the thermotropic behavior of these compounds was studied using differential scanning calorimetry. The formation of thermotropic mesophases is indicated by the C→LC and LC→I phase transitions of DDGC, TDGC and CGC (see Table 1). In this context, DGC has a particular position, since, although forming lyotropic solutions in aqueous medium, it does not form thermotropic phases, as shown by the absence of LC→I phase transition in its DSC thermogram.

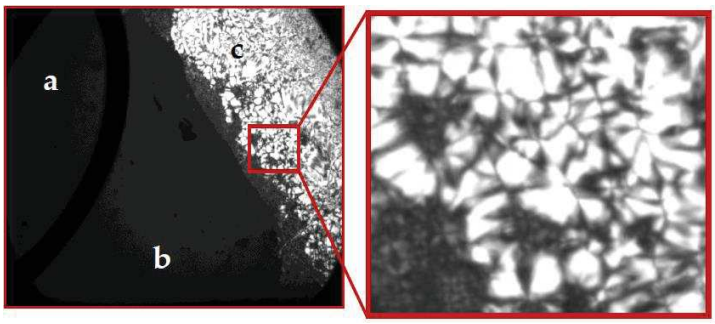


**Figure 1. Polarizing micrographs of DGC at 2.5× original magnification**: (a) air phase; (b) isotropic phase; (c) anisotropic phase.

### 2.2.1 Krafft Temperature, Critical Micelle Concentration, and Micelle Dissociation

Figure 2 illustrates the variations of the specific conductance of micellar aqueous solutions as a function of the temperature for the guanidinium surfactants studied in the present paper. With the sole exception of DGC, these plots exhibit a break, which indicates a noticeable change in the surfactant solubility and may be used to determine the Krafft temperature, $T_K$.[26, 27] The following values have been inferred from the temperature dependency of the specific conductance: 292 ± 1 K (19 ± 1 °C), DDGC; 304 ± 1 K (31 ± 1 °C), TDGC; 314 ± 1 K (41 ± 1 °C), CGC. For DDGC, the Krafft temperature is, within the margin of error, in a good agreement with the value reported by Miyake *et al.*[7]

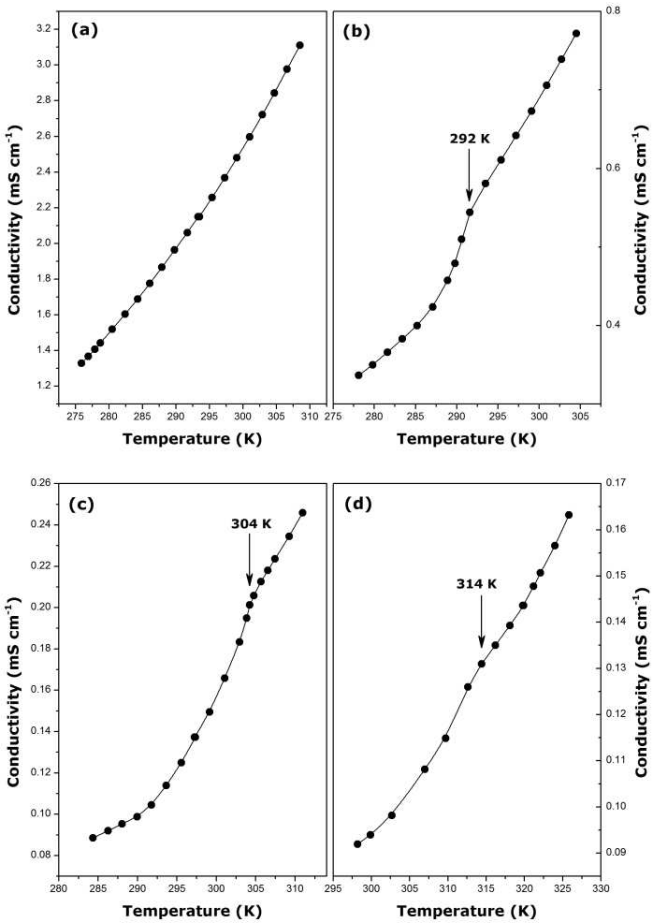


**Figure 2. Plots of the specific conductance against temperature for micellar aqueous solutions of guanidinium cationic surfactants**: (a) DGC ($m$ = 31.72 mmol·kg$^{-1}$); (b) DDGC ($m$ = 8.01 mmol·kg$^{-1}$); (c) TDGC ($m$ = 2.55 mmol·kg$^{-1}$); and (d) CGC ($m$ = 0.7 mmol·kg$^{-1}$).

Since no such break has been observed in Figure 2a, the Krafft temperature of DGC should be lower than 276 K (3 °C), *i.e.* the lowest temperature to be obtained in the measuring system used. As for classical ionic surfactants,[2] the Krafft temperature increases with the increase of the length of the alkyl chain. Compared to their alkyltrimethylammonium bromide or chloride homologues, the guanidinium type cationics appear to have much higher $T_K$ values (e.g., $T_K$ = 293 K, CTAB; $T_K$ = 284 K, CTAC[28]). This also means that aqueous solutions of alkylguanidinium surfactants are more difficult to handle, especially in the case of CGC, where solvent evaporation may pose a serious problem.

In the next series of experiments, surface tension of surfactant solutions was determined at a constant temperature higher than the corresponding $T_K$ value. The results are presented in Figure 3. The appearance of a shallow minimum close to the CMC, especially for DGC, might be interpreted as being the result of some surface-active impurities in the solutions, although the uncertainty of the surface tension measurements should not be forgotten here. Note that the high purity of the surfactant samples was confirmed by the NMR and FT-IR studies.

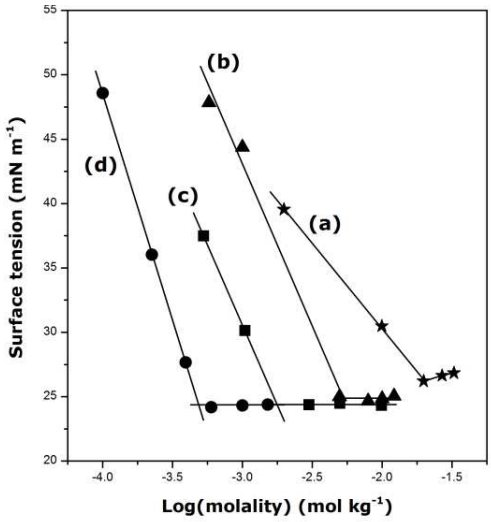


**Figure 3. Plots of the surface tension against logarithm of the bulk molality for aqueous solutions of guanidinium cationic surfactants**: (a) DGC at 298 K; (b) DDGC at 298 K; (c) TDGC at 306 K; and (d) CGC at 317 K.

When analyzing Figure 3, the emphasis should be placed on the evaluation of the surfactant efficiency in lowering the surface tension of water. For example, DDGC decreases the surface tension down to about 24 ± 2 mN·m$^{-1}$ above the CMC at 298 K, whereas dodecyltrimetylammonium chloride (DTAC) shows much lower efficiency (*i.e.*, 42 mN·m$^{-1}$ at

298 K[29]). This result is in agreement with those reported by other authors.[7, 19] The propensity of guanidinium head-group to form hydrogen bonds may be considered to account for this reinforced surface activity of guanidinium cationics compared with their alkyltrimethylammonium homologues. The collective action of intermolecular hydrogen bonds makes water a highly structured liquid even at room temperature.[3] When the surfactant units are adsorbed at the water-air interface in an oriented fashion, new hydrogen bonds between water molecules and guanidinium head-groups may form easily, thereby preventing water molecules from binding as tightly to one another and thus lowering the tension of the surface. In the case of TDGC and CGC, the temperature dependence of the surface tension should be additionally taken into account, since water loses some of its peculiar structure properties at higher temperatures.[30] From plots of the surface tension *versus* the logarithm of a solution molality, it is also possible to evaluate the critical micelle concentration (CMC) or the area ($A_{min}$) per adsorbed surfactant unit at the solution–air interface based on the Gibbs equation.[2] The following values have been obtained in the present work: CMC = 21 mmol·kg$^{-1}$ and $A_{min}$ = 1.4 nm$^2$, DGC; CMC = 5.3 mmol·kg$^{-1}$ and $A_{min}$ = 0.8 nm$^2$, DDGC; CMC = 1.8 mmol·kg$^{-1}$ and $A_{min}$ = 0.8 nm$^2$, TDGC; CMC = 0.5 mmol·kg$^{-1}$ and $A_{min}$ = 0.6 nm$^2$, CGC. In comparison with alkyltrimethylammonium chlorides containing the same alkyl chains and studied at the same temperature (*i.e.*, $C_{10}$ and $C_{12}$),[31] the guanidinium-type surfactants self-assemble at relatively lower CMC values. On the other hand, the alkylguanidinium cations occupy more surface area per molecule at the solution-air interface. Different shapes of the polar head-groups should be taken into account in rationalizing this last observation. Indeed, the ammonium group can be described as a nearly spherical bowl, thus leading to a $C_{3v}$ symmetry of the long-chain-substituted ammonium surfactants.[32] On the contrary, the guanidinium group has a planar shape with a $C_{3h}$ symmetry.[33] The present results show that the lengthening of the alkyl chain by two methylene groups causes a steady decrease in the $A_{min}$ value, which thereby points out the increasingly enhanced adhesion of alkylguanidinium units within the adsorbed monolayer. This trend is at variance with the very high compactness of the surfactant monolayer already postulated by Miyake *et al.* for DDGC based on the $A_{min}$ value of 0.37 nm$^2$.[7] Even though the small number of points in the molality region close to the break points in Figure 3 makes the resulting CMC and $A_{min}$ values less precise here, there are no strong indications for unusually close packing of alkylguanidinium cations at the solution–air interface.

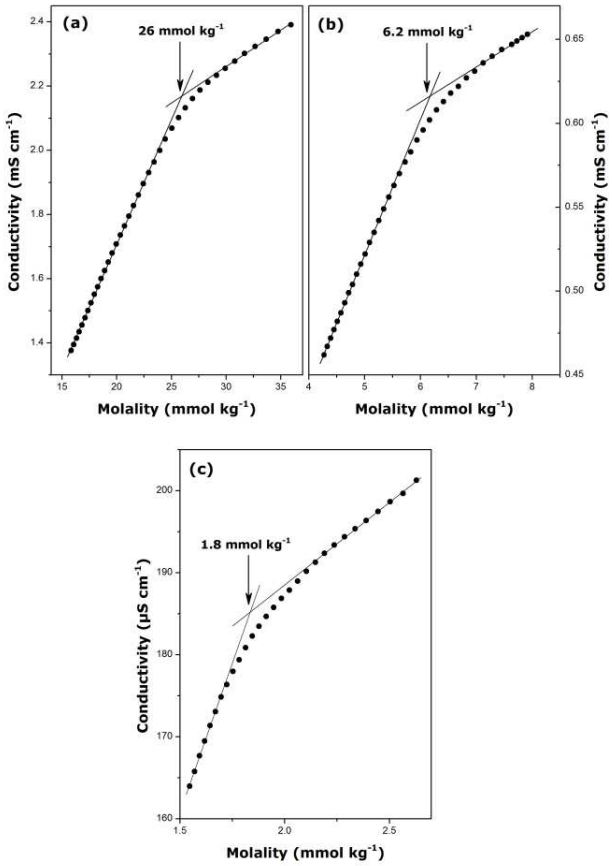


**Figure 4. Plots of the specific conductance against bulk concentration for aqueous solutions of guanidinium cationic surfactants**: (a) DGC at 298 K; (b) DDGC at 298 K; and (c) TDGC at 306 K.

More reliable values of micellization parameters for guanidinium surfactants have been inferred from the measurements of the specific conductance of aqueous solutions. For comparative purposes, the conductivity measurements were carried above the Krafft temperature: at 298 K, DGC and DDGC, and at 306 for TDGC. Taking into account the high Krafft temperature of the $C_{16}$-homologue and given the difficulty in carrying out precise experiments at too high temperatures, further estimation of the main micellization parameters was restricted only to the first three members of the surfactant series. The conductivity *vs.* concentration plots are given in Figure 4 and the resulting values of CMC and counter-ion binding, β, to the micelle have been collected in Table 2.

**Table 2.** Critical micelle concentration, CMC, and degree of counter-ion binding to the micelle, β, for guanidinium cationic surfactants.

| Surfactant | Temperature (K) | CMC (mmol·kg$^{-1}$) | β | $\Delta_{mic}G°$ (kJ·mol$^{-1}$) |
|---|---|---|---|---|
| DGC | 298 | 26 ± 1 | 0.71 ± 0.01 | −22.3 ± 0.6 |
| DDGC | 298 | 6.2 ± 0.3 | 0.74 ± 0.01 | −28.3 ± 0.9 |
| TDGC | 306 | 1.8 ± 0.1 | 0.72 ± 0.01 | −33.6 ± 0.9 |

It should be noted here that the changes in the solution conductivity above the CMC observed in Figures 2 and 4 are not very abrupt, which likely indicates that some partial $Cl^-$ dissociation renders the micelles less effective charge carriers than the monomers. Of course, this hypothesis argues against the full counter-ion binding to the guanidinium micelles, at variance with the β values close to unity as reported previously.[7, 19] The existence of globular micelles at smaller surfactant concentrations (still above the CMC), as revealed by the polarizing micrographs in Figure 1, additionally corroborates the conclusion with respect to the β parameters drawn in the present work. The comparison between alkylguanidinium cationics and their alkyltrimethylammonium homologues[7, 34-36] indicates that the former form less ionized micelles. Miyake *et al.* have explained this increased counter-ion binding by a much closer packing of the DDGC units in micelles under the action of hydrogen bonds, thereby making the surface charge density higher than that of DTAC.[7]

The generally used rule for ionic surfactants[2] that the CMC is divided by 4 on the addition of two methylene groups still holds approximately in this case. On the contrary, the β parameter seems to be much less sensitive to the alkyl chain length and temperature.[34, 35]

With the estimates of the two parameters, it was possible to determine the standard Gibbs free energy of micellization ($\Delta_{mic}G°$) of the surfactant under given conditions, using the following expression:[2, 37]

$$\Delta_{mic}G° = RT\,(1 + \beta)\,\ln X_{CMC} \qquad (1)$$

where $X_{CMC}$ is the mole fraction of the surfactant in the aqueous solution at the CMC. In this formulation, $\Delta_{mic}G°$ represents the Gibbs free energy of transfer of 1 mole of the surfactant solute from the aqueous phase to the micellar pseudo-phase. The resulting $\Delta_{mic}G°$ values have been added to Table 2. As for all types of single-chain surfactants, the micellization of guanidinium cationics is a spontaneous phenomenon that is accompanied by a decrease in the Gibbs free

energy. The $\Delta_{mic}G°$ change involved in the transfer of a methylene unit of the hydrophobic group from an aqueous environment to the interior of the micelle at 298 K can be calculated from the two values obtained for DGC and DDGC. An increase in the length of the hydrophobic group makes $\Delta_{mic}G°$ more negative by about 3.0 kJ per methylene group, which corresponds well to values usually reported for conventional surfactants.[2, 37, 38]

### 2.2.2 Thermal Effects of Micelle Formation in Various Aqueous Media

Isothermal titration calorimetry (ITC) can provide useful information about the outcome of molecular interactions involved in the micellization phenomenon.[39, 40] Given the high $T_K$ temperatures of alkylguanidinium surfactants, the ITC equipment offers a better possibility of controlling the loss of water due to evaporation. An example of thermograms recorded during dilution calorimetry measurements is given in Figure 5a. The integration of peaks appearing in this thermogram leads to the determination of the total enthalpy changes during successive injections, $\Delta_{inj}H_i$ [39,40]. The resulting thermal effects may be summed up to obtain the cumulative enthalpy of dilution per mole of the surfactant, $\Delta_{dil}H_{cum}$, which can be expressed in the following manner:[39, 40]

$$\Delta_{dil}H_{cum} = \sum_{k=1}^{i} \frac{\Delta_{inj}H_k}{n_2^{inj}} = i \cdot \left[ \Phi_H\left(m_2^i\right) - \Phi_H\left(m_2^0\right) \right] \qquad (2)$$

where $i$ is the number of successive injections, $n_2^{inj}$ is the number of moles of the surfactant solute (say component 2) injected into the calorimetric ampoule during each injection; $\Phi_H(m_2)$ represents the apparent molal enthalpy of the surfactant corresponding to a given molality $m_2$, $m_2^0$ is the molality of the stock solution. Taking into account the relationship between the apparent molal enthalpy, $\Phi_H(m_2)$, and the partial molal enthalpy, $\overline{h_2}(m_2)$, linear dependence of $\Delta_{dil}H_{cum}$ against surfactant molality in Figure 5b indicates that $\overline{h_2}$ is a constant function of the molality in the pre-micellar and post-micellar regions.[39] Therefore, the intersection of the two linear portions provides estimate of the CMC for the surfactant in a given environment. In addition, the plot of $\Delta_{dil}H_{cum}$ as a function of the injection number in Figure 5c is also represented as two straight lines intersecting at the CMC. In accordance with Equation (2), the standard enthalpy of micelle formation per mole of surfactant, $\Delta_{mic}H°$, is determined easily from the difference between the slopes of the two linear regression segments.[39]

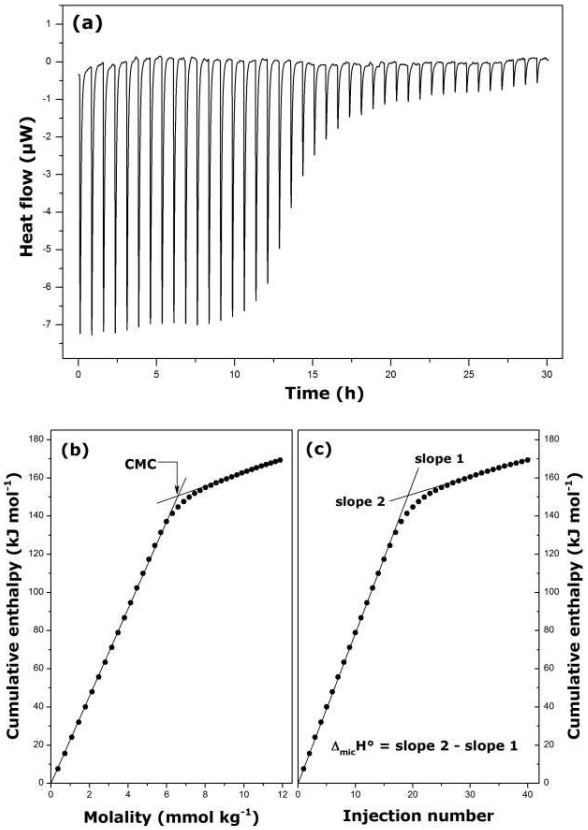


**Figure 5. Results of calorimetry measurements of the cumulative enthalpy of dilution obtained by injecting a 60 mmol·kg$^{-1}$ aqueous solution of DDGC into deionized water at 298 K**: (a) records of 40 successive injections of 5 µL aliquots into a 1 mL glass ampoule containing initially 800 µL of deionized water (the equilibration time between 2 injections was set at 45 min); (b) cumulative enthalpy of dilution as a function of the equilibrium surfactant molality; (c) cumulative enthalpy of dilution as a function of the injection number.

Figure 6 shows that the linearity of the $\Delta_{dil}H_{cum}$ *vs.* injection number plots is preserved for DGC and DDGC in presence of the background NaCl electrolyte. Similar curves were obtained for all alkylguanidinium and alkyltrimethylammonium surfactants studied here. The values of CMC and $\Delta_{mic}H°$ were inferred accordingly from such data. These parameters have been collected in Table 3.

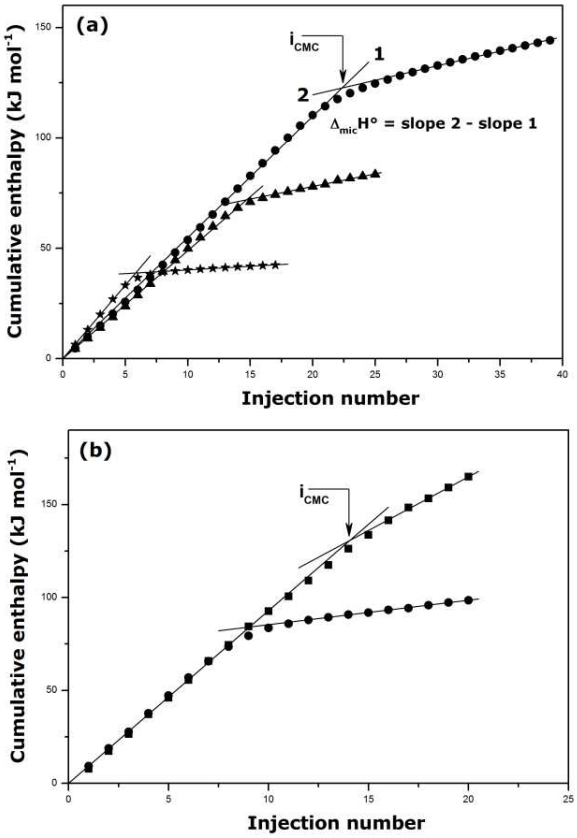


**Figure 6. Effect of NaCl addition on the cumulative enthalpy of dilution per mole of** DGC (a) and DDGC (b) determined by Isothermal Titration Calorimetry at 298 K: single-solute solution (circles), 0.001 NaCl solution (triangles), 0.01 NaCl solution (squares), 0.1 NaCl solution (stars). The enthalpy of dilution has been plotted as a function of the injection number to illustrate the direct calculation of the enthalpy of surfactant micellization.

The discrepancies between the corresponding CMC values obtained in conductimetry and calorimetry experiments are obviously due to the differences in the sensitivity and reliability of the two methods and further data processing (e.g., the sharpness of the break in the concentration dependence of a given physical property[41]).

With the knowledge of such thermodynamic functions as $\Delta_{mic}G°$ (Table 2) and $\Delta_{mic}H°$ (Table 3), it is possible to calculate the standard molar entropy of micellization, $\Delta_{mic}S°$, for DGC, DDGC, and TDGC in single-component solutions. The following values have been obtained: $T{\cdot}\Delta_{mic}S° = 17.8 \pm 0.9$ kJ·mol$^{-1}$, DGC at 298 K; $T{\cdot}\Delta_{mic}S° = 20.5 \pm 2$ kJ·mol$^{-1}$, DDGC at 298 K; $T{\cdot}\Delta_{mic}S° = 16.1 \pm 0.8$ kJ·mol$^{-1}$, TDGC at 306 K. When there is less than 14 carbon atoms in the alkyl chain, the negative values of $\Delta_{mic}G°$ are mainly due to the positive values of $\Delta_{mic}S°$, $\Delta_{mic}H°$, even

negative, being smaller than the value of $T \cdot \Delta_{mic}S°$. As for other types of surfactants, micellization of guanidinium cationics is an entropy-driven process owing to the transfer of the hydrophobic tails from the water environment to the micelle core.[3, 42, 43] Therefore, the downward trends in the CMC with lengthening the alkyl chain, increasing the salt content, and decreasing the temperature, as observed qualitatively for DTAC, TTAC, DGC, and DDGC in Table 3, may be considered as consistent with the reinforcement of the hydrophobic effect in relation with changes in the peculiar solvent structure or in the micelle size and shape. In the case of TDGC, the enthalpy and entropy contributions to $\Delta_{mic}G°$ are almost equal (but still opposite in sign) and the phenomenon also becomes enthalpy-driven. When analyzing the variations of $\Delta_{mic}H°$ in Table 3, it should always be remembered that the thermal effect of micellization is a result of the interplay among various competitive or co-operative interactions; besides the hydrophobic interaction, the outcome of forces operating among the ionized head-groups, counter-ions and water molecules constitutes the most important contribution.

**Table 3.** Critical micelle concentration, CMC, and standard enthalpy of micelle formation per mole of the surfactant, $\Delta_{mic}H°$, for guanidinium cationic surfactants.

| Surfactant | Solvent | Temperature (K) | CMC (mmol·kg$^{-1}$) | $\Delta_{mic}H°$ (kJ·mol$^{-1}$) |
|---|---|---|---|---|
| DTAC | $H_2O$ | 298 | 21.5 ± 0.1 | 5.1 ± 0.2 |
| DTAC | 0.01 M NaCl | 298 | 18.1 ± 0.1 | 4.2 ± 0.1 |
| DTAC | 0.1 M NaCl | 298 | 8.6 ± 0.1 | 3.6 ± 0.1 |
| TTAC | $H_2O$ | 298 | 5.0 ± 0.1 | 2.2 ± 0.2 |
| TTAC | 0.1 M NaCl | 298 | 3.3 ± 0.4 | 1.1 ± 0.2 |
| TTAC | $H_2O$ | 318 | 6.0 ± 0.4 | −8.9 ± 0.2 |
| DGC | $H_2O$ | 298 | 28.4 ± 0.1 | −4.5 ± 0.1 |
| DGC | 0.001 M NaCl | 298 | 25.5 ± 0.6 | −4.2 ± 0.3 |
| DGC | 0.01 M NaCl | 298 | 22.7 ± 0.2 | −4.0 ± 0.1 |
| DGC | 0.1 M NaCl | 298 | 9.6 ± 0.3 | −6.4 ± 0.1 |
| DDGC | $H_2O$ | 298 | 6.2 ± 0.2 | −7.8 ± 0.5 |
| DDGC | 0.001 M NaCl | 298 | 5.7 ± 0.2 | −9.0 ± 0.1 |
| DDGC | 0.01 M NaCl | 298 | 3.5 ± 0.1 | −9.5 ± 0.5 |
| DDGC | $H_2O$ | 306 | 6.6 ± 0.4 | −12.3 ± 0.9 |
| DDGC | $H_2O$ | 310 | 7.3 ± 0.4 | −13.0 ± 0.4 |
| TDGC | $H_2O$ | 306 | 1.5 ± 0.3 | −17.5 ± 0.3 |

By far the most important conclusion drawn from the analysis of Table 3 is that the micellization of alkylguanidinium chlorides is an exothermic phenomenon, irrespective of the experimental conditions used. From this point of view, this micellization behavior is at variance with the endothermic micelle formation observed here for their alkyltrimethylammonium homologues. A more detailed comparison with the thermodynamic parameters reported in the literature for various ionic surfactant indicates that this behavior is rather similar to that exhibited by alkyltrimethylammonium bromides with the same hydrophobic tails, even though the micellization of the guanidinium cationics studied occurs at lower CMC values.[44] The latter conclusion may be easily rationalized since the degrees of counter-ion binding to the micelle are similar in both cases, and $Cl^-$ is known to be more effective than $Br^-$ in salting out the surfactant cation and thus depressing the CMC.[2] In accordance with some previously reported results,[35, 36] a passage from endothermic to exothermic micellization for alkyltrimethylammonium chlorides is favored with increasing the temperature and NaCl addition to the aqueous phase (see the results reported for DTAC and TTAC in Table 3). From the viewpoint of enthalpy, the present alkylguanidinium surfactants thus behave as their alkyltrimethylammonium homologues at higher temperatures and salt contents. This clearly points towards the guanidinium head-group as being responsible for the particularly exothermic character of micellization.

When the DDGC units self-assemble to form micelles in the presence of background electrolyte, only the first addition of NaCl to the aqueous phase makes $\Delta_{mic}H°$ much less negative, and the thermal effect then seems to level off. This likely means that the DDGC micelles are fairly compact already in single-component solutions, but not to the degree proposed by Miyake *et al.*[7] They then attain their optimal shape and size (e.g., maximum aggregation number) at low ionic strengths. For the same tail lengths, the fractions of surfactant units in the micellized state should be thus much greater than those characterizing the cationic micelles of alkyltrimethylammonium chlorides. For DGC in the presence of NaCl content up to 0.01 $mmol \cdot kg^{-1}$, a small decrease in the CMC is paralleled by a near constant value of $\Delta_{mic}H°$. Here, the salt addition to the aqueous phase does not cause much change in the self-aggregation behavior of the guanidinium type surfactants. High NaCl contents (of the order of 0.1 $mmol \cdot kg^{-1}$) render the phenomenon again more exothermic with the concomitant decrease in the CMC. Since the pre-micellar and post-micellar parts of the $\Delta_{dil}H_{cum}$ *vs.* injection number plots preserve their linear character (see Figure

6-a), it may be argued that the DGC micelles formed at high ionic strengths have a different shape from what is observed in single-solute solutions or at lower NaCl contents.

A stronger counter-ion binding in the Stern layer and hydrogen bonding with water molecules are also to be taken into account. Stronger interactions in the polar mantle of the micelle likely account for the enthalpy gain when the cationic head-groups are transferred from the aqueous environment to the micelle mantle. The increased magnitude of the exothermic micellization for longer hydrophobic tails may still be explained on the same basis when postulating the concomitant increase in the micelle aggregation number.

## 2.3 Conclusions

With their Griffin's hydrophilic-lipophilic balance (HLB) ranging between 4 and 6, straight-chain guanidinium cationics DGC, DDGC, TDGC, CGC are less soluble in water and more surface-active than alkyltrimethylammonium bromides or chlorides having the same hydrophobic tails. These conclusions are corroborated by the following trends inferred from the experimental studies undertaken within the framework of the present work:

- For DDGC, TDGC, CGC, the Krafft temperature ranges between 292 and 314 K, and it increases strongly with the addition of methylene units to the surfactant hydrophobic tail.
- The presence of DDGC, TDGC, and CGC units in the aqueous solution decreases its surface tension down to about 24 $mN \cdot m^{-1}$ above the CMC, irrespective of the surfactant structure and temperature.
- The binding of chloride counter-ions to the micelle is about 70%, similar to that in the micelles of alkyltrimethylammonium bromides and much greater than in the case of alkyltrimethylammonium chlorides; it appears hardly dependent on the tail length and temperature.
- Micellization of guanidinium cationics, especially those with long alkyl chains, may be described as both entropy and enthalpy-driven; the critical micelle concentration, CMC, decreases and the standard enthalpy of micellization per mole of surfactant, $\Delta_{mic}H°$, becomes more negative (the process is more exothermic) upon lengthening the hydrocarbon tail.
- The addition of the background NaCl electrolyte to the aqueous phase causes a steady decrease in the CMC and renders the micellization process more exothermic; depending on the tail length, the alkylguanidinium micelles may attain their optimum shape and size at a given NaCl content, and further salt addition may result in the formation of micelles likely differing in shape and size.

Compared to alkyltrimethylammonium chlorides, the increased surface activity of alkylguanidinium surfactants, and the fact that micelle formation is much more exothermic and occurs at much lower CMC values, may be ascribed to the hydrogen-binding capacity of the guanidinium head-group, which promotes the formation of more compact micelles together with a stronger $Cl^-$ binding in the corresponding Stern layer.

**References**


1. Ramanathan, M.; Shrestha, L.K.; Mori, T.; Ji, Q.; Hill, J.P.; Ariga, K. Amphiphile nanoarchitectonics: From basic physical chemistry to advanced applications. *Phys. Chem. Chem. Phys.* **2013**, *15*, 10580-10611.
2. Rosen, M.J. *Surfactants and interfacial phenomena, third edition*. John Wiley & Sons: New York, 2004.
3. Tanford, C. *The hydrophobic effect: Formation of micelles and biological membranes*. Wiley-Interscience: New York, 1973.
4. Robb, I.D. *Specialist surfactants*. Blackie Academic and Professional: London, 1997.
5. Zhang, G.; Han, F.; Zhang, G. New family of trisiloxane surfactants. *Tenside Surfact. Det.* **2006**, *43*, 146-150.
6. He, J.; Wang, X.; Morill, M.; Shamsi, S.A. Amino acid bound surfactants: A new synthetic family of polymeric monoliths opening up possibilities for chiral separations in capillary electrochromatography. *Anal. Chem.* **2012**, *84*, 5236-5242.
7. Miyake, M.; Yamada, K.; Oyama, N. Self-assembling of guanidine-type surfactant. *Langmuir* **2008**, *24*, 8527-8532.
8. Mingarro, I.; Lukovic, D.; Vilar, M.; Perez-Gil, J. Synthetic pulmonary surfactant preparations: New developments and future trends. *Curr. Med. Chem.* **2008**, *15*, 393-403.
9. Wu, S.-H.; Mou, C.-Y.; Lin, H.-P. Synthesis of mesoporous silica nanoparticles. *Chem. Soc. Rev.* **2013**, *42*, 3862-3875.
10. Soler-Illia, G.J.D.; Sanchez, C.; Lebeau, B.; Patarin, J. Chemical strategies to design textured materials: From microporous and mesoporous oxides to nanonetworks and hierarchical structures. *Chem. Rev.* **2002**, *102*, 4093-4138.
11. Alothman, Z.A. A review: Fundamental aspects of silicate mesoporous materials. *Materials 5*, 2874-2902.
12. El Hankari, S.; Hesemann, P. Guanidinium vs. Ammonium surfactants in soft-templating approaches: Nanostructured silica and zwitterionic-silica from complementary precursor–surfactant ion pairs. *Eur. J. Inorg. Chem.* **2012**, 5288-5298.
13. Russell, V.A.; Ward, M.D. Molecular crystals with dimensionally controlled hydrogen-bonded nanostructures. *Chem. Mater.* **1996**, *8*, 1654-1666.

14. Ward, M.D. Directing the assembly of molecular crystals. *Mrs Bulletin* **2005**, *30*, 705-712.

15. Ward, M.D. Design of crystalline molecular networks with charge-assisted hydrogen bonds. *Chem. Commun.* **2005**, 5838-5842.

16. El-Hankari, S.; Huo, J.; Ahmed, A.; Zhang, H.; Bradshaw, D. Surface etching of hkust-1 promoted via supramolecular interactions for chromatography. *J. Mater. Chem. A* **2014**, *2*, 13479-13485.

17. Makhatadze, G.I.; Privalov, P.L. Protein interactions with urea and guanidinium chloride - a calorimetric study. *J. Mol. Biol.* **1992**, *226*, 491-505.

18. Arakawa, T.; Timasheff, S.N. Protein stabilization and destabilization by guanidinium salts. *Biochemistry* **1984**, *23*, 5924-5929.

19. Song, Y.; Li, Q.; Li, Y. Self-aggregation and antimicrobial activity of alkylguanidium salts. *Colloids Surf., A* **2012**, *393*, 11-16.

20. Katritzky, A.R.; Rogovoy, B.V. Recent developments in guanylating agents. *Arkivoc* **2005**, 49-87.

21. Isobe, T.; Iskikawa, T. 2-chloro-1,3-dimethylimidazolinium chloride. 1. A powerful dehydrating equivalent to dcc. *J. Org. Chem.* **1999**, *64*, 6984-6988.

22. El Kadib, A.; Hesemann, P.; Molvinger, K.; Brandner, J.; Biolley, C.; Gaveau, P.; Moreau, J.J.E.; Brunel, D. Hybrid materials and periodic mesoporous organosilicas containing covalently bonded organic anion and cation featuring mcm-41 and sba-15 structure. *J. Am. Chem. Soc.* **2009**, *131*, 2882-2892.

23. Dräger, G.; Solodenko, W.; Messinger, J.; Schön, U.; Kirschning, A. A new reagent and its polymer-supported variant for the amidination of amines. *Tetrahedron Lett.* **2002**, *43*, 1401-1403.

24. Scott, F.L.; Odonovan, D.G.; Reilly, J. Studies in the pyrazole series .3. Substituted guanidines. *J. Am. Chem. Soc.* **1953**, *75*, 4053-4054.

25. Sasaki, D.Y.; Alam, T.M. Solid-state p-31 nmr study of phosphonate binding sites in guanidine-functionalized, molecular imprinted silica xerogels. *Chem. Mater.* **2000**, *12*, 1400-1407.

26. Bales, B.L.; Benrraou, M.; Zana, R. Krafft temperature and micelle ionization of aqueous solutions of cesium dodecyl sulfate. *J. Phys. Chem. B* **2002**, *106*, 9033-9035.

27. Manojlović, J.Ž. The krafft temperature of surfactant solutions. *Thermal Science* **2012**, *16*, S631-S640.

28. Di Michele, A.; Brinchi, L.; Di Profio, P.; Germani, R.; Savelli, G.; Onori, G. Effect of headgroup size, temperature and counterion specificity on cationic micelles. *J. Colloid Interf. Sci.* **2011**, *358*, 160-166.

29. Ikeda, N.; Sanefuji, N.; Lu, K.K.; Aratono, M.; Motomura, K. Surface adsorption and micelle formation of the mixture of n-methylated dodecylammonium chloride and ammonium chloride. *J. Colloid Interf. Sci.* **1994**, *164*, 439-443.

30. Kavanau, J.L. *Water and solute-water interactions*. Holden-Day: San Francisco, 1964.

31. Rosen, M.J.; Li, F.; Morrall, S.W.; Versteeg, D.J. The relationship between the interfacial properties of surfactants and their toxicity to aquatic organisms. *Env. Sci. Technol.* **2001**, *35*, 954-959.

32. Oxton, I.A.; Knop, O.; Falk, M. Determination of the symmetry of the ammonium ion in crystals from the infrared spectra of the isotopically dilute ammonium-d1(1+) species. *J. Phys. Chem.* **1976**, *80*, 1212-1217.

33. Angell, C.L.; Sheppard, N.; Yamaguchi, A.; Shimanouchi, T.; Miyazawa, T.; Mizushima, S. The infra-red spectrum, structure, and normal vibrations of the guanidinium ion. *Trans. Faraday Soc.* **1957**, *53*, 589-600.

34. Ikeda, S. Stability of spherical and rod-like micelles of ionic surfactants, in relation to their counterion binding and modes of hydration. *Colloid Polym. Sci* **1991**, *269*, 49-61.

35. Sarač, B.; Bešter-Rogač, M. Temperature and salt-induced micellization of dodecyltrimethylammonium chloride in aqueous solution: A thermodynamic study. *J. Colloid Interf. Sci.* **2009**, *338*, 216-221.

36. Kroflič, A.; Sarač, B.; Bešter-Rogač, M. Influence of the alkyl chain length, temperature, and added salt on the thermodynamics of micellization: Alkyltrimethylammonium chlorides in nacl aqueous solutions. *J. Chem. Thermodyn.* **2011**, *43*, 1557-1563.

37. Zana, R. Critical micellization concentration of surfactants in aqueous solution and free energy of micellization. *Langmuir* **1996**, *12*, 1208-1211.

38. Zajac, J.; Chorro, C.; Lindheimer, M.; Partyka, S. Thermodynamics of micellization and adsorption of zwitterionic surfactants in aqueous media. *Langmuir* **1997**, *13*, 1486-1495.

39. Chaghi, R.; de Ménorval, L.-C.; Charnay, C.; Derrien, G.; Zajac, J. Interactions of phenol with cationic micelles of hexadecyltrimethylammonium bromide studied by titration calorimetry, conductimetry, and h-1 nmr in the range of low additive and surfactant concentrations. *J. Colloid Interf. Sci.* **2008**, *326*, 227-234.
40. Chaghi, R.; de Ménorval, L.-C.; Charnay, C.; Derrien, G.; Zajac, J. Competitive solubilization of phenol by cationic surfactant micelles in the range of low additive and surfactant concentrations. *Langmuir* **2009**, *25*, 4868-4874.
41. Mysels, K.J.; Mujerjee, P. Reporting experimental data dealing with critical micelle concentrations (cmcs) of aqueous surfactant systems. *Pure Appl. Chem.* **1979**, *51*, 1083-1089.
42. Aranow, R.H.; Witten, L. The environmental influence on the behavior of long chain molecules. *J. Phys. Chem.* **1960**, *64*, 1643-1648.
43. Aranow, R.H.; Witten, L. Additional comments on thermodynamics of environmental changes of methylene group. *J. Chem. Phys.* **1965**, *43*, 1436-1437.
44. Zajac, J. Calorimetry at the solid-liquid interface. In *Calorimetry and thermal methods in catalysis*, Auroux, A., Ed. Springer-Verlag: Berlin-Heidelberg, 2013; pp 197-270.

# Part II

## Alkylguanidinium Based Ionic Liquids in a Screening Study for the Removal of Anionic Pollutants from Aqueous Solution

## Summary

# 1 Introduction

Ionic liquids are unique solvents which consist entirely of ions.[1] Due to their unique properties such as high chemical and thermal stability, inflammability, low vapor pressure and high ionic conductivity, ionic liquids found numerous applications as solvents for organic synthesis and catalysis, in electrochemistry, as electrolyte batteries, fuel cells, and as media for polymerization processes. Due to their unusual self-aggregation properties, ionic liquids are referred as 'supramolecular solvents' which also opened new routes in materials science, in nanoparticle synthesis or as reaction media in ionothermal syntheses.

Imidazolium derivatives are by far the most studied class of ionic liquids. In contrast, ionic liquids based on guanidinium entities are much scarcer, and mostly peralkylated guanidinium ions were reported. [2, 3] Here, we report monoalkyl guanidinium bis-trifluoromethane sulfonimides as a new class of functional ionic liquids. The particularity of these new ionic liquids is based on the cationic guanidinium group which confers specific properties to the ionic liquids. The guanidine/guanidinium substructure exhibits very particular physico-chemical behaviour. It is a relevant functional group widely present in Nature both in proteins *via* the essential amino acid arginine and in a variety of natural products. Guanidine is a strong base (pKa=13.6) and therefore exists in aqueous solution as protonated guanidinium cation. The guanidine/guanidinium couple possesses unique electronic, physico-chemical and steric characteristics such as superbasicity and the ability to undergo π-cation interactions. Its ability to form strong H-bonding interactions together with the planar arrangement with $C_{2h}$ symmetry are useful features in the field of materials' science, for example in view of the formation of molecular materials.[4] Guanidinium salts therefore display big differences compared to conventional imidazolium type ionic liquids. In view of their self aggregation and coordination properties, long-chain substituted guanidinium halides behave differently compared to other cationic surfactants such as ammonium or imidazolium based amphiphiles.[5-7] Guanidinium surfactants have also been used as structure directing agents in template directed hydrolysis-polycondensation reactions of nanostructured ionosilica phases.[8] Finally, guanidinium sulfonimides have been immobilized on nanostructured silica materials *via* sol-gel approaches.[9]

Ionic liquids are intensively studied in separation sciences.[10] As ILs are still rather expensive, special attention has been paid on the limitation of IL quantity in separation processes. For this

reason, liquid-liquid microextraction processes play an increasingly important role.[11] On the other side, removal of anionic dyes from aqueous solutions using imidazolium based ionic liquids has already been studied.[12] It appears that the extraction process is generally driven by hydrophilic/hydrophobic interaction of the dyes with the ionic liquid phase. For this reason, long alkyl chain substituted ionic liquids gave better results compared to their short chain substituted counterparts. In this work, we will show that the extraction processes involving guanidinium based ionic liquids involve a different mechanism and different types of interaction on the molecular level.

The concept of task-specific ionic liquids (TSILs) usually consists of the chemical grafting of functional organic groups on either cation or anion of the ionic liquid.[13] We already used this approach for accessing task-specific ionic liquids as recyclable ligands in asymmetric catalysis[14, 15] and as extractant in liquid-liquid separation.[16]

In this chapter, we report guanidinium based ionic liquids as a new class of task-specific ionic liquids. Due to the versatility and the particular bonding properties of the guanidinium groups, chemical functionality is conferred by the cationic substructure of the ionic liquid itself. For this reason, we can consider that monoalkylguanidinium salts such as hexylguanidinium *bis*-trifluoromethane sulfonimide ($C_6$Gua $NTf_2$, figure 1) are indeed task-specific ionic liquids. We investigated these new compounds in liquid-liquid extraction of anionic pollutants from aqueous solutions. We focused in particular on the sequestration of an organic dye (methyl orange, MO), an anionic drug (diclofenac, DCF, Figure 1) and a metallic anion (chromate). Our work highlights the particular properties of guanidinium based ionic liquids compared to other water immiscible ionic liquids, *i.e.* butyl-methyl-imidazolium *bis*-triflimide ($C_4$mim $NTf_2$).

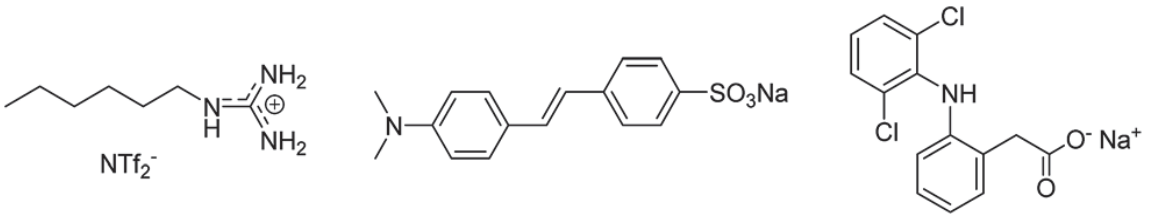


**Figure 1. Structures of hexylguanidinium bis-trifluoromethane sulfonimide ($C_6$Gua $NTf_2$ left), the anionic dye methyl orange (MO middle) and the anionic drug diclofenac (DCF right)**

# 2 Results and discussion

## 2.1 Guandinium ionic liquid: synthesis and characterisation

Firstly we studied the synthesis of a variety of monoalkylated guanidinium based ionic liquids. Primary amines were efficiently converted into alkylguanidinium bis-trifluoromethane sulfonimides in a two-step sequence. In the first step, guanidinium chlorides were synthesized by reacting primary amines with 1H-pyrazole-1-carboxamidine hydrochloride.[8] The resulting guanidinium chlorides were used for anion metathesis reactions with lithium bis-trifluoromethane sulfonimide anions (Figure 2). We synthesized different ionic liquids with variable alkyl chain length: hexyl, octyl and decylguanidinium bis-trifluoromethane sulfonimides $C_xGua\ NTf_2$ (x = 6, 8, 10).

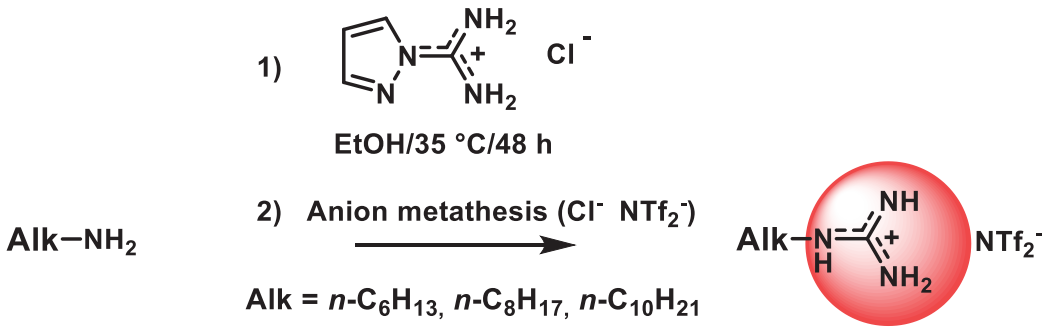


**Figure 2. Synthesis of the guanidinium type ionic liquids**

These new compounds were characterized by $^{1}H$, $^{13}C$ NMR, IR, mass spectroscopy, differential scanning calorimetry (DSC) and thermogravimetric analysis.

$C_6Gua\ NTf_2$: $^{1}H$ NMR (MeOH-$d_4$): δ = 0.96 (3H, m); 1.38 (6H, m); 1.62 (2H, m); 3.19 (2H, 't'). $^{13}C$ NMR (MeOH-$d_4$): δ = 13.35; 22.53; 26.27; 28.71; 31.46; 41.58; 120.13 (q, J = 320Hz); 157.47. FT-IR (neat) $\nu_{max}/cm^{-1}$ 3461, 3372, 3304, 3233, 2960, 2935, 2863, 1658, 1625, 1607, 1343, 1186, 1129, 1050. HRMS [ESI+] calcd. for $C_7H_{18}N_3$ $(M)^+$ 144.1501; found 144.1503.

$C_8Gua\ NTf_2$: $^{1}H$ NMR (MeOH-$d_4$): δ = 0.93 (3H, m); 1.37 (10H, m); 1.58 (2H, m); 3.19 (2H, 't'). $^{13}C$ NMR (MeOH-$d_4$): δ = 13.50; 22.68; 26.61; 28.76; 29.23; 29.26; 31.90; 41.59; 120.12 (q, J = 320Hz); 157.44. FT-IR (neat): $\nu_{max}/cm^{-1}$ 3461, 3373, 3308, 3240, 2929, 2859, 1658, 1626, 1343, 1187, 1130, 1051. HRMS [ESI+] calcd. for $C_9H_{22}N_3$ $(M)^+$ 172.1814; found 172.1815.

$C_{10}$Gua $NTf_2$: $^{1}$H NMR (MeOH-$d_4$): δ = 0.91 (3H, m); 1.32 (14H, m); 1.60 (2H, m); 3.17 (2H, 't'). $^{13}$C NMR (MeOH-$d_4$): δ = 13.03; 22.31; 26.26; 28.45; 28.90; 29.01, 29.23 (2H); 31.63; 41.10; 119.80 (q, J = 320Hz); 157.16. FT-IR (neat): $\nu_{max}/cm^{-1}$ 3461, 3372, 3306, 3233, 2927, 2857, 1658, 1625, 1344, 1189, 1130, 1052. HRMS [ESI+] calcd. for $C_{11}H_{26}N_3$ $(M)^+$ 200.2127; found 200.2128.

All alkylguanidinium bis-trifluoromethane sulfonimides are liquid at room temperature and do not display any noticeable phase transition between -50 and 130°C (Figure 3) and therefore are room-temperature ionic liquids (RTILs).

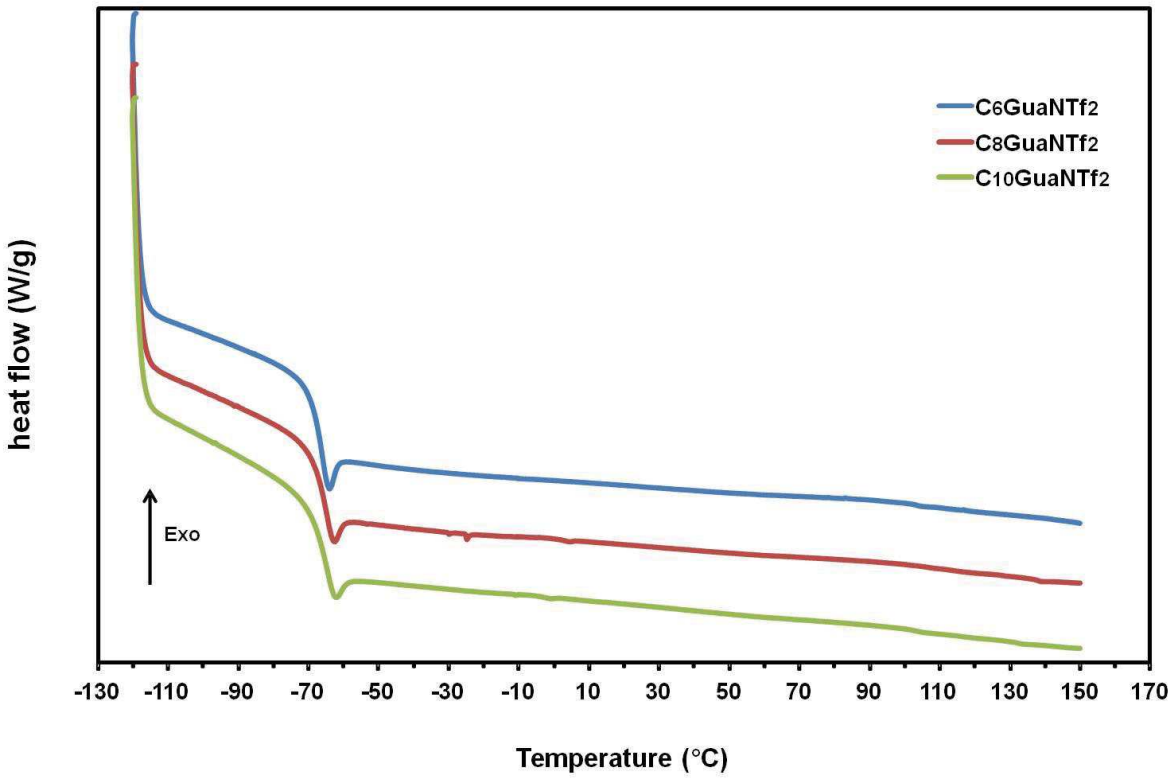


**Figure 3. DSC thermograms guanidinium type ionic liquid**

It has to be mentioned that the guanidinium bis-trifluoromethane sulfonimides are thermally highly stable. Thermogravimetric experiment with $C_6$Gua $NTf_2$ (Figure 4) indicate that degradation starts at ca. 380°C. The thermal stability of this IL therefore is slightly lower than observed for $C_4$mim $NTf_2$.[17]

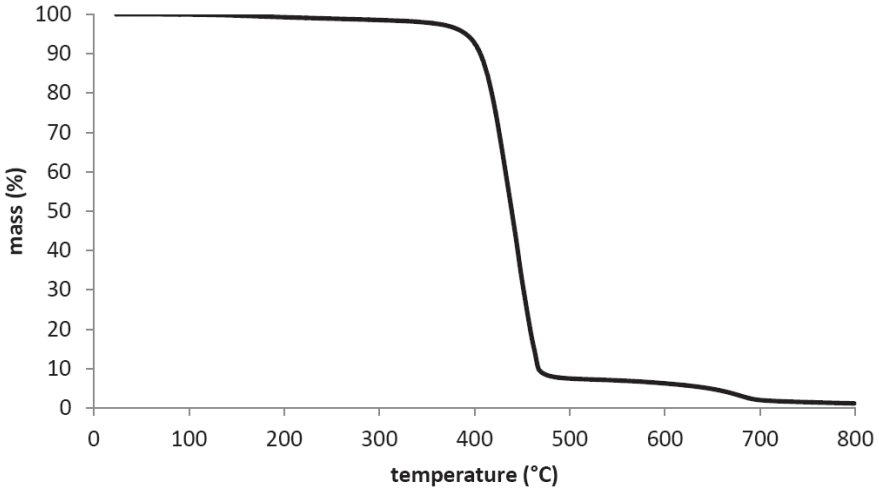


**Figure 4. TGA plot of $C_6$Gua $NTf_2$ (heating rate: 10°C/min, under argon)**

These ionic liquids show a low water content in dried ionic liquid and even in saturated ionic liquid with water, these results are obtained by Karl fisher measurement (Table 1) and show a great similarity with classical ionic liquid (e.g. imidazolium).[17]

**Table 1. Water contnet of dried and water saturated ionic liquid**

| Sample | Water content (dried) | Water content (saturated) |
|---|---|---|
| **$C_6$Gua $NTf_2$** | 300 ppm | 22500 ppm |
| **$C_8$Gua $NTf_2$** | 300 ppm | 21400 ppm |
| **$C_{10}$Gua $NTf_2$** | 500 ppm | 22200 ppm |

The Table 2 regroup the viscosity measurement of guanidinium ionic liquid performed at 25°C and at 5 m.s-1 shear rate. The results show that guanidnium based ILs are moderately viscous compounds with viscosities from 420-480 cP, are although being approx. six times higher than those measured for imidazolium bis-trifluoromethane sulfonimides such as $C_4$mim $NTf_2$, which is typical for a number of other ionic liquids.[17] Similarly to imidazolium type ILs, increasing alkyl

chain length resulted in increasing viscosity of the guanidinium type ILs.[17]

**Table 2. Viscosities of the Guanidinium based ionic liquids**

| Sample | Viscosity (cP) |
|---|---|
| **$C_6$Gua $NTf_2$** | 421 |
| **$C_8$Gua $NTf_2$** | *n.d.* |
| **$C_{10}$Gua $NTf_2$** | 479 |
| *for comparison:* | |
| **$C_4$mim $NTf_2$** | 69 |

## 2.2 liquid-liquid extraction

Then we studied the use of these new ionic liquids in liquid-liquid extraction of anionic pollutants. In a first time, we focused on the sequestration of methyl orange (MO), an anionic dye (figure 1). Figure 5 shows the biphasic water/IL solutions after contacting the MO containing water phase with $C_6$Gua $NTf_2$ (left) and $C_4$mim $NTf_2$ (right). At a first glance, the transfer of the anionic dye from the water into the IL phase using the guanidinium IL can directly be visualized by the decolouration of the water phase. In contrast, using the imidazolium IL $C_4$mim $NTf_2$, the anionic dye is rather homogenously distributed between the water and the IL phase (Figure 5, right). This result gives a first indication that the separation properties of guanidinium and imidazolium ILs differ by a large extent.

**Figure 5. Biphasic water/IL solutions after contacting the MO containing water phase with $C_6$Gua $NTf_2$ (left) and $C_4$mim $NTf_2$ (right)**

We than studied the sequestration of MO using different guanidinium based ILs more in detail. The distribution of the MO between the water and the IL phase was quantified via UV-Vis-spectroscopy (λ= 466 nm). This technique allows the determination of the distribution coefficient D according to the general formula

$$D = ([MO_{init}] - [MO_{eq}]) / [MO_{eq}]$$

In a first series of experiments, we studied the extraction of small quantities of MO, i.e. using a large excess of the IL (Table 3). Under standard conditions, we contacted approx. 100 mg of the ILs $C_6$Gua $NTf_2$, $C_8$Gua $NTf_2$ and $C_{10}$Gua $NTf_2$ with an aqueous solution (3 mL) containing 1, 2, 4 and 10 mol-% of MO. The biphasic solution was stirred during 15 h at room temperature, and the quantity of the MO remaining in the water phase was determined via UV/Vis-spectroscopy. It clearly appears that all guanidinium based ILs efficiently adsorb MO. Analysis of the supernatant water phase shows that in all cases > 99% of MO is transferred into the IL phase (D > 99, Table 3, entries 1-12). The increasing D values can be related to the fact that in all experiments, nearly identical MO concentrations were found in the aqueous phase after contacting with the guanidinium ILs. Interestingly, long chain substituted ILs ($C_{10}$Gua $NTf_2$) gave slightly higher distribution coefficients compared to the short chain counterparts ($C_6$Gua $NTf_2$). This trend can be related to the higher hydrophobicity in the former ILs. Hydrophilic/hydrophobic interaction has already shown to be the driving force of separation

processes involving imidazolium based ILs.[12] For seek of comparison, we performed identical experiments using a conventional IL, namely $C_4$mim $NTf_2$. These experiments showed that the use of $C_4$mim $NTf_2$ resulted in considerably lower distribution coefficients indicating much less efficient MO transfer towards the IL phase (Table 3, entries 13-16).

**Table 3. Liquid-liquid extraction of MO using $C_x$Gua $NTf_2$ and $C_4$mim $NTf_2$**

| Entry | Quantity of IL /mg (mmol) | Quantity of MO/mg (mmol)[a] | MO/IL ratio | $C_{init}$ / mmol/L | $C_{eq}$ / mmol/L | D | Percentage of extracted anion / % |
|---|---|---|---|---|---|---|---|
| | | | ***with $C_6$Gua $NTf_2$*** | | | | |
| **1** | 100.6 (0.237) | 0.76 (2.33) | 0.01 | 0.78 | 0.0047 | 165 | 99.40% |
| **2** | 100.0 (0.236) | 1.60 (4.90) | 0.02 | 1.63 | 0.0065 | 249 | 99.60% |
| **3** | 101.1 (0.238) | 3.23 (9.88) | 0.04 | 3.29 | 0.0061 | 542 | 99.80% |
| **4** | 100.6 (0.237) | 7.80 (23.8) | 0.1 | 7.95 | 0.0058 | 1375 | 99.90% |
| | | | ***with $C_8$Gua $NTf_2$*** | | | | |
| **5** | 100.5 (0.222) | 0.73 (2.24) | 0.01 | 1.11 | 0.0052 | 214 | 99.50% |
| **6** | 100.6 (0.222) | 1.47 (4.50) | 0.02 | 2.23 | 0.006 | 369 | 99.70% |
| **7** | 100.1 (0.221) | 2.93 (8.96) | 0.04 | 4.44 | 0.0068 | 654 | 99.80% |
| **8** | 101.0 (0.221) | 7.27 (22.2) | 0.1 | 11.06 | 0.0057 | 1951 | 99.90% |
| | | | ***with $C_{10}$Gua $NTf_2$*** | | | | |
| **9** | 100.3 (0.209) | 0.69 (2.10) | 0.01 | 1.05 | 0.0046 | 226 | 99.60% |
| **10** | 100.0 (0.208) | 1.36 (4.15) | 0.02 | 2.08 | 0.0058 | 355 | 99.70% |
| **11** | 100.2 (0.209) | 2.74 (8.38) | 0.04 | 4.17 | 0.0064 | 653 | 99.80% |
| **12** | 100.1 (0.208) | 6.81 (20.8) | 0.1 | 10.4 | 0.0042 | 2494 | 100.00% |
| | | | ***with $C_4$mim $NTf_2$*** | | | | |
| **13** | 104.5 (0.249) | 0.80 (2.43) | 0.01 | 1.21 | 0.94 | 0.29 | 22.39% |
| **14** | 110.6 (0.264) | 1.55 (4.74) | 0.018 | 2.37 | 1.808 | 0.31 | 23.79% |
| **15** | 102.3 (0.244) | 3.15 (9.61) | 0.04 | 4.79 | 3.879 | 0.23 | 19.04% |
| **16** | 105.5 (0.252) | 7.75 (23.7) | 0.09 | 11.87 | 8.834 | 0.34 | 25.56% |

[a] dissolved in 3 mL of water.

After having ascertained the ability of the novel guanidinium ILs to adsorb efficiently MO at low concentrations, we investigated the anion exchange capacity of these novel compounds. For this purpose, we performed extraction experiments using higher molar ratios between the IL and MO together with reduced IL quantity. In this second series of experiments, we contacted approx. 10 mg of the $C_x$Gua $NTf_2$ ILs with approx. 20, 40, 60, 80 mol-% and an equimolar amount of MO dissolved in water (Table 4). Once again, our results show that the guanidinium ILs adsorb efficiently the anionic dye. For all studied ILs, we observed decreasing D values with increasing MO quantities. Furthermore, the highest distribution coefficients were observed with the long chain substituted $C_{10}$Gua $NTf_2$. More specifically, for extraction experiments involving $C_{10}$Gua $NTf_2$ with 20 and 38 mol-% of MO, the dye concentration in the aqueous phase was below the

detection limit (Table 4, entries 11/12). In all cases, the distribution coefficients remain high up to a dye/IL ratio of 0.8, but strongly decrease for equimolar dye/IL amounts. These experiments clearly show that at least 80% of the guanidinium cations of the ILs can be used for anion extraction.

**Table 4. Liquid-liquid extraction of MO using high $C_6$Gua $NTf_2$ / MO ratios**

| Entry | Quantity of IL /mg (mmol) | Quantity of MO/mg (mmol)[a] | MO/IL ratio | $C_{init}$ / mmol/L | $C_{eq}$ / mmol/L | D | Percentage of extracted anion / % |
|---|---|---|---|---|---|---|---|
| | | | ***with $C_6$Gua $NTf_2$*** | | | | |
| **1** | 10.0 (23.5) | 1.58 (4.8) | 0.2 | 1.61 | 0.014 | 114 | 99.1% |
| **2** | 9.9 (23.3) | 3.24 (9.9) | 0.42 | 3.29 | 0.024 | 136 | 99.3% |
| **3** | 10.3 (24.3) | 4.88 (14.9) | 0.61 | 4.95 | 0.039 | 127 | 99.2% |
| **4** | 10.1 (23.8) | 6.49 (19.8) | 0.83 | 6.61 | 0.081 | 81 | 98.8% |
| **5** | 10.4 (24.5) | 7.82 (23.9) | 0.97 | 7.95 | 0.964 | 8 | 87.9% |
| | | | ***with $C_8$Gua $NTf_2$*** | | | | |
| **6** | 10.0 (22.1) | 1.46 (4.5) | 0.2 | 2.23 | 0.0005 | 4930 | 100% |
| **7** | 10.5 (23.2) | 2.92 (8.9) | 0.38 | 4.45 | 0.002 | 2237 | 100% |
| **8** | 10.0 (22.1) | 4.35 (13.3) | 0.6 | 6.64 | 0.003 | 2276 | 100% |
| **9** | 10.2 (22.6) | 5.81 (17.8) | 0.79 | 8.85 | 0.01 | 871 | 99.9% |
| **10** | 10.4 (23.0) | 7.29 (22.3) | 0.97 | 11.06 | 0.612 | 17 | 94.5% |
| | | | ***with $C_{10}$Gua $NTf_2$*** | | | | |
| **11** | 10.2 (21.2) | 1.36 (4.2) | 0.2 | 2.08 | <0.0001 | >10000 | 100% |
| **12** | 10.4 (21.7) | 2.73 (8.3) | 0.38 | 4.17 | <0.0001 | >10000 | 100% |
| **13** | 10.0 (20.8) | 4.09 (12.5) | 0.6 | 6.25 | 0.005 | 1175 | 99.9% |
| **14** | 10.2 (21.2) | 5.45 (16.6) | 0.78 | 8.32 | 0.004 | 2007 | 100% |
| **15** | 10.0 (20.8) | 6.86 (21.0) | 1.01 | 10.4 | 0.545 | 18 | 94.8% |

[a] dissolved in 3mL of water.

It has to be mentioned that, with increasing MO/IL ratio, the IL layer tends to solidify. This trend is due to the formation of crystalline $C_x$Gua $(NTf2)_{1-x}(MO)_x$ systems. Indeed, the characterization of the formed $C_6$Gua $(NTf_2)_{0.9}(MO)_{0.1}$ phase via $^1$H NMR spectroscopy nicely indicates a molar ratio between the guanidinium cation and the MO anion of 1 : 0.12 (Figure 6), what is in very good agreement with the amount of added MO. This result indicates that the extraction involves an anion exchange mechanism and is driven by the high affinity of the guanidinium groups towards the sulfonate groups of MO.

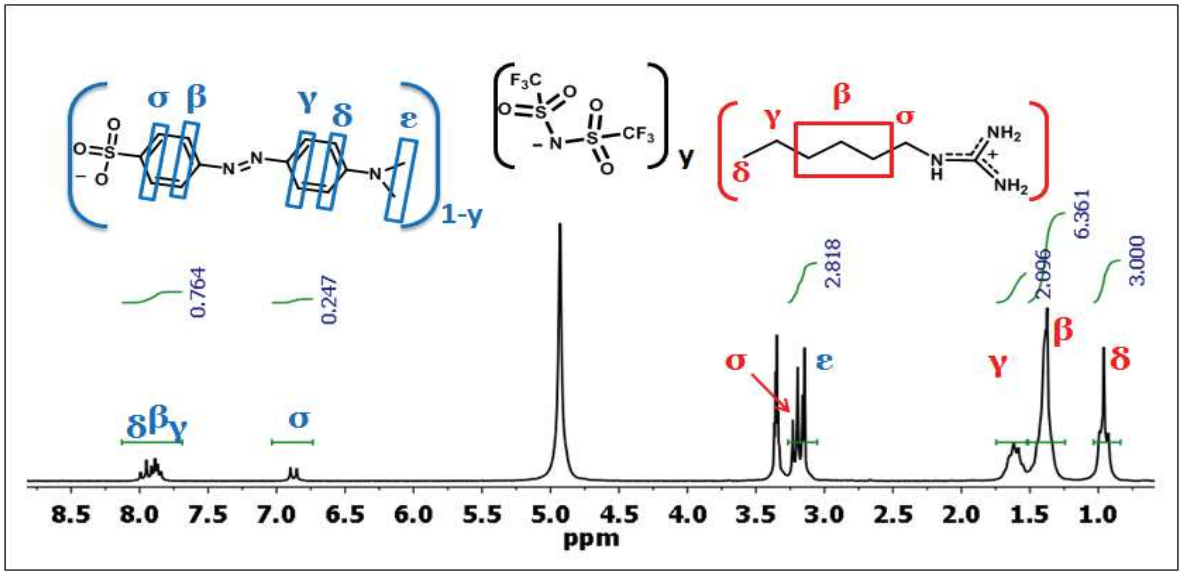


**Figure 6. $^{1}$H liquid NMR spectra of the $C_6$Gua $(NTf_2)_{0.9}(MO)_{0.1}$ phase (solvent:MeOD)**

In order to generalize our approach, we investigated the sequestration properties of the guanidinium type ILs for the extraction of other anionic species, i.e. an anionic drug (diclofenac, DCF) and a metallic anion (chromate). Both species are of high environmental and sanitary concern: DCF is a widely used non steroidal anti-inflammatory drug which is, together with its metabolites, among the most frequently detected pharmaceutical residues in water bodies.[18] Chromate, widely present in the effluents of many industries including tanning, electroplating paints, dyes etc., is a hazardous pollutant and recognized as a human cancerogen.

In this case, we used $C_6$Gua $NTf_2$ ionic liquid for the extraction of DCF and chromate anions, for low concentration of extracts; we contacted 100 mg of $C_6$Gua $NTf_2$ with approx. 1, 2, 4, 6, 10% of DCF and chromate dissolved in 3 ml of water. For high concentration, we contacted the same quantity of IL with approx. 20, 40, 60, 80% and an equimolar amount of DCF and chromate respectively. The results obtained were compared with those of imidazolium based ionic liquid. 100 mg of $C_4$mim $NTf_2$ was contacted with DCF and chromate solution at low concentration.

**Table 5. Liquid-liquid extraction of DCF and chromate using $C_6$Gua $NTf_2$ in low anion/IL ratios**

| Entry | Quantity of IL /mg (mmol) | Quantity of MO/mg (mmol)[a] | MO/IL ratio | $C_{init}$ / mmol/L | $C_{eq}$ / mmol/L | D | Percentage of extracted anion / % |
|---|---|---|---|---|---|---|---|
| | | | ***DCF*** | | | | |
| **1** | 99.8 (0.235) | 0.9 (2.74) | 0.01 | 0.91 | 0.033 | 27 | 96.40% |
| **2** | 101.7 (0.240) | 1.8 (5.45) | 0.02 | 1.82 | 0.022 | 82 | 98.80% |
| **3** | 99.9 (0.235) | 3.6 (11.0) | 0.05 | 3.65 | 0.016 | 228 | 99.60% |
| **4** | 102.3 (0.241) | 5.4 (16.5) | 0.07 | 5.44 | 0.031 | 172 | 99.40% |
| **5** | 101.8 (0.240) | 7.0 (21.9) | 0.09 | 7.24 | 0.032 | 225 | 99.60% |
| **6** | 101.3 (0.239) | 8.6 (27.1) | 0.11 | 9.02 | 0.046 | 196 | 99.50% |
| | | | ***Chromate*** | | | | |
| **7** | 107.9 (0.254) | 0.46 (2.4) | 0.01 | 1.21 | 0.38 | 2.1 | 68.80% |
| **8** | 103.2 (0.243) | 0.86 (4.4) | 0.02 | 2.23 | 0.76 | 2 | 66.20% |
| **9** | 102.1 (0.241) | 1.7 (8.8) | 0.04 | 4.42 | 1.66 | 1.7 | 62.40% |
| **10** | 102.4 (0.241) | 2.5 (13.0) | 0.05 | 6.57 | 2.74 | 1.4 | 58.30% |
| **11** | 101.3 (0.239) | 3.4 (17.3) | 0.07 | 8.76 | 4.08 | 1.1 | 53.50% |
| **12** | 102.6 (0.242) | 4.8 (24.6) | 0.1 | 12.3 | 4.97 | 1.5 | 59.50% |

[a] dissolved in 3 mL of water for experiments with DCF, in 2 mL of water for experiments with chromate.

The results obtained with $C_6$Gua $NTf_2$ and low anion/IL ratios are given in table 5. Both DCF and chromate are extracted towards the IL phase. However, results for DCF are slightly lower compared to those of MO, and chromate is extracted in a considerably lower extent.

This behaviour is due to the hydrophobic character of the IL which favours the adsorption of organic anions, whereas metallic or mineral anions display a lower affinity. Similar results were obtained with $C_6$Gua $NTf_2$ and high anion/IL ratios (Table 6). It has to be mentioned that nor DCF neither chromate are adsorbed in noticeable amounts by imidazolium ILs (Table 7). The fact that guanidinium salts adsorb these pollutants more efficiently is a clear sign of the contribution of the guanidinium substructure towards the extraction performances of these compounds.

**Table 6. Extraction of diclofenac (DCF) and Chromate using $C_6$Gua $NTf_2$ in high anion/IL ratios**

| Entry | Quantity of IL /mg (mmol) | Quantity of MO/mg (mmol)[a] | MO/IL ratio | $C_{init}$ / mmol/L | $C_{eq}$ / mmol/L | D | Percentage of extracted anion / % |
|---|---|---|---|---|---|---|---|
| | | | ***DCF*** | | | | |
| **1** | 101 (23.8) | 7.63 (23.99) | 0.10 | 7.918 | 0.0504 | 156.17 | 99.4% |
| **2** | 100.2 (23.61) | 15.2 (47.778) | 0.20 | 15.754 | 0.1124 | 139.11 | 99.3% |
| **3** | 100.6 (23.71) | 30.48 (95.82) | 0.40 | 31.776 | 0.3485 | 90.17 | 98.9% |
| **4** | 102.3 (24.11) | 46.72 (146.9) | 0.61 | 48.384 | 1.1406 | 41.42 | 97.6% |
| **5** | 100.8 (23.75) | 60.52 (190.2) | 0.80 | 63.186 | 4.2482 | 13.87 | 93.3% |
| **6** | 101.2 (23.85) | 75.92 (238.7) | 1.00 | 76.947 | 13.0286 | 4.91 | 83.1% |
| | | | ***Chromate*** | | | | |
| **7** | 102.6 (0.242) | 4.77 (24.56) | 0.10 | 12.26 | 4.97 | 1.468 | 59.5% |
| **8** | 101.5 (0.239) | 8.99 (46.28) | 0.19 | 23.12 | 13.53 | 0.709 | 41.5% |
| **9** | 100 (0.236) | 17.95 (92.43) | 0.39 | 45.83 | 29.16 | 0.572 | 36.4% |
| **10** | 100.1 (0.236) | 26.5 (136.47) | 0.58 | 67.54 | 48.75 | 0.386 | 27.8% |
| **11** | 100.8 (0.238) | 36.34 (187.15) | 0.79 | 92.74 | 68.39 | 0.356 | 26.3% |
| **12** | 100.2 (0.236) | 43.88 (225.98) | 0.96 | 111.17 | 77.27 | 0.439 | 30.5% |

**Table 7. Extraction of diclofenac (DCF) and Chromate using the imidazolium IL $C_4$mim $NTf_2$ in low anion/IL ratios**

| Entry | Quantity of IL /mg (mmol) | Quantity of MO/mg (mmol)[a] | MO/IL ratio | $C_{init}$ / mmol/L | $C_{eq}$ / mmol/L | D | Percentage of extracted anion / % |
|---|---|---|---|---|---|---|---|
| | | | ***DCF*** | | | | |
| **1** | 100.5 (0.24) | 0.87 (2.73) | 0.01 | 0.907 | 0.913 | 0.000 | 0.0% |
| **2** | 100.3 (0.239) | 1.74 (5.46) | 0.02 | 1.819 | 1.728 | 0.053 | 5.0% |
| **3** | 100.1 (0.239) | 3.49 (10.95) | 0.05 | 3.649 | 3.532 | 0.033 | 3.2% |
| **4** | 100.1 (0.239) | 5.19 (16.32) | 0.07 | 5.442 | 5.226 | 0.041 | 4.0% |
| **5** | 100.2 (0.239) | 6.95 (21.85) | 0.09 | 7.242 | 7.116 | 0.018 | 1.7% |
| **6** | 100.2 (0.239) | 8.62 (27.1) | 0.11 | 9.024 | 8.687 | 0.039 | 3.7% |
| | | | ***Chromate*** | | | | |
| **7** | 101.5 (0.242) | 0.464 (2.39) | 0.01 | 1.196 | 1.187 | 0.0075 | 0.7% |
| **8** | 101.8 (0.243) | 0.932 (4.8) | 0.02 | 2.383 | 2.304 | 0.0344 | 3.3% |
| **9** | 100.4 (0.239) | 1.86 (9.56) | 0.04 | 4.768 | 4.607 | 0.0351 | 3.4% |
| **10** | 100 (0.238) | 2.8 (14.41) | 0.06 | 7.172 | 7.173 | 0 | 0% |
| **11** | 101.6 (0.242) | 3.71 (19.08) | 0.08 | 9.513 | 9.523 | 0 | 0% |
| **12** | 100.4 (0.239) | 4.67 (24.02) | 0.10 | 11.925 | 11.752 | 0.0147 | 1.4% |

## 2.3 ionic liquid regeneration

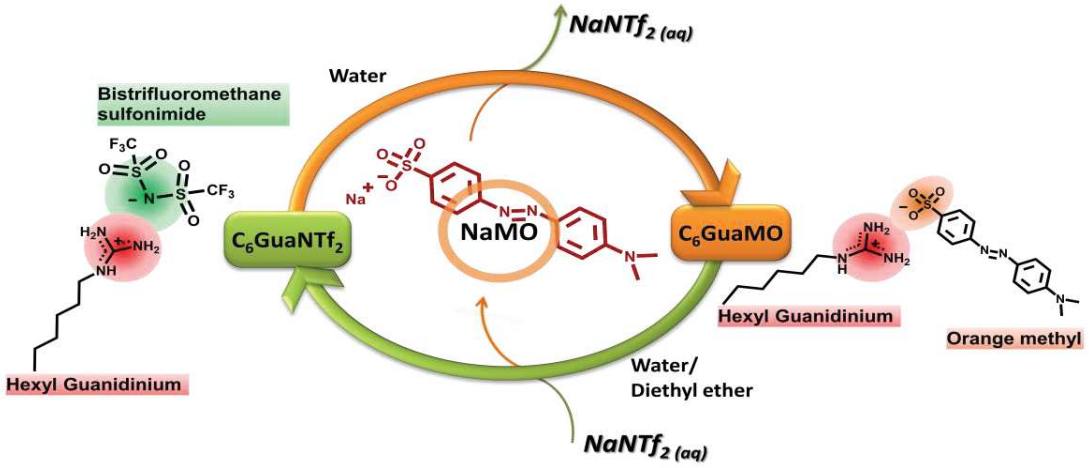


**Figure 7. Extraction-regeneration cycle of $C_6$Gua $NTf_2$ in the separation of MO**

For green and sustainable process engineering, the regeneration of the extractants is of particular interest. Here, this issue is of importance as, besides its notable toxicity, the bis-trifluoromethane sulfonimide anion is not biodegradable and tends to accumulate in the biosphere.[19] We therefore studied the recycling of the guanidinium ionic liquids in view of the development of an extraction/regeneration cycle. Firstly, the sequestration of anionic pollutants towards the IL phase involves a transfer of the bis-trifluoromethane sulfonimide anion into the water phase. We were able to form new guanidinium $NTf_2$ ILs via a simple addition of hexylguanidinium chloride. The newly formed $C_x$Gua $NTf_2$ show identical characteristics compared to the initially synthesized material. Another interesting feature of the guanidinium ILs is their atypical miscibility with some organic solvents. We observed that the guanidinium ILs are completely miscible in diethyl ether in every IL/solvent ratio. This behaviour opens new possibilities for a simple and straightforward IL regeneration after liquid–liquid extraction (Figure 7). In fact, treatment of the formed $C_x$Gua $(NTf2)_{1-x}(MO)_x$ systems with an aqueous $M^+$ $NTf2^-$ solution followed by addition of diethyl ether gave a biphasic system containing the MO in the aqueous phase and the newly formed $C_x$Gua $NTf_2$ in the ether phase. We also used the expelled bis-trifluoromethane sulfonimide anion obtained in the water phase as described above for this purpose. Evaporation of the organic solvent gave the recycled $C_x$Gua $NTf_2$ (Figure 8). In this way, our work

demonstrates the possibility to re-use both cation and anion of the guanidinium based ionic liquids and to build up a closed extraction–regeneration cycle (Figure 7).

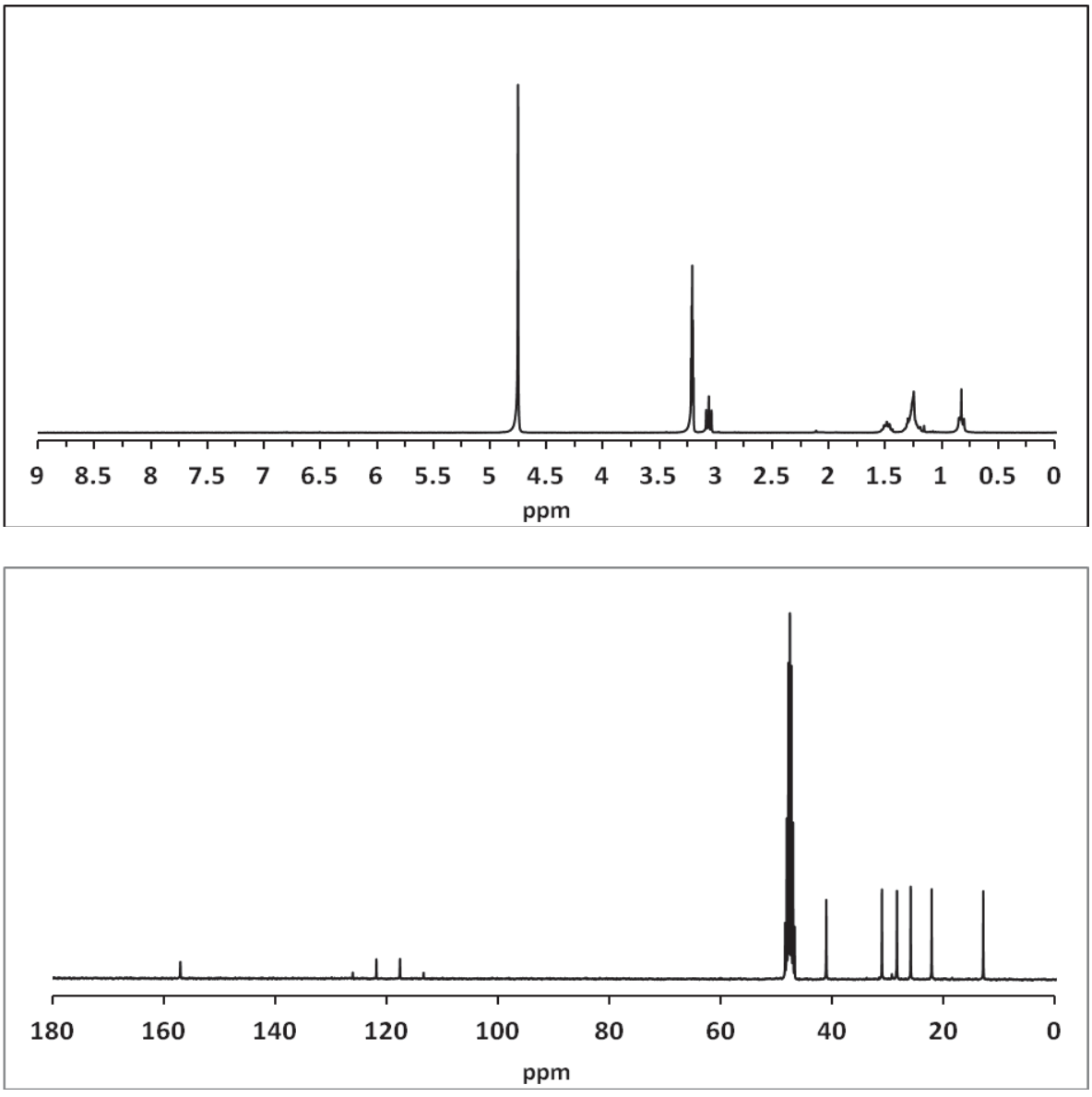


**Figure 8. $^{1}H$ (upper) and $^{13}C$ liquid NMR (lower) spectra of the recovered $C_6Gua\ (NTf_2)$ phase**

This extraction–regeneration cycle can also be performed with other organic anions such as diclofenac, which behaves similarly compared to MO in the liquid–liquid extraction process.

Although metallic anions such as chromate led to considerably lower distribution coefficients, the extraction–regeneration can be performed in a similar way as the cyclic process is driven by the extraction of the IL into the ether phase. As a consequence, chromate was recovered from the aqueous phase, too, as visually evidenced by the coloration of the water phase (Figure 9). Finally, the ionic liquid was successfully recovered from the ether phase as indicated by its liquid NMR spectrum (Figure 10).

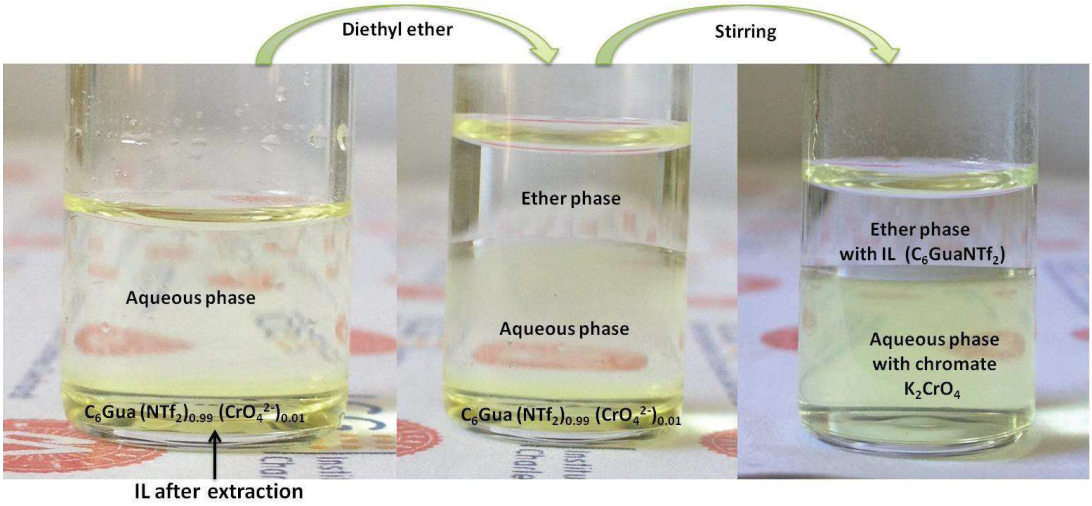


**Figure 9. regeneration of chromate and $C_6GuaNTf_2$ ionic liquid**

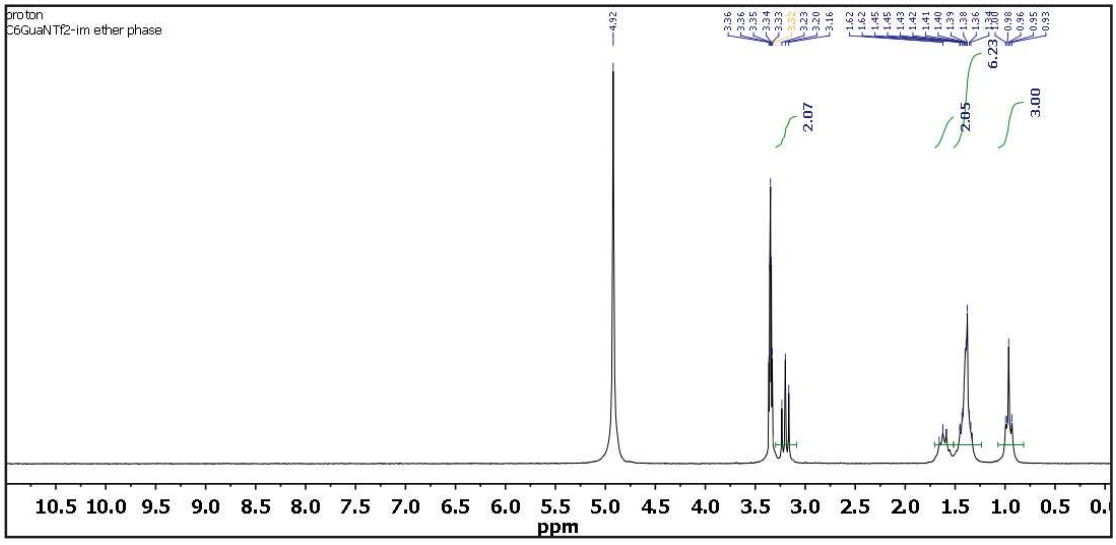


**Figure 10. $^1$H liquid NMR spectra of the recovered $C_6Gua\ (NTf_2)$ in ether phase**

## 3 Conclusion

In conclusion, we synthesized a series of new monoalkylguanidinium bis-trifluoromethane sulfonimide ionic liquids. These novel compounds appear as functional ('task-specific') ionic liquids due to the presence of cationic guanidinium groups, able to create strong interactions with various anionic substrates via combined ionic interactions and hydrogen bonding. Here, the high potential of guanidinium based ILs in separation was monitored via the extraction of an anionic dye (methyl orange, MO), an anionic drug (diclofenac) and a metallic anion (chromate). Significant differences were found regarding the extraction efficiency of these different anionic species. The best results were found for MO, and DCF was also efficiently sequestrated. In contrast, chromate was separated in significantly lower extent. We attribute these results to the high affinity of organic anions towards the hydrophobic IL phase. This result is supported by the fact that decyl substituted guanidinium IL $C_{10}$Gua $NTf_2$ gave better results than related octyl or hexyl guanidinium compounds. In contrast, mineral or metallic anions show a less pronounced affinity towards the guanidinium IL phase. It has to be mentioned that in all cases, the guanidinium based ILs gave considerably better results compared to their imidazolium counterparts. Finally, we introduced a closed separation-regeneration cycle involving the guanidinium based ionic liquids which is of interest for sustainable process engineering. Our ongoing work in this field focusing on the separation of traces of pollutants of real environmental solutions will be reported in due course.

**References**


1. Wasserscheid, P.; Welton, T., *Ionic Liquids in Synthesis, Second Edition*. Wiley-VCH Verlag GmbH & Co. KGaA: Weinheim, Germany, 2008.

2. Gao, Y.; Arritt, S. W.; Twamley, B.; Shreeve, J. M., Guanidinium-based ionic liquids. *Inorg. Chem.* **2005,** 44, (6), 1704-1712.

3. Carrera, G.; Frade, R. F. M.; Aires-de-Sousa, J.; Afonso, C. A. M.; Branco, L. C., Synthesis and properties of new functionalized guanidinium based ionic liquids as non-toxic versatile organic materials. *Tetrahedron* **2010,** 66, (45), 8785-8794.

4. Ward, M. D., Directing the assembly of molecular crystals. *MRS Bull.* **2005,** 30, (10), 705-712.

5. Miyake, M.; Yamada, K.; Oyama, N., Self-assembling of guanidine-type surfactant. *Langmuir* **2008,** 24, (16), 8527-8532.

6. Song, Y.; Li, Q.; Li, Y., Self-aggregation and antimicrobial activity of alkylguanidium salts. *Colloid Surface A* **2012,** 393, 11-16.

7. Bouchal, R.; Hesemann, P.; Prelot, B.; Zajac, J., Micellization behavior of long chain substituted alkylguanidinium surfactants. *manuscript under preparation* **2016**.

8. El Hankari, S.; Hesemann, P., Guanidinium vs. Ammonium Surfactants in Soft-Templating Approaches: Nanostructured Silica and Zwitterionic-Silica from Complementary Precursor–Surfactant Ion Pairs. *European Journal of Inorganic Chemistry* **2012**, (32), 5288-5298.

9. El Kadib, A.; Hesemann, P.; Molvinger, K.; Brandner, J.; Biolley, C.; Gaveau, P.; Moreau, J. J. E.; Brunel, D., Hybrid Materials and Periodic Mesoporous Organosilicas Containing Covalently Bonded Organic Anion and Cation Featuring MCM-41 and SBA-15 Structure. *Journal of the American Chemical Society* **2009,** 131, (8), 2882-2892.

10. Han, X.; Armstrong, D. W., Ionic liquids in separations. *Accounts Chem. Res.* **2007,** 40, (11), 1079-1086.

11. Han, D.; Tang, B.; Lee, Y. R.; Row, K. H., Application of ionic liquid in liquid phase microextraction technology. *J. Sep. Sci.* **2012,** 35, (21), 2949-2961.

12. Pei, Y. C.; Wang, J. J.; Xuan, X. P.; Fan, J.; Fan, M., Factors affecting ionic liquids based removal of anionic dyes from water. *Env. Sci. Technol.* **2007,** 41, (14), 5090-5095.

13. Fei, Z. F.; Geldbach, T. J.; Zhao, D. B.; Dyson, P. J., From dysfunction to bis-function: On the design and applications of functionalised ionic liquids. *Chem. Eur. J.* **2006,** 12, (8), 2122-2130.

14. Gadenne, B.; Hesemann, P.; Moreau, J. J. E., Ionic liquids incorporating camphorsulfonamide units for the Ti-promoted asymmetric diethylzinc addition to benzaldehyde. *Tetrahedron Letters* **2004,** 45, (44), 8157-8160.

15. Gadenne, B.; Hesemann, P.; Moreau, J. J. E., Easily recoverable BINOL ligand with ionic tag for asymmetric catalysis. *Tetrahedron Asymmetr.* **2005,** 16, (11), 2001-2006.

16. Ouadi, A.; Gadenne, B.; Hesemann, P.; Moreau, J. J. E.; Billard, I.; Gaillard, C.; Mekki, S.; Moutiers, G., Task-specific ionic liquids bearing 2-hydroxybenzylamine units: Synthesis and americium-extraction studies. *Chem.-Eur. J.* **2006,** 12, (11), 3074-3081.

17. Huddleston, J. G.; Visser, A. E.; Reichert, W. M.; Willauer, H. D.; Broker, G. A.; Rogers, R. D., Characterization and comparison of hydrophilic and hydrophobic room temperature ionic liquids incorporating the imidazolium cation. *Green Chemistry* **2001,** 3, (4), 156-164.

18. Rabiet, M.; Togola, A.; Brissaud, F.; Seidel, J.-L.; Budzinski, H.; Elbaz-Poulichet, F., Consequences of treated water recycling as regards pharmaceuticals and drugs in surface and ground waters of a medium-sized Mediterranean catchment. *Environmental Science & Technology* **2006,** 40, (17), 5282-5288.

19. Ranke, J.; Stolte, S.; Stoermann, R.; Arning, J.; Jastorff, B., Design of sustainable chemical products - The example of ionic liquids. *Chemical Reviews* **2007,** 107, (6), 2183-2206.

# Chapter III

## Ionosilica type hybrid materials bearing ammonium entities: structuration and ion exchange

The following chapter will highlight some of the main designs of nano- and multi-scale structured ionosilicas materials shaped as nanoparticles, powders and monoliths with additional functionalities and outstanding properties in the fields of separation and nanomedicine. In particular, we will discuss the control of different synthesis parameters such as temperature, concentration of various reagents and time in order to obtain materials with specific architectures and morphologies. To achieve these goals, we initiated several collaborations with other research groups at the European level. We divided this chapter into three parts.

*i*) Part I: In this part, the potential of mesoporous ionosilicas bearing ammonium groups for the adsorption and release of different non-steroidal anti-inflammatory molecules was investigated. Due to the strong adsorption capacity of ionosilicas for charged molecules, the obtained materials were then evaluated for the application as adsorbents in wastewater treatment. Our study concerned the adsorption process driven *via* electrostatic interaction between anionic drugs (diclofenac and sulindac) and positively charged sites in ionosilicas. The physico-chemical properties of the loaded materials were investigated *via* Fourier transform infrared spectroscopy, UV-Vis spectroscopy, thermogravimetric analysis and gas-volumetric analysis. The results obtained in this section are obtained in the frame of a short term scientific mission supported by the European COST Action MP1202. This work was in collaboration with Dr. Gloria Belier and Dr. Ivana Miletto at the University of Torino Dipartimento di Chimica and NIS (Centre for Nanostructured Interfaces and Surfaces). The results obtained in this part were published at *New Journal of Chemistry*. DOI: 10.1039/c6nj01473a.

*ii*) Part II: The study achieved in the first part allowed us to get an idea about the behavior of ionosilica materials for the adsorption of active ingredients. For this reason, periodic mesoporous ionosilica nanoparticles with ammonium walls were synthesized from a trisilylated ammonium precursor. The nanoparticles display uniform diameter particles size less than 100 nm together with ordered hexagonal pore architecture and high specific surface area. The nanoparticles are completely biocompatible *in vitro* and *in vivo* and are efficiently endocytosed by macrophages. Diclofenac delivery was studied. The loaded nanoparticles are very efficient in inhibiting lipopolysaccharide (LPS) induced inflammation. This work was performed in collaboration with different institutes of the University of Montpellier. At ICGM with Jean- Olivier Durand and

Clarence Charnay. At the Institut de Biomolécules Max Mousseron, all the biological experiments were performed by Mogane Daurat and Magali Gary-Bobo.

*iii*) Part III: with the aim to develop continuous flow processes for the adsorption and extraction of anionic molecules, we studied the synthesis of ionosilica monoliths. Here, we present the first results of monoliths synthesis containing amine or ammonium functionalities. The as synthesized monoliths display trimodal hierarchical porous structure (micro, meso, and macroporosity) obtained via high internal phase emulsion process and lyotropic mesophases. This work was performed at Centre de Recherche Paul Pascal (CRPP) of Bordeaux in collaboration with Pr. Rénal Backov.

# Part I

## Ionosilicas as efficient adsorbents for the separation of diclofenac and sulindac from aqueous media

## Summary

# 1 Introduction

A large volume of pharmaceuticals is used for the prevention, diagnosis and treatment of diseases in humans and animals. In industrialized countries, the average annual consumption of pharmaceuticals is estimated to be between 50 and 150 g per capita. Most pharmaceuticals are not completely degraded after application. As a result, pharmaceutical metabolites and some unchanged forms of these compounds are excreted and subsequently enter the ecosystem.[1] For this reason, efficient methods for the removal of drugs and their metabolites from wastewater and effluents are required. Non steroidal anti-inflammatory drugs (NSAID) are among the most abused drugs in developed countries; among them, diclofenac (DCF) and sulindac (SUL, Figure 1) are widely used to reduce inflammation and to relieve pain, working as an analgesic in conditions such as in arthritis or acute injury. The annual consumption of both drugs is of several hundreds of tons per year (diclofenac: approx. 900 tons).[2] Diclofenac and its metabolites are among the most frequently detected pharmaceutical residues in water bodies thus far.[3] After oral administration, these drugs are eliminated in rather short periods. For example, the elimination half-life of diclofenac in the human body is of about 2 h. Approximately 65% of the dosage is excreted through urine in which six diclofenac metabolites have been identified, in particular partially oxidized species.[4]

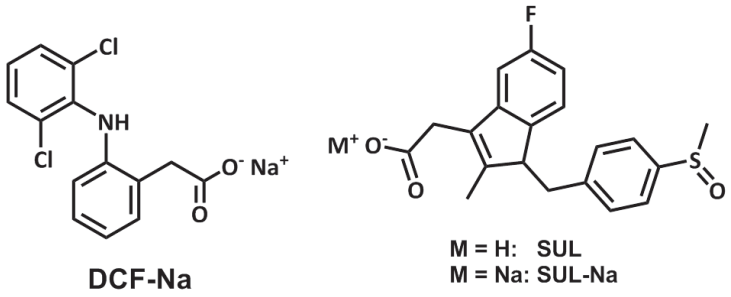


**Figure 1. Structures of the drugs used in the present study.**

Silica based materials are well established and widely used for separation processes and the sequestration of pollutants.[5] Mesoporous silica such as HMS[6] and SBA-15[7] were previously used for the adsorption of pharmaceuticals such as carbamazepine, diclofenac and ibuprofen.[8, 9]

The surface functionalization of nanostructured silica mesophases allows accessing a large variety of tailor made materials for the separation of both organic and inorganic pollutants. For example functionalized silica-based porous materials with

trimethysilyl,[10] aminopropyl[11, 12] and mercaptopropyl groups[8] display enhanced the adsorption capacity of pharmaceuticals components. In the field of organic/inorganic materials, ion exchange involving silica based materials containing ionic groups appear as an interesting way for the sequestration of charged species, in particular of oxo-anions such as arsenate, chromate, perrhenate or pertechnetate.[13-18] Here, we investigated ionosilicas as efficient adsorbing materials for anionic drugs and compared with silica material type MCM-41. Ionosilicas are defined as silica hybrid materials containing covalently bound ionic species and recently emerged as interesting functional materials for several applications in catalysis and separation.[15, 19, 20] Ionosilicas combine high porosity, regular architecture on the mesoscopic level with an unmatched chemical versatility, induced by the high variability and the high number of incorporated ionic species. In our recent work, we focused on the formation of structured ionosilicas via bottom-up approaches using ionic precursors.[21-23]

This strategy allowed accessing a large variety of porous silica hybrid materials containing different types of ionic groups and displaying various textures. Here, we report that ionosilicas are efficient adsorbents for the sequestration of drugs from aqueous solutions. We used an ammonium type ionosilica (Figure 2) for adsorption experiments of the anionic drugs diclofenac and sulindac.

## 2 Results and discussion

### 2.1 Materials synthesis

We used an ammonium type ionosilica for the separation experiments. The material **A** (Figure 2) was synthesized following published procedures by hydrolysis-polycondensation procedures from the corresponding *tris*-trimethoxysilylated precursor in the presence of anionic surfactant.[24, 25] This strategy allows obtaining nanostructured ammonium based ionosilica materials with regular pore. After elimination of the surfactant by repeated washing with ethanolic hydrochloric acid, we obtained an ionosilica containing ammonium chloride entities (Figure 2). The X-ray diffractogram (Figure 3-a) of the material A shows the (100), (110) and (200) reflections, indicating 2d hexagonal architecture. Nitrogen sorption experiment (Figure 3-b) confirms that the material is highly porous (SBET = 1038 $m^2.g^{-1}$) and shows

relatively high pore volume (0.55 $cm^3$ $g^{-1}$). BJH analysis of the adsorption branch of the isotherm indicates narrow pore size distribution centered at 2 nm.

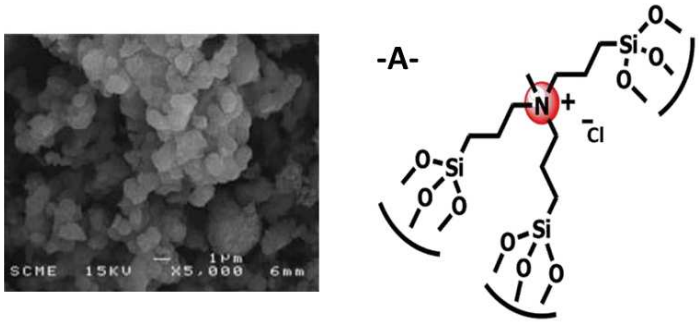


**Figure 2. SEM image (left) of an ionosilica material containing ammonium groups and structure of the ammonium groups in material A (right).**

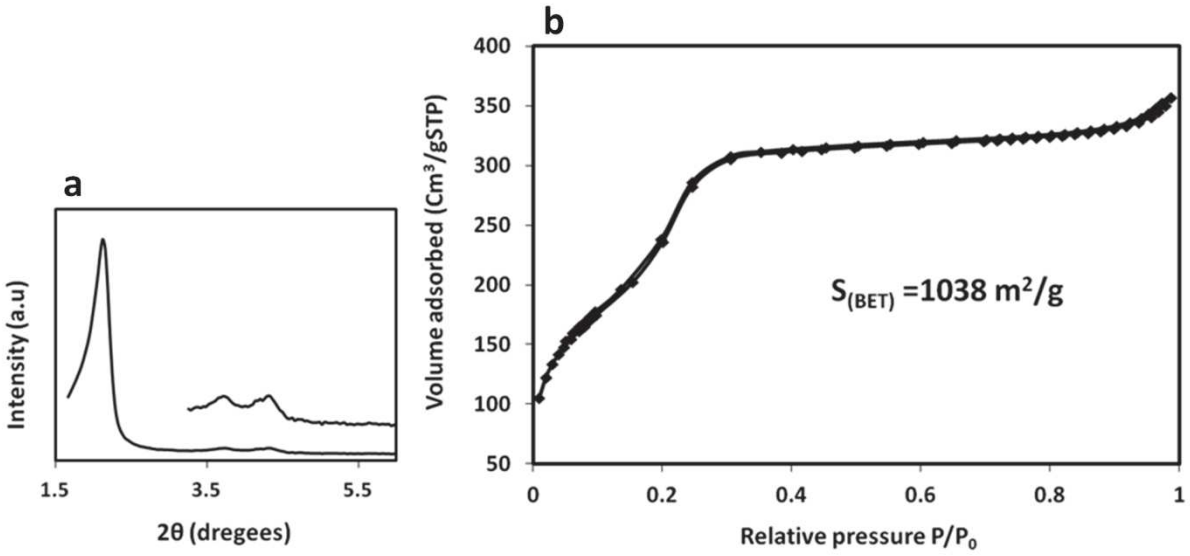


**Figure 3. a) X-ray diffraction pattern of Material A, b) Nitrogen sorption isotherm of material A**

## 2.2 Adsorption experiments with diclofenac and sulindac

Here, we evaluated the potential of porous ammonium hybrid ionosilica for the adsorption of the anionic drugs diclofenac and sulindac. Diclofenac is usually supplied and used in pharmaceutical formulations as potassium or sodium salt, whereas sulindac is usually commercialized in its acidic form and it is thus neutral (pKa = 4.7). We therefore used commercial diclofenac sodium salt (**DCF-Na**) and sulindac (**SUL**), and we prepared the sodium salt of sulindac (**SUL-Na**) by overnight treatment of the acidic form of sulindac in sodium hydroxide solution (Figure 1).

The adsorption ability of the ionosilica material **A** was monitored towards **DCF-Na**, **SUL-Na** and **SUL**. All drugs were employed to test their adsorption from high concentration solutions (0.03M) at a molar drug-ionosilica ratio of 1.1 : 1, resulting in the **A-DCF-Na/HC**, **A-SUL-Na/HC** and **A-SUL** samples. In the case of diclofenac **DCF-Na**, experiments were also carried out using a diluted drug solution (3.82 $\mu g \cdot ml^{-1}$ / $1.2 \cdot 10^{-5}$ M) at a 1:6000 drug-ionosilica wt.-ratio in order to study the ability to adsorb traces of the drug, more realistic for real environmental waters (sample **A-DCF-Na/LC**). Furthermore, the loading was repeated on this sample in order to test the re-usability of the ionosilica as drug adsorbent. The corresponding ionosilica loaded samples were labeled as **HC** when prepared from high concentration solutions, and **LC** when prepared from low concentration ones.

For the drug adsorption experiments, the drugs were dissolved in a suitable solvent (deionized water in the case of **DCF-Na** and **SUL-Na** and ethanol in the case of **SUL**). Then, the ionosilica material was added to the solution. After 24 h stirring at room temperature, the suspensions were filtered and the solids were recovered and dried under vacuum at room temperature overnight. The adsorption of the drugs within the ionosilica material was qualitatively monitored *via* FT-IR and solid state NMR spectroscopies. The quantification of the loading within the ionosilica material was assessed *via* TGA measurements and UV-Vis absorption and emission spectroscopies of the supernatant, depending on the concentration**.**

## 2.3 Characterization of loaded drug material

### 2.3.1 Infrared spectroscopy

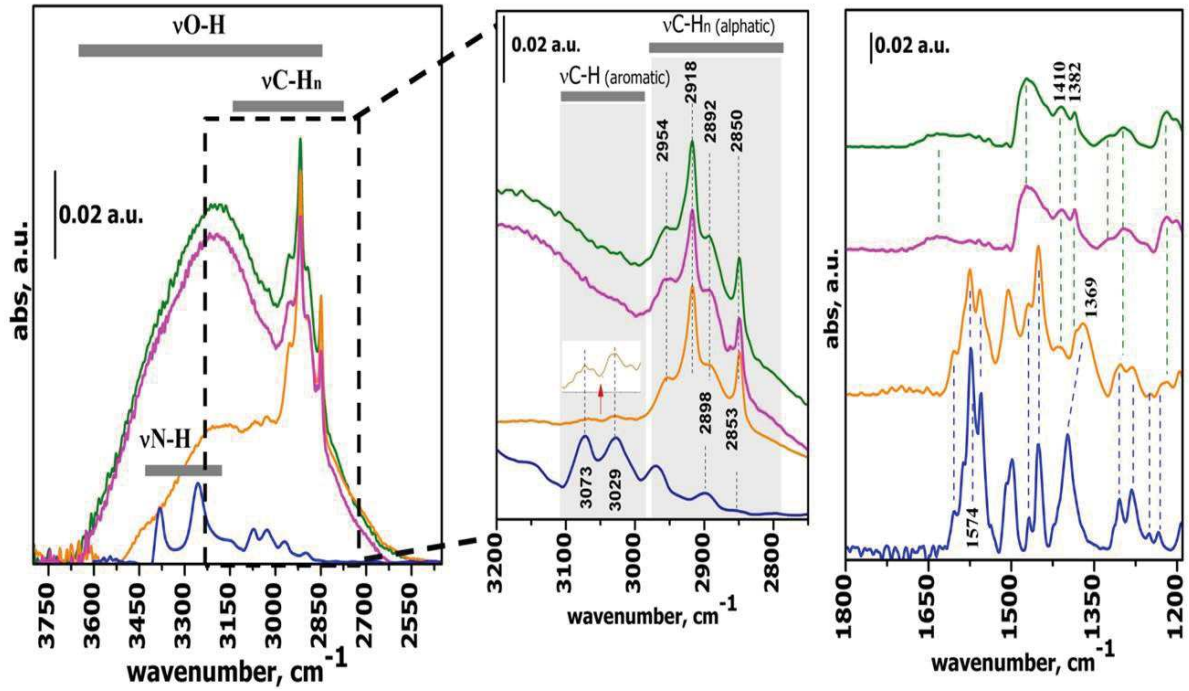


**Figure 4. FT-IR spectra of DCF-Na (blue curve), ionosilica material A (green curve), drug/ionosilica complexes DCF-Na/HC (orange curve) and DCF-Na/LC (pink curve). Spectra in panel C are vertically translated for the sake of clarity.**

FT IR spectroscopy was used to get a first information about the adsorbing process of the drugs. Figure 4 shows the FTIR spectra of **DCF-Na**, measured in ATR mode, and of the ionosilica material **A** before and after loading with DCF-Na. The latter spectra were measured in transmission mode on self supported pellets. Although the infrared spectrum of the **A-DCF-Na/HC** sample (Figure 4, orange curve) is dominated, in the high frequencies range, by the signals of the ionosilica material, the signals due to the drug are visible (absorption bands at 3073/3029 $cm^{-1}$). However, the characteristic absorption bands are more clearly visible in the low frequency range of the spectrum (absorption band at 1574 $cm^{-1}$).[26-28] Moreover, the broad absorption in the 3600-2500 $cm^{-1}$ range, typical of hydrogen-bonding interactions decreases on sample **A-DCF-Na/HC**, thus testifying the involvement of surface groups with the drug. On the contrary, in the case of the **A-DCF-Na/LC** sample (Figure 4, pink curve), the drug content is too low to generate visible changes in the spectrum of the parent ionosilica

material. It is clear that after interaction with the ionosilica material, diclofenac molecules remain in the carboxylate form, as indicated by the presence of signals at 1574 and 1369 $cm^{-1}$, which can be attributed to antisymmetric and symmetric stretching of the carboxylate group.[29] The slight shift of the lower frequency carboxylate peak observed in the drug/ionosilica complex with respect to the spectrum of the drug itself can be related to a modified interaction between the carboxylate ion and the cationic moiety of the ionosilica. To conclude the IR spectroscopic characterization of the solids, signals characteristic for diclofenac are clearly visible only in the high loaded sample **A-DCF-Na/HC**. The adsorbed diclofenac quantity is too low to be detected in the material **A-DCF-Na/LC** *via* FT-IR spectroscopy.

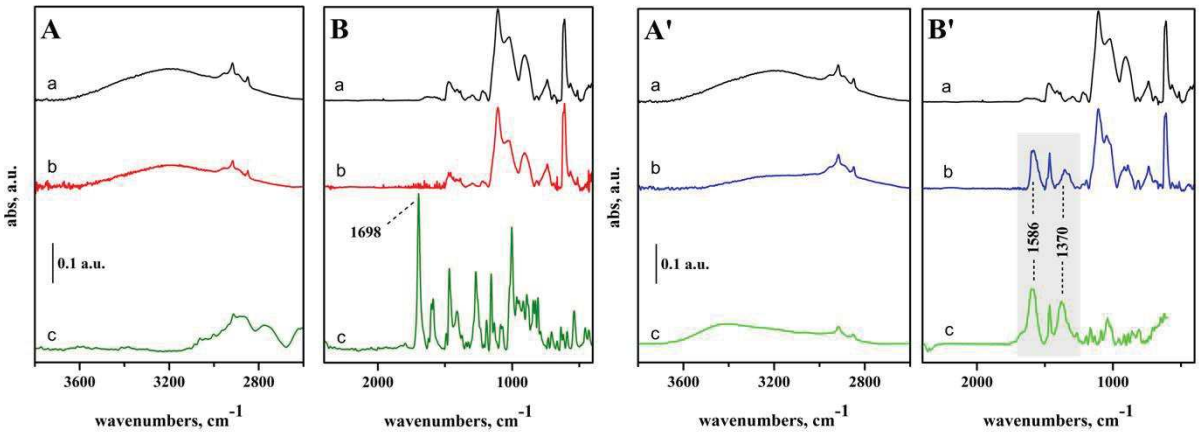


**Figure 5. A, B. FTIR spectra of Material A (curve a),** A-SUL/HC (curve b) and SUL in solid form (curve c)**; A',B': FTIR spectra of Material A (curve a),** A-SUL-Na/HC (curve b) and SUL-Na in solid form (curve c).

The adsorption of the sodium salt of sulindac **SUL-Na**, monitored via FT-IR spectroscopy, gave similar results. In Figure 5, shows panel A and B FTIR spectra of Material A, sulindac and of the corresponding hybrid system A-SUL/HC. The spectral profile of A-SUL/HC is coincident with the spectra of Material **A**; no signals ascribable to Sulindac molecule are present. On the contrary, in the case of sample A-SUL-Na/HC, in which Sulindac Sodium salt was adsorbed, typical signals ascribable to carboxylate moieties of SUL-Na molecules are clearly observable, confirming the successful incorporation of the drug in Material A. This is a clear indication for a selective adsorption of anionic compounds, whereas neutral compounds are not adsorbed by the ionosilica material.

### 2.3.2 Solid state NMR spectroscopy

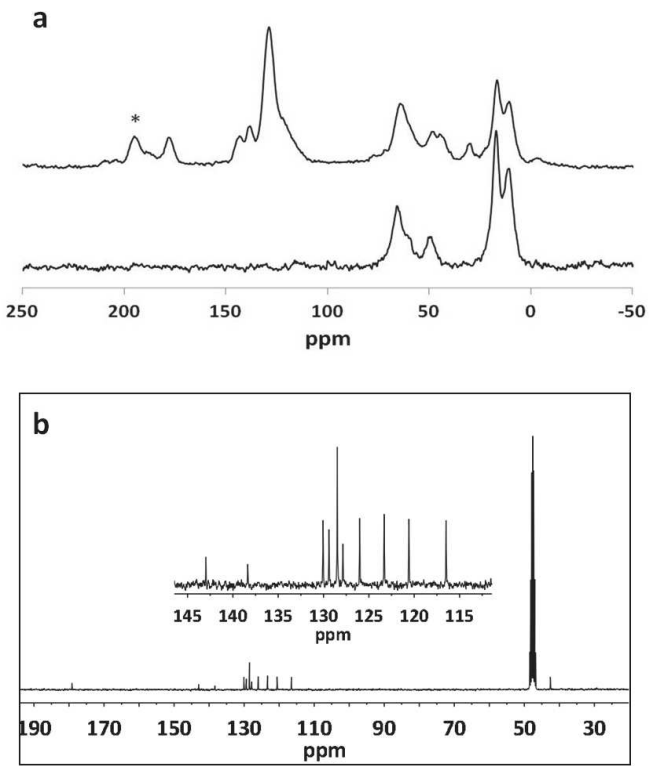


**Figure 6. a) Upper, solid state $^{13}$C CP-MAS NMR spectra of the parent ionosilica material A and lower, solid state $^{13}$C CP-MAS NMR spectra of the diclofenac loaded sample A-DCF-Na/HC and b) $^{13}$C NMR of sodium diclofenac in deuterium methanol.**

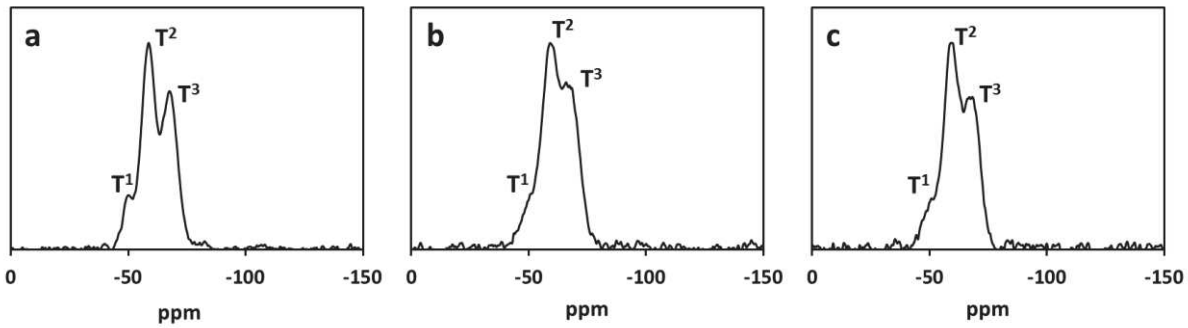


**Figure 7. Solid state $^{29}$Si CP-MAS NMR spectra: a)** parent ionosilica material A, **b)** diclofenac loaded sample A-DCF-Na/HC and **c)** sulindac loaded sample A-SUL-Na/HC.

The characterization of the pure ionosilica and the DCF loaded samples *via* solid state NMR spectroscopy confirms these results. Whereas the $^{29}$Si CP-MAS NMR spectra of the loaded sample **A-DCF-Na/HC** (Figure 7-a) do not show noticeable differences compared to the spectrum of the parent material **A** (Figure 7-b), significant changes can be observed in the $^{13}$C

CP-MAS NMR spectra of the parent ionosilica material **A** and the diclofenac loaded sample **A-DCF-Na/HC** (Figure 6-a). The spectrum of the pure ionosilica **A** shows the three signals of the propyl linkers and the signal relative to the methyl group directly attached to the nitrogen atom. The spectrum of the DCF-loaded sample shows, additionally to the signals of the ionosilica material, a set of intense peaks characteristic for the DCF anions, in particular in the aromatic region (110-150 ppm). Furthermore, in nice agreement to the $^{13}C$ NMR spectrum of diclofenac in solution (Figure-b), the signals at 45 ppm and 179 ppm can be assigned to the methylene and the carboxylate group of the drug molecule, respectively. The high intensity of the signals characteristic of the diclofenac anions, in particular in the aromatic region, indicates a high loading of the ionosilica material and, accordingly, a high adsorption efficiency of the ionosilica towards diclofenac. However, it is not possible to quantify the amount of adsorbed diclofenac from the $^{13}C$ CP-MAS NMR spectrum. The $^{29}Si$ and $^{13}C$ CP-MAS NMR spectrum of the sulindac loaded sample **A-SUL-Na/HC** shown in Figure 7-c and Figure 8-a give similar information respectively. In fact the $^{13}C$ CP-MAS NMR spectrum shows the signals characteristic for the ionosilica material A with additional signals characteristic for sulindac drug. We found set of intense peaks in aromatic region in concordance with $^{13}C$ NMR spectrum of sulindac in solution as shown in Figure 8-b.

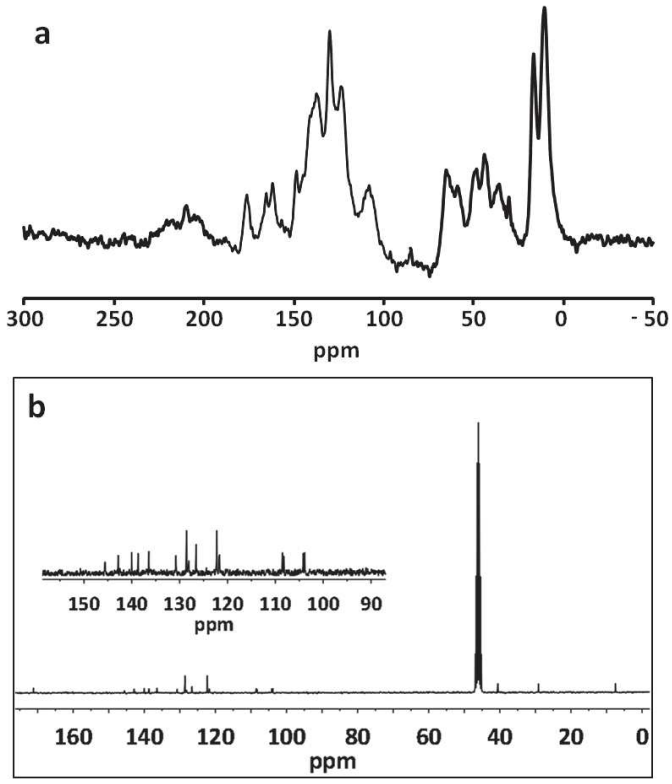


**Figure 8. a) Solid state $^{13}C$ CP-MAS NMR spectra of the sulindac loaded sample A-SUL-Na/HC and b) $^{13}C$ NMR of sulindac in deuterium methanol.**

After having ascertained qualitatively that the drugs were adsorbed onto the ionosilica material, we were interested to quantify the amount of adsorbed drug. We therefore calculated the adsorption capacity and the encapsulation efficiency μ of the material by thermogravimetric analysis of the loaded ionosilica samples and by spectroscopic analysis of the supernatant after the loading procedure via UV-Vis spectroscopy.

### 2.3.3 Thermogravimetric analysis (TGA)

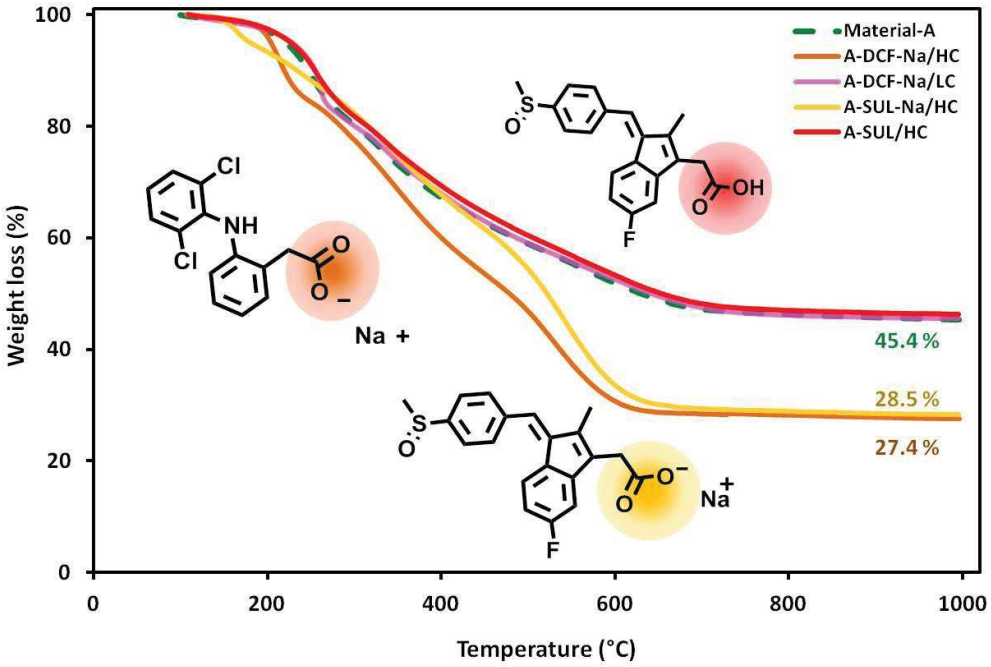


**Figure 9. Thermogravimetric analysis: A -ionosilica material (green dashed curve) and drug/ionosilica complexes DCF-Na/HC (orange curve), DCF-Na/LC$_1$ (pink curve), SUL-Na/HC (yellow curve) and SUL/ HC (red curve).**

The TGA thermograms under air of the parent ionosilica material **A** and the loaded samples after adsorption with **A-DCF-Na/HC**, **A-SUL-Na/HC** and **A-SUL/HC** are given in Figure 9. The thermogram of the pure ionosilica material **A** indicates that the material is stable up to ca. 180°C. The slight weight loss below 180°C can be ascribed to the desorption of physically adsorbed water. The chemical decomposition of the material starts at 200°C and ends at ca. 700°C. The product of this thermal decomposition is pure silica. For the pure material **A**, we observed a weight loss of 54.7%, which is slightly higher than the expected theoretical value (48.1%). This higher weight loss can be explained by incomplete condensation and the presence of silanol groups within the material after the hydrolysis polycondensation

procedure, resulting in additional elimination of water during the calcination process. Regarding the thermograms of the samples loaded with the anionic drugs **A-DCF-Na/HC** and **A-SUL-Na/HC**, we observed a significantly higher mass loss of 73.7% and 72,5%, respectively. This increase is due to the adsorption of considerable amounts of the anionic drugs. In fact, the maximal mass loss we can expect for complete anion exchange reaction is of 74.2% and 76.6% for the materials **A-DCF-Na/HC** and **A-SUL-Na/HC**, respectively. Taking into account the elimination of the organo-ionic group together with the anionic drug during the calcinations, we can estimate the mount of adsorbed drug to be of 90% in the case of **DCF-Na** and of 68% in the case of **SUL-Na** (Table 1, entries 1 and 2). The experimentally obtained values indicate once more that the ionosilica material adsorbs relatively high amounts of the anionic drugs **DCF-Na** and **SUL-Na**. In contrast, the thermogram of the sample **A-SUL/HC**, obtained from an adsorption of the neutral **SUL** compound, is similar to the original ionosilica material, thus indicating that sulindac in its neutral form is hardly adsorbed by the ionosilica material. This result is of considerable interest as it clearly indicates that the ionosilica material selectively adsorbs anionic species, whereas neutral compounds are not adsorbed. We can therefore conclude that the adsorption of drugs is driven by anion exchange.

In the case of the material **A-DCF-Na/LC**, obtained by contacting the ionosilica material **A** with a solution containing a considerably lower DCF concentration (*vide supra*), the thermogram shows a similar shape and similar weight loss compared to the parent material **A**. This result can be explained by the low quantity of the adsorbed diclofenac, which is too low to be detected *via* TGA.

### 2.3.4 UV-vis absorption and emission spectroscopy

Finally, we addressed the adsorption of the anionic drugs via spectroscopic analysis of the supernatant after the loading procedure. All these results are reported in Table 1, together with the results of the thermogravimetric analyses.

In order to determine the saturation limit of the ionosilica, we firstly contacted the material with a high amount of the anionic drugs diclofenac and sulindac. As previously described, a 30 mL of a 0.03 M solution of **DCF-Na** and sulndac **SUL-Na** (corresponding to a quantity of 0.9 mmol of diclofenac /sulindac) was treated with 0.3 g of the ionosilica. This quantity of the

material **A** contains approx. 0.86 mmol of immobilized ammonium entities. Hence, the used anionic drugs were used in slight excess related to the amount of cationic sites in the ionosilica material **A**. The characterization of the supernatant solutions after contacting with the material **A** showed that both diclofenac and sulindac, in their sodium salt form, are efficiently adsorbed by the ionosilica material. The upper saturation limit of material **A** for the adsorption of diclofenac and sulindac are 2.55 mmol/g and 1.59 mmol/g corresponding to 88% and 65% for **A-DCF-Na/HC** and **A-SUL-Na/HC**, respectively (Table 1, entries 1/2). Furthermore, we found that the neutral form of sulindac is not adsorbed by the ionosilica material **A**, thus confirming the results obtained by TGA (Table 1, entry 3). Once more, these results confirm that the separation process is driven by anion exchange. However, it has to be mentioned that the adsorption process, carried out in aqueous media, led to a complete collapse of the mesopore architecture of the material. As already described above, material **A** is a material displaying mesoporosity (average pore diameter: ~2nm, specific surface area: > 1000 $m^2/g$. After adsorption of **DCF-Na** and **SUL-Na**, the different resulting materials displayed considerably lower specific surface area and, in particular, no mesoporosity (see annex). The collapse of the mesopore architecture can be explained by rearrangements *via* reversible siloxane (Si-O-Si) opening and closing reactions.

**Table 1. Encapsulation efficiency (μ) and the adsorption capacity (mmol/g) of the prepared samples measured by different techniques**

| entry | Samples | UV/Vis Supernatant analysis [a] | | Thermogavimetric analysis [c] |
|---|---|---|---|---|
| | | Q (mmol/g) | μ (%) | μ (%) |
| **1** | **A-DCF-Na/HC** | 2.55 | 88 | 90 |
| **2** | **A-SUL-Na/HC** | 1.59 | 65 | 68 |
| **3** | **A-SUL/HC** | 0 | 0 | 0 |
| **4** | **A-DCF-Na/LC$_1$** | n.d. | 98 | - |
| **5** | **A-DCF-Na/LC$_2$** [b] | n.d. | 99 | - |

[a] analysis was carried out by UV-Vis absorption spectroscopy in the case of HC samples and by UV-Vis emission spectroscopy in the case of LC samples

[b] **DCF-Na/LC$_2$** was prepared by loading procedure using a low concentrated **DCF-Na** solution on **DCF-Na/LC$_1$** sample

% $\mu = (C_i-C_f)/C_i$ where $C_i$ is the initial diclofenac concentration, while $C_f$ is the diclofenac concentration after exchange with the material (24 hours).

Q = (mole of loaded drug / weight of the material)

[c] The encapsulation efficiency μ estimated by TGA was determined by the mass ratio as a percentage of anionic drug after loading and of chloride before loading compared to the mass molar ratio of the two compounds

$$\% \mu = \frac{((\%\ \text{mass of anionic drug after loading})/(\%\ \text{mass of chloride before loading}))}{(M_{\text{anionic drug}}/M_{\text{chloride}})}$$

Furthermore, to get an idea on the adsorption of DCF-Na on pure silica and the contribution of the ionic entities of ionosilica material, we performed the adsorption of DCF-Na on MCM-41 mesoporous silica.[30] Similarly to the experiments involving the ionosilica material **A**, the adsorption capacity was quantified using spectroscopic analysis of the supernatant after the loading and thermogravimetric analysis. We obtained 0.16 mmol/g by analyzing the supernatant using UV spectroscopy and 0.09 mmol/g by analyzing the complex drug/material by ATG (Figure 10 and Table 2). These results show that pure silica absorb diclofenac but at very low quantity compared with ionosilica material. Once again, the presence of cationic entities in the ionosilica material framework increased to a large extent the adsorption capacity of anionic drug.

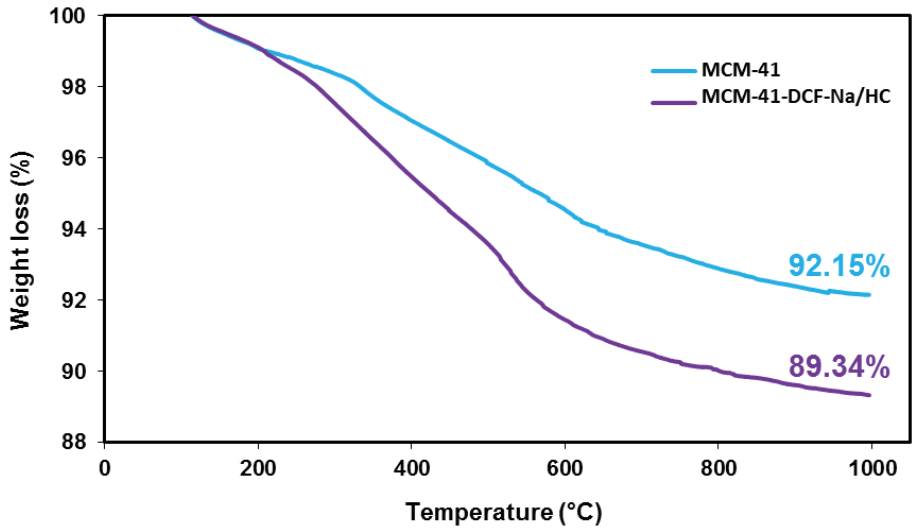


**Figure 10. Thermogravimetric analysis: silica material (blue curve), DCF/silica complex (purple curve).**

**Table 2. Adsorption capacity Q of silica measured by different techniques.**

| entry | Sample | UV/Vis Supernatant analysis [a] | Thermogavimetric analysis [b] |
|---|---|---|---|
| | | Q (mmol/g) [c] | Q (mmol/g) [c] |
| 1 | MCM-41-DCF-Na/HC | 0.156 | 0.088 |

$Q_{(uv)} = (C_{init} - C_{final})$/ weight of the material
where $C_{init}$ is the initial diclofenac concentration, while $C_{final}$ is the diclofenac concentration after 24 h exchange with the material.

$Q_{(ATG)}$ = [(weight loss of MCM-41) – (weight loss of MCM-41-DCF-Na)] / [(mass molar of DCF-Na)*(weight of the material)]

Finally, we studied the uptake ability of the ionosilica material **A** with highly diluted drug solutions. These studies are of particular importance as low concentrations of pollutants are more similar to real conditions in waste water bodies. For this purpose, we contacted the material twice with a $1.2 \cdot 10^{-5}$ M aqueous solution of **DCF-Na**, thus yielding the materials **DCF-Na/LC$_1$** (after the first contact) and **DCF-Na/LC$_2$** (after the second contact) Both procedures, involving the same material, led to an almost complete adsorption of the anionic drug onto the material (Table 1, entries 4 and 5). These results indicate the high affinity of the anionic drugs towards the ionosilicas and indicate that the material can be used as efficient anion trap even for low concentrations of pollutants. The material is therefore highly interesting for applications under real environmental conditions. As in the experiences involving solutions containing high drug concentrations, the adsorption of traces of anionic drugs led to a material displaying low porosity and no mesoporous contribution. The decrease of specific surface area after the adsorption process is therefore independent of the quantity of adsorbed drug, but is related to rearrangement reactions of the material in aqueous solution.

## 2.4 Release test experiments

In a last set of experiences, we addressed the release of the drugs from the ionosilica material. In this way, the material was characterized with regard to its adsorption/release performances and recyclability. The stability of the drug/ionosilica complex was verified by release test, which was carried out with the **A-DCF-Na/HC** sample using distilled water as solvent medium. The release was monitored over 32 h via UV-Vis absorption spectroscopies assessing that less than 3% of the loaded drug was released from the different complexes (see

annex for details). Release tests carried out in acidic media (hydrochloric acid, pH=3) with the same sample **A-DCF-Na/HC** gave similar results, thus proving the high stability of the drug-ionosilica system. These results can be both explained by the high affinity of the anionic drug towards the ionosilica material, and the trapping of the anionic compound within the material, *i.e.* the irreversible capture of the drug *via* the collapse of the mesoporous architecture of the adsorbent material.

## 3 Conclusion

In summary, we have demonstrated that nanostructured cationic ionosilicas bearing quaternary ammonium groups are efficient and re-usable adsorbents with high capacity and high selectivity towards to anionic drugs. The materials show high capacities up to 2.55 mmol/g. However, the capacity of the material depends on the nature of the studied adsorbent: the smaller and more hydrophilic sodium diclofenac **DCF-Na** is adsorbed in higher amount compared to the bigger and more hydrophobic sodium-sulindac **SUL-Na**. The ionosilica is a highly efficient adsorbent even for traces of anionic drugs, thus highlighting the high affinity of these compounds towards the material. In contrast, no adsorption was observed using the drugs in the acidic, neutral form. Finally, the high affinity of anionic species towards the ionosilica material was also monitored via drug release tests involving loaded samples. No significant drug release was observed after contacting the sample during 32h both with water or hydrochloric acid solution (pH=3). However, it has to be mentioned that these treatments led to a complete collapse of the pore structure of the material, and a completely non-porous material was recovered after these tests.

**References**


1. Luo, Y.; Guo, W.; Ngo, H. H.; Long Duc, N.; Hai, F. I.; Zhang, J.; Liang, S.; Wang, X. C., A review on the occurrence of micropollutants in the aquatic environment and their fate and removal during wastewater treatment. *Science of the Total Environment* **2014,** 473, 619-641.

2. Zhang, Y.; Geissen, S.-U.; Gal, C., Carbamazepine and diclofenac: Removal in wastewater treatment plants and occurrence in water bodies. *Chemosphere* **2008,** 73, (8), 1151-1161.

3. Rabiet, M.; Togola, A.; Brissaud, F.; Seidel, J.-L.; Budzinski, H.; Elbaz-Poulichet, F., Consequences of treated water recycling as regards pharmaceuticals and drugs in surface and ground waters of a medium-sized Mediterranean catchment. *Environmental Science & Technology* **2006,** 40, (17), 5282-5288.

4. Tang, W., The metabolism of diclofenac - Enzymology and toxicology perspectives. *Curr. Drug Metab.* **2003,** 4, (4), 319-329.

5. Walcarius, A.; Mercier, L., Mesoporous organosilica adsorbents: nanoengineered materials for removal of organic and inorganic pollutants. *Journal of Materials Chemistry* **2010,** 20, (22), 4478-4511.

6. Tanev, P. T.; Pinnavaia, T. J., Mesoporous silica molecular sieves prepared by ionic and neutral surfactant templating: A comparison of physical properties. *Chemistry of Materials* **1996,** 8, (8), 2068-2079.

7. Zhao, D. Y.; Feng, J. L.; Huo, Q. S.; Melosh, N.; Fredrickson, G. H.; Chmelka, B. F.; Stucky, G. D., Triblock copolymer syntheses of mesoporous silica with periodic 50 to 300 angstrom pores. *Science* **1998,** 279, (5350), 548-552.

8. Suriyanon, N.; Punyapalakul, P.; Ngamcharussrivichai, C., Mechanistic study of diclofenac and carbamazepine adsorption on functionalized silica-based porous materials. *Chemical Engineering Journal* **2013,** 214, 208-218.

9. Bui, T. X.; Choi, H., Adsorptive removal of selected pharmaceuticals by mesoporous silica SBA-15. *Journal of Hazardous Materials* **2009,** 168, (2-3), 602-608.

10. Bui, T. X.; Pham, V. H.; Le, S. T.; Choi, H., Adsorption of pharmaceuticals onto trimethylsilylated mesoporous SBA-15. *Journal of Hazardous Materials* **2013,** 254, 345-353.

11. Bui, T. X.; Kang, S. Y.; Lee, S. H.; Choi, H., Organically functionalized mesoporous SBA-15 as sorbents for removal of selected pharmaceuticals from water. *Journal of Hazardous Materials* **2011,** 193, 156-163.

12. Zhu, Y. F.; Shi, J. L.; Li, Y. S.; Chen, H. R.; Shen, W. H.; Dong, X. P., Storage and release of ibuprofen drug molecules in hollow mesoporous silica spheres with modified pore surface. *Microporous and Mesoporous Materials* **2005,** 85, (1-2), 75-81.
13. Lee, B.; Im, H. J.; Luo, H. M.; Hagaman, E. W.; Dai, S., Synthesis and characterization of periodic mesoporous organosilicas as anion exchange resins for perrhenate adsorption. *Langmuir* **2005,** 21, (12), 5372-5376.
14. Lee, B.; Bao, L. L.; Im, H. J.; Dai, S.; Hagaman, E. W.; Lin, J. S., Synthesis and characterization of organic-inorganic hybrid mesoporous anion-exchange resins for perrhenate (ReO4-) anion adsorption. *Langmuir* **2003,** 19, (10), 4246-4252.
15. Petrova, M.; Guigue, M.; Venault, L.; Moisy, P.; Hesemann, P., Anion selectivity in ion exchange reactions with surface functionalized ionosilicas. *Physical Chemistry Chemical Physics* **2015,** 17, (15), 10182-10188.
16. Zhu, L.; Zhang, C.; Liu, Y.; Wang, D.; Chen, J., Direct synthesis of ordered N-methylimidazolium functionalized mesoporous silica as highly efficient anion exchanger of Cr(VI). *Journal of Materials Chemistry* **2010,** 20, (8), 1553-1559.
17. Idris, S. A.; Alotaibi, K. M.; Peshkur, T. A.; Anderson, P.; Morris, M.; Gibson, L. T., Adsorption kinetic study: Effect of adsorbent pore size distribution on the rate of Cr (VI) uptake. *Microporous and Mesoporous Materials* **2013,** 165, 99-105.
18. Yoshitake, H.; Yokoi, T.; Tatsumi, T., Adsorption of chromate and arsenate by amino-functionalized MCM-41 and SBA-1. *Chemistry of Materials* **2002,** 14, (11), 4603-4610.
19. Ciriminna, R.; Hesemann, P.; Moreau, J. J. E.; Carraro, M.; Campestrini, S.; Pagliaro, M., Aerobic oxidation of alcohols in carbon dioxide with silica-supported ionic liquids doped with perruthenate. *Chem.-Eur. J.* **2006,** 12, (20), 5220-5224.
20. Motos-Perez, B.; Roeser, J.; Thomas, A.; Hesemann, P., Imidazolium-functionalized SBA-15 type silica: efficient organocatalysts for Henry and cycloaddition reactions. *Applied Organometallic Chemistry* **2013,** 27, (5), 290-299.
21. Nguyen, T. P.; Hesemann, P.; Tran, T. M. L.; Moreau, J. J. E., Nanostructured polysilsesquioxanes bearing amine and ammonium groups by micelle templating using anionic surfactants. *Journal of Materials Chemistry* **2010,** 20, (19), 3910-3917.
22. El Hankari, S.; Motos-Perez, B.; Hesemann, P.; Bouhaouss, A.; Moreau, J. J. E., Periodic mesoporous organosilica from zwitterionic precursors. *Chemical Communications* **2011,** 47, (23), 6704-6706.
23. Nguyen, T. P.; Hesemann, P.; Moreau, J. l. J. E., i-Silica: Nanostructured silica hybrid materials containing imidazolium groups by hydrolysis-polycondensation of disilylated bis-

N,Nâ€²-alkyl-imidazolium halides. *Microporous and Mesoporous Materials* **2011,** 142, (1), 292-300.

24. Nguyen, T. P.; Hesemann, P.; Thi, M. L. T.; Moreau, J. J. E., Nanostructured polysilsesquioxanes bearing amine and ammonium groups by micelle templating using anionic surfactants. *Journal of Materials Chemistry* **2010,** 20, (19), 3910-3917.

25. El Hankari, S.; Motos-Perez, B.; Hesemann, P.; Bouhaouss, A.; Moreau, J. J. E., Pore size control and organocatalytic properties of nanostructured silica hybrid materials containing amino and ammonium groups. *Journal of Materials Chemistry* **2011,** 21, (19), 6948-6955.

26. Saha, A. K.; Ray, S. D., Effect of cross-linked biodegradable polymers on sustained release of sodium diclofenac-loaded microspheres. *Brazilian Journal of Pharmaceutical Sciences* **2013,** 49, (4), 873-888.

27. Bratu, I.; Astilean, S.; Ionesc, C.; Indrea, E.; Huvenne, J. P.; Legrand, P., FT-IR and X-ray spectroscopic investigations of Na-diclofenac-cyclodextrins interactions. *Spectrochimica Acta Part a-Molecular and Biomolecular Spectroscopy* **1998,** 54, (1), 191-196.

28. Ramachandran, E.; Ramukutty, S., Growth, morphology, spectral and thermal studies of gel grown diclofenac acid crystals. *Journal of Crystal Growth* **2014,** 389, 78-82.

29. Griffith, P. R., *Introduction to Vibrational Spectroscopy*. John Wiley & Sons Ltd.: New York, 2006.

30. Beck, J. S.; Vartuli, J. C.; Roth, W. J.; Leonowicz, M. E.; Kresge, C. T.; Schmitt, K. D.; Chu, C. T. W.; Olson, D. H.; Sheppard, E. W.; McCullen, S. B.; Higgins, J. B.; Schlenker, J. L., A NEW FAMILY OF MESOPOROUS MOLECULAR-SIEVES PREPARED WITH LIQUID-CRYSTAL TEMPLATES. *Journal of the American Chemical Society* **1992,** 114, (27), 10834-10843.

# Part II

## Biocompatible periodic mesoporous ionosilica nanoparticles with ammonium walls, application to drug delivery

## Summary

# 1 Introduction

The development of original methods for efficient and targeted drug delivery is still a major challenge in nanomedecine. The elaboration of various types of nanometric drug carrier vehicles is currently a field of intense research activity[1-4] and various organic or inorganic materials have been prepared as theranostic agents such as polymers, palladium, iron, gold and silica.

In the area of functional silica materials, Periodic Mesoporous Organosilicas (PMO) materials were independently introduced in the year 1999 by the research groups Inagaki, Ozin and Stein.[5-7] These materials are obtained by template directed hydrolysis-polycondensation procedures starting from di- or oligosilylated organic precursors in the presence of structure directing agents and in absence of a silica source (*e.g.* tetraethyl-*ortho*-silicate, TEOS). A large variety of bulk PMO materials was synthesized from a wide variety of organosilica precursor in the meantime.[8]

Reaching the nanoscale with PMO materials is still a major challenge, [9, 10] as examples of PMO nanoparticles are scarce. In 2006, Lu *et al.* reported for the first time hollow PMO nanospheres with 100-400 nm of diameter.[11] The preparation of aqueous colloidal mesoporous nanoparticles was only reported in 2011 by the Kuroda group.[12] In 2012, Guan *et al.* reported the first ordered and monodisperse PMO nanoparticles with cage-type and cylindrical mesostructures.[10] The approach of combining a homogenous dispersion of the organic groups within nanoparticles of controlled size and texture offers the possibility to control the interfacial, chemical and physico-chemical properties of these objects. [9, 13] For this reason, PMO nanoparticles appear as original nanoobjects with tunable surface properties which offer new perspectives in catalysis[14] and nanomedecine.[9, 13, 15]

As described in the introduction chapter, ionosilicas are defined as periodic mesoporous organosilicas constituted of ionic building blocks, recently emerged as a new family of functional materials.[19-21] Ionosilicas combine high porosity, regular architecture on the mesoscopic level with an unmatched chemical versatility, induced by the high variability and the high number of homogeneously distributed ionic species.[22]

However ionosilicas were only available in bulk at the macroscopic scale. In this thesis we performed the synthesis of ionosilica nanoparticles with uniform and homogeneous particle size. This new form of ionosilica is essentially interesting for the application in several domains such as nanocatalysis, imaging and nanomedecine. We describe here in particular the synthesis of

ionosilica nanoparticles bearing ammonium substructures using a binary surfactant system. These ionosilica nanoparticles were then used as nano-carriers for the vehiculation of anti-inflammatory (sodium diclofenac).

## 2 Synthesis of ionosilica nanoparticles by Stöber method

In this thesis, the goal is the synthesis of ionosilica nanoparticles with controlled morphology and texture. For the application in biomedical purpose, synthesis of particles with size less than 200 nm is highly desired.[9, 13] Hereafter, the influence of synthesis conditions such as: precursor and surfactant quantity, temperature, catalyst and control of hydrolysis / condensation reactions are discussed and optimized.

At first glance, we tried to synthesize bridged polysilsesquioxane (BPS) nanoparticles from ionic precursor following Stöber method. The synthesis was catalyzed using ammonia and without surfactant. After varying the precursor concentration and the ammonia, we were able to obtain nanoparticles with 100-150 nm diameter size. But after 4 h aging, the nanoparticles suspensions condense and form a bulk gel. When the nanoparticles were recovered by centrifugation directly after the synthesis we obtained a rigid solid. As a result, in both cases the nanoparticles tend to agglomerate and form micrometric aggregates. These results suggest that the particles as formed are highly condensed. Therefore we obtained a bulk BPS gel of identical chemical composition.
Secondly, we used an anionic surfactant to generate porosity and also to avoid the aggregation. This synthesis was in the same condition as PBS nanoparticles. The only change is the addition of an anionic surfactant and consequently the formation of lyotropic phase. In this case also, we obtained nanoparticle agglomeration after aging of 4 h. The nanoparticles suspension transforms to a gel after 15 hours.

The obtained results show that in the presence of surfactant or not, the nanoparticles tend to aggregate and form bulk BPS gel (Figure 1). This behavior was previously observed by Shea *et al.*[28] by using a hydrophilic organic silylated precursor.

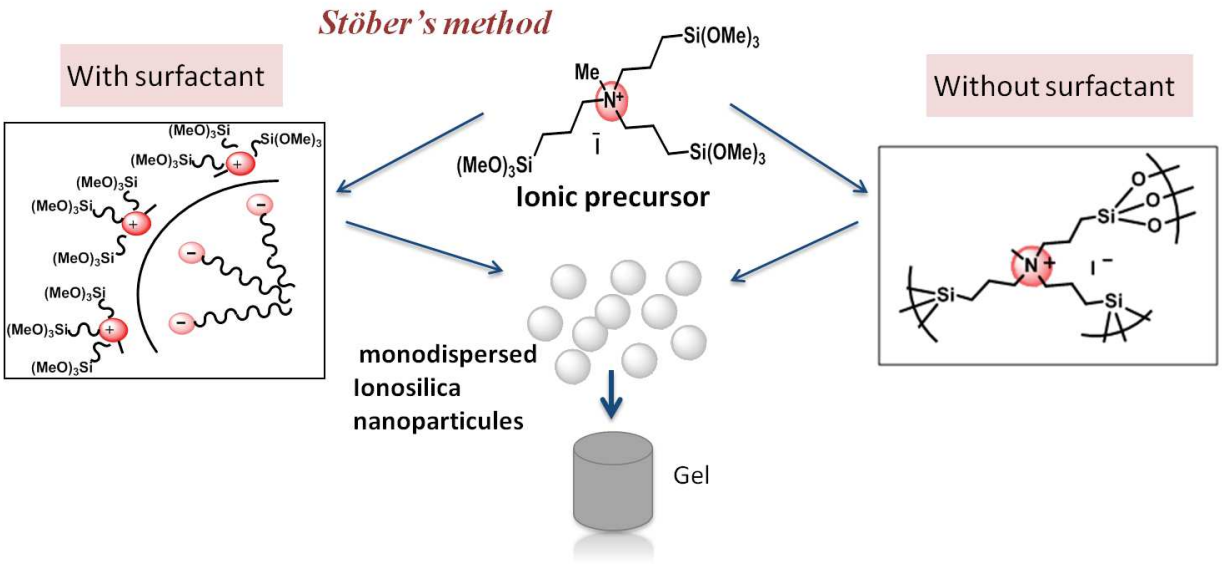


**Figure 1. Illustration of the formation of bulk gel by the agglomeration of silsesquioxane nanoparticles**

Models used to discuss the growth of silica particles under Stöber conditions may help to explain these results. There are two well-accepted particle growth models for the process; "monomer addition"[29] and "controlled aggregation".[30-32] The condensation of partially hydrolyzed soluble monomers results in nucleation. In the first model, the particle grows only by addition of hydrolyzed monomers to surface $Si\text{-}O^-$ groups. In the latter model, once the particles have reached a certain size, the growth is only by aggregation *see* Figure 2. In the SEM images, the spheres appear to be composed of smaller nanoparticles with diameters approximately 5-10 nm, suggesting that the "controlled aggregation" model may be important for the growth of silsesquioxane nanoparticles.

In our case, the nanoparticle growth model is proposed. This is supported by the fact that the nanoparticles size increase with time aging.

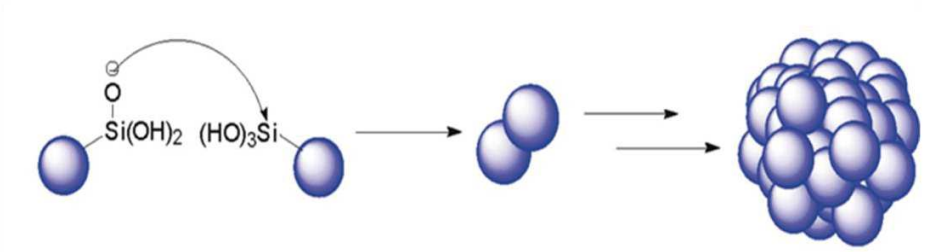


**Figure 2. Mechanism for particle growth.**

## 2.1 Surface recovery system

To avoid this particle agglomeration and prevent the particles bridging, a surface recovery system was here applied. For this purpose, we used a binary surfactant system (ionic surfactant / nonionic surfactant). The ionic surfactant acts a template to generate porosity and the nonionic surfactant recovers the surface particle. This method was reported by Imai *et al.*[33] A cationic surfactant (CTAB) in combination with a co-polymer triblock surfactant (F127) were used with TEOS as silica source under basic condition. Small mesoporous silica nanoparticles with hexagonal pore architecture were obtained. The results demonstrate that the presence of F127 decrease the particle size and avoid agglomeration.

In our study, the formation of surfactant / precursor ion pairs is crucial to generate porosity. For this reason we used an anionic surfactant (SHS, sodium hexadecyl sulfate) for the mesostructuring and nonionic surfactant (F127, triblock copolymer) for the particle recovery. The synthesis was performed following a modified Stöber method. An ammonium precursor was used in the presence of ammonia as a catalyst.

DLS measurements indicate the formation of monodispersed nanoparticles with diameter size of 100 - 200 nm (Figure 3-a). TEM images show particle size of less than 100 nm (Figure 3-b). After 10 hours aging the particle size did not change. These results show clearly that the presence of the co-polymer triblock prevents the particles bridging and condensation.

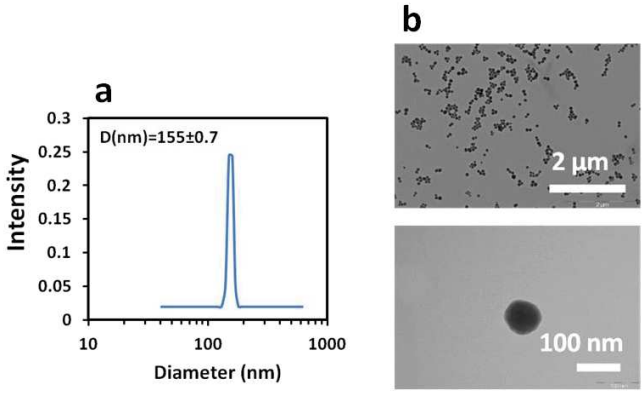


**Figure 3. a) DLS measurement (ethanol as solvent) b) TEM images of the formed ionosilica nanoparticles by binary surfactant system after 15 h aging.**

The mechanism for the inhibition of particles' agglomeration is illustrated in Figure 4 and can be explained as follow: First, there is formation of precursor / surfactant ion pairs by electrostatic interaction between the anionic surfactant head groups with the cationic sites of the precursor. In the second step, the grain agglomeration was inhibited by the addition of a nonionic surfactant (F127) which recovers the surface of the primary nanoparticles via hydrogen bonding.

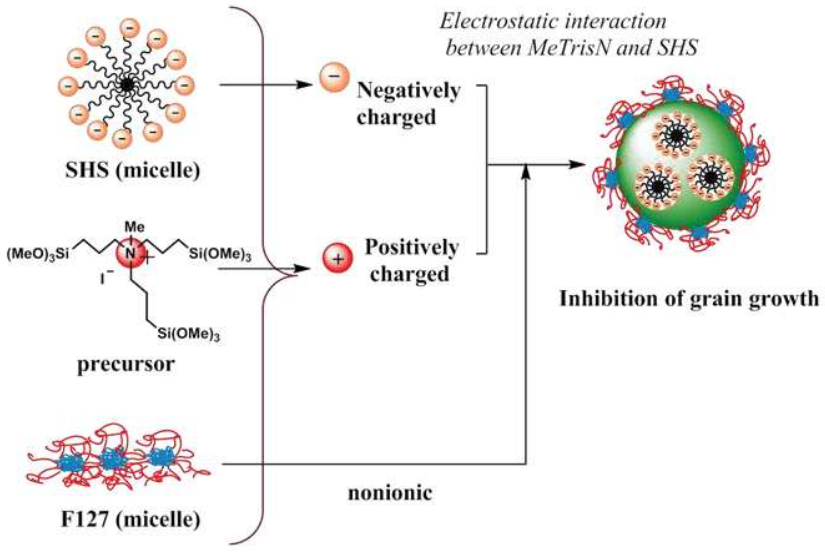


**Figure 4. Synthesis process of ionosilica nanoparticles via binary surfactant system.**

After having ascertained the formation of the nanoparticles, we proceed to the washing and surfactants extraction step. The as-synthesized nanoparticles were isolated by centrifugation and washed with ethanol. For the surfactants extraction we used an acidic ethanol solution hydrochloric acid at 2 M (HCl/ ethanol). However the extraction step involves an increase in the particle size. DLS measurements show that particles diameter increase from 100-150 nm to 250-350 nm. These results suggest that there is at least an agglomeration of two particles. To avoid this association, we used ammonium chloride $NH_4Cl$ ethanol solution for the surfactant extraction. Using this salt, we observed that the particle size did not change during extraction.

## 2.2 Synthesis optimization

Using the binary surfactant system we were able to synthesize nanoparticles with diameter size less than 200 nm. Then the synthesis was optimized to control the morphology, size and texture properties. Here different synthesis parameters were studied such as:

- Quantity of surfactants.
- Stirring rate.
- Hydrolysis / condensation reactions.
- Effect of F127.

A synthesis model is described as follows: a suitable amount of the anionic surfactant (SHS) was dissolved in 30 ml of water at 70°C for 1 hour. After the complete surfactant dissolution, 600 µl of ammonia ($NH_4OH_{aq}$) at 0.1 M was then added to the mixture followed by 10 mg of F127 under stirring. To this solution, an ammonium precursor solution (200 mg of MeTrisN with 2 ml of PrOH) was added drop by drop. The solution mixture was let to stir for 15 h at 70°C.

### 2.2.1 Effect of SHS Concentration, stirring rate and F127 concentration

In our case, the further desired use of these nanoparticles is for drug delivery as the basis of nanodevices. For the absorption of drugs within the nanoparticle, the porosity is highly desired. Here, we will show the effect of the quantity of surfactant and stirring rate on the specific surface area of the formed nanoparticles.

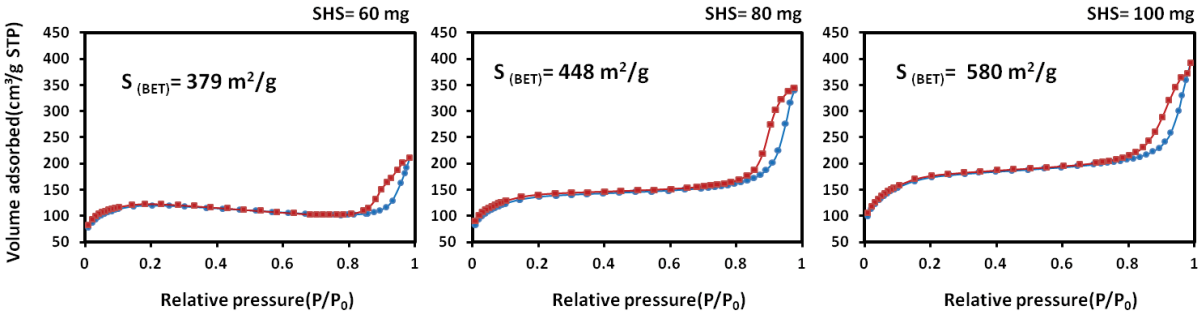


**Figure 5. Nitrogen adsorption desortion isotherms of the synthesized nanoparticles with the variation of the SHS quantity 60, 80 and 100 mg corresponding to the surfactant/precursor molar ratio of 0.61, 0.75 and 1.**

Firstly, we synthesized nanoparticles with increasing the quantity of anionic surfactant (SHS) at fixed stirring rate of 700 rpm. The amounts of SHS were: 60, 80 and 100 mg corresponding to the surfactant / precursor molar ratio of 0.61, 0.75 and 1. In all these cases, the concentration of SHS was up then 10 times the critical micelle concentration ($CMC_{(SHS)}$ = 5.5 $10^{-4}$ M).[34] Nitrogen adsorption – desorption measurements were used in order to investigate the effect of the surfactant concentration on the textural properties of the as- synthesized nanoparticles. The nitrogen sorption isotherms are shown in Figure 5. All the curves display an isotherm of type IV, an adsorption at low relative pressure in the range of $P/P_0$ = 0.14-0.2. These adsorption indicates that the nanoparticles contain relatively small pores (supramicro-porosity).[35, 36] Furthermore at high pressure, a hysteresis loop $H^1$ was observed indicating the intergranular porosity. For the nanoparticles synthesized with surfactant amount of 60, 80 and 100 mg we obtained 379, 448 and 580 $m^2/g$ of BET specific surface area respectively (Figure 5). These results show that when the surfactant / precursor molar ratio increases the BET surface area increases. A maximum was obtained with nanoparticles synthesized with equimolar surfactant / precursor ratio. This can be explained by the fact that the formation of nanostructured ionosilicas involves the formation of defined precursor / surfactant ion pairs. The organo-ionic group of the silylated precursor promotes the structuration process during the template directed hydrolysis-polycondensation reaction.

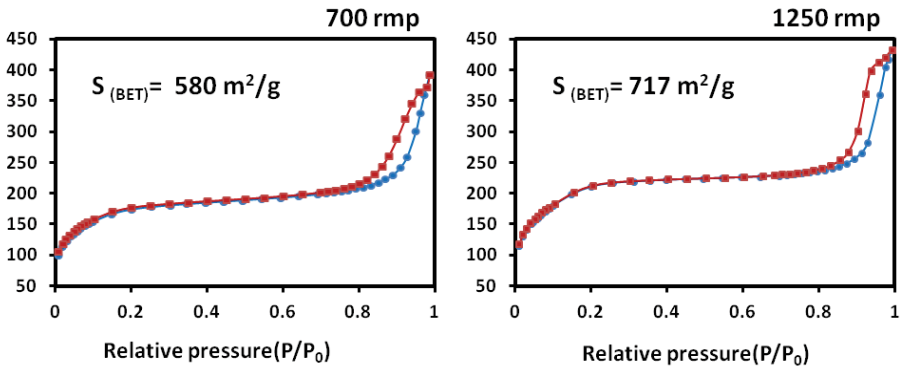


**Figure 6. Nitrogen sorption isotherms of ionosilica nanoparticles synthesized wit different stirring rate.**

It is well known that the stirring rates have a large effect on the nanoparticle polydispersity and diameter size, [37, 38] even on the specific surface area. In our study, the stirring rate was found to be a key parameter to control the specific surface area of the nanoparticles. Figure 6 gives the nitrogen isotherms of ionosilica nanoparticles synthesized in a binary surfactant system with 100 mg of SHS at two different stirring rates at 700 and 1250 rpm. At 700 rpm we obtained nanoparticles with $S_{BET}$ = 580 $m^2/g$ but when increasing the stirring rate to 1250 rpm, we observed an increase in the specific surface area to 717 $m^2/g$.

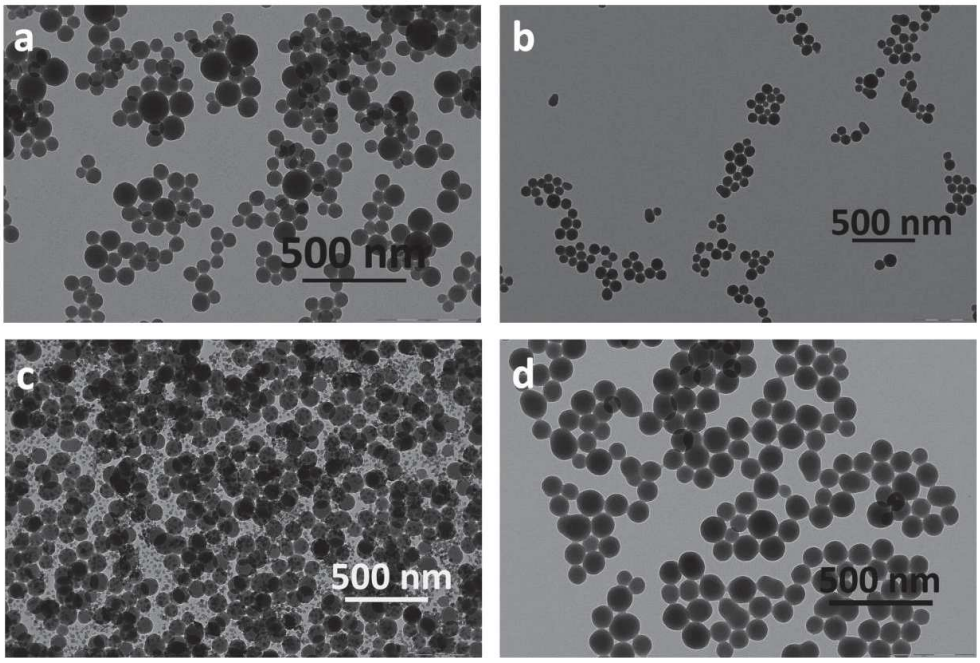


**Figure 7. TEM images of the ionosilica nanoparticles with the variation of the amount of F127:** a) 10 mg, b) 20 mg, c) 40 mg, d) 60 mg.

After the determination of the suitable amount of SHS and the stirring rate, we studied the effect of F127 concentration on the particle size and morphology. The nanoparticles were prepared with 100 mg of SHS at 1250 rpm stirring rate. The concentration of F127 was varied in the range of 24.3, 48.7, 97.4 and 146 mM corresponding to 10, 20, 40 and 60 mg respectively. TEM images (Figure 7) show that there is no a drastic variation in the particle size. The diameter sizes were 82.4, 77.2, 103.2 and 110.7 corresponding to 10, 20, 40 and 60 mg respectively (Figure 8). These results show that at very high amount of F127 the particle size increases slightly. The smaller particle size obtained is with 20 mg of F127.

Our results are completely different in comparison with mesoporous silica nanoparticle synthesized in binary surfactant system.[38, 39] Kim et al.,[38]reported that the increase of the F127 amount, the average particle size decrease from 500 to 70 nm.

In our case, the reason for increasing particle size by F127, is still unclear and also demands further investigation.

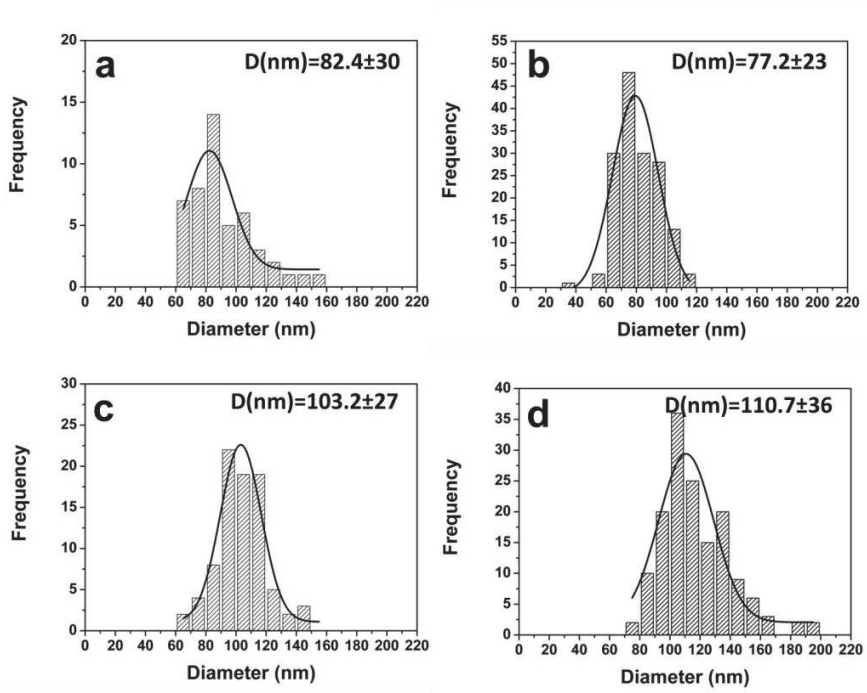


**Figure 8. Particle size distribution of the ionosilica nanoparticles with the variation of the amount of F127 obtained by TEM**: a) 10 mg, b) 20 mg, c) 40 mg, d) 60 mg.

### 2.2.2 Effect of the synthesis conditions on particles formation

After having established the amount of surfactants, precursor and the stirring speed, we will discuss, in the following section, two parameters in the formation of ionosilica nanoparticles. Firstly, we studied the effect of hydrolysis / condensation reactions on the particle formation. In one synthesis, the hydrolysis and condensation of the precursor were performed simultaneously by adding the ammonia in the reaction medium before the precursor; resulting nanoparticles called **$NP_{is}$-A**. In the other, we started by the precursor hydrolysis followed by the condensation step and this was achieved by adding ammonia after the precursor in the reaction medium; resulting nanoparticles called **$NP_{is}$-B**. Secondly, a study on the surface recovery of nanoparticles was then performed to verify the effect of the addition of F127 before or after particles formation. It is noted that, for **$NP_{is}$-A** and **$NP_{is}$-B** samples, the F127 was added after particles formation. The sample called **$NP_{is}$-C** was synthesized in the same condition as **$NP_{is}$-B** but the F127 was added before particles formation.

All these samples (**$NP_{is}$-A, $NP_{is}$-B** and **$NP_{is}$-C**) were characterized by several techniques: electron microscopy (TEM), scanning electron microscopy (SEM), dynamic light scattering (DLS) and nitrogen sorption.

In the following, we will discuss separately these two parameters.

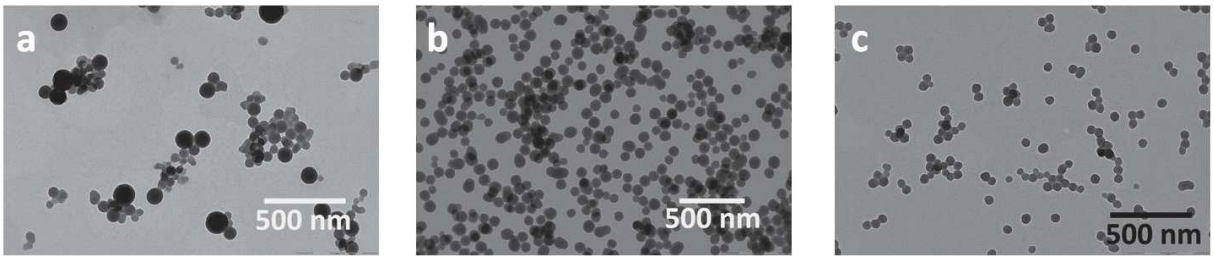


**Figure 9. TEM images of a). $NP_{is}$-A, b). $NP_{is}$-B and c). $NP_{is}$-C.**

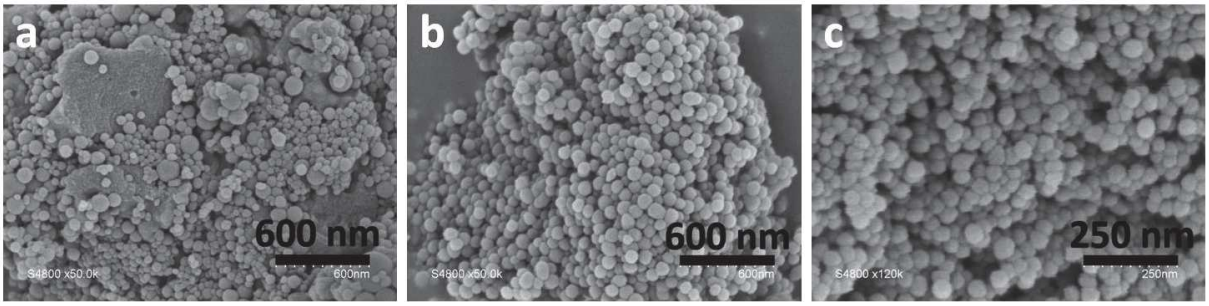


**Figure 10. SEM images of a). $NP_{is}$-A, b). $NP_{is}$-B and c). $NP_{is}$-C.**

About the first parameter (the effect of hydrolysis / condensation reactions on the nanoparticles formation). TEM and SEM images (Figure 9-a, b and Figure 10-a, b) correspond to **$NP_{is}$-A** and **$NP_{is}$-B** samples respectively. In the case of **$NP_{is}$-A** sample, the nanoparticles were not uniform. The diameter size was from 20 nm to 160 nm. In contrast, for **$NP_{is}$-B** sample, the particles were homogeneous with diameter size centered at ~ 87 nm (Figure 11-a, b). The dynamic light scattering gives a diameter size of ~ 190 nm for **$NP_{is}$-A** and ~ 136 nm for **$NP_{is}$-B** *see* Figure 12-a and b respectively. These diameters are larger than those given by TEM. This is due to the presence of the surrounding solvent and some particles agglomeration. Usually, the hydrodynamic diameter is larger than particle diameter given by TEM or SEM. Moreover, we observed that the hydrodynamic diameter of **$NP_{is}$-A** is higher than of **$NP_{is}$-B**. These results show that the hydrolysis of the precursor before the adding of ammonia, and consequently the condensation step, gives smaller and homogenous particles.

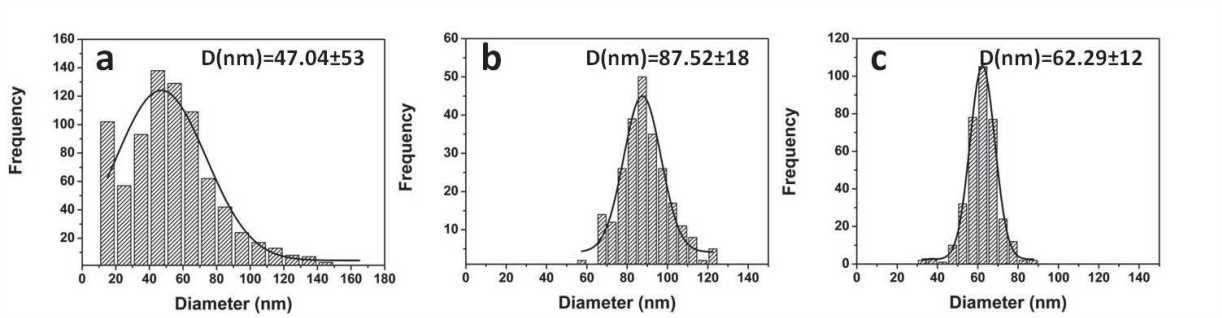


**Figure 11. Particle size distribution obtained by TEM of a). $NP_{is}$-A, b). $NP_{is}$-B and c). $NP_{is}$-C.**

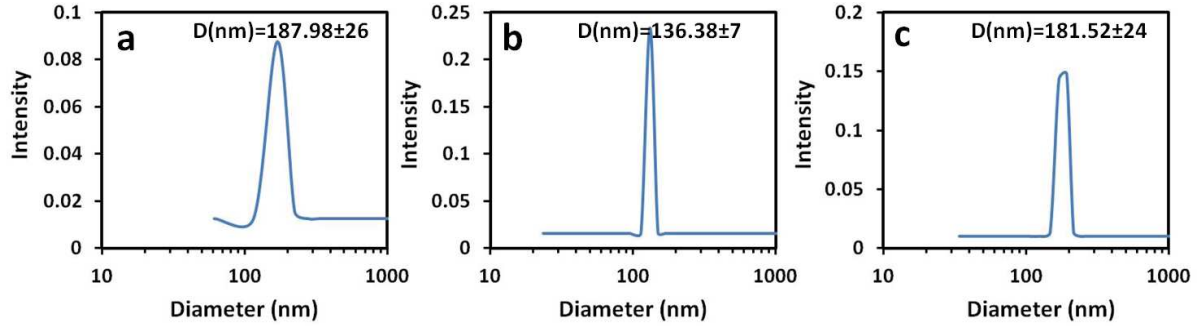


**Figure 12. Particle size distribution obtained by DLS of a). $NP_{is}$-A, b). $NP_{is}$-B and c). $NP_{is}$-C.**

The nitrogen sorption measurements were then carried out on **$NP_{is}$-A** and **$NP_{is}$-B** nanoparticles. The isotherm obtained from **$NP_{is}$-A** (Figure 13-a) shows a warm-like type 4 in which the adsorption and the desorption branches did not coincide. This behavior can be explained by the

presence of organic moieties in the material framework making it less rigid and morphologically less stable. The specific surface area $S_{BET}$ was about of 121 $m^2/g$.

In the case of **$NP_{is}$-B**, we observed an isotherm of type 4 as shown in Figure 13-b. The template signature can be observed around 0.2 relative pressures. Furthermore, the curve displays an additional capillary adsorption at high relative pressures, which can be attributed to the intergrain porosity. The specific surface area $S_{BET}$ of **$NP_{is}$-B** was 310 $m^2/g$. This value is larger than for **$NP_{is}$-A** sample**.** Once again, the results of nitrogen sorption indicate that the separation of the two reaction hydrolysis and condensation steps give different results. Thus the precursor pre-hydrolysis before adding the ammonia gives better results on nanoparticles formation.

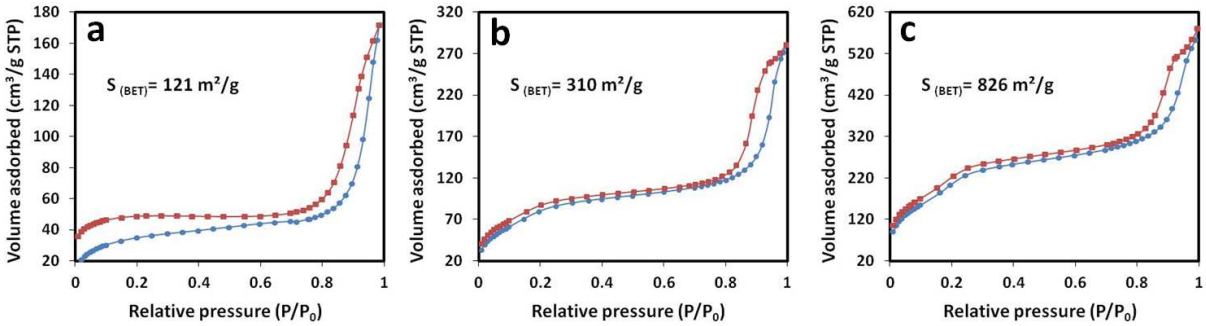


**Figure 13. Nitrogen sorption isotherms of a). $NP_{is}$-A, b). $NP_{is}$-B and c). $NP_{is}$-C.**

Regarding the second parameter (the effect of the addition of F127 before or after particles formation), TEM and SEM images (Figure 9-c and Figure 10-c respectively) give an average diameter of ~62 nm for **$NP_{is}$-C**, smaller than for **$NP_{is}$-B** (~87 nm) (Figure 11-c). All these observations show that the adding of F127 before particle formation decreases the nanoparticles diameter size. DLS measurement shows 180 nm diameter sizes for **$NP_{is}$-C**. We observed that the hydrodynamic diameter of **$NP_{is}$-C** was bigger than **$NP_{is}$-B** (Figure 12-c). This can be explained by the fact that there is some particles agglomeration.

Finally, the nitrogen sorption gives a concordance result, the adsorption - desorption isotherms (Figure 13-c) of **$NP_{is}$-C** have the same behavior as for **$NP_{is}$-B**. The specific surface area $S_{BET}$ is about 826 $m^2/g$. This value is more than two times higher than **$NP_{is}$-B**. These results suggest that the adding of F127 before particle formation gives higher surface area and low particle size.

According to these results, we selected the **$NP_{is}$-C** synthesis condition. We obtained particles with diameter size of about 64 nm with high specific surface area up to 800 $m^2/g$.

### 2.2.3 Effect of the ammonia concentration

Previous study on the effect of ammonia on particles size variation was reported. Gua *et al.*[10] reported ethylene–PMO nanoparticle in which they observed a decrease in particles size when the ammonia concentration varied from 2.2 M to 0.14 M. Ikari *et al.*[40] observed the same behavior on the synthesis of silica nanoparticles using the binary surfactant system.

Here, we studied the variation of ammonia amount for the control of particle size. We choose **$NP_{is}$-C** synthesis condition and we varied the ammonia concentration of the reaction medium. The amount of ammonia ($NH_4OH_{aq}$) at 0.1 M concentration was varied as follow: 450, 600, 800 µl and 1, 1.4, 1.8 ml resulting to **$NP_{is}$-D- a, b, c, d, e, f** respectively. TEM images (Figure 14 and Figure 15) show that the particle size did not change considerably. The range size was ~ 81, 56, 84, 88, 74, 57 nm for **$NP_{is}$-D- a, b, c, d, e, f** respectively. In general, the particle size decreases from ~ 80 to ~ 50 nm with increasing the ammonia concentration. Except with 600 µl, the size was found to be 56 nm and did not follow the same behavior.

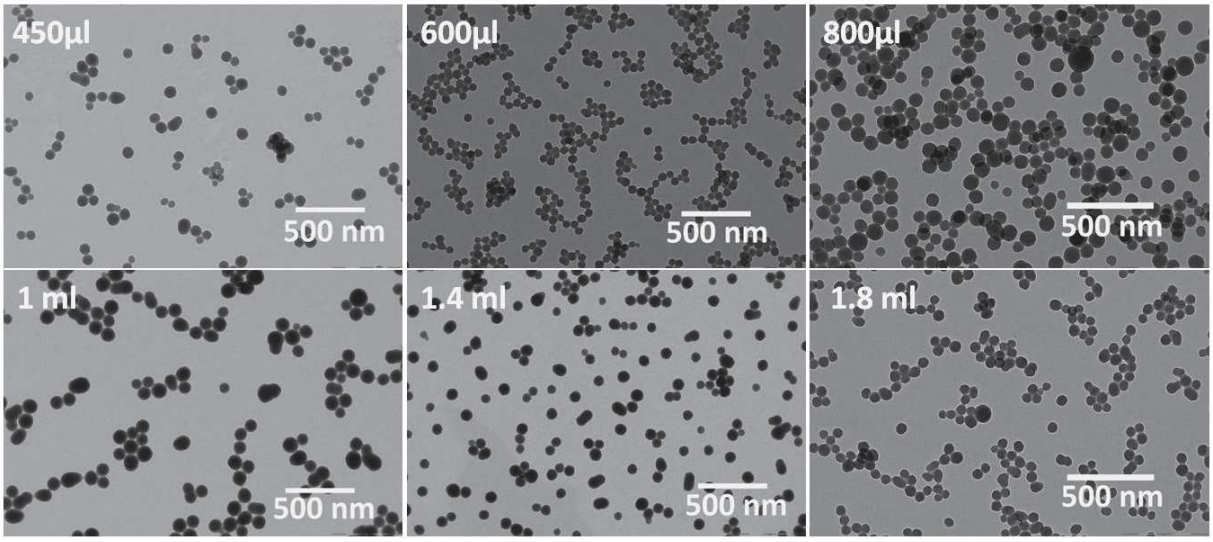


**Figure 14. TEM images of ionosilica nanoparticles with the variation of the amount of ammonia solution at 0.1 M**: 450, 600, 800 µl and 1, 1.4, 1.8 ml.

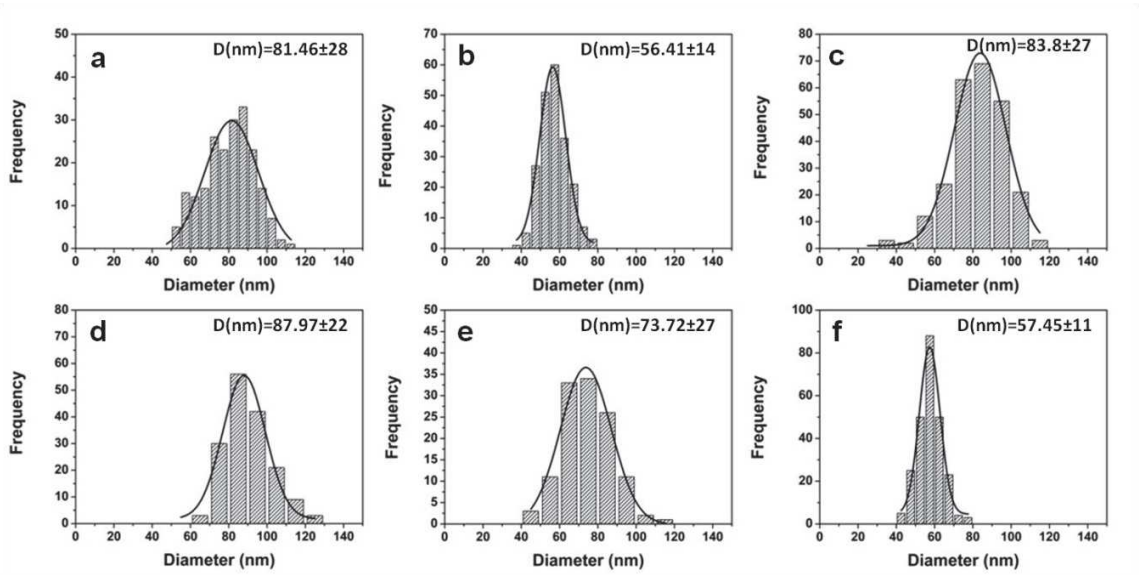


**Figure 15. Particle size distribution obtained by TEM of ionosilica nanoparticles as a function ammonia quantity:** 450, 600, 800 µl and 1, 1.4, 1.8 ml corresponding to a, b, c, d, e, f

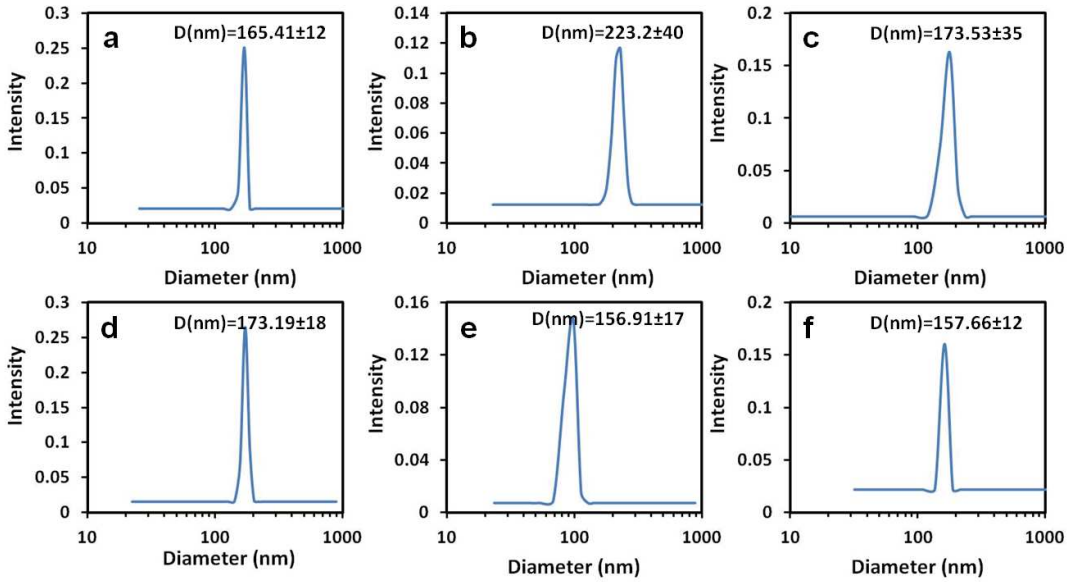


**Figure 16. Particle size distribution obtained by DLS of ionosilica nanoparticles as a function ammonia quantity**: 450, 600, 800 µl and 1, 1.4, 1.8 ml corresponding to a, b, c, d, e, f

The hydrodynamic diameters of **$NP_{is}$-D- a, b, c, d, e, f** samples (Figure 16) were measured using DLS. The observed hydrodynamic diameters are less than 250 nm in all cases and display slightly larger diameters than those observed in the corresponding TEM images. This can easily be

understood as the hydrodynamic diameters are generally larger than the core particle sizes observed by TEM.

Finally, the surface properties of the **$NP_{is}$-D- a, b, c, d, e, f** samples were determined via nitrogen sorption. The different nitrogen sorption isotherms are given in Figure 17. All the nitrogen sorption isotherms show type 4 isotherm. A rapid increase in the adsorption branches was observed at low relative pressures ($P/P_0$), indicating that the nanoparticles contain relatively small pores.[35] Each sample displays an additional capillary condensation of $N_2$ at high relative pressures ($P / P_0 > 0.90$), These phenomena can be attributed to the intergrain porosity. Specific surface area $S_{BET}$ with ammonia concentration increase did not present a linear change. We observed that the surface area increases as the particle size decreases.

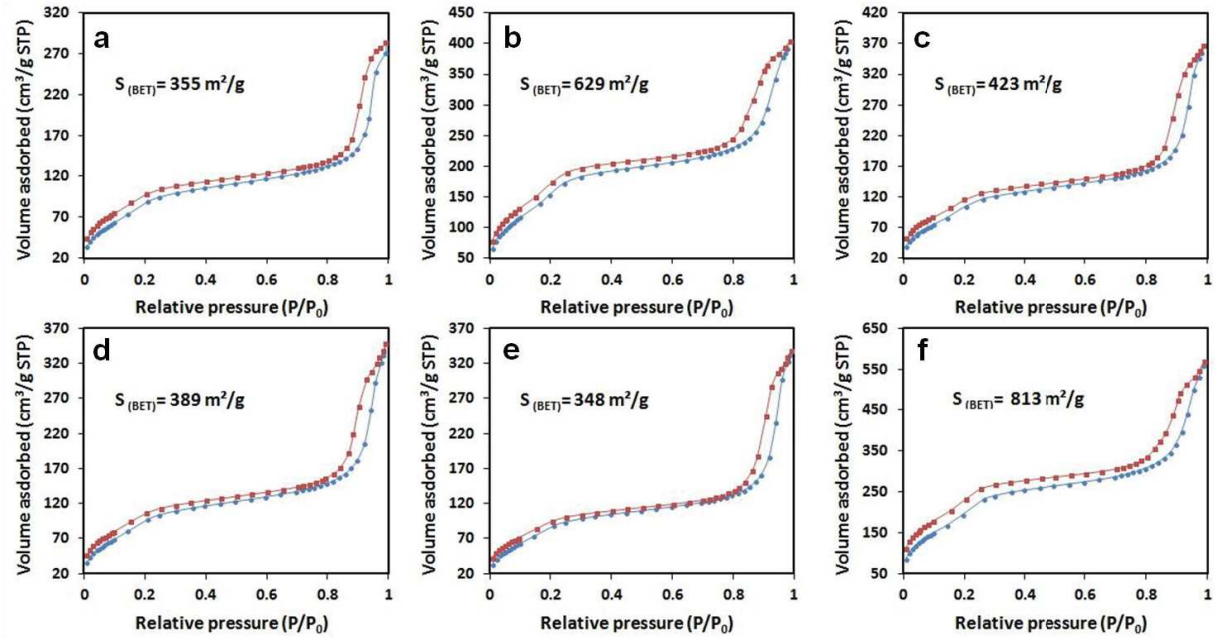


**Figure 17. Nitrogen sorption isotherms of ionosilica nanoparticles as a function ammonia quantity**: 450, 600, 800 µl and 1, 1.4, 1.8 ml corresponding to a, b, c, d, e, f

To summarize, we studied the variation of several parameters in order to optimize and control the size and textural properties of nanoparticles. The results are as following:

- The increase of SHS surfactant concentration induces the increase of the nanoparticles specific surface area. The maximum was reached with nanoparticles synthesized using an equimolar surfactant / precursor ratio.
- The stirring rate was observed to be a key parameter on the nanoparticles specific surface area.
- The separation of precursor hydrolysis and condensation steps yields to well polydispersed nanoparticles.
- The variation of F127 concentration did not affect the nanoparticle's shape. In contrast, the nanoparticles diameter size changes.
- The adding of F127, in the reaction medium before the particle formation, yields to smaller nanoparticles diameter size together with highest specific surface area than the sample prepared with adding F127 after particle formation.
- Finally, we observed that the variation of the amount of ammonia did not affect the particles size considerably and did not change linearly. However, we observed an increase of specific surface area $S_{BET}$ as the particles size decreases.

## 3 Synthesis of ionosilica nanoparticles for the biomedical application

The study of different synthesis parameters for the control of textural and morphological properties enabled us to synthesize nanoparticles with size of the order of 100 nm with an important surface property. As already described, the ultimate aim of this study is to synthesize particles containing ammonium group for use in the field of drug delivery.

In the following to improve the biocompatibility of the nanoparticles, a silyl PEG was added in the end of the synthesis. A complete study on the different characterization of nanoparticles was performed. *In vitro*, *in vivo* and bio-distribution investigations were performed in order to address the cytotoxicity and biocompatibility of ionosilica nanoparticles. Finally, the ionosilica nanoparticles were loaded with diclofenac (DCF), an anionic non-steroidal anti-inflammatory drug (NSAID) which was chosen as model drug to monitor the potential of the ionosilica nanoparticles to be used as drug carrier vehicles.[41, 42]

## 3.1 Synthesis and characterization of ionosilica nanoparticles

### 3.1.1 Synthesis of pegylilated ionosilica nanoparticles

Briefly, the ionosilica nanoparticles were synthesized as follows. In an aqueous mixture of sodium hexadecylsulfate SHS at 70°C, an ammonium precursor solution was added drop by drop under vigorous stirring to promote the precursor hydrolysis during 20mn. To this solution, a triblock copolymer F127 aqueous mixture was added. After 5 min, the condensation process was catalyzed by an ammonium solution followed by an addition of an aqueous PEG solution at the end. The reaction then was conducted for 15 h at 1250 rpm at 70°C. The as-synthesized NPs were collected by centrifugation and washed twice with ethanol before template extraction with an ethanolic ammonium chloride solution *see* annex for more details.

Figure 18 illustrated the nanoparticles formation. As explained before: the synthesis was based on the balance between the ordered assembly of cationic organic ammonium precursor (precursor **A**) and an anionic surfactant (SHS). The formation of precursor-surfactant ion pairs was followed by the inhibition of grain agglomeration. This was achieved by the addition of a nonionic surfactant (F127) which efficiently adsorbs on the surface of the primary nanoparticles *via* hydrogen bonding. Finally, addition of a silylated poly(ethylene glycol) precursor 'Silyl PEG' further stabilized the nanoparticles and avoided particle agglomeration. As PEG is a biocompatible group,[33, 39, 43] the surface functionalization of the ionosilica nanoparticles also enhances their biocompatibility. The obtained as-synthesized ionosilica nanoparticles with filled pores (**$NP_{is}$-as**) were then used to access bare particles with empty pores (**$NP_{is}$-bare**) *via* washing procedures.

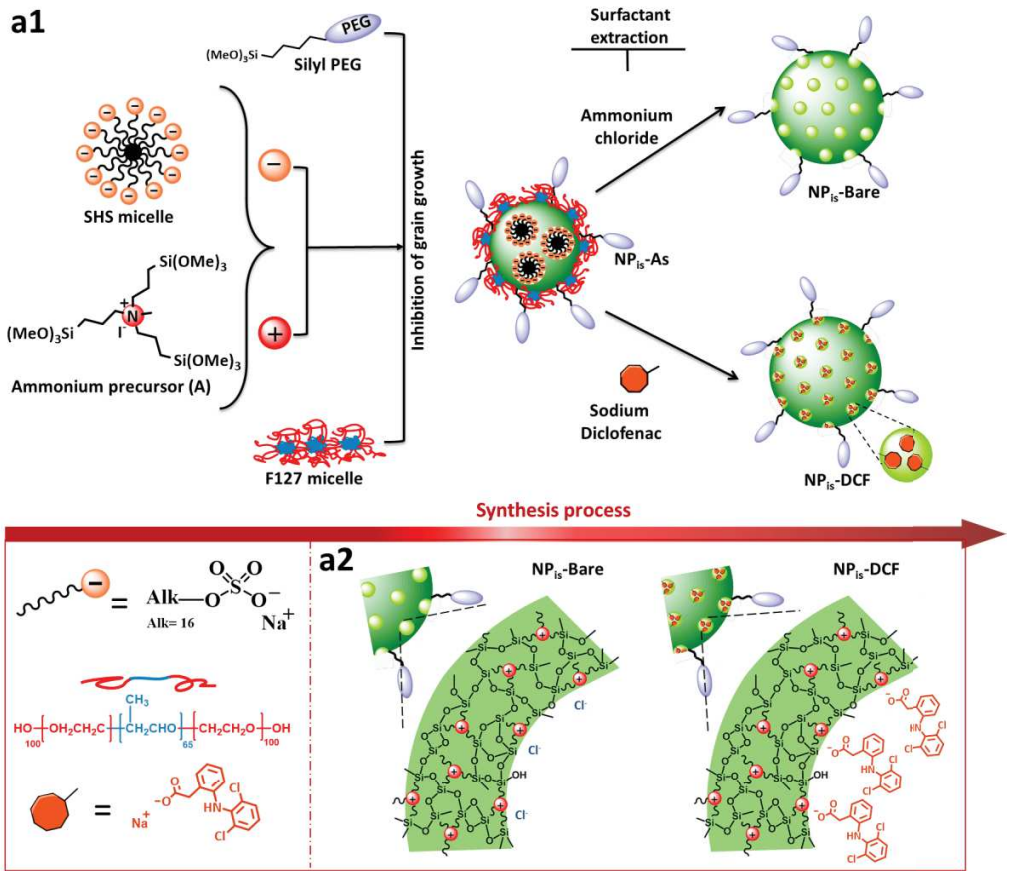


**Figure 18. a1) Illustration of the preparation of ionosilica nanoparticles and the template extraction, a2) schematic illustration of ionosilica framework with ammonium group and the composition of internal pore of $NP_{is}$-bare and $NP_{is}$-DCF.**

Diclofenac loaded ionosilica nanoparticles (**$NP_{is}$-DCF**) (Figure 18-a1, Figure 18-a2) were obtained *via* direct anion exchange of the as-synthesized ionosilica nanoparticles (**$NP_{is}$-as**) with diclofenac sodium salt (**DCF-Na**).

The successful formation of ionosilica nanoparticles **$NP_{is}$-as** was indicated by electron microscopy (TEM) and dynamic light scattering (DLS). TEM images of these particles (Figure 19-b) show spherical objects with a diameter of approximately 80-100 nm. The particle size determined by DLS is higher (148 nm), as DLS takes into account the surface located PEG-groups and adsorbed F127 polymers which increase the hydrodynamic diameter of the particles (Figure 19-b).

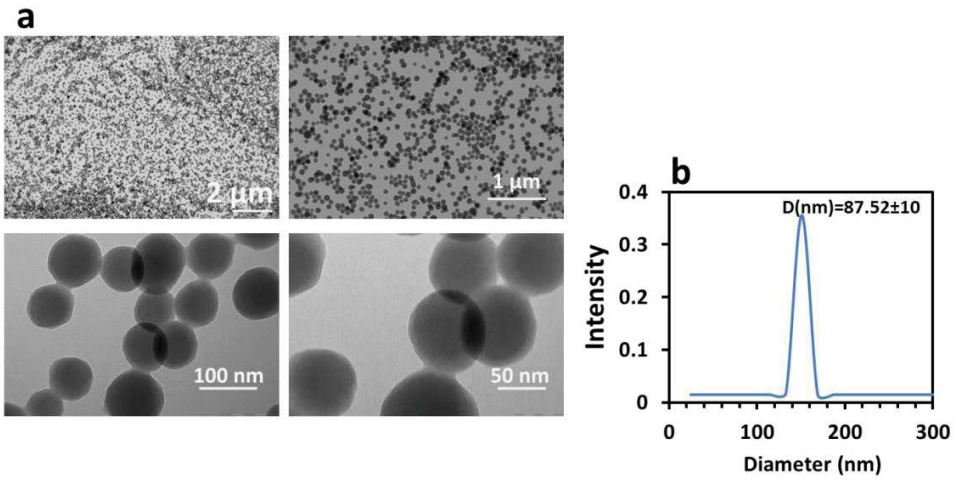


**Figure 19. a) TEM images and b) DLS measurement of $NP_{is}$-as.**

After having ascertained the formation of ionosilica / surfactant nanoparticles, we focused on surfactant elimination in order to access porous ionosilica nanoparticles. For this purpose, the **$NP_{is}$-as** nanoparticles were treated with an ethanolic ammonium chloride solution. The obtained nanoparticles **$NP_{is}$-bare** were very similar in size and shape compared to the **$NP_{is}$-as** particles. TEM and SEM images (Figure 20-a and Figure 21) indicate an average diameter of approximately 90 nm and a hydrodynamic diameter of 148 nm (Figure 20-d and Figure 20-c), in nice agreement with the results obtained for **$NP_{is}$-as**.

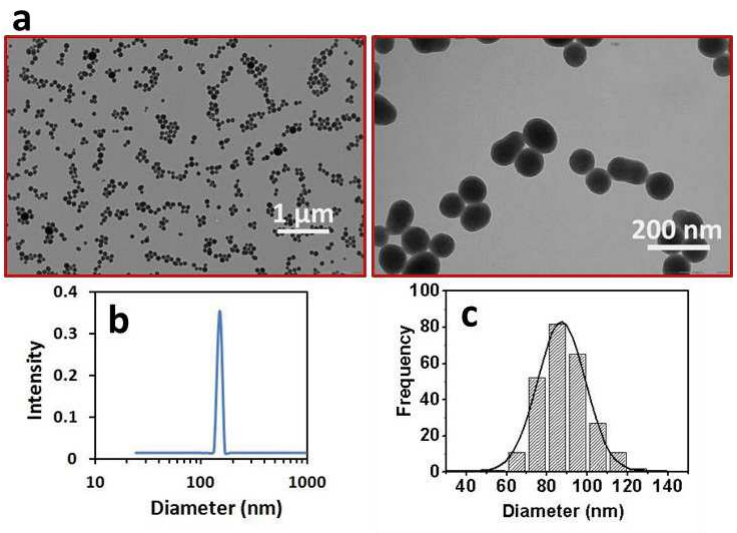


**Figure 20. a) TEM images of $NP_{is}$-bare. b). Particle size distribution of $NP_{is}$-bare obtained by TEM. c) DLS measurement of $NP_{is}$-bare.**

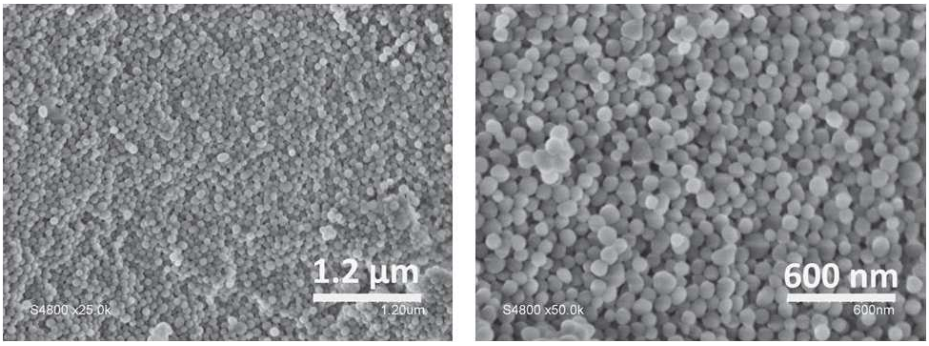


**Figure 21. SEM images of $NP_{is}$-bare.**

In the following, we characterized the **$NP_{is}$-bare** nanoparticles more in detail in order to confirm the chemical integrity of the ionic building block, and to determine the surface properties of the material. For this purpose, we performed $^{13}C$ CP-MAS and $^{29}Si$ CP-MAS solid state NMR and infrared spectroscopy, nitrogen sorption, X-ray diffraction and zeta potential measurements.

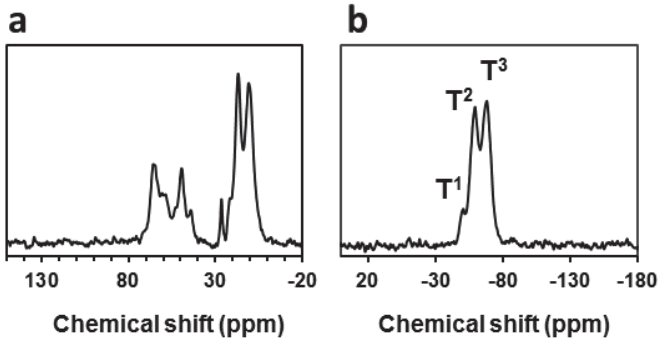


**Figure 22. a) 13C cross-polarization magic angles spinning (CP-MAS) spectra of $NP_{is}$-bare nanoparticles.**

First, the $^{13}C$ CP-MAS spectrum of **$NP_{is}$-bare** (Figure 22-a) displays three signals related to *n*-propyl chains of the precursor at 10.7, 16.8 and 49.7 ppm, respectively. Additionally, the two signals around 60-70 ppm can be assigned to the methyl group directly attached to the nitrogen atom and to the PEG groups located on the surface of nanoparticles. The $^{29}Si$ CP MAS NMR spectra of the material (Figure 22-b) shows three signals characteristic of the T units confirming the formation of a siloxane framework. The highest intensity was found for the $T^2$ and $T^3$ signals, which are assigned to $R\underline{Si}(OSi)_2OH$ and $R\underline{Si}(OSi)_3$ silicon centers, respectively. These results

prove the presence of ammonium groups within the material and confirm that no degradation of the ionic precursor occurred during hydrolysis polycondensation procedure.

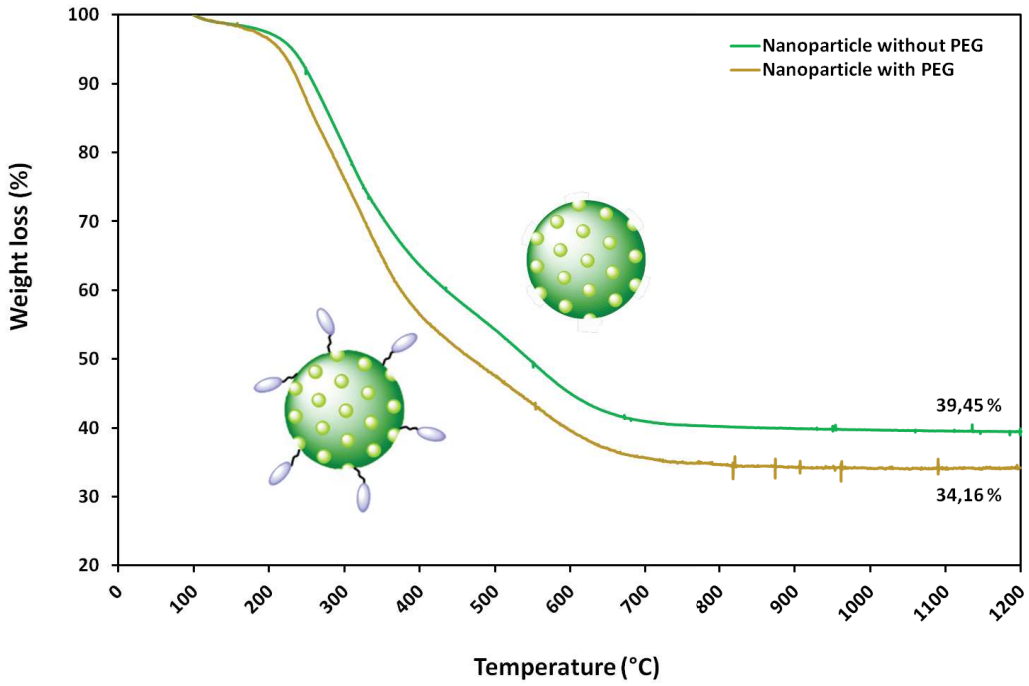


**Figure 23. TGA spectra of ionosilica nanoparticles synthesized with and without PEG performed under air.**

Thermogravimetric analysis of ionosilica nanoparticles with and without surface functionnalization were carried out in order to show with an indirect way the presence of silyl PEG on the surface of nanoparticles, the measurements were carried out under air by heating from 30 to 1200 °C at a rate of 5°C/min, the thermogram of $NP_{is}$-PEG (Figure 23) show an additional weight loss in comparison with the thermogram of $NP_{is}$ indicating the presence of silyl PEG with 5% weight (PEG / Nanoparticles).

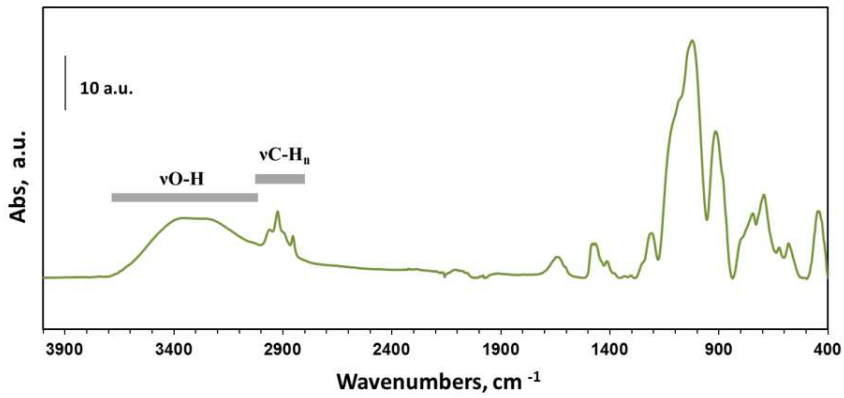


**Figure 24. FT-IR spectra of ionosilica nanoparticles $NP_{is}$-bare.**

These results were confirmed by FT-IR spectroscopy. The FT-IR spectrum of **$NP_{is}$-bare** (Figure 24) shows (C-H) stretching vibrations of methylene groups at 3000-2840 $cm^{-1}$. Moreover, the spectrum is dominated by strong absorption bands between 1150 - 1000 $cm^{-1}$ which can be assigned to the siloxane network.[44] The FT-IR spectrum of the nanoparticles is in nice agreement with those of previously reported bulk ionosilica.[16, 17]

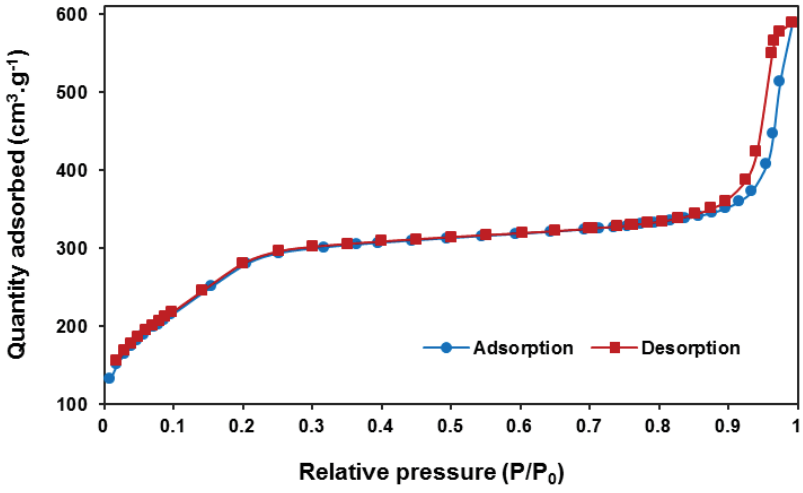


**Figure 25. Nitrogen adsorption-desorption isotherm of $NP_{is}$-bare nanoparticles.**

The surface properties of the **$NP_{is}$-bare** nanoparticles were determined *via* nitrogen sorption. The nitrogen sorption isotherm is given in Figure 25-c. The BET surface area of the materials was of 1034 $m^2.g^{-1}$. This result indicated that the anionic surfactant was eliminated in large extent from

the pores. The nitrogen adsorption isotherm of the **$NP_{is}$-bare** nanoparticles shows two separated adsorption steps. The first adsorption step occurred at low partial pressure ($P/P_0 < 0.2$) and indicates mesoporosity with a pore size of ~2.0 nm. This mesoporosity is due to the template effect of the anionic surfactant during the template directed hydrolysis-polycondensation process.[45] Secondly, a strong nitrogen uptake at high relative pressure ($P/P_0 > 0.8$) can be observed. This phenomenon can be related to nitrogen adsorption by the void spaces between the nanoparticles and therefore indicates intergranular porosity.

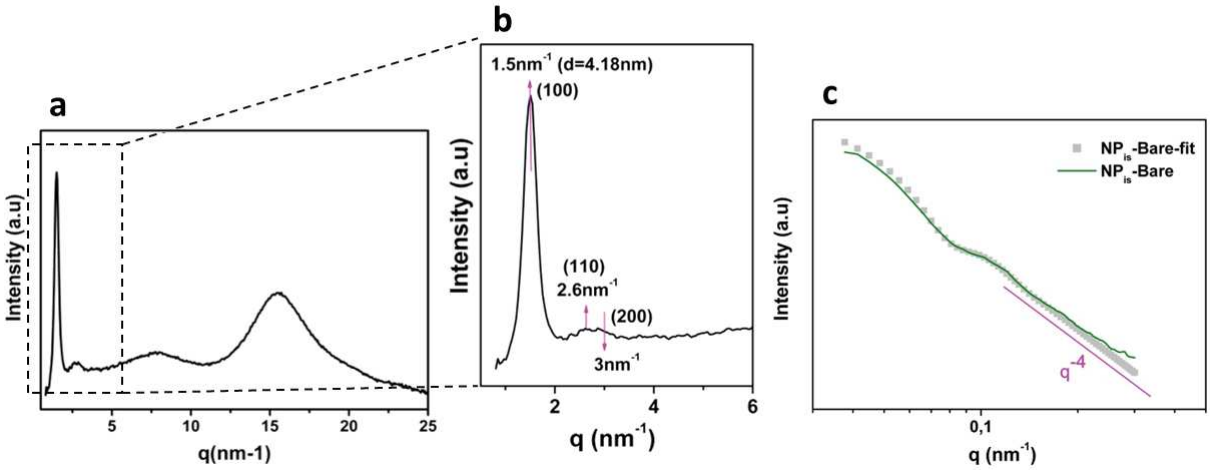


**Figure 26. a and b) X-ray diffractogram of $NP_{is}$-bare. c) SAXS patterns of $NP_{is}$-bare.**

Finally, XRD and SAXS measurements were performed to get more information about the architecture of the material on the mesoscopic length scale and the particle size. Figure 26-a and Figure 26-b display the XRD pattern of **$NP_{is}$-bare** nanoparticles. The diffractogram displays an intense peak at q = 1.5 $nm^{-1}$, and a low intense and larger contribution which could fit with 2 contributions at q = 2.6 and 3 $nm^{-1}$ (Figure 26-b). These three peaks with index (100), (110) and (200), respectively, indicate the regular repetition of cylindrical pore arrangement, separated by hybrid silica walls, in accordance with a hexagonal 2D structure. Considering the existence of walls between the cylinders, the distance D between the center of cylinders should be $D = 2d_{100} / \sqrt{3}$ for a hexagonal 2D structure, with $d_{100} = 2\pi/q_{100} = 4.2$ nm. We found then D = 4.8 nm corresponding to the wall thickness plus the cylinders diameter. The broad peak centered at q = 15 $nm^{-1}$ confirmed the amorphous nature of the silica hybrid walls[46, 47] as demonstrated in Figure 26-b. Small angle X-ray scattering (SAXS) was performed to measure the average diameter size

and size polydispersity of nanoparticles.-The SAXS profile (position of intensity oscillations of the form factor as shown on Figure 26-c) is directly related to the particle size and size polydispersity. A fit profile was performed using the Sasfit software (Figure 26-c) giving a radius of 52 nm (+/- 1 nm) for **$NP_{is}$-bare** with radius variance of 0.18. The intensity decrease of SAXS profile should follow a power law in $q^{-4}$ for dense particles (as indicated in Figure 26-c) for fitted curve). For experimental data, SAXS profile shows that the exponent of the power low is less than 4, indicating that the particles density is not homogeneous at the nm scale. This result is coherent with the existence of two phases with two different densities inside the nanoparticles (pores and walls).

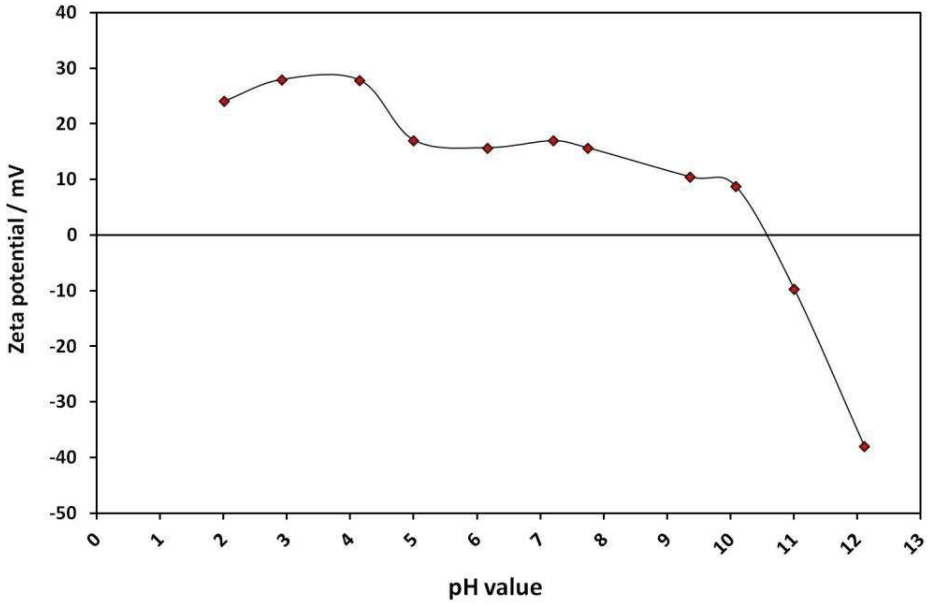


**Figure 27. Zeta potential of $NP_{is}$-bare at pH ranging from 2 to 12. The nanoparticles were dispersed in a 1 mM KOH aqueous solution.**

The surface charge of **$NP_{is}$-bare** was checked using zeta-potential measurements at different pH. We observed that the isoelectric point (IEP) of **$NP_{is}$-bare** was found at slightly basic medium (pH ~ 10,5) *see* Figure 27. This much higher value compared to silica ($IEP_{SiO2}$: pH ~ 2), can be explained by the presence of cationic ammonium groups within ionosilica framework, thus compensating the negative charge of silanolates ($Si\text{-}O^-$) located at the surface of the nanoparticles in alkaline solution.

All these results clearly indicate that highly porous ionosilica nanoparticles displaying ordered pore arrangements were obtained starting from the *tris*-silylated ammonium precursor **A**. TEM, SEM, DLS and SAXS gave concordant results regarding the particle size. Solid state NMR and FT-IR spectroscopy confirmed the chemical constitution and integrity of the ionic building blocks.

## 3.2 Diclofenac loading into the ionosilica nanoparticles

In the following, we investigated the use of these functional **$NP_{is}$-bare** nanoobjects in the area of drug delivery. For this purpose, we synthesized diclofenac (**DCF**) loaded nanoparticles directly *via* anion exchange on the as-synthesized **$NP_{is}$-as** nanoparticles, *i. e.* loading and template elimination were carried out simultaneously in order to preserve the porosity of the material. For this purpose, the ionosilica nanoparticles were contacted with an ethanolic sodium diclofenac solution (C = 0.51 mM) under sonication for 25 min at room temperature. This procedure was repeated three times. The resulting nanoparticles (**$NP_{is}$-DCF**) were then washed three times with ethanol to remove all physisorbed surfactant and DCF. The loading of diclofenac on ionosilica nanoparticles was monitored by UV-Vis, FT-IR and Energy-dispersive X-ray (EDX) spectroscopies.

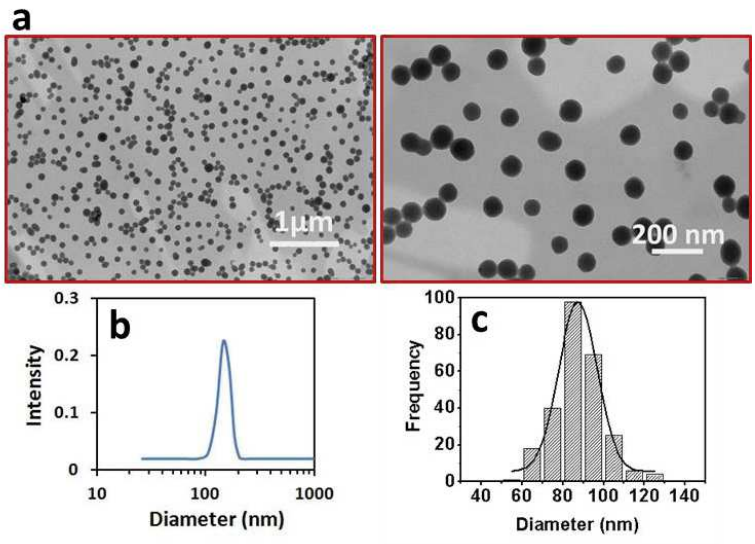


**Figure 28. a) TEM images of $NP_{is}$-bare. b). Particle size distribution of $NP_{is}$-bare obtained by TEM. c) DLS measurement of $NP_{is}$-bare.**

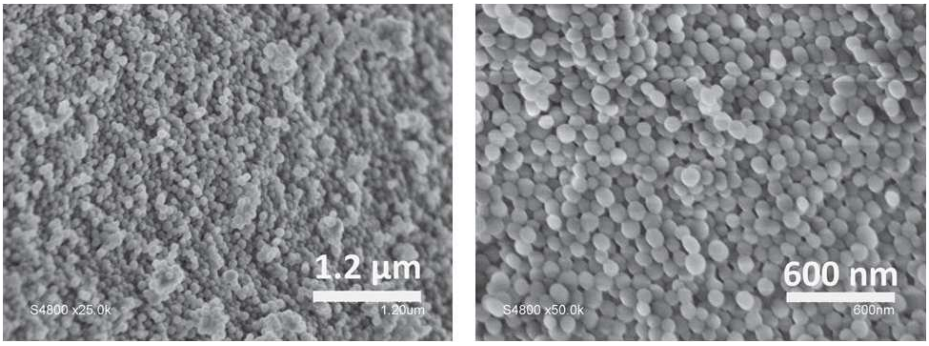


**Figure 29. SEM images of $NP_{is}$-DCF**

TEM, SEM and SAXS measurements indicated that **$NP_{is}$-DCF** show very similar shape and size compared to **$NP_{is}$-as** and **$NP_{is}$-bare** nanoparticles (TEM: 90 nm, SAXS: 94 nm) (Figure 28-a and c, Figure 29 and Figure 30-a). Once again, the particle size determined by DLS is significantly higher (150 nm) due to surface located PEG groups (Figure 28-c). The fact that we measured very similar particle size for all three materials **$NP_{is}$-as**, **$NP_{is}$-bare** and **$NP_{is}$-DCF** indicates that neither surfactant elimination from the pores nor anion exchange with **DCF-Na** into the ionosilica nanoparticles affects the particle geometry in terms of particle size, geometry or particle size distribution. The pore arrangement of **$NP_{is}$-DCF** was verified using X-ray diffraction. The diffractogram (Figure 30-b) shows an intense (100) reflection at 1.5 $nm^{-1}$ as observed with **$NP_{is}$-bare** but the (110) and (200) reflections are hardly identified. Finally, the surface charge of **$NP_{is}$-DCF** was checked by zeta potential indicating the positively charge contributed by the presence of ammonium substructures (see Table 1).

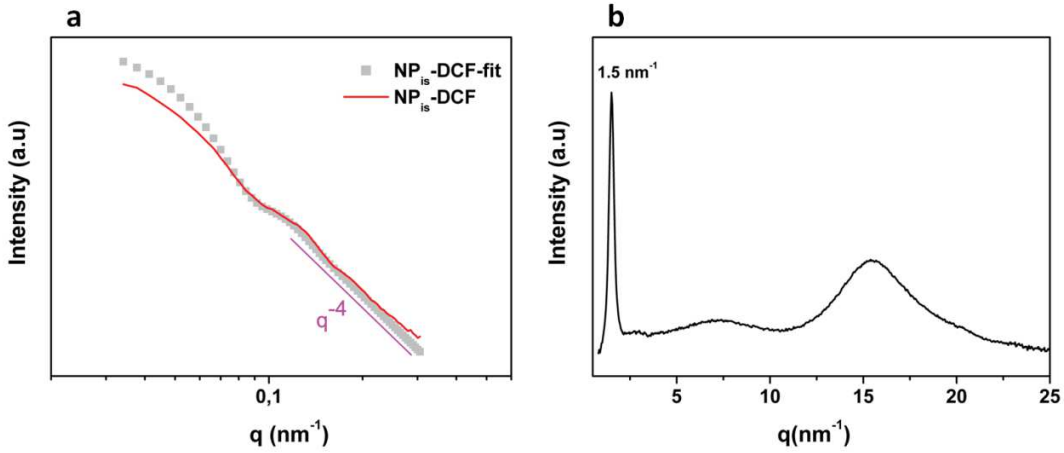


**Figure 30. SAXS and XRD pattern of $NP_{is}$-DCF a, b respectively.**

**Table 1:** Zeta potential of **$NP_{is}$-DCF**

| Sample | Zeta Potential (mV) | pH |
|---|---|---|
| **$NP_{is}$-DCF** | 31.3 | 6.47 |

The nanoparticles were dispersed in a 1 mM KOH aqueous solution.

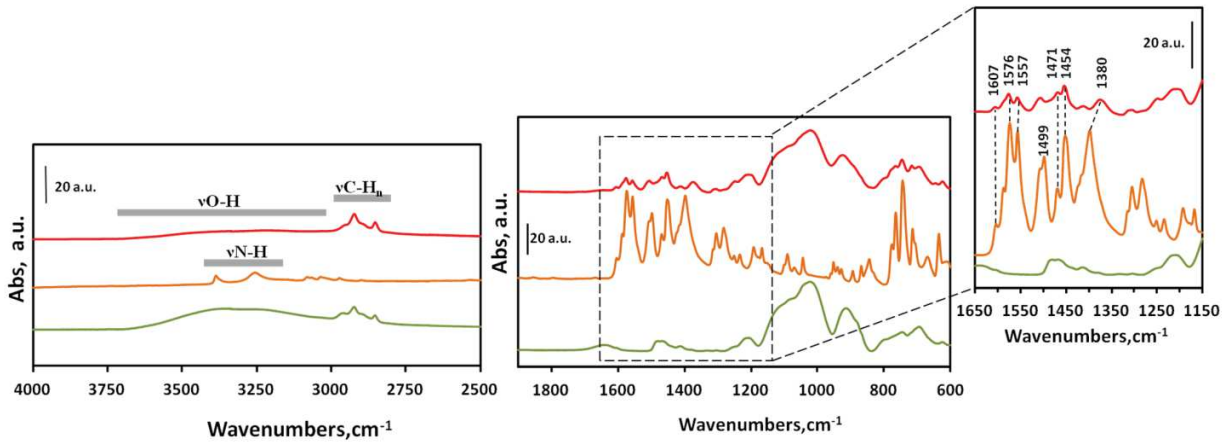


**Figure 31. FT-IR spectra of ionosilica nanoparticles $NP_{is}$-DCF (red curve), DCF-Na (orange curve), $NP_{is}$-bare (green curve).**

The DCF-loading onto the ionosilica nanoparticles was determined by UV-visible spectroscopy using the followed equation:

$$C_{DCF} = (C_{initial} - C_{final})/\text{nanoparticle mass}$$

We measured that the ionosilica nanoparticles adsorbed 1.54 mmol/g of **DCF-Na** (mol DCF/1 g of nanoparticles) corresponding to 49% *w/w*. This high quantity of immobilized DCF is explained by the high affinity of the anionic drug towards the immobilized cationic ammonium groups. UV-vis spectroscopy was also performed on the **$NP_{is}$-DCF** nanoparticles suspended in ethanol. The absorbance spectrum of the nanoparticles shows a strong absorption band characteristic for diclofenac, thus indicating the adsorption of diclofenac into ionosilica nanoparticles (Figure 32). The adsorption of DCF anions was also monitored *via* FT-IR spectroscopy. The FT-IR spectrum of **$NP_{is}$-DCF** clearly shows the antisymmetric and symmetric stretching of carboxylate group of DCF at 1576 and 1380 cm$^{-1}$ (Figure 31), in addition to the characteristic absorption bands of the ionosilica nanoparticle **$NP_{is}$-as**. The slight shift in the lower frequency absorption compared to

the spectrum of **DCF-Na** indicates the interaction between the carboxylate ion and the cationic moiety of the ionosilica nanoparticle.

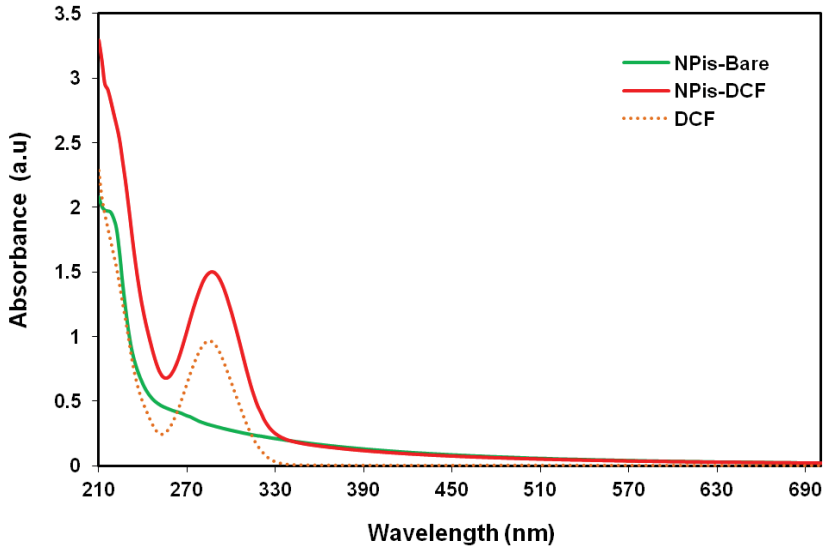


**Figure 32. UV-Vis absorbance spectra of $NP_{is}$-bare, $NP_{is}$-DCF and DCF**; the nanoparticles **$NP_{is}$-bare** and **$NP_{is}$-DCF** were suspended in ethanol at 15.3 µg/ml and 3.6 µg/ml respectively, **DCF-Na** was dissolved in ethanol at concentration of 0.63 mM.

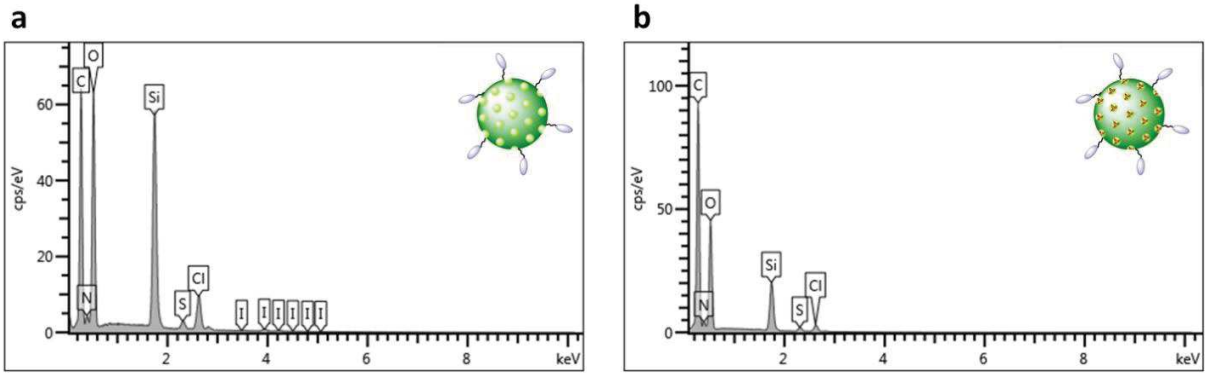


**Figure 33. EDX spectra of $NP_{is}$-bare (a) and $NP_{is}$-DCF (b).**

Finally, energy-dispersive X-ray spectroscopy (EDX) was performed on **$NP_{is}$-DCF** in order to get information on the amount of anionic surfactant traces remaining in the loaded nanoparticles. In fact, EDX analysis of **$NP_{is}$-DCF** indicates that approximately 70% of the anionic surfactant was replaced by DCF (Figure 33). However, the presence of residual SHS in the sample does not raise toxicological problems due to the low harmfulness of sulfate/sulfonate surfactants.[48, 49] Our synthetic strategy is therefore particularly adapted for the preparation of nano objects for the

biomedical use. This issue is of particular interest as ammonium type structure directing agents like CTAB, usually used in silica based nanoparticles' syntheses, display considerably higher toxicity and often lead to cellular death even at low concentrations.[50]

### 3.2.1 *In vitro* and *in vivo* invistigations

The cytotoxicity effect of **$NP_{is}$-bare** and **$NP_{is}$-DCF** nanoparticles was evaluated using MTT assay on RAW 264.7 cells. As depicted in Figure 34-a, following a 24 h treatment with increasing concentrations of nanoparticles, **$NP_{is}$-bare** and **$NP_{is}$-DCF** had no effect on RAW 264.7 cell growth. Even after 72 h, **$NP_{is}$-bare** and **$NP_{is}$-DCF** displayed only a very slight effect on RAW 264.7 cell growth (Figure 34-b). These results clearly demonstrate the biocompatibility of ionosilica nanoparticles and their suitability for further biomedical use.

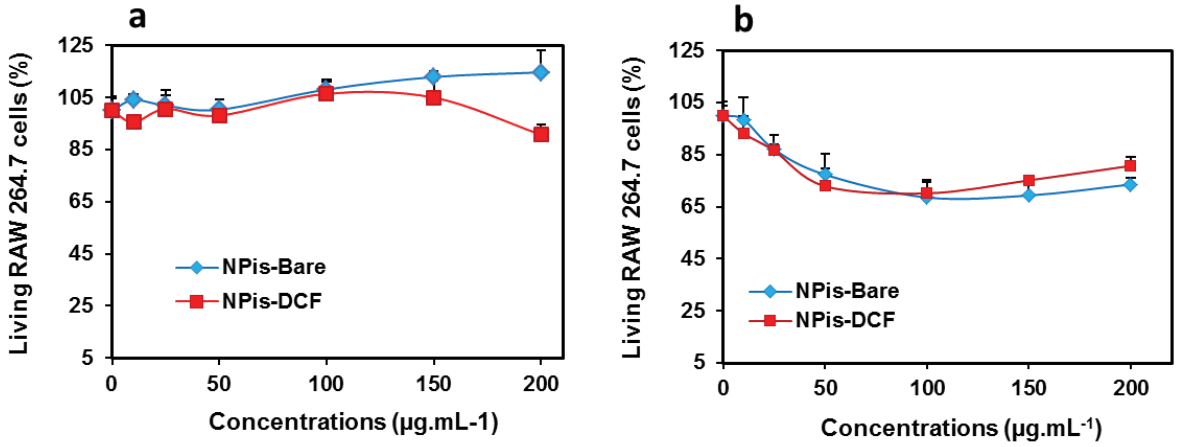


**Figure 34. Effect of $NP_{is}$-bare and $NP_{is}$-DCF nanoparticles on RAW 264.7 cells viability.** RAW 264.7 cells incubated with increasing concentrations of $NP_{is}$-DCF and $NP_{is}$-bare nanoparticles during x h and submitted to a MTT assay. Results are percentage of living cells compared to untreated cells. Values are means ± standard deviations of 3 experiments. a) x= 24, b) x= 72.

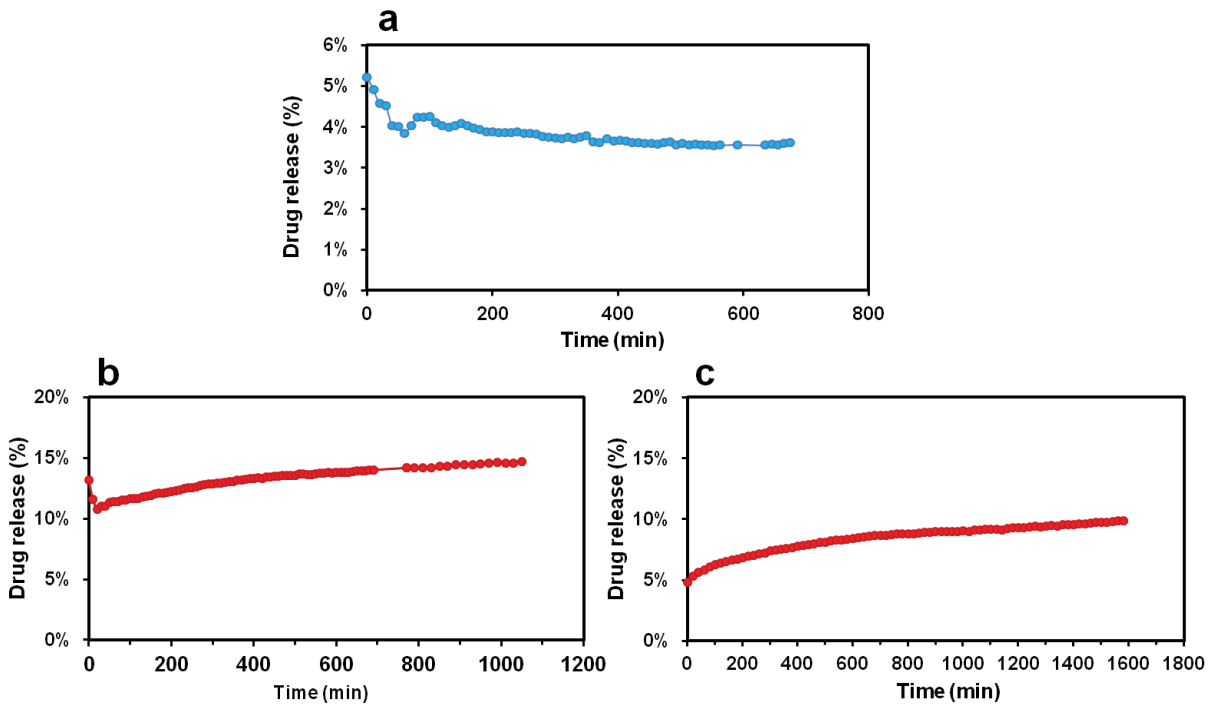


**Figure 35. In vitro diclofenac release from NPis-DCF: a) in water at pH 5.5. b) in $KH_2PO_4$ water solution (11mM, pH 5.6), c) in $KH_2PO_4$ water solution (the sample was the same as (b) the release medium was removed and replaced by the same quantity of $KH_2PO_4$ water.**

The diclofenac release from **$NP_{is}$-DCF** was performed in vitro using deionized water at pH 5.5 and monopotassium phosphate ($KH_2PO_4$) aqueous solution at pH 5.6 as release medium. In deionized water we observed only 5% **DCF** release (Figure 35-a). In the case of monopotassium phosphate $KH_2PO_4$ aqueous solution as release medium, the solution was replaced after 18 h by the same quantity in order to mimic the real condition (the monopotassium phosphate is usually present in culture medium). We found 15% **DCF** release in the first release (Figure 35-b) and 10% in the second (Figure 35-c), we obtained 25% **DCF** release by adding the results of both releases. This demonstrated that **$NP_{is}$-DCF** nanoparticles release drug by fraction not directly in a single quantity. All these results show clearly that the release of diclofenac was conducted *via* ion exchange reaction in the presence of anionic molecules and suggest drug target and release inside cells in the suitable medium.

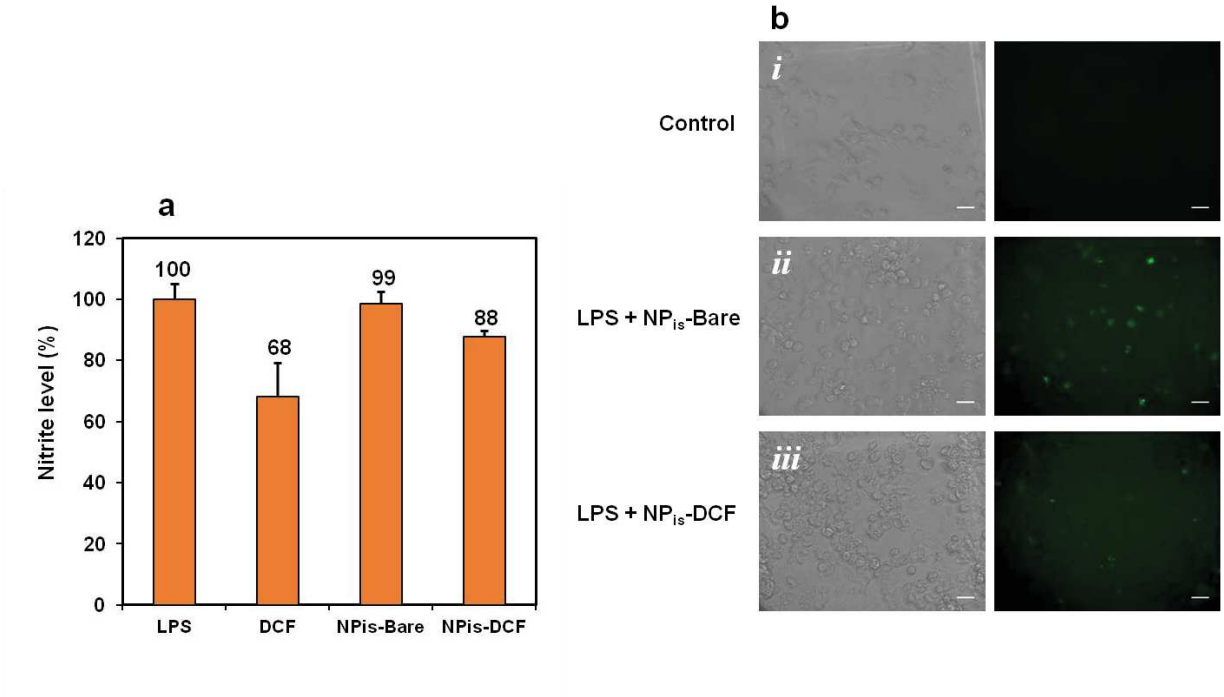


**Figure 36. a) Effect of nanoparticles on LPS-induced nitrite production in RAW 264.7 cells.** Nitrite level assayed in the culture medium of RAW 264.7 cells stimulated with LPS (25 ng.mL$^{-1}$) for 2 h, followed by a 24 h treatment with 100 µg.mL$^{-1}$ of $NP_{is}$-bare, $NP_{is}$-DCF and DCF-Na in a concentration corresponding the one contained in $NP_{is}$-DCF. Values are mean percentages ± standard deviations of 2 experiments**. b) Detection of intracellular ROS by DCFDA assay in RAW 264.7 cells.** Oxidative stress was observed in RAW 264.7 cells with the DCFDA that fluoresces when exposed to intracellular peroxides. (*i*) Control cells. (*ii*) Cells treated with LPS (25 ng.mL-1) and with NPis-bare nanoparticles. (*iii*) Cells treated with LPS (25 ng.mL-1) and NPis-DCF nanoparticles. Scale bar 10 µm.

To estimate the biomedical potential of such nanoparticles loaded with **DCF**, their anti-inflammatory effect was studied. **$NP_{is}$-DCF** and **$NP_{is}$-bare** were incubated with RAW 264.7 cells in which inflammation was LPS-induced. More precisely, RAW 264.7 cells were treated for 2 h with LPS (25 ng.mL$^{-1}$), followed by treatment with 100 µg.mL$^{-1}$ of **$NP_{is}$-bare**, **$NP_{is}$-DCF** nanoparticles and **DCF-Na** in a concentration equivalent to the one contained in **$NP_{is}$-DCF**. Figure 36-a shows that **$NP_{is}$-DCF** could decrease nitrite production induced by LPS on RAW 264.7 cells of 12% which is lower than the value observed for **DCF-Na** alone (32%). This lower anti-inflammatory effect is explained by slow **DCF** release from the nanoparticles as indicated above. As expected, **$NP_{is}$-bare** have no effect on LPS-induced nitrite production. All these results demonstrate the capacity of ionosilica nanoparticles to be used as drug delivery system.

To confirm the drug delivery efficacy of **$NP_{is}$-DCF**, their capacity to reverse oxidative stress LPS-induced was analyzed by dichlorofluorescin diacetate (DCFDA) assay on RAW 264.7 cells. These macrophages were treated for 2 h at a concentration of 25 ng.mL$^{-1}$ with LPS to induce the ROS production. Then, the pre-treatment was followed by an incubation of 100 µg. mL$^{-1}$ of **$NP_{is}$-DCF** and **$NP_{is}$-bare** for 24 h. We observed that cells incubated with LPS and **$NP_{is}$-DCF** exhibit a lower green fluorescence than cells treated with LPS and **$NP_{is}$-bare** (Figure 36-b). This confirmed that **$NP_{is}$-DCF** released **DCF** in culture cells and decreased inflammatory reactions induced by LPS treatment, such as ROS production.

This effect could be attributed to the efficient endocytosis of ionosilica nanoparticles by macrophages as demonstrated in Figure 37. We prepared fluorescent ionosilica nanoparticles **$NP_{is}$-FITC** by contacting **$NP_{is}$-bare** with an ethanol solution of fluorescein isothiocyanate **(FITC)** at 0.1:1 (FITC : **$NP_{is}$-bare**) molar ratio. The adsorption of **FITC** on ionosilica nanoparticles involved a sonication step of 30 min at 30°C followed by several washing steps with ethanol. The resulting fluorescent **$NP_{is}$-FITC** nanoparticles were then incubated in culture cells at concentration of 100 µg.mL$^{-1}$ for 24 h. Fluorescent imaging of living cells showed that nanoparticles were progressively internalized by RAW 264.7 cells. **$NP_{is}$-FITC** is quickly internalized after 3 h of incubation after 9 h, and a maximum internalization was observed after 24 h (Figure 37). All together, these results demonstrate the highly efficient uptake of ionosilica nanoparticles by macrophages and their efficiency in drug delivery.

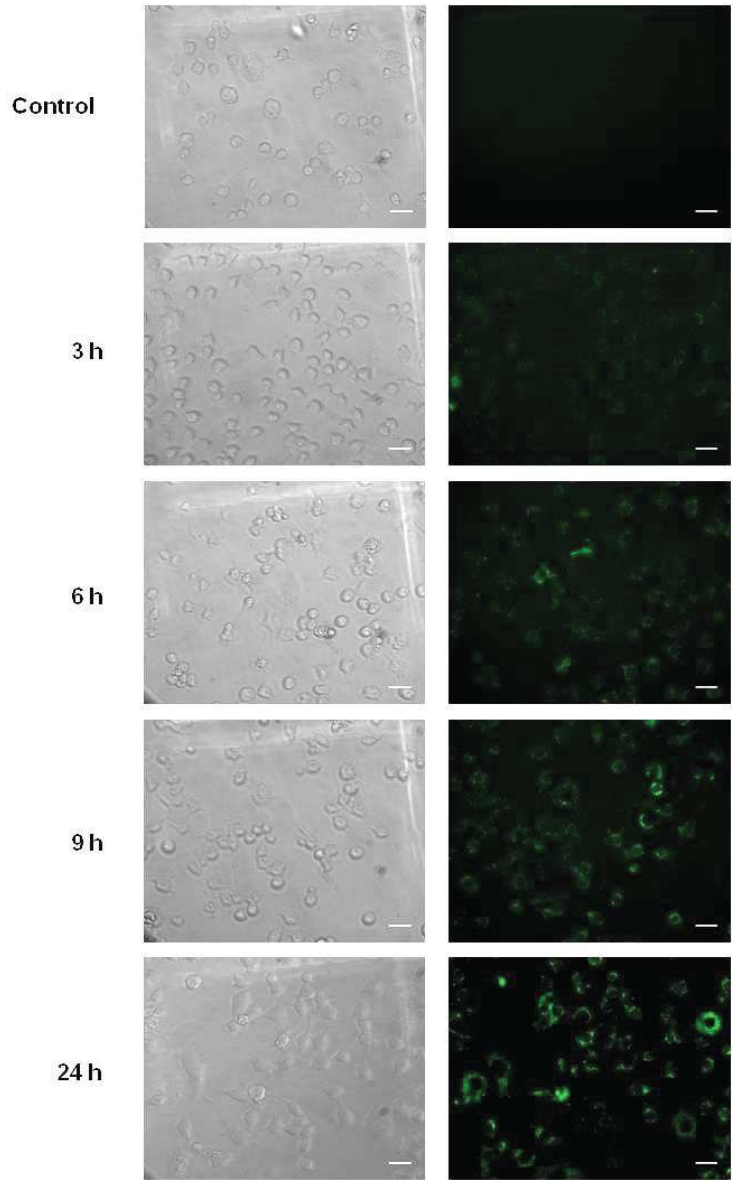


**Figure 37. Imaging of cell uptake of $NP_{is}$-FITC. Transmission microscopy (left) and fluorescence imaging (right) of RAW 264.7 cells**, incubated or not (control) during different times (3 h, 6 h, 9 h and 24 h) with NPis-FITC (100 µg.mL-1) exhibiting a green fluorescence inside cells. Scale bar 10 µm.

To estimate the *in vivo* biocompatibility of ionosilica nanoparticles, 2 groups of mice were constituted (n=4) and injected intravenously with physiological serum supplemented or not (Control) with NPis-bare nanoparticles to reach a final concentration in the animal of 40 $mg.kg^{-1}$ (Figure 38). This concentration is relatively high and corresponds to already used doses for acute toxicity studies in mice.[51] However, the dispersibility of the solution of physiological serum

added with nanoparticles was remarkably good and we observed no problems related to particles' agglomeration or precipitation over the whole time of the experiment. One week after the injection, mice were sacrificed. The histological analysis did not show any structural modifications on liver, kidney and spleen (Figure 38-a). Moreover, no significant differences between control and treated mice for the biomarkers such as ALT (liver), IL-6 (systemic inflammation) and creatinine (kidney) were observed (Figure 38-b, c, d), confirming the functional integrity of organs involved in the metabolism. These results obtained in mice demonstrated the biocompatibility of ionosilica nanoparticles and their potential for biomedical use.

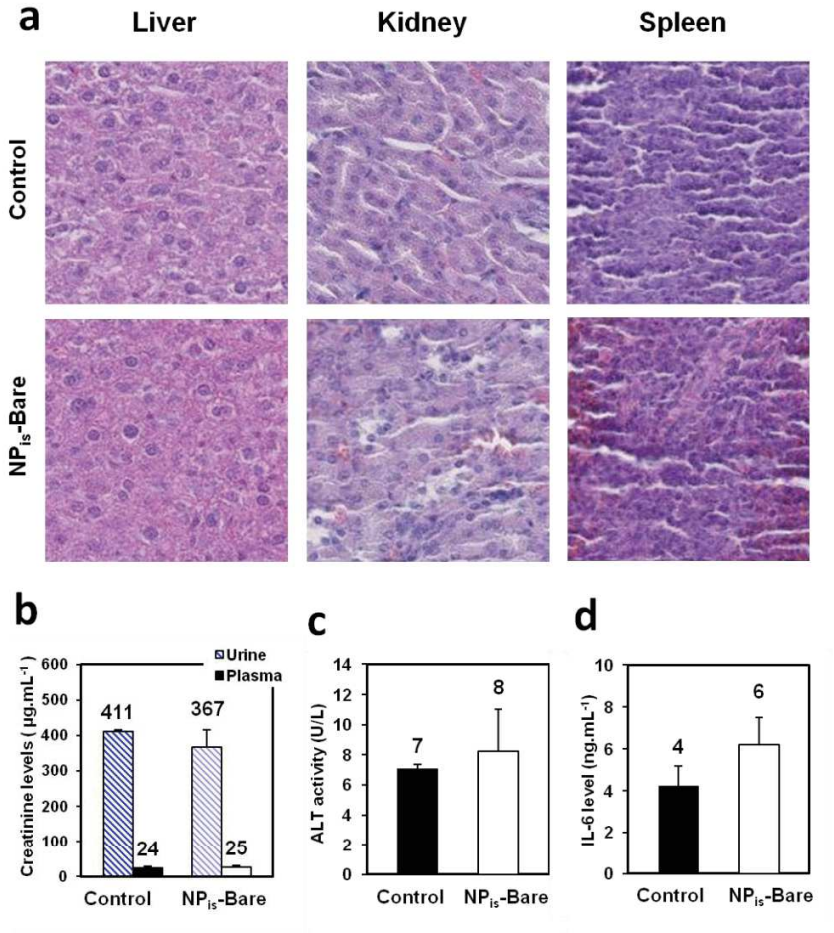


**Figure 38. a) Hematoxylin-eosin stained sections from paraffin-embedded tissues of control and treated mice observed at magnification x 100. b) Plasma and urine levels of renal biomarker (creatinine). c) Plasma levels of biomarkers of the liver (ALT). d) Plasma levels of systemic inflammation (IL-6).**

## 4 Conclusion

In summary, we report original ionosilica nanoparticles with ammonium substructures within the silica network. These ionosilica nanoparticles were successfully synthesized using a binary surfactant system. Different synthesis conditions were studied to control the textural and morphological properties. These original nano objects were synthesized exclusively from a silylated ammonium precursor and display highly uniform particle size less than 100 nm together with high specific surface area up to 1000 $m^2.g^{-1}$ and regular pore arrangement. The average pore size is centered at approximately 1.9 nm. Both *in vitro* and *in vivo* cytotoxicity investigations of ionosilica nanoparticles displayed high biocompatibility. This feature is in part due to the original nanoparticles synthesis strategy involving anionic surfactants instead of more toxic cationic surfactants. Finally, ionosilica nanoparticles can be used as drug transport vehicles. We show that the nanoparticles can be loaded with anionic drugs (diclofenac) *via* anion exchange. Furthermore, we observed that drug release depends on the composition of the release medium. Our results indicate the high potential of these functional and hydrophilic ionosilica nanoparticles in drug delivery.

**References**


1. Boisselier, E.; Astruc, D., Gold nanoparticles in nanomedicine: preparations, imaging, diagnostics, therapies and toxicity. *Chemical Society Reviews* **2009,** 38, (6), 1759-1782.

2. Fatieiev, Y.; Croissant, J. G.; Julfakyan, K.; Deng, L.; Anjum, D. H.; Gurinov, A.; Khashab, N. M., Enzymatically degradable hybrid organic-inorganic bridged silsesquioxane nanoparticles for in vitro imaging. *Nanoscale* **2015,** 7, (37), 15046-15050.

3. Ouvinha de Oliveira, R.; de Santa Maria, L. C.; Barratt, G., Nanomedicine and its applications to the treatment of prostate cancer. *Annales Pharmaceutiques FranÃ§aises* **2014,** 72, (5), 303-316.

4. Mura, S.; Nicolas, J.; Couvreur, P., Stimuli-responsive nanocarriers for drug delivery. *Nat. Mater.* **2013,** 12, (11), 991-1003.

5. Inagaki, S.; Guan, S.; Fukushima, Y.; Ohsuna, T.; Terasaki, O., Novel mesoporous materials with a uniform distribution of organic groups and inorganic oxide in their frameworks. *Journal of the American Chemical Society* **1999,** 121, (41), 9611-9614.

6. Asefa, T.; MacLachlan, M. J.; Coombs, N.; Ozin, G. A., Periodic mesoporous organosilicas with organic groups inside the channel walls. *Nature* **1999,** 402, (6764), 867-871.

7. Melde, B. J.; Holland, B. T.; Blanford, C. F.; Stein, A., Mesoporous sieves with unified hybrid inorganic/organic frameworks. *Chemistry of Materials* **1999,** 11, (11), 3302-3308.

8. Hoffmann, F.; Cornelius, M.; Morell, J.; Froba, M., Silica-based mesoporous organic-inorganic hybrid materials. *Angew. Chem.-Int. Edit.* **2006,** 45, (20), 3216-3251.

9. Croissant, J. G.; Cattoen, X.; Man, M. W. C.; Durand, J. O.; Khashab, N. M., Syntheses and applications of periodic mesoporous organosilica nanoparticles. *Nanoscale* **2015,** 7, (48), 20318-20334.

10. Guan, B. Y.; Cui, Y.; Ren, Z. Y.; Qiao, Z. A.; Wang, L.; Liu, Y. L.; Huo, Q. S., Highly ordered periodic mesoporous organosilica nanoparticles with controllable pore structures. *Nanoscale* **2012,** 4, (20), 6588-6596.

11. Djojoputro, H.; Zhou, X. F.; Qiao, S. Z.; Wang, L. Z.; Yu, C. Z.; Lu, G. Q., Periodic mesoporous organosilica hollow spheres with tunable wall thickness. *Journal of the American Chemical Society* **2006,** 128, (19), 6320-6321.

12. Urata, C.; Yamada, H.; Wakabayashi, R.; Aoyama, Y.; Hirosawa, S.; Arai, S.; Takeoka, S.; Yamauchi, Y.; Kuroda, K., Aqueous Colloidal Mesoporous Nanoparticles with Ethenylene-Bridged Silsesquioxane Frameworks. *Journal of the American Chemical Society* **2011,** 133, (21), 8102-8105.

13. Wei, Y.; Li, X. M.; Zhang, R. Y.; Liu, Y.; Wang, W. X.; Ling, Y.; El-Toni, A. M.; Zhao, D. Y., Periodic Mesoporous Organosilica Nanocubes with Ultrahigh Surface Areas for Efficient CO2 Adsorption. *Sci Rep* **2016,** 6, 11.

14. Liu, J.; Yang, H. Q.; Kleitz, F.; Chen, Z. G.; Yang, T.; Strounina, E.; Lu, G. Q.; Qiao, S. Z., Yolk–Shell Hybrid Materials with a Periodic Mesoporous Organosilica Shell: Ideal Nanoreactors for Selective Alcohol Oxidation. *Advanced Functional Materials* **2012,** 22, (3), 591-599.

15. Lu, N.; Tian, Y.; Tian, W.; Huang, P.; Liu, Y.; Tang, Y. X.; Wang, C. Y.; Wang, S. J.; Su, Y. Y.; Zhang, Y. L.; Pan, J.; Teng, Z. G.; Lu, G. M., Smart Cancer Cell Targeting Imaging and Drug Delivery System by Systematically Engineering Periodic Mesoporous Organosilica Nanoparticles. *ACS Appl. Mater. Interfaces* **2016,** 8, (5), 2985-2993.

16. El Hankari, S.; Motos-Perez, B.; Hesemann, P.; Bouhaouss, A.; Moreau, J. J. E., Pore size control and organocatalytic properties of nanostructured silica hybrid materials containing amino and ammonium groups. *J. Mater. Chem.* **2011,** 21, (19), 6948-6955.

17. Nguyen, T. P.; Hesemann, P.; Tran, T. M. L.; Moreau, J. J. E., Nanostructured polysilsesquioxanes bearing amine and ammonium groups by micelle templating using anionic surfactants. *J. Mater. Chem.* **2010,** 20, (19), 3910-3917.

18. Lee, B.; Im, H. J.; Luo, H. M.; Hagaman, E. W.; Dai, S., Synthesis and characterization of periodic mesoporous organosilicas as anion exchange resins for perrhenate adsorption. *Langmuir* **2005,** 21, (12), 5372-5376.

19. Nguyen, T. P.; Hesemann, P.; Moreau, J. l. J. E., i-Silica: Nanostructured silica hybrid materials containing imidazolium groups by hydrolysis-polycondensation of disilylated bis-N,Nâ€²-alkyl-imidazolium halides. *Microp. Mesop. Mater.* **2011,** 142, (1), 292-300.

20. Hesemann, P.; Nguyen, T. P.; El Hankari, S., Precursor Mediated Synthesis of Nanostructured Silicas: From Precursor-Surfactant Ion Pairs to Structured Materials. *Materials* **2014,** 7, (4), 2978-3001.

21. Che, S.; Garcia-Bennett, A. E.; Yokoi, T.; Sakamoto, K.; Kunieda, H.; Terasaki, O.; Tatsumi, T., A novel anionic surfactant templating route for synthesizing mesoporous silica with unique structure. *Nat. Mater.* **2003,** 2, (12), 801-805.

22. Nguyen, T. P.; Hesemann, P.; Gaveau, P.; Moreau, J. J. E., Periodic mesoporous organosilica containing ionic bis-aryl-imidazolium entities: Heterogeneous precursors for silica-hybrid-supported NHC complexes. *J. Mater. Chem.* **2009,** 19, (24), 4164-4171.

23. Ju, Y. H.; Webb, O. F.; Dai, S.; Lin, J. S.; Barnes, C. E., Synthesis and characterization of ordered mesoporous anion-exchange inorganic/organic hybrid resins for radionuclide separation. *Ind. Eng. Chem. Res.* **2000,** 39, (2), 550-553.

24. Hesemann, P.; Prelot, B.; Trens, P.; Thach, U. D.; Zajac, J., *manuscript in preparation*.

25. Zhu, L.; Zhang, C.; Liu, Y.; Wang, D.; Chen, J., Direct synthesis of ordered N-methylimidazolium functionalized mesoporous silica as highly efficient anion exchanger of Cr(VI). *J. Mater. Chem.* **2010,** 20, (8), 1553-1559.

26. Petrova, M.; Guigue, M.; Venault, L.; Moisy, P.; Hesemann, P., Anion selectivity in ion exchange reactions with surface functionalized ionosilicas. *Phys. Chem. Chem. Phys.* **2015,** 17, (15), 10182-8.

27. Bouchal, R.; Miletto, I.; Thach, U. D.; Prelot, B.; Berlier, G.; Hesemann, P., Ionosilicas for drug removal from wastwater. *manuscript submitted* **2016**.

28. Hu, L. C.; Khiterer, M.; Huang, S. J.; Chan, J. C. C.; Davey, J. R.; Shea, K. J., Uniform, Spherical Bridged Polysilsesquioxane Nano- and Microparticles by a Nonemulsion Method. *Chemistry of Materials* **2010,** 22, (18), 5244-5250.

29. Matsoukas, T.; Gulari, E., Self-sharpening distributions revisitedâ€”polydispersity in growth by monomer addition. *Journal of Colloid and Interface Science* **1991,** 145, (2), 557-562.

30. Bogush, G. H.; Zukoski, C. F., Uniform silica particle precipitation: An aggregative growth model. *Journal of Colloid and Interface Science* **1991,** 142, (1), 19-34.

31. Bogush, G. H.; Zukoski, C. F., Studies of the kinetics of the precipitation of uniform silica particles through the hydrolysis and condensation of silicon alkoxides. *Journal of Colloid and Interface Science* **1991,** 142, (1), 1-18.

32. Van Blaaderen, A.; Van Geest, J.; Vrij, A., Monodisperse colloidal silica spheres from tetraalkoxysilanes: Particle formation and growth mechanism. *Journal of Colloid and Interface Science* **1992,** 154, (2), 481-501.

33. Suzuki, K.; Ikari, K.; Imai, H., Synthesis of silica nanoparticles having a well-ordered mesostructure using a double surfactant system. *J. Am. Chem. Soc.* **2004,** 126, (2), 462-463.

34. Mittal, K. L.; Lindman, B., *Surfactant in solution*. Springer science and Business media, LLC: Gainesville, 1991.

35. Sun, T.; Ying, J. Y., Synthesis of microporous transition-metal-oxide molecular sieves by a supramolecular templating mechanism. *Nature* **1997,** 389, (6652), 704-706.

36. Sonwane, C. G.; Bhatia, S. K., Characterization of Pore Size Distributions of Mesoporous Materials from Adsorption Isotherms. *The Journal of Physical Chemistry B* **2000,** 104, (39), 9099-9110.

37. Croissant, J.; Cattoen, X.; Man, M. W. C.; Dieudonne, P.; Charnay, C.; Raehm, L.; Durand, J. O., One-Pot Construction of Multipodal Hybrid Periodic Mesoporous Organosilica Nanoparticles with Crystal-Like Architectures. *Advanced Materials* **2014,** 27, (1), 145-149.

38. Kim, T.-W.; Chung, P.-W.; Lin, V. S. Y., Facile Synthesis of Monodisperse Spherical MCM-48 Mesoporous Silica Nanoparticles with Controlled Particle Size. *Chemistry of Materials* **2010,** 22, (17), 5093-5104.

39. Chen, Z. D.; Li, X.; He, H. Y.; Ren, Z. H.; Liu, Y.; Wang, J.; Li, Z.; Shen, G.; Han, G. R., Mesoporous silica nanoparticles with manipulated microstructures for drug delivery. *Colloid Surface B* **2012,** 95, 274-278.

40. Ikari, K.; Suzuki, K.; Imai, H., Structural control of mesoporous silica nanoparticles in a binary surfactant system. *Langmuir* **2005,** 22, (2), 802-806.

41. Agotegaray, M.; Palma, S.; Lassalle, V., Novel Chitosan Coated Magnetic Nanocarriers for the Targeted Diclofenac Delivery. *J. Nanosci. Nanotechnol.* **2014,** 14, (5), 3343-3347.

42. Goncalves, R. M.; Leite Pereira, A. C.; Pereira, I. O.; Oliveira, M. J.; Barbosa, M. A., Macrophage response to chitosan/poly-(gamma-glutamic acid) nanoparticles carrying an anti-inflammatory drug. *J. Mater. Sci. - Mater. Med.* **2015,** 26, (4).

43. Ikari, K.; Suzuki, K.; Imai, H., Structural control of mesoporous silica nanoparticles in a binary surfactant system. *Langmuir* **2006,** 22, (2), 802-806.

44. Chukin, G. D.; Malevich, V. I., Infrared spectra of silica. *J. Appl. Spectrosc.* **1977,** 26, (2), 223-229.

45. Yokoi, T.; Yoshitake, H.; Tatsumi, T., Synthesis of anionic-surfactant-templated mesoporous silica using organoalkoxysilane-containing amino groups. *Chem. Mater.* **2003,** 15, (24), 4536-4538.

46. Kalapathy, U.; Proctor, A.; Shultz, J., A simple method for production of pure silica from rice hull ash. *Bioresource Technol.* **2000,** 73, (3), 257-262.

47. Wang, L.; Lu, A.; Wang, C.; Zheng, X.; Zhao, D.; Liu, R., Nano-fibriform production of silica from natural chrysotile. *J. Colloid Interf. Sci.* **2006,** 295, (2), 436-439.

48. Krebs, F. C.; Miller, S. R.; Malamud, D.; Howett, M. K.; Wigdahl, B., Inactivation of human immunodeficiency virus type 1 by nonoxynol-9, C31G, or an alkyl sulfate, sodium dodecyl sulfate. *Antivir. Res.* **1999,** 43, (3), 157-173.

49. Young, F. M.; Phungtamdet, W.; Sanderson, B. J. S., Modification of MTT assay conditions to examine the cytotoxic effects of amitraz on the human lymphoblastoid cell line, WIL2NS. *Toxicol. in Vitro* **2005,** 19, (8), 1051-1059.

50. Whitehead, K.; Karr, N.; Mitragotri, S., Safe and effective permeation enhancers for oral drug delivery. *Pharmaceut. Res.* **2008,** 25, (8), 1782-1788.

51. Yu, Y.; Li, Y.; Wang, W.; Jin, M.; Du, Z.; Li, Y.; Duan, J.; Yu, Y.; Sun, Z., Acute Toxicity of Amorphous Silica Nanoparticles in Intravenously Exposed ICR Mice. *Plos One* **2013,** 8, (4).

# Part III

## Synthesis of hybrid silica monoliths bearing amine and ammonium functionalities.

## Summary

# 1 Introduction

The fabrication of new multifunctional and complex systems is often motivated by the emergence of "biomimetic and bioinspired" construction approaches.[1] Porous materials bearing hierarchical organization of the network (as found in almost all biominerals) are highly desired for a broad variety of applications, such as in separation techniques, absorbers and heterogeneous catalysis, etc.[2-4]

The preparation of materials with simultaneous tailoring of morphology (monoliths, fibers etc.) and pore structures on different length scales has emerged as a promising field of further investigation with an extensive scope.[5] Recently, monoliths have attracted the attention of researchers in various fields,[6-9] especially in the field of separation science.[10, 11] The generation and dispersion of immiscible droplets combined with conventional soft-templating methods allowed the development of new foaming processes for the fabrication of hierarchically structured monolithic materials with controlled and accessible porosity and good mechanical properties.[1] Ideal monolithic material should have several important properties. excellent chemical and mechanical stability to ensure good practicability and an ease of preparation and tailorability for widespread applications.[12]

The special interest is silica-based organic–inorganic hybrids monoliths. They combine the attractive properties of stable inorganic framework with a tailor-made functionality that can be tuned by the choice of an appropriate organic functionality.[9] In the field of hybrid material, periodic mesoporous organosilicas (PMOs) synthesized from bridged silane precursors contain a regular arrangement of active organic species in their frameworks.[13, 14] Their surface hydrophilicity– hydrophobicity properties, mechanical and hydrothermal stabilities can be finely controlled by the choice of organic functionalities and pore structure.[15, 16] So that these materials are very useful in treating bio-macromolecules.[17 18] However, synthesis of Periodic Mesoporous Organosilicas (PMOs) monoliths is more difficult due to the variability of the silica precursors. Different organic functionalities usually require specific optimization of the synthetic conditions to obtain ordered mesostructures.[15]

In this chapter, we synthesized organo-silica based hybrid monoliths containing amine and ammonium substructures with hierarchical trimodal porous structure (micro, meso, and

macroporosity). These hierarchical pores structures were obtained via high internal phase emulsion (HIPE) process and lyotropic mesophases.[11]

The incorporation of organic functionalities has been achieved in two pathways, by co-condensation process and by using only an organosilylated precursor. Different synthesis conditions were investigated in order to optimize the synthesis of hybrid silica monoliths containing organic functionalities.

Morphology and structure of the as-synthesized monoliths have been characterized by several techniques: Scanning electron microscopy with mercury intrusion porosity used in order to investigate the textural properties at macroscopic length scale, nitrogen sorption and $^{29}Si$ solid state NMR spectroscopy used to study the textural properties at the meso- microscopic length scale and the integration of the amine and ammonium functionalities in the material scaffold respectively.

## 2 Description of the studied system

Herein we make use two processes to synthesize hybrid silica monoliths with amine and ammonium functionalities. The incorporation of organic functionalities (amine and ammonium) has been achieved in two pathways; Firstly via co-condensation process by simultaneous reaction of tetraethoxyorthosilicate (TEOS) and silylated organic precursors (tris(3-(trimethoxysilyl)propyl)amine (TrisN) and methyl-(tris(3-trimethoxysilyl)propyl) ammonium iodide (MeTrisN) *see* Figure 1 where the organosilane precursors are incorporated into the reaction medium and participate in the whole synthesis. Secondly by using only ammonium precursor MetrisN (Figure 1) that leads to periodic mesoporous organosilicas (PMOs). Different synthesis conditions were investigated in order to optimize the synthesis of hybrid silica monolith with highest concentration of ionic substructures.

Due to the difference of the reactivity of organosilane precursors, it is to note that the incorporation of organic functionalities in the silica framework is often difficult to reach. In order to obtained hybrid monoliths with hierarchical porosity, the synthesis often requires synthesis optimization.[15]

Considering the co-condensation process, the integration of amine and ammonium functionalities was achieved by the use of two organosilane precursors: tris(3-(trimethoxysilyl)propyl)amine (**TrisN**) and methyl-(tris(3-trimethoxysilyl)propyl) ammonium iodide (**MeTrisN**), see Figure 1. in the presence of silica precursor TEOS. The quantity of the organosilane precursors were varied from 5, 10, 20 to 40 weight %.

The syntheses were performed in the presence of cationic surfactant or anionic surfactant tetradecyltrimethylammonium bromide **TTAB** or sodium dodecyl sulfate **SDS** respectively. For each case the synthesis was promoted either by the addition of by hydrochloric acid at 37% or ammonia at 0.1 M.

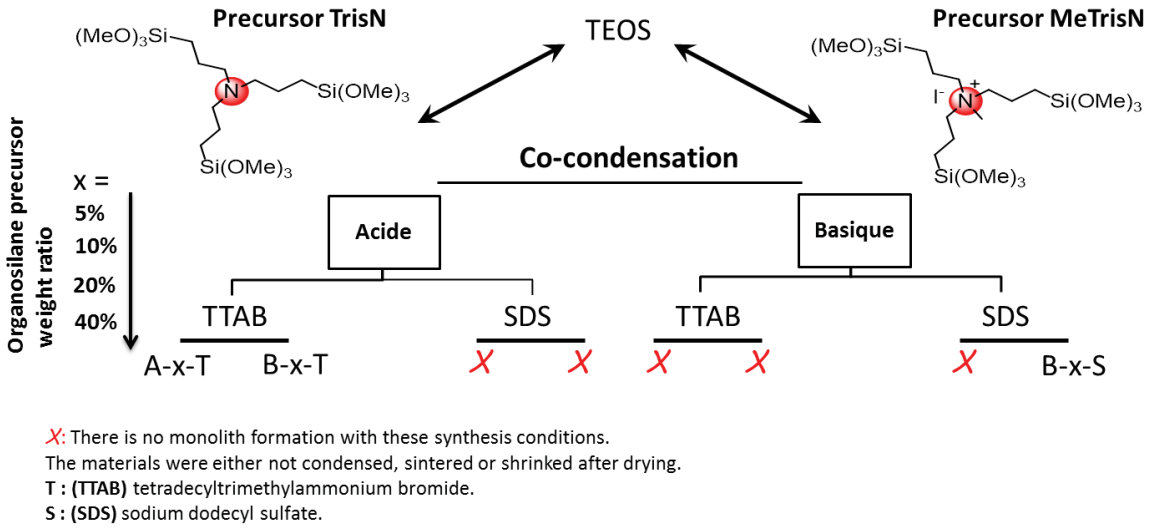


**Figure 1. Different synthesis conditions to obtain hybrid monolith via co-condensation process.** Using the precursors tris(3-(trimethoxysilyl)propyl)amine (**TrisN**) and methyl-(tris(3-trimethoxysilyl)propyl) ammonium iodide (**MeTrisN**) as the organic functionalities source. The final obtained monoliths are: **TrisN-x-T**, **MeTrisN-x-T** and **MeTrisN-x-S** where **x** is the concentration of **TrisN** or **MeTrisN**, **T** corresponds to **TTAB** surfactant and **S** to **SDS** surfactant.

To summarise: For the co-condensation process we studied the effect of several parameters on the formation of hybrid silica monolith:

- Organosilane precursor type and concentration.
- Surfactant nature (cationic or anionic).
- Catalysis condition (acid or base).

The monoliths synthesis was performed through a double template process making use of direct emulsion and a lyotropic mesophase (see chapter 1 and chapter2, part1 for more details on surfactant and the formation of lyotropic mesophase). The direct emulsion was used to create the macroporosity while the lyotropic phase acts both to stabilize the oil/water interface and to create micellar induced mesoscopic porosity.

The surfactant used for the synthesis of silica monolith acts both for the stabilization of liquid-liquid interfaces and for silica mesostructuring via lyotropic phase. The concentration of surfactant molecules was fixed to about 80 times the CMC in all performed experiments. Under these conditions, the interfaces are saturated and must have a low viscoelasticity. Furthermore, the self assembly of surfactant molecules in the continuous phase will increase the viscosity and act as a template for the formation of mesoporosity. At the same time, this lyotropic phase stabilize the emulsion and limits the effects of creaming.[11]

An aqueous medium was used as the continuous phase during this study. For this purpose deionized water was used preferentially in order to avoid the interfaces disruption (short-chain alcohols can disrupt the monolayer of surfactants and induce premature coalescence). Furthermore, the aqueous medium was chosen to promote the polymerization of silica precursors.

Concerning the emulsion step, we used a linear alkane (dodecane ($C_{12}H_{26}$)). This compound commonly used in the emulsions has a relatively low viscosity ($\eta$ = 1,5m Pa.s at 20°C), a density of about 0.75 g / $cm^3$ and is nearly insoluble in water. Moreover, this hydrocarbon is barely volatile (vapor pressure of about 0.04 kPa at 20°C) in contrast with alkanes shorter chains such as hexane (vapor pressure of about 16.5 kPa 20°C). This last characteristic should limit the effects of evaporation during the gel aging.
Generally the synthesis of monoliths is following the same strategy as described previously by F. Carn *et al.*[11]. A General synthesis procedure is described as follow:
A very concentrated surfactant aqueous solution more than 80 times the CMC was prepared. 5 g of silica precursor (TEOS with precursor **TrisN** or **MetrisN**) is added drop-by-drop and under stirring to a solution consisting of 16 mL of surfactant solution with 5 ml of acidic or basic solution. The mixture is then left stirring vigorously to promote evaporation of ethanol from the

hydrolysis of silica precursors. After the hydrolysis of the silica precursor is complete, and the solution, initially turbid, became clear. The aqueous solution is then placed in a mortar. The oil phase composed of approximately 30 mL of dodecane is added drop-wise and the emulsification is performed manually using a pestle. The volume fraction of oil is about 67%. The emulsion is then placed in plastic containers and let to age one week in order to allow the polycondensation of the inorganic matrix. The oily phase is then removed by successive washings (3 x 24 h) in 200 mL of an equimolar mixture of tetrahydrofuran (THF) and acetone. The monoliths are dried one week at room temperature, and then thermally treated at 150°C in air for 7 hours (with a temperature rise speed of 2°C per minute). This heat treatment allows the evaporation of remnant organic solvents and consolidates the organic/inorganic walls. For more details on monoliths synthesis *see* annex.

# 3 Results and discussion

After syntheses of the monoliths following different processes and synthesis conditions, the monoliths formation and the effect of several chemical parameters were then studied using several characterization techniques. In the first glance, the as-synthesized monoliths were characterized visually and qualitatively.

## 3.1 Effect of chemical parameters on monolith formation

Materials produced by the synthesis route described above appear as a monolithic shape see Figure 2, the size and shape depend mainly on the used container (typically cylinder with radius of 3 cm and height of 6 cm). However after drying or thermal treatment step, some materials display high densification and sintering effect related to the inorganic polycondensation. In first glance, the calibrated containers acting as a mold allow us to observe qualitatively these characteristics.

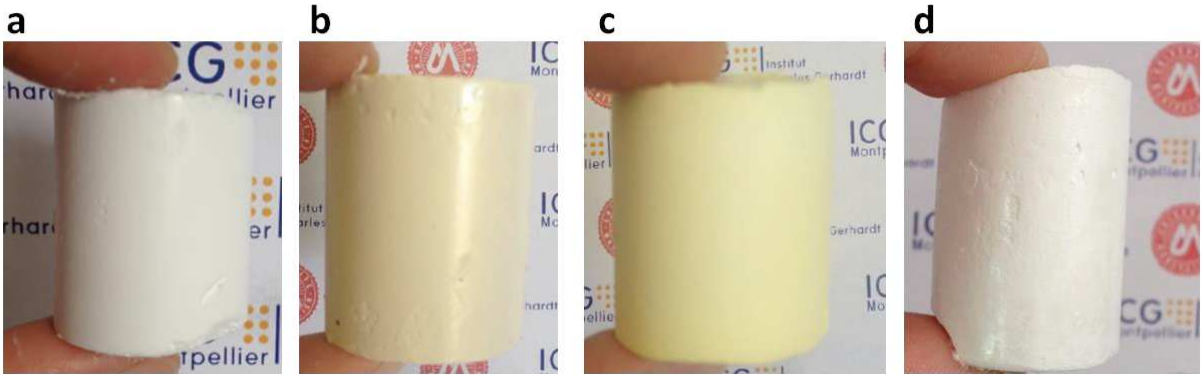


**Figure 2. Photograph of a monolith synthesized for each condition synthesis: a) TrisN-20-T, b) MeTrisN-10-T, c) MeTrisN-40-S and d) MeTrisN-100-S.**

In the following we will discuss qualitatively the shape and mechanical properties of the monoliths obtained with different syntheses conditions. We will discuss separately the monoliths obtained by co-condensation route and PMO monolith.

### 3.1.1 Co-condensation process

In this study, several parameters were used in order to investigate the formation of hybrid silica monolith. Hereafter, we will discuss the effect of the catalyst (acid or base) together with the type of surfactant and precursors (TEOS/amine or ammonium precursors) weight ratio on monolith formation.

#### *3.1.1.1 Catalysis condition and surfactant type effect on monolith formation*

For the synthesis catalyzed with hydrochloric acid at 37% the formation of monoliths was observed only for the synthesis carried out in the presence of cationic surfactant (**TTAB**). The pH of the emulsion is close to zero. This high acidic concentration yields the silica far from its isoelectric point. Therefore the native objects will depict a strong Euclidian character.[20]
In this case, we obtained monoliths using the two organosilane precursors (**TrisN** and **MeTrisN**). Monoliths synthesized with the precursor **TrisN** are called **TrisN-x-T**, while those with the precursor **MeTrisN** are called **MeTrisN-x-T. TrisN** and **MeTrisN** correspond to the added organosilane precursors **TrisN** and **MeTrisN** respectively, **x** is the weight concentration of the organosilica precursors (**x** = 5, 10, 20, 40 %) and **T** is the cationic surfactant **TTAB**.

Using anionic surfactant (**SDS**), the monoliths were either shrinked or sintered. This can be explained by the weak interaction of anionic surfactant with the hydrolyzed silica precursors. As described above, the lyotropic phase was used to stabilize the emulsion and promote the precursors condensation.[11] The very weak interaction between the precursors and the surfactant[14] could form two different phases resulting in
unconsolidated materials.

For syntheses carried out in basic condition, the pH of the emulsion is around 10. At this pH the silica species are present as anions (silanolate).[14] The non-obtaining of monoliths in the presence of **TTAB** could be related to the fact that the interaction of silica species and **TTAB** are not strong enough. Since silicates with a high negatively-charged density can only assemble with the cationic surfactants through strong electrostatic interaction. The surfactant (CTAB)-silica composite can exist stably at a pH greater up to 12.[21]

Considering now the monoliths synthesized in the presence of **SDS**, the monoliths obtained with the precursor **TrisN** display a high shrinkage and sintering effect. In contrast with precursor **MeTrisN**, we observed the formation of well-defined monoliths starting at certain concentration (see Figure 2-d). This observation can be explained by the formation of precursor **MeTrisN / SDS** surfactant ion pairs through the electrostatic interaction between the cationic entities of the precursor (ammonium) and the anionic surfactant head group.[22] Thus stabilizing the emulsion and promoting the condensation rate.[11] Therefore, the precursor **MeTrisN** acts as a structure directing agents as described in the literature.[19, 23] In contrast with precursor **TrisN**, the non-obtaining of monoliths is due to the precursors charge. In fact, at the basic condition the amine group of TrisN is in neutral form.

The monoliths obtained from the precursor **MeTrisN** and **SDS** surfactant are called **MeTrisN-x-S series**, where **MeTrisN** is the organosilica precursor, **x** is the weight ratio of precursor **MeTrisN** (**x** = 5, 10, 20, 40 %) and **S** is the anionic surfactant **SDS**.

#### *3.1.1.2 Precursor concentration on monolith formation*

In the following, the effect of the concentration of amine and ammonium precursor on the formed monoliths is investigated. In the case of monoliths synthesized under acidic condition **TrisN-x-T** and **MeTrisN-x-T series**, mechanical properties of the as-synthesized monoliths did not change by increasing the amount of the organosilane precursor from 5 to 20 w%. Starting from 40 w% the monoliths obtained are shrinked after drying and heat treatment.

All these observations can be explained by the difference of hydrolysis condensation kinetics between **TEOS** and organosilica precursor. In fact **TEOS** and organosilane present large differences in chemical reactivity.[24] These differences can induce the formation of not consolidate material.

Remarkably we noticed the opposite effect with **MeTrisN-x-S** series, monoliths obtained in the presence of **SDS** under basic condition, mechanical properties of monoliths is becoming increasingly important with increasing the precursor **MeTrisN** concentration starting from 20 w%. These observations show that the organic precursor promotes the formation of monolith. In fact with increasing the precursor **MeTrisN** the formation of cationic precursor / anionic surfactant ion pairs increase. Therefore this is a clear demonstration that the well-defined interaction between the silica precursor and surfactant stabilizes the emulsion and promotes the precursors condensation.

In conclusion, we synthesized hybrid monoliths containing amine and ammonium substructures. The monoliths were obtained either under acidic or basic condition. The formation of monoliths under acidic conditions was observed only in the presence of **TTAB**. Contrary with basic way, we obtained monoliths using **SDS** only in the presence of cationic precursor **MeTrisN**.

### 3.1.2 Periodic mesoporous organosilica monolith

Concerning PMO monoliths, the synthesis was recorded following the **MeTrisN-x-S** synthesis condition under basic condition in the presence of anionic surfactant **SDS**. The synthesis of monoliths using exclusively the ammonium precursor was performed. The obtained monolith was called **MeTrisN-100-S** in order to simplify further discussion.

To summarize, using the co-condensation process we synthesized monoliths with different pathways. Under acidic condition with **TTAB**, we obtained monoliths at different organosilane precursor concentration. Furthermore, it is to note that the synthesis of monoliths in the presence of anionic surfactant were not reported previously, here we were able to synthesis monolith with ammonium functionalities in the presence of **SDS**. The syntheses show that the presence of the ammonium precursor promotes the formation of monoliths. Finally, we successfully synthesized PMO monolith starting only from the ammonium precursor. The table below summarizes all the monoliths obtained bearing a good external mechanical property.

**Table 1: Different synthesized monoliths**

| Process | Catalysis condition | Precursor | Surfactant | Obtained monoliths |
|---|---|---|---|---|
| **Co-condensation** | Acid | **TrisN** and **MeTrisN** | **TTAB** | **TrisN-5-T**, **TrisN-10-T**, **TrisN-20-T**, **MeTrisN-5-T**, **MeTrisN-10-T**, **MeTrisN-20-T**. |
| | Basic | **MeTrisN** | **SDS** | **MeTrisN-20-S**, **MeTrisN-40-S** |
| **PMO** | Basic | **MeTrisN** | **SDS** | **MeTrisN-100-S** |

**T** for **TTAB**, **S** for **SDS** and 5, 10, 20, 40 and 100 for the organosilane precursor weight ratio.

## 3.2 Characterization at the macroscopic length scale

### 3.2.1 Scanning electron microscopy (SEM)

In order to understand more in detail the formation of monoliths together with the shrinkage and sintering effect, we observed the textural properties of the as-synthesized monoliths at macroscopic scale using scanning electron microscopy (SEM). In the following we will discuss separately the SEM images of monoliths obtained under acidic condition in the presence of **TTAB** with precursor **TrisN (TrisN-x-T series)** and with precursor **MeTrisN** (**MeTrisN-x-T series**)followed by the monoliths obtained under basic condition in the presence of SDS with precursor MetrisN (**MeTrisN-x-S**). In all these conditions the organic precursor (**TrisN** and **MeTrisN**) concentration was varied from **x** = 5, 10, 20 to 40 w%.

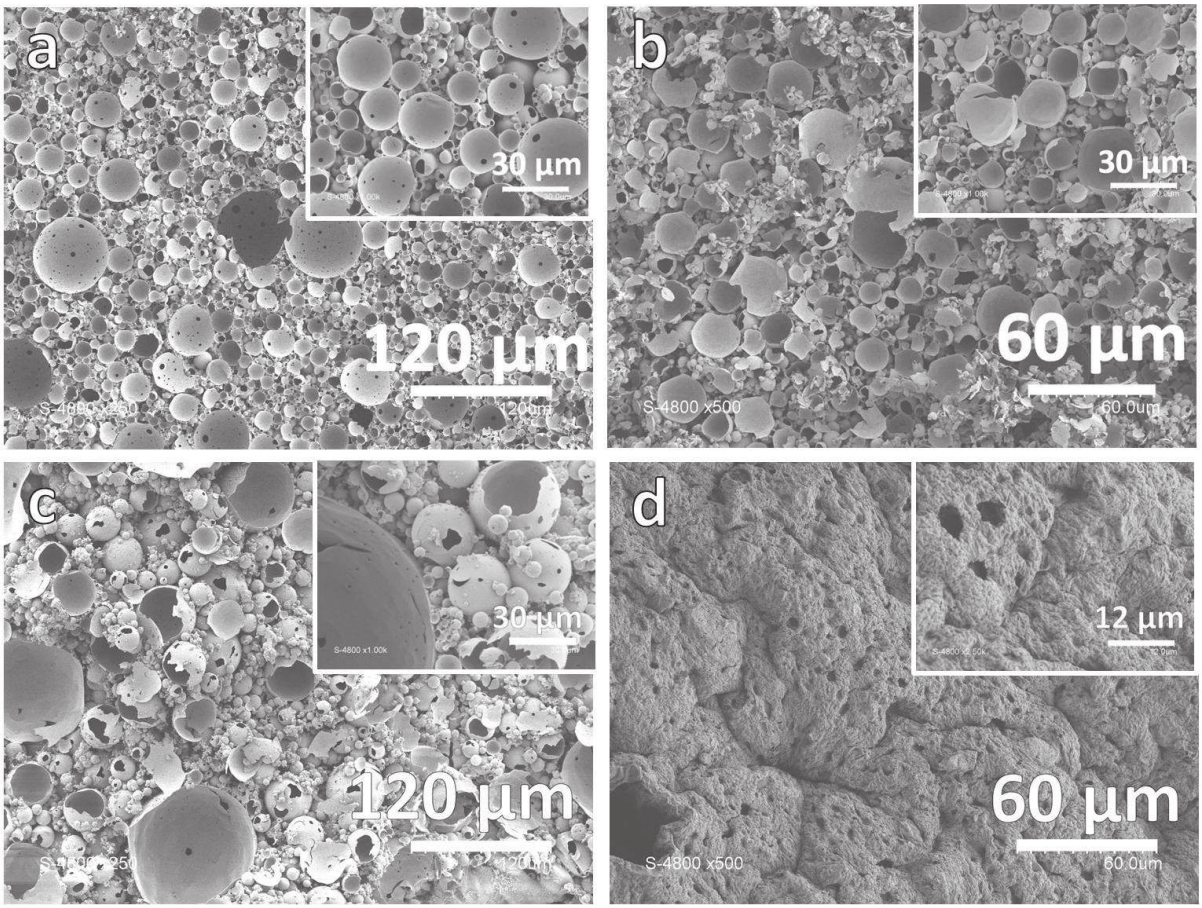


**Figure 3. SEM micrographs of the hybrid monolith-type material synthesized with the precursor TrisN under acidic condition in the presence of TTAB: a) TrisN-5-T, b) TrisN-10-T, c) TrisN-20-T and d) TrisN-40-T.**

The Figure 3 Shows SEM images of the monoliths obtained under acidic condition using **TTAB** with precursor **TrisN** at different concentration. The Figure 3-a, b, c and d correspond to **TrisN-5-T**, **TrisN-10-T**, **TrisN-20-T** and **TrisN-40-T** samples respectively. All samples display hollow spheres aggregation structure except for the material with highest precursor concentration of **TrisN** (**TrisN-40-T)**. The "hollow spheres" aggregation, usually named "cells",[11] induced by oil droplets template removed after intensive washing, are rather polydisperse in size ranging from 5 to 63 µm for **TrisN-5-T** sample, 3 to 28 µm and 4 to 95 µm for **TrisN-10-T** and **TrisN-20-T** respectively. Furthermore we observed that these cells are connected together and the holes that separate two adjacent macroscopic cells are called "cell windows".[11]

As previously mentioned by Backov *et al.*[11, 25] the presence of these hollow spheres demonstrates that mineralization starts at the water interface (interface acting as a defect where the nucleation enthalpy is lowered) and then extends moderately to the water phase, without polymerizing throughout the hydrophilic continuous phase.

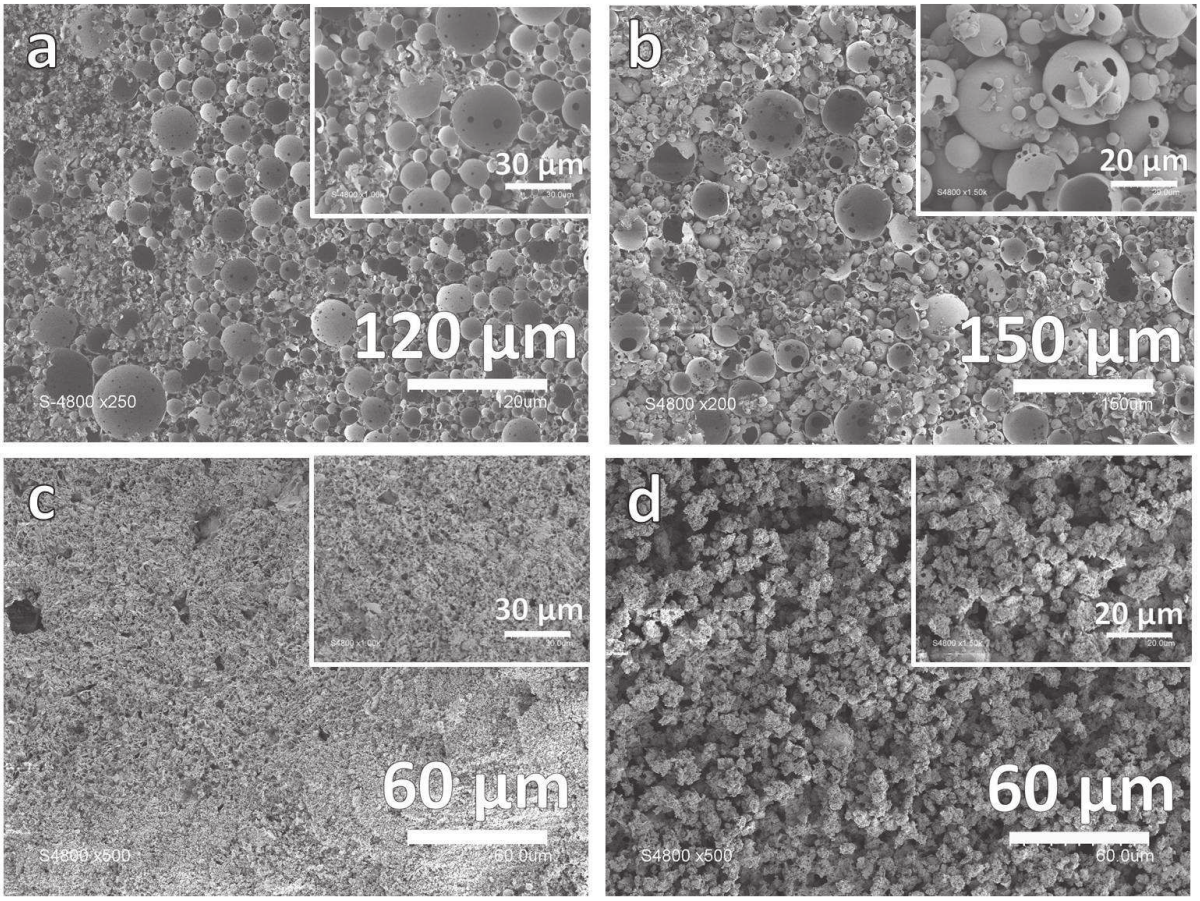


**Figure 4. SEM micrographs of the monoliths synthesized with the precursor MeTrisN under acidic condition in the presence of TTAB: a) MeTrisN-5-T, b) MeTrisN-10-T, c) MeTrisN-20-T and d) MeTrisN-40-T.**

Regarding the materials with ammonium precursor **MeTrisN** under acid condition in the presence of **TTAB**, the typical hollow spheres were observed for the monoliths with 5 and 10 w% of precursor **MeTrisN** (**MeTrisN-5-T** and **MeTrisN-10-T** in Figure 4-a and b respectively). These cells are also polydisperse in size about 4 to 65 µm diameter range. For the monolith with 20 w% of precursor **MeTrisN** (**MeTrisN-20-T)** the structures collapse partially as shown in Figure 4-c. However, the presence of small spheres of 3 to 9 µm was observed. In contrast,

material with highest percentage of precursor **MeTrisN** (**MeTrisN-40-T)** displays no presence of hollow spheres (Figure 4-d).

All these observations show that for the monoliths displaying shrinkage and sintering effect described above, their textural properties do not show the hollow spheres aggregation. In contrast the monoliths with a good mechanical property display the hollow spheres aggregation induced by oil droplets

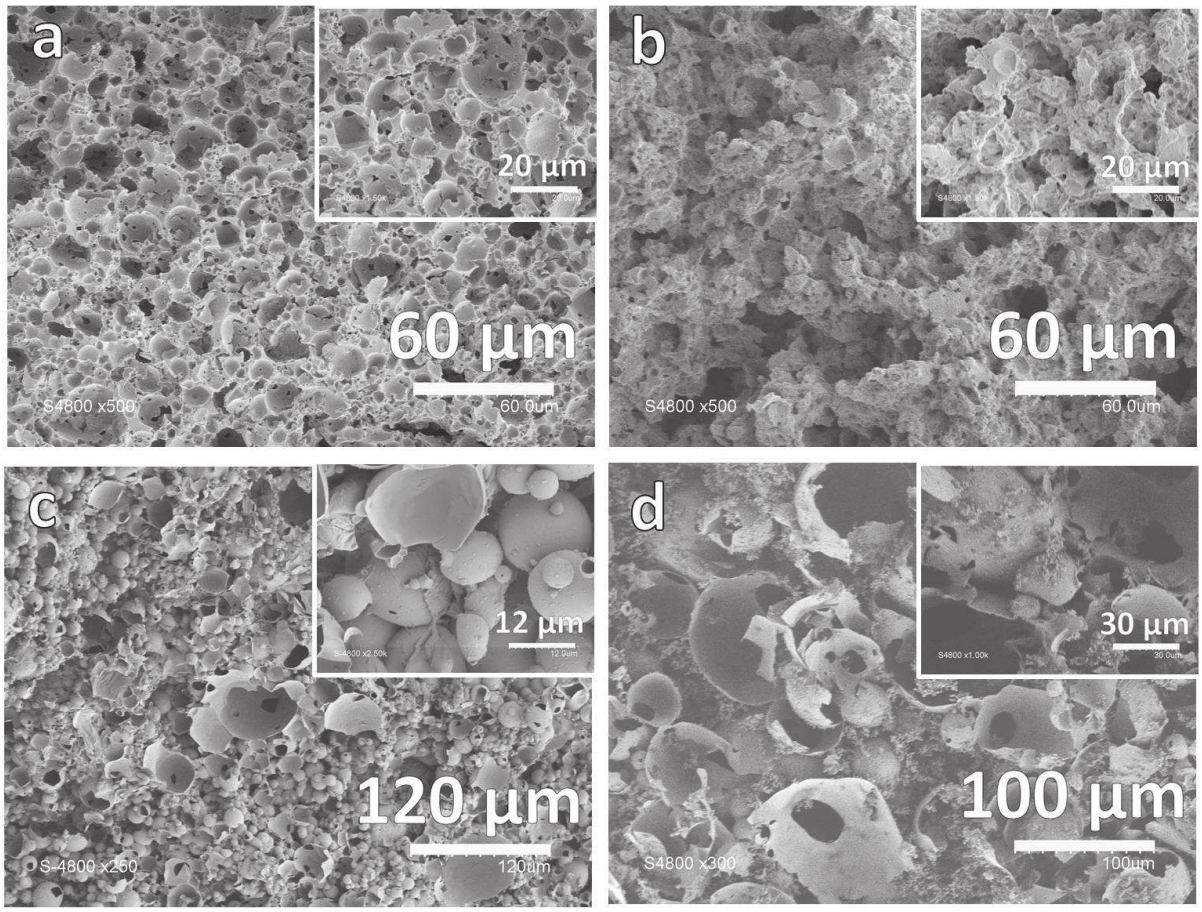


**Figure 5. SEM micrographs of the hybrid monolith-type material synthesized with the precursor MeTrisN under basic condition in the presence of SDS: a) MeTrisN-5-S, b) MeTrisN-10-S, c) MeTrisN-20-S and d) MeTrisN-40-S.**

In the following we observed the same behaviors with the monoliths obtained under basic condition in the presence of **SDS** and precursor **MeTrisN** at different concentration (**MeTrisN-x-S)**. The hollow aggregations were observed only with the monoliths with defined exterior shape. In fact, monoliths with 5 and 10 w% of precursor **MeTrisN** display a high densification and sintering effect. Their textural properties observed by SEM show some macroscopic void space

in the case of 5 w% but the material with 10 w% show a continuous phase without a characteristic shape. Concerning the monoliths with higher percentage, here 20 and 40 w% (see Figure 5-c and d), the macroscopic textures of the monoliths resemble a "hollow spheres" aggregation. We observed 30 to 70 µm and 20 to 100 µm diameter range for **MeTrisN-20-S** and **MeTrisN-40-S** samples respectively. Moreover with **MeTrisN-40-S** sample, we observed, in addition of the hollow spheres, the formation of very small particles surrounding the macroscopic spheres. These particles are 1.2 to 3 µm in diameter size.

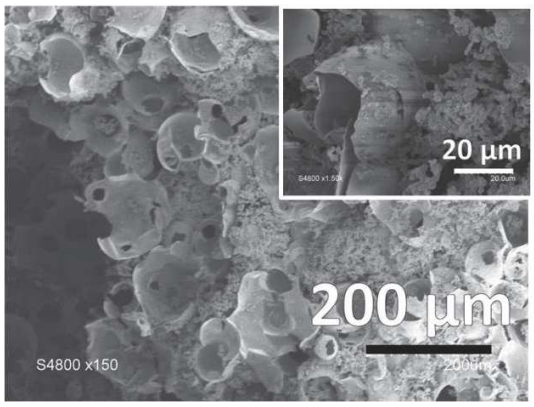


**Figure 6. SEM micrographs of the PMO monolith material (MeTrisN-100-S) synthesized with the precursor MeTrisN under basic condition in the presence of SDS.**

Finally, the PMO monolith **MeTrisN-100-S** was characterized by SEM, the Figure 6 depicts a "hollow spheres" aggregation with pore opening connecting two adjacent cells. These cells are rather polydisperse in size ranging from 20 to 140 µm. In addition we also observed the formation of small particles around the cells (Figure 6) with diameters size of 1.8 to 7 µm.

Regarding all the monoliths synthesized under basic condition and in the presence of **SDS**, the hollow spheres aggregation show an increase with the weight ration of the precursor. This behavior is due to probably of both to the highest reactivity of the precursor **MeTrisN** and to the presence of alcohol. Indeed, the time of the emulsification reduce with the precursor quantity leading to larger diameter size and the presence of propanol which is used to promote the organosilane precursor solubilization in aqueous phase can induce the premature coalescence.

Considering these all results, we observed that the formation of monoliths without any shrinkage or sintering effect require a strong precursor / surfactant interaction. The SEM characterization showed that the formation of monoliths is observed only with the formation of hollow spheres

induced by oil droplets, suggesting that the precursor condensation starts at the oil/water interfaces then extends to the core continuous phase as described previously by Backov *et al.*[11, 25] For further characterization we selected the monoliths which present a good mechanical stability bearing macroporosity as observed by SEM. We then selected the materials: **TrisN-5-T**, **TrisN-10-T**, **TrisN-20-T**, **MeTrisN-5-T**, **MeTrisN-10-T**, **MeTrisN-20-T**, **MeTrisN-20-S**, **MeTrisN-40-S** and **MeTrisN-100-S** for further characterization. These materials were characterized by means of intrusion / extrusion mercury measurements, nitrogen sorption and solid state NMR spectroscopy.

### 3.2.2 Mercury intrusion porosity measurements

In order to better quantify the macroscale void space distribution we performed the mercury intrusion porosity measurements. Here we have to specify that mercury intrusion porosimetry measures the size of the macroscopic pore ‘‘windows’’ between the emulsion templated cells and not the diameter of the cells themselves. Also, we have to note that all the materials described in this work display a scaffold with mechanical strength high enough to endure mercury porosity measurements, which is an important property.

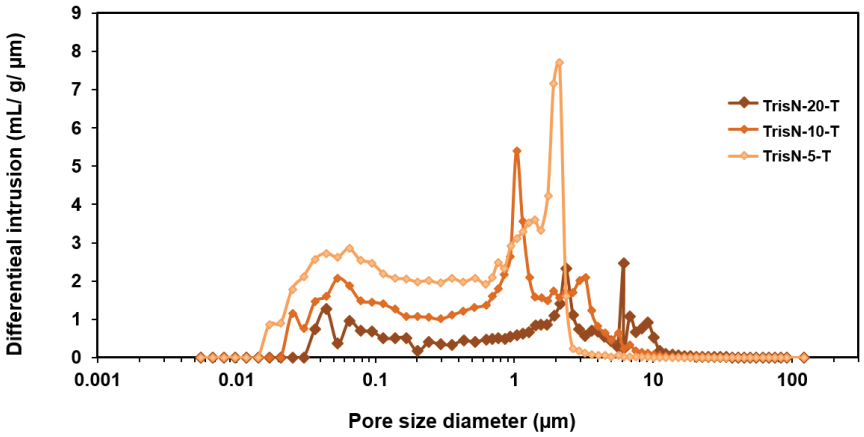


**Figure 7. Macroscopic pore sizes distribution obtained through mercury intrusion porosimetry of monoliths obtained under acidic condition in the presence of TTAB and with the precursor TrisN at different weight ration: TrisN-5-T, TrisN-10-T and TrisN-20-T samples.**

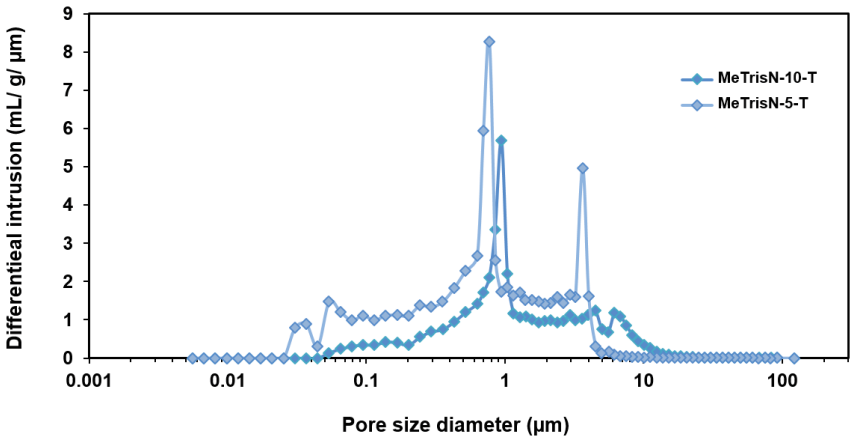


**Figure 8. Macroscopic pore sizes distribution obtained through mercury intrusion porosimetry of monoliths obtained under acidic condition in the presence of TTAB and with the precursor MeTrisN at different weight ratios: MeTrisN-5-T and MeTrisN-10-T samples.**

The Figure 7 and Figure 8 correspond to the macroporous size distribution of the monoliths obtained under acidic condition in the presence of **TTAB** with the precursor **TrisN** and **MeTrisN** corresponding to **TrisN-x-T** and **MeTrisN-x-T** series respectively. In general the distributions display two sets of windows. First, we have the window that intrinsically connects two adjacent microporous cells that observed previously by Carn *et al.*[11] called "internal junctions". Moreover, considering the aggregated "hollow spheres" textural aspect of macropores, we have to consider window emerging from aggregation between several hollow spheres. This is what is called "external junctions".

In addition, we observed that the pore range increases with the precursor concentration. Regarding the **TrisN-x-T** monoliths series we have pores range of 0.01 – 3 µm, 0.017 – 6 µm and 0.025 – 10 µm which corresponds to **TrisN-5-T, TrisN-10-T** and **TrisN-20-T** respectively. For the monoliths obtained with precursor **MeTrisN**, we have 0.03 − 5 µm for **MeTrisN-5-T** and 0.05 – 12 µm for **MeTrisN-10-T**. This increase of porosity with the precursor concentration can be related to the hollow spheres diameter size. In fact, as depicted by SEM images the hollow spheres aggregation increase with the precursor concentration, leading to an increase of diameter of cell windows (internal junction). Moreover, at this condition the emulsion phase becomes decreasingly compact with the increase of spheres diameter. As a result the continuous phase is not completely polymerized inducing the increase in the second porosity (external junction).

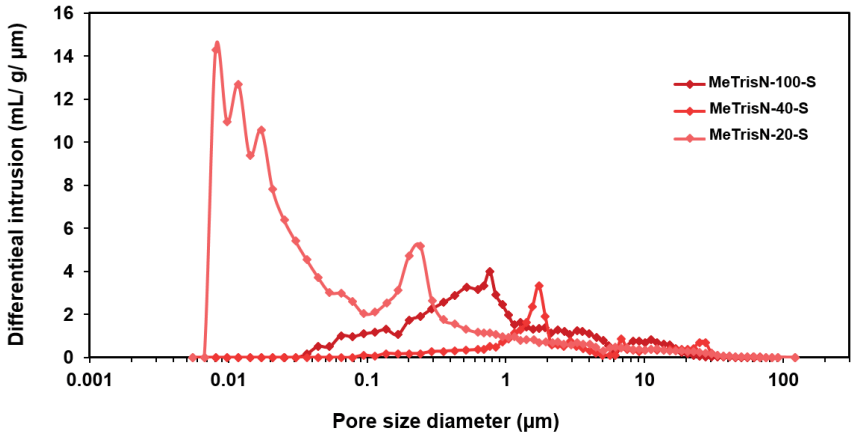


**Figure 9. Macroscopic pore sizes distribution obtained through mercury intrusion porosimetry of monoliths obtained under basic condition in the presence of SDS and with the precursor MeTrisN at different weight ratios: MeTrisN-20-S, MeTrisN-40-S and MeTrisN-100-S samples**

Finally, the Figure 9 shows the size distribution of monoliths obtained under acidic condition in the presence of **SDS** and precursor **MeTrisN** (**MeTrisN-x-S** series). For the sample **MeTrisN-20-S**, the bimodal character was observed but the two sets windows are closer. The pores related to the internal junctions in the range of 0.01 – 0.1 µm are more important. Rather than **MeTrisN-40-S** sample which displays only one set window, the pores size distribution is located at values greater than 0.3 µm. In contrast, PMO monolith (**MeTrisN-100-S)** displays a very polydispersity distribution ranging from 0.030 µm to 11 µm. Even more these observations are related to the emulsion step.

**Table 2. Mercury intrusion porosimetry data.**

| Entry | Materials | Intrusion volume ($cm^3.g^{-1}$) | Porosity (%) | Bulk density ($g.cm^{-3}$) | Skeletal density ($g.cm^{-3}$) |
|---|---|---|---|---|---|
| **1** | **TrisN-5-T** | 9.6 | 92 | 0.1 | 1.23 |
| **2** | **TrisN-10-T** | 9.9 | 94 | 0.1 | 1.64 |
| **3** | **TrisN-20-T** | 9.2 | 92 | 0.1 | 1.22 |
| **4** | **MeTrisN-5-T** | 10.1 | 92 | 0.1 | 1.3 |
| **5** | **MeTrisN-10-T** | 11.8 | 94 | 0.08 | 1.39 |
| **6** | **MeTrisN-20-S** | 15.4 | 94 | 0.06 | 1 |
| **7** | **MeTrisN-40-S** | 17.5 | 96 | 0.05 | 1.4 |
| **8** | **MeTrisN-100-S** | 17.5 | 90 | 0.05 | 0.5 |

Nevertheless, looking more precisely at the mercury porosimetry data collected in Table 2, we observe for all the samples the porosity is equal or more than 90%. The volume intrusion of the monolith synthesized under acidic condition **TrisN-x-T** and **MeTrisN-x-T** series is between 9.2 and 11.8 $cm^3.g^{-1}$ (Table 2, entries 1-5). Interestingly, for the samples synthesized under basic condition (**MeTrisN-x-T** series) the intrusion volume is more important. The sample **MeTrisN-20-S** displays 15.4 $cm^3.g^{-1}$ and **MeTrisN-40-S** with **MeTrisN-100-S** show intrusion volume of about 17.5 $cm^3.g^{-1}$ (Table 2, entries 6-8).

There are two parameters that can influence the value of the bulk density; the amount of the added hybrid precursor and the fraction of the void space. We noticed for the series **TrisN-x-T**, the bulk density was 0.1 $g.cm^{-3}$ (Table 2, entries 1-3) and does not change depending on the precursor **TrisN** concentration. We observed a similar result for the **MeTrisN-x-T** series (Table 2, entries 4 and 5), nevertheless a slight decrease in bulk density for the **MeTrisN-10-T** sample comparing with **MeTrisN-5-T** sample was observed. Finally, **MeTrisN-x-S** series show a lower bulk density, we observe 0.06 and 0.05 $g.cm^{-3}$ see Table 2, entries 6-8. This decrease in density is accompanied by an increase in the volume of intrusion.

These results show that the apparent density value is related with the fraction of the void space. As observed by SEM and also from the mercury porosimetry measurements, the pore size is much more important in basic medium. So we associated this behavior to the way in which the inorganic network grows in the continuous phase. Indeed, we found that the continuous phase has a large volume occasionally when it is not fully mineralized. Under these conditions, a second source of porosity is added from drops of oils and polydispersity increases.

### 3.3 Hypothesis formation monoliths mechanism

It is important to note that the shrinkage and sintering effect of monolith was observed when the organic precursor weight ratio increase (up to 20%) with monoliths synthesized under acidic condition. These effects are due to the difference of reactivity of **TEOS** and organosilane precursor. In contrast under basic condition, the effects decrease with the increasing the organosilane weight ratio. This observation is a nice demonstration that the ammonium precursor

acts as a structure directing agent. These observations are in direct relation with the fact that the condensation as previously mentioned certainly starts at the oil-water interface. In fact the oil-water interface might promote silica condensation by minimizing the nucleation enthalpy, acting as a defect. In addition, the strong interaction of the precursor and surfactant might be crucial for the formation of the monoliths. In fact, it is well known that the oil-water interface of an emulsion is associated with a higher surfactant concentration than the core of the continuous aqueous phase. [11, 25] In this specific region of high surfactant concentration should enhance silica condensation. This consideration might explain why the silica condensation first starts at the oil-water interface and then extend up to the wall core.

## 3.4 Characterization at the mesoscopic and microscopic length scale

After ascertained the formation of monoliths and having characterized their morophology on a macroscopic length scale, we proceed to their characterization at the micro and mesoscpic length scale. First the nitrogen sorption measurements were used in order to quantify the porosity induced by the used surfactant as well as the associated surface area. The second characterization $^{29}$Si solid state NMR spectroscopy was used to confirm the structural integrity of the immobilized organic functionalities (amine and ammonium) after the hydrolysis condensation.

### 3.4.1 Nitrogen sorption measurements

In the following, we studied the textural properties of the as-synthesized monoliths using adsorption-desorption of nitrogen measurements. The Figure 10 shows the adsorption-desorption isotherms of **TrisN-x-T** series. The shape of the isotherm of **TrisN-5-T** sample (Figure 10-a) corresponds to type I with a capillary condensation at low relative pressures characteristic to the microporosity. A similar isotherm was observed in the case of sample **TrisN-10-T** with a slight hysteresis at relative pressure > 0.4 as illustrated by the Figure 10-b. This hysteresis can be attributed to the presence of mesoporosity. Regarding **TrisN-20-T** sample (Figure 10-c), the isotherm shows a type 4 with a hysteresis at higher relative pressures > 0.4 indicating the presence of mesoporosity. Concerning the specific surface area determined by BET, we observed a surface area of 723, 484 and 481 $m^2.g^{-1}$ for samples **TrisN-5-T**, **TrisN-10-T** and **TrisN-20-T** respectively.

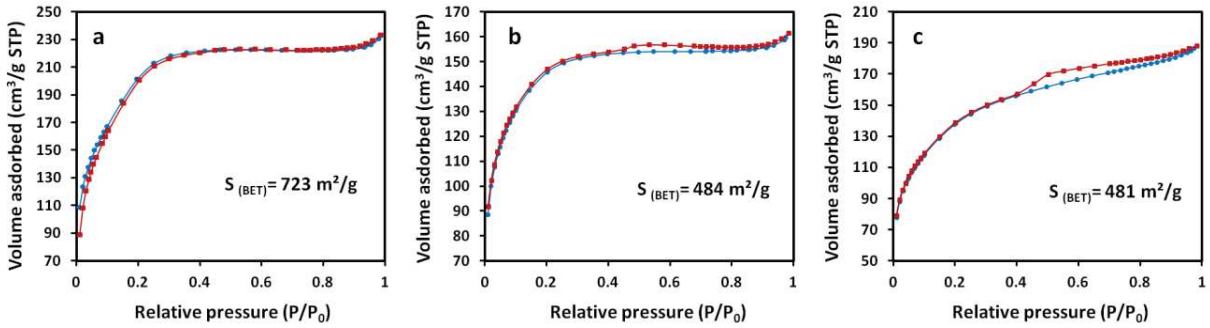


**Figure 10. Nitrogen adsorption-desorption isotherm of monoliths obtained under acidic condition in the presence of TTAB and with the precursor TrisN (TrisN-x-T series): a) TrisN-5-T, b) TrisN-10-T, c) TrisN-20-T.**

For the **MeTrisN-x-T** series, the samples **MeTrisN-5-T** and **MeTrisN-10-T** show an isotherm type 1 with condensation at low relative pressure (Figure 11-a and b). The sample **MeTrisN-20-T** show an isotherm type 4 with a hysteresis around 0.4 relative pressures. Furthermore a condensation at high pressure can be observed indicating the macroporosity (Figure 11-c). The specific surface area determined by BET is about 480 and 557 $m^2.g^{-1}$ for the samples **MeTrisN-10-T** and **MeTrisN-20-T** respectively. The sample **MeTrisN-5-T** shows a highest surface BET more than 960 $m^2.g^{-1}$.

The monoliths obtained under acidic condition show a specific surface area $S_{BET}$ decreases with the increase of organosilane precursor (**TrisN** or **MeTrisN**). This is due to that **TTAB** surfactant interacts with silica precuosor (**TEOS**) and not with amine and ammonium precursor. As a result the decrease of **TEOS** concentration induces the decrease of the surfactant / precursor interaction followed by the decrease in the specific surface area $S_{BET}$.

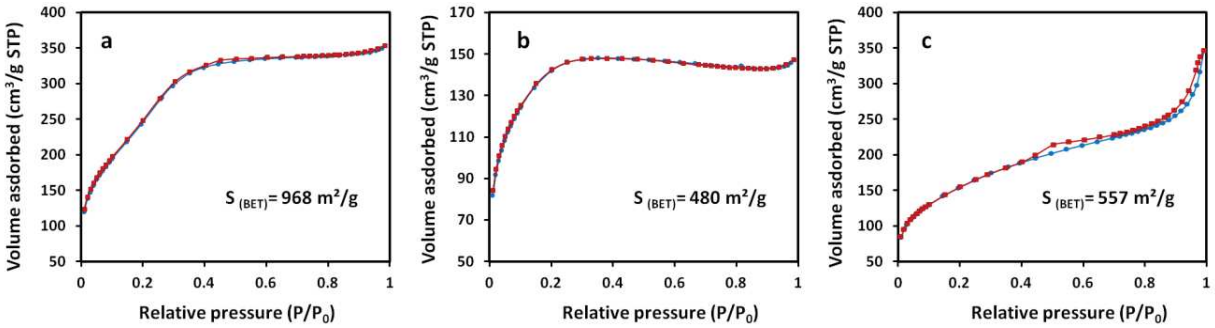


**Figure 11. Nitrogen adsorption-desorption isotherm of monoliths obtained under acidic condition in the presence of TTAB and with the precursor MeTrisN (**MeTrisN-**x-T series): a)** MeTrisN-**5-T, b)** MeTrisN-**10-T, c)** MeTrisN-**20-T.**

Regarding the isotherms of the monoliths obtained under basic condition in the presence of **SDS** and **MeTrisN** precursor (**MeTrisN-x-S** series) as shown in the Figure 12, all the isotherms display different behavior depending on the concentration of precursor **MeTrisN**. The sample **MeTrisN-20-S** shows an isotherm type 4 with a hysteresis at high relative pressure. A type 1 was observed for the sample **MeTrisN-40-S** with condensation at low relative pressure characteristic to the microporosity. Finally, the PMO material **MeTrisN-100-S** display an isotherm type 4 with a hysteresis above 0.4 relative pressures. Concerning the BET specific surface area, we observe smaller surface area than those obtained under acidic condition. In this case synthesis optimization is required in order to improve the mesoporous contribution.

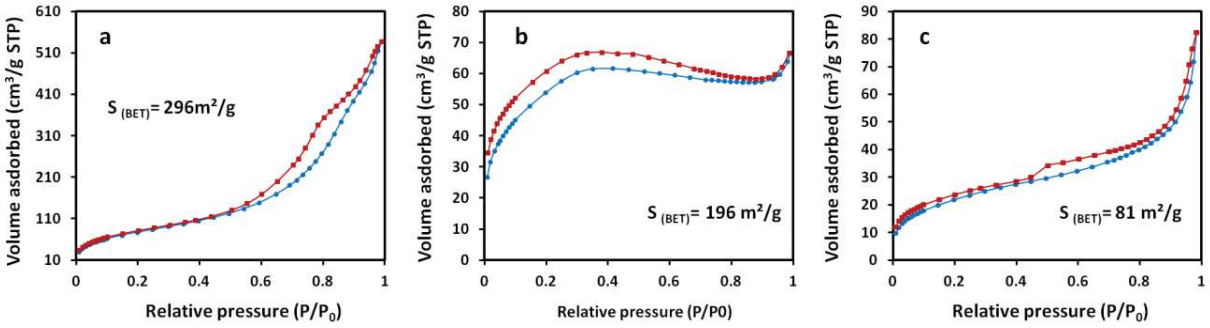


**Figure 12. Nitrogen adsorption-desorption isotherm of monoliths obtained under basic condition in the presence of SDS and with the precursor MeTrisN (MeTrisN-x-S series): a) MeTrisN-20-S, b) MeTrisN-40-S, c) MeTrisN-100-S.**

To summarize, we synthesized hybrid monoliths with amine and ammonium substructures. The monoliths display a microporosity and mesoporosity depending on the synthesis condition and the concentration of the organosilane. Under acidic condition, we obtained a more important specific surface area.

### 3.4.2 Solid state NMR spectroscopy

The synthesis of these hierarchical open-cell functional hybrid monoliths via sol-gel involves hydrolysis and condensation of different precursors, bearing different hydrolysis condensation kinetics when compared with TEOS. Since TEOS and organosilanes present large differences in chemical reactivity, it is important to know the co-condensation degree of the silicate species in the final monoliths. Solid state $^{29}$Si NMR spectroscopy appears as a powerful tool to determine

the local chemical environment around the Si atoms and, therefore, allows the identification of the different siloxane species.

At this stage, we have to specify that $^{29}Si$ sites are labelled with the conventional $T^n$ and $Q^n$ notation *see* Figure 13. Thus, T refers to functional $RSiO_3^-$ units resulting from hydrolysis and condensation of organosilane precursors, while Q species are associated with $SiO_4^-$ units from the silica framework. In this notation, n corresponds to the number of bridging oxygen atoms surrounding the silicon and R to the organic chain.

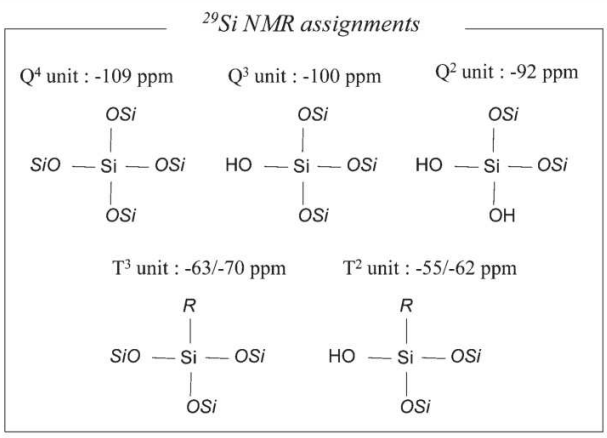


**Figure 13. Assignments of the $^{29}Si$ NMR signals to the silicate species according to the conventional notation.**

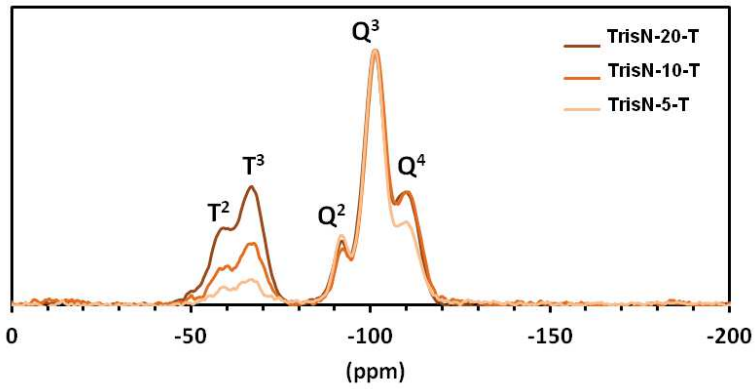


**Figure 14. $^{29}Si$ CP MAS spectra of monoliths obtained under acidic condition in the presence of TTAB and with the precursor TrisN (TrisN-x-T series).**

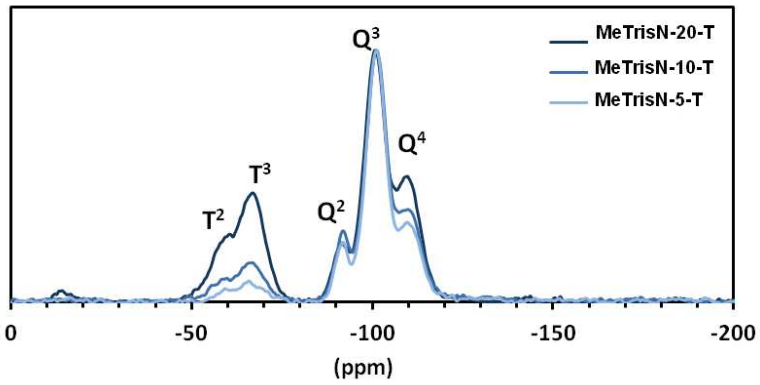


**Figure 15. $^{29}$Si CP MAS spectra of monoliths obtained under acidic condition in the presence of TTAB and with the precursor MeTrisN (MeTrisN-x-T series).**

Figure 14 and Figure 15 illustrate the $^{29}$Si MAS NMR spectra recorded for the samples **TrisN-x-T** and **MeTrisN-x-T**. All spectra show two groups of signals at chemical shifts (δ) of around -50/-70 ppm and -100/-110 ppm, characteristic of the T and Q units respectively. The presence of not fully O bridging silane species, i.e., $Q^2$ (-92 ppm), $Q^3$ (-100 ppm), and $T^2$ (-58 ppm) units, besides those of $Q^4$ (-109 ppm) and $T^3$ -66 ppm units, indicates that the organically modified silica is not completely condensed. On the other hand, it must be noticed that $Q^n$ and $T^n$ signals appear at the same chemical shift in all the spectra. The intense of $T^n$ units significantly increase with the quantity of organosilane precursor used during the synthesis.

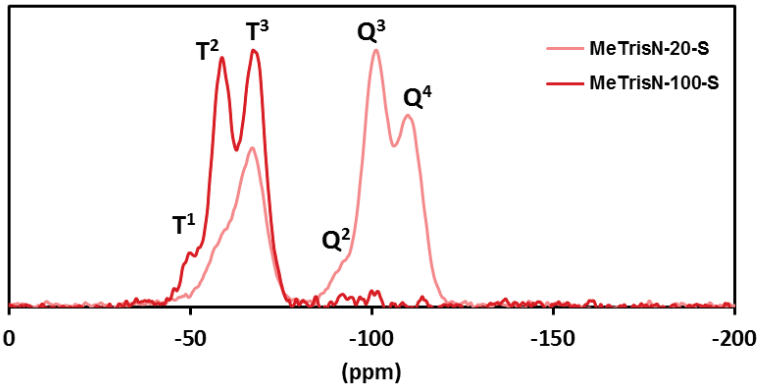


**Figure 16. $^{29}$Si CP MAS spectra of monoliths obtained under basic condition in the presence of SDS and with the precursor** MeTrisN **(**MeTrisN-**x-S series).**

The Figure 16 illustrates the $^{29}$Si MAS NMR spectra of **MeTrisN-20-S** and **MeTrisN-100-S** samples. Like **TrisN-x-T** and **MeTrisN-x-T** series, **MeTrisN-20-S** spectra show the presence of

T and Q units. In contrast, $T^2$ units at (-58 ppm) are hardly identified suggesting the near complete condensation of organosilane precursor. Regarding the PMO monolith **MeTrisN-100-S**, the spectra show only the $T^n$ units. At -50, -67, 59 ppm related to $T^1$, $T^2$ and $T^3$ sites, respectively. The complete absence of Q–resonances in the $^{29}Si$ spectrum indicates that no Si-C bond cleavage occurred during the hydrolysis-condensation and reflect high chemical stability of the precursor under the hydrolysis-polycondensation reactions.

The results obtained from the $^{29}Si$ MAS NMR spectroscopy confirm the incorporation of the organosilane precursors within the hybrid silica monolith scaffold. However, complementary characterizations such as $^{13}C$ solid NMR spectroscopy and thermogravimetric analysis are necessary to quantify the amine and ammonium groups.

## 4 Conclusion

In the present work, we reported the synthesis of hybrid silica monoliths with amine and ammonium substructures. Well defined monoliths were obtained via co-condensation process under acidic condition with cationic surfactant and under basic condition with anionic surfactant. The synthesis was found to be very sensitive towards several parameters: the charge of the organic group of the organosilane precursor and surfactant as well as the catalysis condition. The study shows that the interaction of the surfactant / precursor is a key parameter for the formation of monoliths. The monoliths obtained show trimodal hierarchical pores structures. However the volume intrusion determined by mercury macroporosity is much higher in the case of monoliths obtained under basic condition. Using the basic catalysis, the monoliths formation was observed only with the ionic precursor. Under these conditions, we were able to incorporate a higher amount of organic functionalities. Finally, we reported the synthesis of PMO monoliths bearing ammonium functionalities homogenously distributed over the whole silica network. However, the optimization of the parameters is highly requested in this part in order to improve the mesoporous specific surface area.

These synthesized monoliths bearing amine and ammonium substructures are particularly interesting in the field of separation and adsorption of molecules. The high concentration of ionic organic group located in the materials' framework enables immobilization of ionic molecules via ion exchange reactions. These materials promote further use in continuous extraction process and in catalysis.

**References**


1. Faustini, M.; Grosso, D.; Boissiere, C.; Backov, R.; Sanchez, C., "Integrative sol-gel chemistry": a nanofoundry for materials science. *Journal of Sol-Gel Science and Technology* **2014,** 70, (2), 216-226.
2. Sanchez, C.; Lebeau, B.; Chaput, F.; Boilot, J. P., Optical properties of functional hybrid organic-inorganic nanocomposites. *Advanced Materials* **2003,** 15, (23), 1969-1994.
3. Prouzet, E.; Ravaine, S.; Sanchez, C.; Backov, R., Bio-inspired synthetic pathways and beyond: integrative chemistry. *New Journal of Chemistry* **2008,** 32, (8), 1284-1299.
4. Chung, C. M.; Chou, T. P.; Cao, G.; Kim, J. G., Porous organic-inorganic hybrids for removal of amines via donor-acceptor interaction. *Materials Chemistry and Physics* **2006,** 95, (2-3), 260-263.
5. Dutta, S.; Bhaumik, A.; Wu, K. C. W., Hierarchically porous carbon derived from polymers and biomass: effect of interconnected pores on energy applications. *Energy & Environmental Science* **2014,** 7, (11), 3574-3592.
6. El Kadib, A.; Chimenton, R.; Sachse, A.; Fajula, F.; Galarneau, A.; Coq, B., Functionalized Inorganic Monolithic Microreactors for High Productivity in Fine Chemicals Catalytic Synthesis. *Angew. Chem.-Int. Edit.* **2009,** 48, (27), 4969-4972.
7. Nakanishi, K.; Kobayashi, Y.; Amatani, T.; Hirao, K.; Kodaira, T., Spontaneous formation of hierarchical macro-mesoporous ethane-silica monolith. *Chemistry of Materials* **2004,** 16, (19), 3652-3658.
8. Park, S. S.; An, B.; Ha, C. S., High-quality, oriented and mesostructured organosilica monolith as a potential UV sensor. *Microporous and Mesoporous Materials* **2008,** 111, (1-3), 367-378.
9. Ungureanu, S.; Laurent, G.; Deleuze, H.; Babot, O.; Achard, M. F.; Popa, M. I.; Sanchez, C.; Backov, R., Syntheses and characterization of new organically grafted silica foams. *Colloids and Surfaces a-Physicochemical and Engineering Aspects* **2010,** 360, (1-3), 85-93.
10. Marechal, A.; Jarrosson, F.; Randon, J.; Dugas, V.; Demesmay, C., In-line coupling of an aptamer based miniaturized monolithic affinity preconcentration unit with capillary electrophoresis and Laser Induced Fluorescence detection. *Journal of Chromatography A* **2015,** 1406, 109-117.

11. Carn, F.; Colin, A.; Achard, M. F.; Deleuze, H.; Sellier, E.; Birot, M.; Backov, R., Inorganic monoliths hierarchically textured via concentrated direct emulsion and micellar template. *Journal of Materials Chemistry* **2004,** 14, (9), 1370-1376.

12. Wu, C.; Liang, Y.; Yang, K. G.; Min, Y.; Liang, Z.; Zhang, L. H.; Zhang, Y. K., Clickable Periodic Mesoporous Organosilica Monolith for Highly Efficient Capillary Chromatographic Separation. *Analytical Chemistry* **2016,** 88, (3), 1521-1525.

13. Asefa, T.; MacLachlan, M. J.; Coombs, N.; Ozin, G. A., Periodic mesoporous organosilicas with organic groups inside the channel walls. *Nature* **1999,** 402, (6764), 867-871.

14. Hoffmann, F.; Cornelius, M.; Morell, J.; Froba, M., Silica-based mesoporous organic-inorganic hybrid materials. *Angew. Chem.-Int. Edit.* **2006,** 45, (20), 3216-3251.

15. Zhou, Y.; Wan, M. M.; Gao, L.; Lin, N.; Lin, W. G.; Zhu, J. H., One-pot synthesis of a hierarchical PMO monolith with superior performance in enzyme immobilization. *J. Mat. Chem. B* **2013,** 1, (12), 1738-1748.

16. Zhong, H.; Zhu, G. R.; Yang, J.; Wang, P. Y.; Yang, Q. H., Periodic mesoporous hybrid monolith with hierarchical macro-mesopores. *Microporous and Mesoporous Materials* **2007,** 100, (1-3), 259-267.

17. Lin, N.; Gao, L.; Chen, Z.; Zhu, J. H., Elevating enzyme activity through the immobilization of horseradish peroxidase onto periodic mesoporous organosilicas. *New Journal of Chemistry* **2011,** 35, (9), 1867-1875.

18. Zhou, Z.; Inayat, A.; Schwieger, W.; Hartmann, M., Improved activity and stability of lipase immobilized in cage-like large pore mesoporous organosilicas. *Microporous and Mesoporous Materials* **2012,** 154, 133-141.

19. Hesemann, P.; Nguyen, T. P.; El Hankari, S., Precursor Mediated Synthesis of Nanostructured Silicas: From Precursor-Surfactant Ion Pairs to Structured Materials. *Materials* **2014,** 7, (4), 2978-3001.

20. Brinker, C. J.; Scherer, G. W., *SOL-GEL SCIENCE, the physics and chemistry of sol-gel processing*. Academic press, INC: San Diego, 1990.

21. Wu, S.-H.; Mou, C.-Y.; Lin, H.-P., Synthesis of Mesoporous Silica Nanoparticles. *Chemical Society Reviews* **2013,** 42, (9), 3862-3875.

22. Nguyen, T. P.; Hesemann, P.; Thi, M. L. T.; Moreau, J. J. E., Nanostructured polysilsesquioxanes bearing amine and ammonium groups by micelle templating using anionic surfactants. *Journal of Materials Chemistry* **2010,** 20, (19), 3910-3917.
23. Gao, C. B.; Che, S. A., Organically Functionalized Mesoporous Silica by Co-structure-Directing Route. *Advanced Functional Materials* **2010,** 20, (17), 2750-2768.
24. Van Blaaderen, A.; Van Geest, J.; Vrij, A., Monodisperse colloidal silica spheres from tetraalkoxysilanes: Particle formation and growth mechanism. *Journal of Colloid and Interface Science* **1992,** 154, (2), 481-501.
25. Brun, N.; Hesemann, P.; Laurent, G.; Sanchez, C.; Birot, M.; Deleuze, H.; Backov, R., Macrocellular Pd@ionic liquid@organo-Si(HIPE) heterogeneous catalysts and their use for Heck coupling reactions. *New Journal of Chemistry* **2012,** 37, (1), 157-168.

# General conclusion

In this thesis, we have shown that the presence of ionic entities within functional ionic systems offers different properties and application area. We studied two families of compounds: guanidinium salts and ionosilica materials.

Concerning guanidinium salts, we synthesized monoalkylguanidinium surfactants and ionic liquids. Firstly, surface activity and micelle formation of alkylguanidinium chlorides with long alkyl chain were studied by combining ionic conductivity and surface tension measurements with isothermal titration calorimetry. Our results show a clear relationship between alkyl chain length and self-aggregation behavior. Compared to alkyltrimethylammonium chlorides, the increased surface activity of alkylguanidinium surfactants, and the fact that micelle formation is much more exothermic and occurs at much lower CMC values, may be ascribed to the hydrogen-bonding capacity of the guanidinium head-group, which promotes the formation of more compact micelles together with a stronger $Cl^-$ binding in the corresponding stern layer.

The use of guanidinium substructures in ionic liquid for the extraction and the removal of anionic molecules from aqueous solution was investigated. For this purpose, we synthesized a series of new monoalkylguanidinium bis-trifluoromethane sulfonimide ionic liquids. The high potential of guanidinium based ILs in separation was monitored via the extraction of an anionic dye (methyl orange, MO), an anionic drug (diclofenac) and a metallic anion (chromate). We observed a high affinity of organic anions towards the hydrophobic IL phase. It has to be mentioned that in all cases, the guanidinium based ILs gave considerably better results compared to their imidazolium counterparts. Finally, we successfully introduced a closed separation-regeneration cycle of guanidinium ionic liquid. These ionic liquids could then be re-used via sample ion exchange reaction.

Regarding ionosilica materials, their potential for waste water treatment was here investigated. In fact, we have demonstrated that nanostructured cationic ionosilicas bearing quaternary ammonium groups are efficient and re-usable adsorbents with high capacity and high selectivity towards to anionic drugs. Ionosilicas are highly efficient adsorbents even for traces of anionic drugs, thus highlighting the high affinity of these compounds towards the material. Finally, the release tests show no significant drug release. However, it has to be

mentioned that these treatments led to a complete collapse of the pore structure of the material, and a completely non-porous material was recovered after these tests.

The synthesis of ionosilica at nanometric scale was then reported. We synthesized ionosilica nanoparticles with ammonium substructures within the silica network. These original nano objects were synthesized exclusively from a silylated ammonium precursor and display highly uniform particle size less than 100 nm together with high specific surface area up to 1000 $m^2.g^{-1}$ and regular mesoporearrangement. Both *in vitro* and *in vivo* cytotoxicity investigations of ionosilica nanoparticles displayed high biocompatibility. This feature is in part due to the original nanoparticles synthesis strategy involving anionic surfactants instead of more toxic cationic surfactants. Finally, we showed that the nanoparticles can be loaded with anionic drugs (diclofenac) *via* anion exchange. Furthermore, we observed that drug release depends on the composition of the release medium. Our results indicate the high potential of these functional and hydrophilic ionosilica nanoparticles in drug delivery.

With the aim to develop continuous flow processes for the adsorption and extraction of anionic molecules, the synthesis of hybrid silica monoliths with amine and ammonium substructures was studied. The synthesis co-condensation process was found to be very sensitive towards several parameters: the charge of the organic group of the organosilane precursor and surfactant as well as the catalysis conditions. The study shows that surfactant/precursor interactions are a key parameter for the formation of monoliths. The monoliths obtained *via* co-condensation process show trimodal hierarchical pores structures (micro, meso and macro). Moreover, the synthesis of periodic mesoporous organosilica (PMO) monoliths bearing homogenously distributed ammonium functionalities over the whole silica network was obtained under basic condition bearing hierarchical porosity.

For each part presented in this manuscript, improvements can be considered:

1. It is possible to use the guanidinium ionic liquid for separation of traces of pollutants of real environmental solutions.
2. Ionosilica nanoparticles with ammonium entities may be used in the field of cancer therapy by the incorporation of anionic anticancer drugs via simple ion exchange. Furthermore, the synthesis of ionosilicas nanoparticles with different ionic groups such as guanidinium and phosphonium is an excellent perspective in the fields of imaging, nanomedicine and nanocatalysis.
3. Regarding the monoliths with ammonium subtructures, the synthesis optimization must be carried out to increase the mesoporous surface area. However, complementary characterizations such as thermogravimetric analysis and $^{13}C$ solid NMR spectroscopy are necessary to quantify the amine and ammonium groups within the monoliths scaffold. The high concentration of ionic organic group located in these monolithic materials allows the immobilisation of ionic molecules via ion exchange thus promoting a future use in the continuous extraction process.

# Annex

# 1 Experimental section-Chapter II-Part I

## Materials and Methods

## Chemicals

ACS reagent acetone and absolute methanol were purchased from Sigma-Aldrich (St Quentin Fallavier, France). Cationic surfactants used for comparative purposes, dodecyltrimethylammonium chloride (DTAC) and tetradecyltrimethylammonium chloride (TTAC), were also the products of Sigma-Aldrich with a high purity (purum, ≥98.0%). ACS reagent 1H-Pyrazol-1-carboxamidine hydrochloride and primary amines, decylamine, dodecylamine, tetradecylamine, and hexadecylamine were obtained from ABCR (Karlsruhe, Germany). All chemicals were employed without further purification. The 18.2 MΩ-cm water utilized in calorimetry, conductivity, and surface tension measurements was obtained with the aid of a combined Purite Select Analyst (France Eau, Fargues St Hilaire, France) and PURELAB® Classic (ELGA LabWater, Atony, France) water purification system.

### Synthesis and Characterization of the Guanidinium Surfactants

$^{1}H$ and $^{13}C$ spectra in solution were recorded on Bruker AC 250 or Bruker Avance 400 spectrometers (Bruker, Rheinstetten, Germany) at room temperature. Deuterated chloroform and deuterated methanol were used as solvent for liquid NMR experiments, and chemical shifts are reported as δ values in parts per million relative to tetramethylsilane. FT-IR spectra were measured on a Perkin-Elmer 1000 FT-IR spectrometer (Perkin Elmer, Waltham, MA, USA); the samples were prepared as KBr pellets.

Decyl-, dodecyl-, tetradecyl- and hexadecylguanidinium chlorides were obtained as crystalline solids in high yield from the corresponding primary alkylamines by reaction with 1H-pyrazole-1-carboxamidine hydrochloride following the procedure published by Sasaki et al. [25]. In a general procedure, the monoalkyl-guanidinium salts were synthesized as follows. The primary amine (5.5 mmol) and 1H-Pyrazole-1-carboxamidine hydrochloride (5 mmol, 0.73 g) were dissolved in 10 mL of methanol. The resulting homogeneous solution was stirred during 20 h at 313 K. After this time, the solvent was evaporated and the formed pyrazole was eliminated by sublimation. The resulting guanidinium salt was purified by repeated recrystallization in

acetone. After drying at 323 K under vacuum, the pure products were obtained as white powders in 80%–90% yield. The purity of the monoalkyl-guanidinium salts was checked via liquid NMR spectroscopy, as specified below.

**Decylguanidinium chloride (DGC)**

$^{1}$H NMR ($CDCl_3$): δ = 0.81 (3H, "t", J = 9.6 Hz); 1.19 (14H, m); 1.54 (2H, m); 3.13 (2H, "q"); 6.94 (4H, bs); 7.62 (1H, "t"). $^{13}$C NMR (MeOH-$d_4$): δ = 14.15; 22.72; 26.84; 28.78; 29.35; 29.40; 29.62; 29.68; 31.95; 41.88; 157.33.

**Dodecylguanidinium chloride (DDGC)**

$^{1}$H NMR ($CDCl_3$): δ = 0.81 (3H, t, J = 6.8 Hz); 1.18 (16H, m); 1.23 (2H, m); 1.54 (2H, q); 3.09 (2H, m); 7.09 (4H, m); 7.67 (1H, s). $^{13}$C NMR ($CDCl_3$): δ = 14.16; 22.74; 26.87; 28.81; 29.40; 29.45; 29.68; 29.76; 29.79; 31.98; 41.91; 157.36. FT-IR (neat) $\nu_{max}/cm^{-1}$ 3391, 3307, 3133, 2952, 2919, 2850, 1670, 1639, 1607, 1557, 1478, 1464, 1385, 1135, 1035, 887, 695.

**Tetradecylguanidinium chloride (TDGC)**

$^{1}$H NMR ($CDCl_3$): δ = 0.90 (3H, "t"); 1.20–1.50 (22H, m); 1.61 (2H, m); 3.17 (2H, m); 7.10 (4H, m); 7.75 (1H, "t"). $^{13}$C NMR ($CDCl_3$): δ =13.49; 22.76; 26.75; 28.93; 29.38; 29.50; 29.68; 29.79 (5 C); 32.10; 41.54; 157.64.

**Cetylguanidinium chloride (CGC)**

$^{1}$H NMR ($CDCl_3$): δ = 0.91 (3H, "t"); 1.20–1.50 (26H, m); 1.66 (2H, m); 3.17 (2H, m); 7.21 (4H, m); 7.85 (1H, "t"). $^{13}$C NMR ($CDCl_3$): δ = 13.02; 22.32; 26.31; 28.50; 28.93; 29.06; 29.25; 29.28; 29.35; 29.37 (5 C); 31.66; 41.09; 157.13.

Furthermore, all mono-alkylguanidinium cations were identified via high-resolution mass spectroscopy (HR-MS) making use of Waters Q-Tof mass spectrometer (Waters, Milford, MA, USA). Table 4 gives a comparison between the calculated and experimentally obtained m/z values.

**Table 4. Results of high-resolution mass spectroscopy experiments with the guanidinium surfactants studied.**

| | Surfactants | | | |
|---|---|---|---|---|
| | DGC | DDGC | TDGC | CGC |
| | $[C_{11}H_{26}N_3]^+$ | $[C_{13}H_{30}N_3]^+$ | $[C_{15}H_{34}N_3]^+$ | $[C_{17}H_{38}N_3]^+$ |
| (ESI+, m/z) [M]+ calc. | 200.2121 | 228.2434 | 256.2747 | 284.3060 |
| (ESI+, m/z) [M]+ found | 200.2127 | 228.2434 | 256.2756 | 284.3061 |

The phase transition temperatures were determined by differential scanning calorimetry (NETZSCH PSC 204 F1 Phoenix was equipped with dinitrogen cryostatic cooling, 5–15 mg samples, 2 $K \cdot min^{-1}$ heating and cooling rates), and calibrated using an indium primary standard. Optical characterization of the compounds and the detection of mesophases were performed with a polarizing microscope (Leitz 12 POL S, Leitz, Wetzlar, Germany), equipped with a 1024 pixel × 768 pixel Sony CCD camera and an Instec hot stage regulated at 0.1 °C. Powder samples were deposited between slides and cover slips and inserted into the hot stage at room temperature. The temperature ramp typically was of 1 $°C \cdot min^{-1}$. The phase transitions were visually detected from the texture changes observed between crossed polarizers. The phase transitions were similarly detected by cooling the samples from the isotropic phase.

## Physical Measurements

The surfactant solutions were prepared on a molality basis by taking the moles of solute dissolved in 1 kg of pure solvent.

### Conductimetry

The specific conductance of aqueous solutions was measured using a CDM210 conductivity meter (Radiometer Analytical, Villeurbanne, France) equipped with a 2-pole platinized XE100 cell. The calibration procedure was performed with a 0.1 $mol \cdot L^{-1}$ KCl standard solution (purchased from VWR Chemicals, Fontenay-sous-Bois, France) at 298 K (25 °C). The

temperature was controlled using an external thermostat (LAUDA RE 206 Chiller/Heater Circulator, Lauda, Roissy-en-France, France) connected to a double-walled water container in which a measuring beaker was placed. The external water circulation loops were insulated, thus reducing the heat exchange with the environment. The solution was homogenized at a constant stirring rate with the aid of a small magnetic stirring bar. A TITRONIC® (Schott Geräte, Mainz, Germany) piston burette was used for delivering precise doses of a given stock solution to the beaker. The main parts of the measuring and dosing systems were placed in a special thermostated cage in order to speed up the temperature stabilization inside the beaker. The actual temperature of the surfactant solution was measured using a T201 temperature sensor (±0.1 °C). At each concentration and temperature, the conductance reading was checked every 20 s until it reached a steady value. The repeatability of the conductivity measurements, estimated from two successive runs, was about ±0.5%.

The critical micelle concentration, CMC, and the degree of counter-ion binding to the micelle, β, were inferred from the plots of the specific conductance against the equilibrium surfactant concentration. For this purpose, each concentration series was made up by progressive injections of a micellar stock solution into the beaker containing initially the pure solvent. The resulting conductivity curves were represented as two linear regression segments having different slopes in the pre-micellar and post-micellar regions and meeting at the breakpoint: The CMC value was determined from the abscissa of the breakpoint, whereas the ratio of the two slopes allowed the evaluation of the β parameter. The relative uncertainties in the CMC and β, related to the precision of the conductivity measurements and further data processing, were less than ±5% and ±1%, respectively.

For the Krafft temperature measurements, the conductivity of a micellar solution was measured as a function of the temperature. The beaker filled with such a solution was cooled down first in a refrigerator at 276 K (3 °C) overnight and then inside the double-walled water container. The temperature of the solution was slowly increased under constant stirring in 1–2 degree steps at intervals of 30 min and its specific conductivity monitored by the same measuring system. The Krafft temperature, $T_K$, was taken at the first distinctive break in the plot of conductivity vs. temperature. The values of $T_K$ were estimated to be reproducible within 1 K.

**Surface Tension Measurements**

The Wilhelmy plate method was employed to measure the equilibrium surface tension of surfactant solutions, making use of a Krüss digital tensiometer K 12 equipped with a platinum plate. The plate was cleaned thoroughly in a burner flame before the first measurement, and was then washed with acetone and carefully dried after each series of measurements. For each surfactant, 5–6 solutions at given concentrations in the submicellar and supermicellar ranges were prepared separately. Special attention has been paid to the temperature stabilization of the solution in the measuring vessel in the tensiometer chamber (20 min). The reliability of the measurement was assessed to be the best for the surfactant solutions above the CMC; here, the repeatability was slightly better than 10%.

**Titration Calorimetry**

The enthalpy changes accompanying the dilution of a surfactant stock solution were monitored by means of a differential TAM III microcalorimeter operating in a heat flow mode. A high precision liquid thermostat (oil heat exchanger with Peltier coolers) maintained the temperature constant within ±0.0001 degrees. The experimental setup was equipped with a computer-controlled micro-syringe injection device allowing small amounts of a micellar stock solution to be injected into a 1 mL glass ampoule, in which a given mass of solvent was initially placed. The same volume of solvent was put in the reference cell. Then, both cells were returned to the microcalorimeter and the thermal equilibrium was reached after 2–4 h. Successive injections of the 5- or 10-μL aliquots of a given stock solution during 10 s resulted in an electric signal directly fed into a computer; the digitized signal representing the related thermal peaks was recorded with an equilibration time of 45 min applied between 2 injections. The homogeneity of the solution inside the measuring calorimetric cell was maintained by means of an agitation system including a gold stirrer rotated at a slow speed of 90 rpm. Integration of the areas under the thermal peaks was performed, and the resulting enthalpy of dilution $\Delta_{inj}H_i$ was related to the amount of surfactant injected into the cell. The molality of each stock solution was chosen to be approximately 10 times the CMC of the surfactant at a given temperature and salt content. The repeatability of the calorimetry measurements was checked thoroughly by carrying out two simultaneous experiments with the use of two microcalorimeters working under the same conditions.

# 2 Experimental section-Chapter II-Part II

## Materials and methods

### Characterization methods

NMR analyses were performed using a Bruker 200 and 300 NMR spectrometer. Deuterated methanol was used as solvent. Chemical shifts are expressed in parts per million (ppm) relative to TMS. The multiplicity of the signals is indicated by the following abbreviations: s (singlet), d (doublet), t (triplet) and m (multiplet). Time of flight (TOF) mass spectrometry analysis was carried out on a mass spectrometer Synapt G2 -S (Waters) equipped with an ESI source. Mass spectra were recorded in the positive ion mode between 100 and 1500 Da. The capillary voltage was 1000 V and the cone voltage 30 V. The temperature of the ion source and desolvation were 120 °C and 250 °C, respectively. Fourier transform infrared (FTIR) spectra were recorded in the 4000-400 cm-1 range using 32 scans at a nominal resolution of 4 cm-1 by means of an AVATAR 320 FTIR spectrometer equipped with an ATR unit. Differential Scanning Calorimetry measurements were carried out on a NETSCH DSC 204-F1 apparatus. DSC thermograms were recorded on raising the temperature from -120 to 150 °C at a heating rate of 10 °C/min under nitrogen atmosphere. Thermogravimetric analyses analysis (TGA) TGA was carried out using a NETSCH 409 PC under air atmosphere. Compounds were heated to from room temperature to 1000 °C at 10 °C/min. UV-Vis absorption spectra were recorded on a UV-SPECORD 210 spectrophotometer (Analytik Jena). Karl Fischer measurements were carried out on Titroline KF trace instrument using hydranal® coulomat E from Sigma Aldrich as Karl Fischer solution. Viscosity measurements were performed with a classical rheological test in plate geometry with 6 cm of diameter and at 200µm in height, the shear rate was fixed at 5 s-1 using a AR2000 rheometer (TA Instruments).

**Synthesis and characterization of the guanidinium based ionic liquids**

The guanidinium bis-trifluoromethane sulfonimides were obtained by reacting the primary amines with 1H-pyrazole-1-carboxamidine hydrochloride and subsequent anion exchange. As an example, the hexylguanidinium bis-trifluoromethane sulfonimide ($C_6$Gua $NTf_2$) was obtained as follows. Hexylamine (18.9 mmol, 1.91 g) and 1H-pyrazole-1-carboxamidine hydrochloride (17.3 mmol, 2.54 g) were dissolved in methanol (30 mL). The resulting homogeneous solution was stirred during 15h at room temperature. After this time, the solvent was evaporated, and the formed pyrazole was eliminated by sublimation. The resulting guanidinium chloride was dissolved in water and mixed with an aqueous solution of lithium bis-trifluoromethane sulfonimide. The title compound demixed from the aqueous solution and was obtained by extraction with dichloromethane. After solvent evaporation, $C_6$Gua $NTf_2$ was obtained as a moderately viscous and colorless liquid. Yield: 6.66g/91%.

# 3 Experimental section-Chapter III-Part I

## Materials

Chemicals Diclofenac sodium salt (98%) and sulindac (99.5%) were purchased from abcr GmbH & Co. KG (Karlsruhe, Germany); the water used for loading and release tests was deionized water from Millipore apparatus; all the other reagents and solvents were from Sigma Aldrich (Milan, Italy and Lyon, France) and were used as received unless otherwise specified. Sodium salt of sulindac (SUL-Na) was prepared by dissolving sulindac in its acidic form with sodium hydroxide at 1 : 1 molar ratio ($5.25 \times 10^{-4}$ mol) in 40 ml of deionized water during 15 h at room temperature. The ionosilica material **A** and the MCM-41 like silica material were synthesized following previously reported procedures.[1, 2]

## Methods

UV-Vis absorption spectra were acquired with a Cary5000 UV-Vis-NIR spectrophotometer (Varian Inc., California USA) in the transmission mode. The UV-Vis analyses were performed at a wavelength of 276 nm for diclofenac and of 330 nm for sulindac.

Photoemission steady-state spectra were acquired using a Fluorolog3 spectrofluorimeter (Horiba, Milan, Italy) equipped with a 450 W Xenon lamp and a Hamamatsu R928 photomultiplier. The spectral response was corrected for the spectral sensitivity of the photomultiplier. In order to evaluate the content of drug in the low concentration loading experiments, calibration curves were prepared in a concentration range from $1 \times 10^{-6}$ M down to $1 \times 10^{-9}$ M.

Thermal gravimetric analyses (TGA) were carried out on a TAQ600 apparatus (TA instruments, Milan, Italy) by heating the samples, after equilibration, from 30 to 1000 °C at a rate of 10 °C $min^{-1}$ in air.

FT-IR spectra were recorded on a Vertex70 spectrophotometer (Bruker, Milan, Italy) equipped with MCT detector and working at 2 $cm^{-1}$ resolution over 64 scans. Samples of ionosilica and drug/ionosilica complexes were in form of self-supporting pellets suitable for transmission IR experiments and placed in a quartz cell equipped with KBr windows and designed for RT studies in vacuum and in controlled atmosphere. Before analysis the samples were outgassed at RT to remove physically adsorbed water. FT-IR spectra of diclofenac sodium

salt, sulindac and sulindac sodium salt were collected in the ATR (Attenuated Total Reflection) mode by using a single reflection diamond ATR accessory (Platinum ATR accessory by Bruker).

Liquid NMR analyses ($^{1}H$ and $^{13}C$) were performed using a Bruker 300 NMR spectrometer. Deuterated methanol was used as solvent. Chemical shifts are expressed in parts per million (ppm) relative to tetramethylsilane.

Solid state $^{13}C$ CP MAS NMR experiments were recorded on a Varian VNMRS 300 MHz solid spectrometer using a two channel probe with 7.5 mm or 3.2 mm $ZrO_2$ rotors. The $^{29}Si$ solid state NMR spectra were recorded using One Pulse (OP) sequences with samples spinning at 6 kHz. For these experiments, $\pi/6$ pulse and 60 s recycling delay were used to obtain quantitative information on the silane–silanol condensation degree. The $^{13}C$ CP MAS spectra were obtained using 3 ms contact time, 5 s recycling delay and 5 kHz spinning rate. The number of scans was in the range 1000–3000 for $^{29}Si$ OP MAS spectra and of 2000–4000 for $^{13}C$ CP MAS spectra.

Gas-volumetric analysis ($N_2$ adsorption–desorption isotherms at liquid nitrogen temperature) was employed to measure specific surface area (SSA), pore volume and pore size with an ASAP 2020 physisorption analyzer (Micromeritics, Norcross, GA, USA). SSA was calculated by the Brunauer–Emmett–Teller method (BET); pore volume and average pore size were estimated using the Barrett–Joyner–Halenda method with the Kruk–Jaroniec–Sayari equation (BJH/KJS). All calculations were performed on the adsorption branch of the isotherm. Prior to analyses, the samples were outgassed overnight at 110 °C.

**Loading of anionic drugs in ionosilica material**

Drug loading experiments were carried out in deionized water (DCF-Na and SUL-Na) or in ethanol (SUL). The drugs were dissolved in the proper solvent at 0.03 M concentration and desired amount of material A was added to the solution in order to obtain a drug : ionosilica molar ratio of 1.1 : 1. The resulting suspensions were stirred at RT for 24 h, then the solid material was recovered by filtration and dried in vacuum at 60 °C, resulting in the A-DCF-Na/HC, A-SUL-Na/HC and A-SUL samples. In the case of DCF-Na, loading experiments from low concentration solutions were carried out. For this purpose, material A was suspended in a $1.2 \times 10^{-5}$ M solution of DCF-Na at a drug : ionosilica molar ratio of 1 : 6000. The resulting suspension was then stirred for 24 h at RT, then the loaded sample was recovered by filtration

and drying under vacuum at 60 °C. The samples prepared through this procedure are addressed to as A-DCF-Na/LC.

**Release tests**

Diclofenac release studies were performed in vitro using deionized water (pH = 6.5) and hydrochloric acid solution (pH = 3) as releases medium. In one type of experiment, a dispersion of 3 ml containing 5 mg of loaded material (DCF-Na/HC) was incubated at room temperature without stirring. Several aliquots of the same dispersions were prepared for independent analysis and samples of the supernatant were withdrawn at prefixed time (15′, 30′, 1, 2, 3, 4, 6…32 h). In another type of experiment, a pellet of 26 mg of the loaded sample was prepared and kept in 13 ml of deionized water under statistic condition at room temperature. The supernatant was removed and replaced by the same quantity of deionized water after prefixed time. The release was monitored by UV-visible spectroscopy by analyzing the supernatant to determine the drug content.

**Loading of diclofenac in silica material type MCM41**

The diclofenac loading on MCM-41 type material was performed in deionized water. Prior 0.3 g of diclofenac was dissolved in deionized water at concentration of 0.03 M, and then 0.3 g of MCM-41 material was added under stirring at RT. After 24 h the solid material was filtered and washed with water followed by dying in vacuum at 60°C, the complex diclofenac-silica material was called MCM-41-DCF-Na/HC.

## Nitrogen adsorption-desorption (BET)

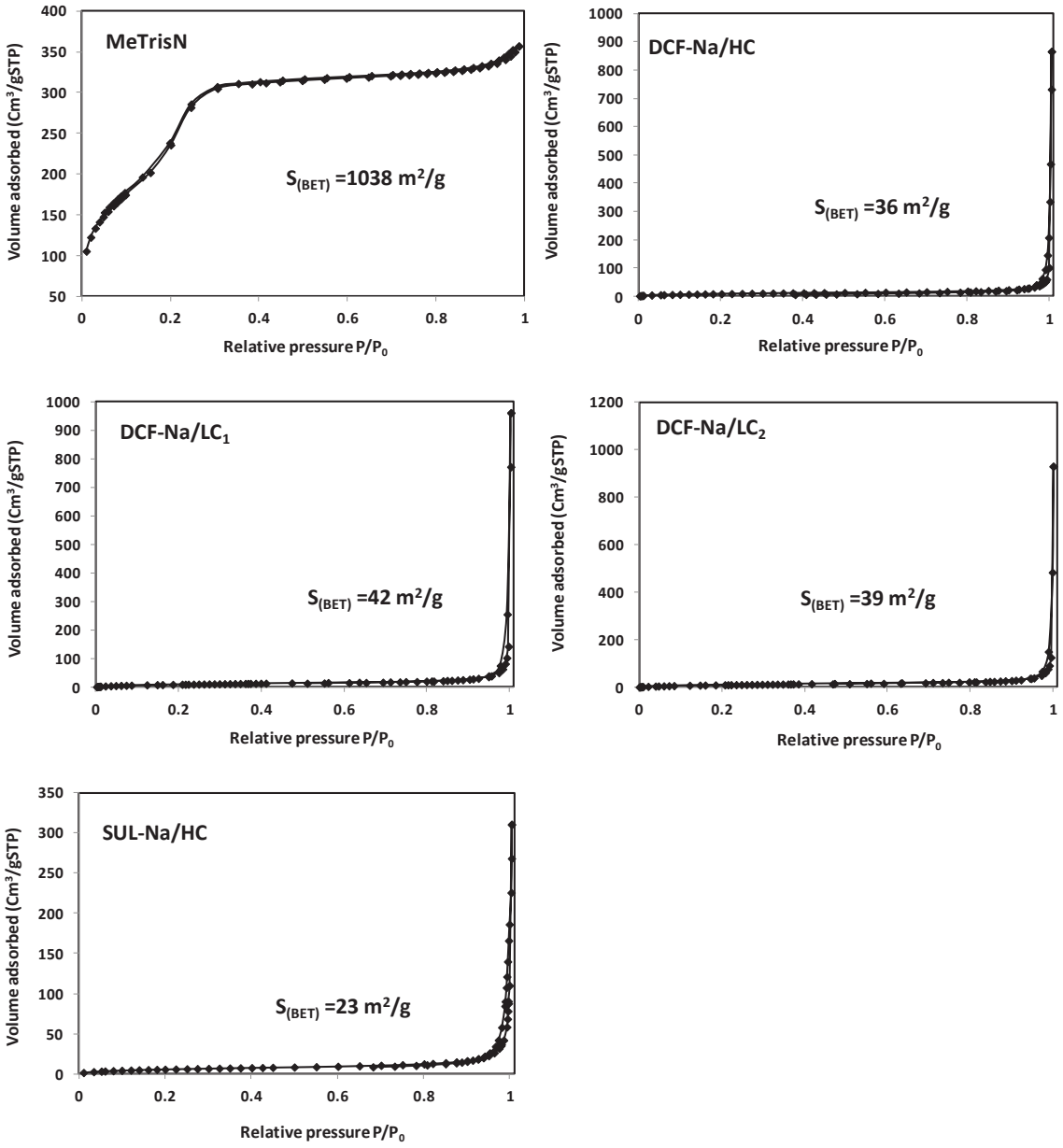


**Figure 1.** Nitrogen sorption isotherms of Material A and drug/material A complexes.

**Release Test**

Figures 2 and 3 show the release efficiency of drug as a function of time of the loaded sample (DCF-Na) in powder form and pellet form respectively in deionized water medium. With powder form the release was constant and the quantity was very small less than 4%, in the case of pellet the release efficiency was around 0.5% and stop after 6 hours. We also obtained a same results in acidic medium pH=3 the release was less than 2%.

According to these results, ionosilica material are strongly adsorbing and retaining the negatively charged Diclofenac molecule, this is supported by the collapse of material's mesoporosity observed with the results obtained from the nitrogen adsorption-desorption (BET),so we could say that ionosilca are a useful traps for sequestration and they have potential for drug removal from wastewater.

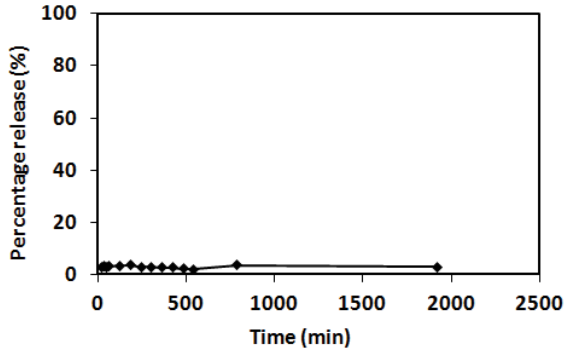


**Figure 2.** Release test with powder sample.

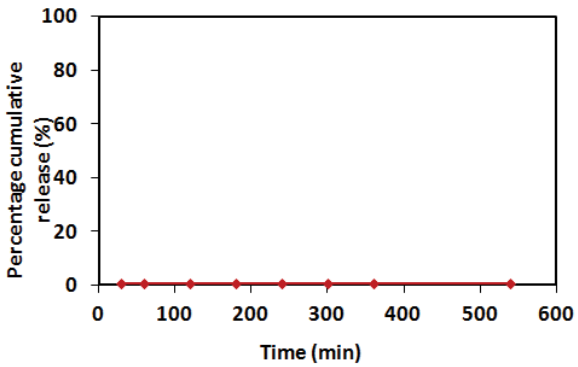


**Figure 3.** Release test with pellet sample.

# 4 Experimental section-Chapter III-Part II

## Materials

(3-Aminopropyl)trimethoxysilane, (3-chloropropyl)trimethoxysilane, (3-iodopropyl)trimethoxysilane, anionic surfactant sodium hexadecyl sulfate (containing 40% sodium stearyl sulfate) and anhydrous 1-propanol were purchased at ABCR. Ammonium hydroxide (28%), hydrochloric acid (HCl, 37%), FITC and iodomethane were obtained from Sigma Aldrich. Ammonium chloride was purchased from Alfa Aesar. Diclofenac sodium salt was purchased from ITC. Silyl PEG-5000 was obtained from RAPP Polymere. All chemicals were used without further purification. Deionized water with resistivity of 18.2 MΩcm was used for the synthesis of the nanoparticles.

## Precursor's synthesis

The syntheses of methyl-(tris(3-trimethoxysilyl)propyl) ammonium iodide was carried out according to the literature.[1, 2]

## Ionosilica nanoparticles synthesis

In a typical synthesis procedure, a solution of sodium hexadecylsulfate SHS (100 mg, 0.3 mmol) and deionized water (30ml) was stirred for 1 hour to form a clear solution at 70°C. 1-propanol solution of the ionorganic precursor (methyl-(tris(3-trimethoxysilyl)propoyl) ammonium iodide) (200 mg, 0.31 mmol) was added drop by drop under vigorous stirring to promote the precursor hydrolysis during 20 min. Then a mixture of nonionic surfactant triblock copolymer F127 (20 mg) in 1 ml of water was added to the solution, followed after 5 min by 600 µl of ammonia (0.1 M), after 10 min an aqueous PEG solution (20 mg of PEG in 1ml of water) was added at the end. The condensation process was conducted for 15 h at 1250 rpm at 70°C. The as-synthesized NPs $NP_{is}$-as were collected by centrifugation and washed twice with ethanol before template extraction with an ethanolic ammonium chloride solution.

**Drug release**

The in vitro Diclofenac release studies were performed using deionized water (pH=5.5) and monopotassium phosphate ($KH_2PO_4$) aqueous solution (pH = 5.6) as release medium. The loaded nanoparticles were incubated at room temperature without stirring. In the case of monopotassium phosphate, the solution was removed and replaced with same quantity in order to mimic the real conditions. The release was monitored by UV-visible spectroscopy.

**Characterization**

Transmission electron microscopy (TEM) images were obtained using a JOEL 1200EX2 instrument; the samples were prepared by deposing an ethanol sample suspension onto a carbon-coated copper grid. Fourier transform infrared (FTIR) spectra were recorded in the 4000-400 $cm^{-1}$ range using 32 scans at a nominal resolution of 4 $cm^{-1}$ with a Perkin Elmer Spectrum2 spectrometer equipped with an ATR unit. Dynamic light scanning (DLS) analyses were performed using a Cordouan Technologies DL135 Particle size analyzer instrument. Zeta potential measurements were carried out at 25°C temperature using a MALVERN instrument. UV-Vis absorption spectra were recorded on a UV-SPECORD 210 spectrophotometer (Analytik Jena). Nitrogen adsorption desorption was employed to measure specific surface area, pore volume and size with a Micromeritics Tristar surface area and porosity analyzer. Specific surface area specific surface area was calculated by the Brunauer-Emmett-Teller method (BET); pore volume and average pore size were estimated using the Barrett-Joyner-Helenda method.All calculations were performed on the adsorption branch of the isotherm. Prior to analyses, the samples were outgassed overnight at 110°C. SEM images were recorded with a FEI instrument. Energy dispersive spectroscopy was performed via an FEI scanning electron microscope. SAXS (small angle X ray scattering) experiments were performed with an in-house setup of the Laboratoire Charles Coulomb, “Réseau X et gamma”, Université Montpellier 2, France. A high brightness low power X- ray tube, coupled with aspheric multilayer optic (GeniX3D from Xenocs) was employed. It delivers an ultralow divergent beam (0.5mrad). Scatterless slits were used to give a clean 0.8mm beam diameter (35 Mphotons/s) at the sample. We worked in a transmission configuration and scattered intensity was measured by a Schneider 2D imageplate

detector prototype, at a distance of 1,9 m from the sample. All Intensities were corrected by transmission and the empty cell contribution was substracted.

**Cell culture**

Murine macrophage 264.7 cells (RAW 264.7) were purchased from ATCC (American Type Culture Collection, Manassas, VA). Cells were cultured in Dulbecco's Modified Eagle's Medium (DMEM)-low glucose including 1 $g.L^{-1}$ glucose and supplemented with 10% foetal bovine serum and antibiotics (100 $U.mL^{-1}$ penicillin and 100 $\mu g.mL^{-1}$ streptomycin). These cells were grown in humidified atmosphere at 37°C under 5% $CO_2$.

**Cell death quantification**

RAW 264.7 cells were seeded into 96-well plates at 1000 cells per well in 200 µL culture medium and allowed to growth for 24 h. The cells were treated with increasing concentrations (0, 10, 25, 50, 100, 150 and 200 $\mu g.mL^{-1}$) of nanoparticles ($NP_{is}$-bare and $NP_{is}$-DCF). After 72 h incubation, a MTT assay was performed to evaluate the toxicity. RAW 264.7 cells were incubated for 4 h with 0.5 $mg.mL^{-1}$ of MTT (3-(4,5-dimethylthiazol-2-yl)-2,5-diphenyltetrazolium bromide; Promega) in media. Then, supernatant was removed, and 150 µL of EtOH/DMSO (1:1) was added to dissolve the precipitated crystals. Absorbance was measured at 540 nm using a microplate reader.

**Measurement of anti-inflammatory properties of nanoparticles**

Increasing concentrations of nanoparticles containing ($NP_{is}$-DCF) or not ($NP_{is}$-bare) diclofenac (DCF) were incubated in culture medium of RAW 264.7 cells. The inflammation was induced with 25 $ng.mL^{-1}$ of LPS. Then, nitrite levels were dosed as described previously (Y Tang et al., 1998) after 24 h. Nitrite measurement reflects the amount of nitric oxide production which is a mediator involved in the inflammatory process.

**Reactive oxygen species (ROS) measurements**

RAW 264.7 cells were seeded into 96-well plates at 1000 cells per well in 200 µL culture medium for 24 h. Then, the cells were pre-treated with LPS (25 $ng.mL^{-1}$) for 2 h, followed by treatment with 100 $\mu g.mL^{-1}$ of $NP_{is}$-bare and $NP_{is}$-DCF nanoparticles for 24 h. The day of the experiment, RAW 264.7 cells were incubated with 20 µM 2', 7'-dichlorofluorescin diacetate (Abcam) for 45 minutes. Finally, RAW 264.7 cells were washed two times with culture medium. Fluorescence microscopy was performed under a 485 nm wavelength excitation.

**Cellular uptake**

The cellular uptake experiment was performed using fluorescence microscopy. RAW 264.7 cells were plated in a 24-well plate in 500 µL culture medium for 24 h. Then, RAW 264.7 cells were treated with 100 $\mu g.mL^{-1}$ of fluorescent nanoparticles conjugated with FITC ($NP_{is}$-FITC) at different times (3 h, 6 h, 9 h and 24 h). The day of experiment, cell medium was removed and RAW 264.7 cells were washed two times with culture medium. Fluorescence microscopy was performed on living cells under a 485 nm wavelength excitation.

**Animals**

Female C57BL/6 8 weeks old mice were used for this study. They were procured from Charles River and housed in the Institutional animal house under standard environmental conditions (23 ± 1°C, 55 ± 5% humidity and 12 hrs/ 12 hrs light/dark cycle) and maintained with free access to standard diet and water. Then, animals were divided into two groups: a control group (n = 4) and a group treated with $NP_{is}$-bare (n = 4). Mice were intravenously injected with 200 µL physiological serum supplemented or not by $NP_{is}$-bare to obtain a final concentration of 40 $mg.kg^{-1}$.

Animal experiments were approved and conducted in accordance with local and national authorities for the care and use of laboratory animals. The accreditation number of the laboratory for the experiments conducted in this work is B34-172-25.

**Preliminary toxicological assessment**

Biochemical assays were performed. The blood samples with heparin were centrifuged at 1 300 rpm for 10 min. The plasma was kept at - 20 °C until analyzed. Liver function was determined from alanine aminotransferase (ALT) activity. Plasma ALT activity was measured according to standard protocol (Infinity, Thermo Scientific). To establish the inflammatory reaction or the systemic toxicity, plasma IL-6 levels were quantified using commercial ELISA kits as described in the manufacturer's protocol (R&D systems). The evaluation of renal function was determined by measuring creatinine levels in plasma and in urine using colorimetric assay at 495 nm with alkaline picrate. Moreover, histopathology was conducted on internal organs of the experimental animals. Liver, spleen and kidney were fixed in 10 % paraformaldehyde, embedded in paraffin and cut 7 µm tick sections in a microtome. Sections were mounted on glass slides. After staining with hematoxylin-eosin, the sections were examined and imaged under a light microscope.

# 5 Experimental section-Chapter III-Part III

## Materials

Tetraethyl-orthosilane (TEOS), tetradecyltrimethylammonium bromide (TTAB), sodium dodecyl sulfate (SDS), dodecane and hydrochloric acid 37% were purchased from Sigma Aldrich. Ammonia 30% was purchased from Carloerba. The reactants were used as received without further purification.

## Precursor's synthesis

The syntheses of tris((3-(trimethosysilyl)propyl)amine (**A**) and methyl-(tris(3-trimethoxysilyl)propyl) ammonium iodide (**B**) were carried out according to the literature.[1]

## Characterization

SEM images were recorded with a FEI instrument. Nitrogen adsorption desorption was employed to measure specific surface area, pore volume and size with a Micromeritics Tristar surface area and porosity analyzer. Specific surface area was calculated by the Brunauer-Emmett-Teller method (BET); pore volume and average pore size were estimated using the Barrett-Joyner-Helenda method. All calculations were performed on the adsorption branch of the isotherm. Prior to analyses, the samples were outgassed overnight at 140°C. Solid state NMR experiments were recorded on a Varian VNMRS 300 MHz solid spectrometer using a two channel probe with 7.5 mm or 3.2 mm $ZrO_2$ rotors. The $^{29}Si$ solid state NMR spectra were recorded using Cross Polarization (CP) sequences with samples spinning at 6 kHz. For these experiments, $\pi/6$ pulse and 60 s recycling delay were used to obtain quantitative information on the silane–silanol condensation degree. The number of scans was in the range 1000–3000.Intrusion/extrusion mercury measurements were performed using a Micrometrics Autopore IV 9500 porosimeter, this to reach the scaffolds macrocellular cells characteristics.

**Monoliths synthesis**

**Synthesis of hybrid monoliths with amine and ammonium functionalities following the co-condensation process.**

The syntheses were carried out in the presence of a cationic and anionic surfactant tetradecyltrimethylammonium bromide TTAB and sodium dodecyl sulfate (SDS) respectively.

16 g of TTAB or SDS aqueous solution at 35 w% or 16% respectively with 5 g of HCl 37%, a mixture of TEOS and ammonium precursor (TEOS:precursor **TrisN** or **MeTrisN**; 5, 10, 20, 40 %), hydrolysis is allowed to take place until a monophasic hydrophilic medium is obtained. The oily phase constituted of 35 g of dodecane is then emulsified drop by drop into the hydrophilic continuous phase using a mortar. The emulsion in then allowed to condense for 1 week at room temperature. The as synthesized monoliths were then washed three times with a tetrahydrofuran / acetone mixture (at 70 / 30 vol %) to extract the oily phase from monolith, the followed by washing with an acid ethanolic solution in order to remove the surfactant. The monoliths were then dried at room temperature for one week and treated thermally at 150°C for 7 hours to favor solvent evaporation and to consolidation of the networks. For basis condition the syntheses were recordered with same procedure replacing the 5 g of acid (HCl) by 5 g of ammonia at 0.1M.

**Synthesis of periodic mesoporous organosilicas monolith bearing ammonium substructures.**

The monolith in this case was synthesized from the ammonium precursor only (precursor **A**) in basic condition. A solution of propanol and organic precursor (3ml PrOH and 2 g precursor **A**) were mixed with SDS aqueous solution at 15% wt containing 5 g of ammonia at 0.1 M. After precursor hydrolysis and the formation of one hydrophilic phase, the emulsion was prepared quickly using 30 g of dodecane. The emulsion was transposed into a canister and left to age for 4 days at room temperature. The resulting material was washed with a mixture of THF and acetone, followed by a surfactant extraction using an acidic ethanol solution and washed at the end by ethanol. The monolith was let to dry at room temperature under air, followed by thermal treatment at 150°c for 7 hours. The monolith is called B-100-S.

1. Nguyen, T. P.; Hesemann, P.; Thi, M. L. T.; Moreau, J. J. E., Nanostructured polysilsesquioxanes bearing amine and ammonium groups by micelle templating using anionic surfactants. *Journal of Materials Chemistry* **2010,** 20, (19), 3910-3917.

2. El Hankari, S.; Motos-Perez, B.; Hesemann, P.; Bouhaouss, A.; Moreau, J. J. E., Pore size control and organocatalytic properties of nanostructured silica hybrid materials containing amino and ammonium groups. *Journal of Materials Chemistry* **2011,** 21, (19), 6948-6955.

# Résumé en Français

## Introduction

L'un des principaux axes de développement chimie réside dans la perception de plus en plus claire, une analyse plus approfondie et une application plus délibérée du paradigme de l'information dans l'élaboration et la transformation de la matière, traçant ainsi le chemin allant de la matière simplement condensée vers celle de plus en plus organisée jusqu'à atteindre des systèmes de complexité croissante.

Les propriétés d'un matériau dépendent à la fois de la nature de ses constituants et de leurs interactions. La chimie supramoléculaire peut donc avoir un fort impact sur la science des matériaux au moyen de la manipulation explicite des forces non covalentes qui maintiennent les constituants ensemble. Ces interactions permettent la conception de matériaux et le contrôle de l'assemblage d'unités appropriées par auto-organisation.
La chimie supramoléculaire est par nature une chimie dynamique étant donné la labilité des interactions moléculaires reliant les composants d'une entité supramoléculaire. La réversibilité de l'association permet un changement continu dans la constitution qui peut être soit interne, (par réarrangement des composants avec la modification de la connectivité entre eux), ou externe (par l'échange, l'incorporation ou l'extrusion des composants), conférant ainsi la plasticité constitutionnelle au système.

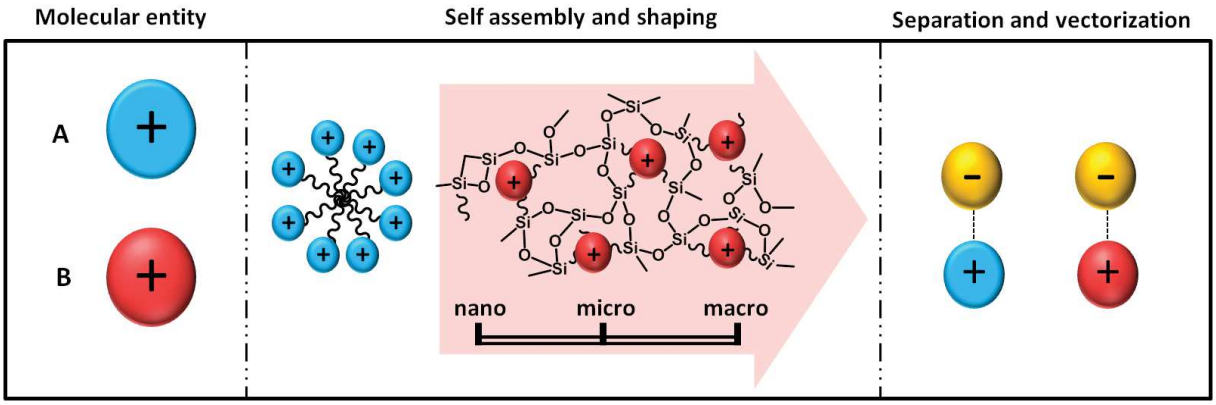


**Figure 1: Représentation schématique des différents systèmes fonctionnels ioniques et applications étudiés.** Entité moléculaire: A) guanidinium et B) ammonium, le comportement l'auto-assemblage du tensioactif et la mise en forme d'ionosilice à différente échelle. Enfin, les différentes applications réalisées sur les liquides ioniques et l'ionosilice par réaction d'échange d'ions.

Cette thèse porte sur différents aspects comme illustré dans la Figure 1: le comportement d'auto-assemblage, la mise en forme du matériau, les réactions d'échange d'ions, le procédé de séparation et la vectorisation de principes actifs. Pour cela, trois systèmes fonctionnels ioniques (tensio-actif, liquide ionique et matériaux d'ionosilices) contenant chacun des entités cationiques (guanidinium et ammonium) ont été étudiés. Considérant ces entités cationiques, nous avons divisé nos systèmes fonctionnels en deux familles de composés: les sels de guanidinium et les matériaux d'ionosilice.

A cet effet nous allons présenter le travail de cette thèse en deux sections. Dans la première nous présenterons les sels de guanidinium accompagnés d'une étude séparée sur les tensio-actifs et les liquides ioniques. Dans la deuxième, nous décrirons les matériaux d'ionosilice en nous focalisant sur le design et la mise en forme de ce type de matériaux en nanoparticules, poudres et monolithes ainsi que sur leur application dans les domaines de séparation et de vectorisation de principes actifs.

## Sel de guanidiniums :

La sous-structure guanidine / guanidinium est un groupe fonctionnel approprié largement répandu dans la nature comme par exemple dans des protéines par l'intermédiaire de l'arginine d'acides aminés essentiels. Guanidine est une base forte et se comporte comme un cation dans une large gamme de pH. Le groupe guanidinium est la base d'une chimie supramoléculaire riche en raison de sa capacité à interagir avec diverses substances par interaction ionique et liaison hydrogène.
Dans cette section nous traiterons de la synthèse et de la caractérisation des composants contenant des sous-structures guanidinium (tensio-actif et liquide ionique).

## Tensio-actif gaunidinium

*Une étude fondamentale a été menée sur le chlorure de guanidinium tensioactif. Ainsi, différentes longueurs de chaîne alkyle de $C_{10}$ à $C_{16}$ ont été synthétisées et caractérisées. Ensuite, une étude physico-chimique du comportement d'auto-assemblage a été réalisée en utilisant différentes techniques de mesure: conductivité, tension superficielle et calorimétrie. Les résultats obtenus sont ensuite comparés avec un tensioactif conventionnel qui est le chlorure d'ammonium quaternaire.*

L'auto-agrégation des molécules amphiphiles et des ions en micelles, vésicules ou membranes formant ainsi des objets supramoléculaires joue un rôle important dans de nombreux domaines comme la biologie, la pharmacie et la science des matériaux. La diversité de ces utilisations a été une force motrice puissante derrière la conception et la préparation de nouvelles familles d'agents tensio-actifs au cours des dernières décennies. La synthèse de matériaux inorganiques mésoporeux par l'utilisation des tensioactifs comme agent de structuration est un bon exemple de la façon dont les efforts dédiés au développement et à la caractérisation de tensioactifs ont conduit aux progrès de la conception et de la synthèse de matériaux avancés à l'architecture poreuse accordable.

L'auto-assemblage et l'activité de surface de longue chaîne de tensioactifs guanidinium ont rarement été étudiés dans les documents scientifiques. Dans cette partie nous présenterons les résultats d'une étude systématique de l'activité de surface et du comportement d'auto-assemblage pour une série de chlorures de mono-alkylguanidinium contenant 10, 12, 14 et 16 atomes de carbone dans la chaîne alkyle (Figure 2). Ces principales caractéristiques ont été déduites à partir des mesures de la conductivité, de la tension de surface et de la calorimétrie.

Généralement, le comportement des tensio-actifs ioniques dans des solutions aqueuses et aux interfaces est un résultat complexe de divers types d'interactions impliquant la chaine hydrophobe du tensioactif, la tête polaire hydrophile, les contre ions ainsi que les molécules capables de former des liaisons hydrogènes avec l'eau ou avec d'autres espèces dissoutes. Dans ce contexte, les études directes de la calorimétrie sur ces interactions peuvent fournir une meilleure compréhension du mécanisme de la synthèse de matériaux poreux en utilisant le tensio-actif comme agent de structuration.

Les mesures de conductivité nous ont permis de déterminer la température de Krafft et la concentration micellaire critique (CMC). La température de Krafft est définie comme la température à laquelle il y a formation des premières micelles. L'augmentation de la

température Krafft ($T_K$) au-delà de la température ambiante avec l'augmentation de la longueur de la chaîne alkyle a été corroborée par la détermination des valeurs de $T_K$ pour les quatre tensio-actifs cationiques étudiés.


**$C_{10}$Gua**:Alk = n-$C_{10}H_{21}$
**$C_{12}$Gua**: = n-$C_{12}H_{25}$
**$C_{14}$Gua**: = n-$C_{14}H_{29}$
**$C_{16}$Gua**: = n-$C_{16}H_{33}$

**Figure 2. Les differents tensio-actifs monoalkyl guanidinium synthétisé.**

Les concentrations micellaires critiques (CMC) des différents tensio-actifs guanidiniums ont été déterminées par les trois techniques de caractérisation. Les résultats montrent une corrélation entre ces différentes techniques indiquant des valeurs de la CMC pour chaque tensio-actif très proches. Avec l'augmentation de deux carbones dans la chaine alkyle on remarque la diminution de la CMC d'un facteur 1/4. A partir des mesures de la calorimétrie, la micellisation des tensio-actifs guanidinium, en particulier ceux avec des chaînes alkyle longues, peut être décrite à la fois comme entropique et enthalpique. L'enthalpie standard de micellisation par mole de tensio-actif, $\Delta_{mic}H°$, devient plus négative (le processus est plus exothermique) avec l'allongement de la chaine hydrocarbonée.
L'ajout du sel NaCl dans la phase aqueuse provoque une diminution constante de la CMC et rend le processus de micellisation plus exothermique; en fonction de la longueur de la chaine alkyle, les micelles d'alkylguanidinium peuvent atteindre leur forme et la taille optimale à une teneur en NaCl donnée.

En comparaison avec les tensio-actifs ammoniums quaternaire (alkyltriméthylammonium chlorures), l'activité superficielle des tensio-actifs alkylguanidinium est plus importante. Le fait que la formation de micelle CMC soit beaucoup plus exothermique et se produit à des valeurs beaucoup plus faibles peut être attribué à la capacité du groupement guanidinium à former des liaisons hydrogène. Ceci favorise la formation de micelles plus compactes et la liaison des contre ions $Cl^-$ plus forte dans la couche de Stern correspondante.

## Liquide ionique

*Dans cette partie, nous avons synthétisé une série de monoalkylguanidinium bis-trifluorométhane sulfonimides à courte chaîne alkyle en tant que nouvelle classe de liquides ioniques fonctionnels utilisés pour l'extraction de composés anioniques. L'extraction a été effectuée par rapport à un colorant organique (orange de méthyle), à un principe actif anionique (Diclofenac) et à un anion métallique (chromate). Afin d'évaluer le potentiel du liquide ionique de guanidinium, nous avons comparé les résultats obtenus avec ceux d'un liquide ionique classique à base d'imidazolium.*

Les liquides ioniques (ILs) sont des solvants uniques qui se composent entièrement d'ions. En raison de leurs propriétés uniques telles que la conductivité ionique élevée, la faible pression de vapeur, la haute stabilité chimique / thermique et l'inflammabilité, les liquides ioniques ont trouvé de nombreuses applications comme solvants dans la synthèse organique et la catalyse ainsi que dans l'électrochimie en tant que batteries à électrolyte.
Les dérivés d'imidazolium sont de loin la classe la plus étudiée de liquides ioniques. En revanche, les liquides ioniques basés sur des entités de guanidinium sont beaucoup plus rares et moins étudiés. Dans la littérature seuls les liquides ioniques à base d'ions guanidinium peralkylés sont rapportés. Dans cette thèse, nous avons étudié les monoalkylguanidium bis-trifluorométhane sulfonimides comme une nouvelle classe de liquides ioniques fonctionnels. La particularité de ces nouveaux liquides ioniques est basée sur le groupement guanidinium cationique qui confère des propriétés spécifiques aux liquides ioniques. La sous-structure guanidine / guanidinium présente un comportement physico-chimique très particulier.

Les liquides ioniques sont étudiés dans la science de séparation. Comme ils sont assez chers, une attention particulière a été portée sur la limitation des quantités utilisées dans les processus de séparation. Pour cette raison, les procédés de microextraction liquide-liquide jouent un rôle de plus en plus important. Par ailleurs, l'élimination des colorants anioniques à partir de solutions aqueuses en utilisant les liquides ioniques à base d'imidazolium a déjà été étudiée. Il apparaît que le procédé d'extraction est généralement entraîné par des interactions hydrophile / hydrophobe entre les colorants et la phase liquide ionique. Pour cette raison, les liquides ioniques à longue chaîne alkyle donne de meilleurs résultats par rapport à leurs homologues à chaîne courte. Dans cette thèse, nous avons montré que les procédés

d'extraction impliquant des liquides ioniques à base de guanidinium impliquent un mécanisme différent et des interactions différentes au niveau moléculaire.

Le concept de liquides ioniques spécifiques à la tâche (TSILs) se compose généralement du greffage chimique des groupements organiques fonctionnels sur le cation ou l'anion du liquide ionique. Dans ce qui suit, nous présentons les liquides ioniques à base de guanidinium comme une nouvelle classe de liquides ioniques spécifiques à la tâche (TSIL). En raison de la polyvalence et des propriétés de liaison spécifiques des groupes guanidinium, la fonctionnalité chimique est conférée à la sous-structure cationique du liquide ionique lui-même. Nous avons étudié ces nouveaux composés dans l'extraction liquide-liquide des polluants anioniques à partir de solutions aqueuses. Nous nous sommes concentrés en particulier sur la séquestration d'un colorant organique (orange de méthyle, MO), d'un médicament anionique (diclofénac, DCF) et d'un anion métallique (chromate). Notre travail met en évidence les propriétés particulières de guanidinium à base de liquides ioniques par rapport aux liquides ioniques non miscibles à l'eau, à savoir 1-butyl-3-methylimidazolium bis(trifluoromethylsulfonyl)imide ($C_4$mim $NTf_2$). L'extraction est suivie par spectroscopie UV-vis en analysant la phase aqueuse.

Les résultats obtenus montrent des différences significatives en ce qui concerne l'efficacité de l'extraction de ces différentes espèces anioniques. Les meilleurs résultats ont été obtenus pour le méthyl orange ainsi que le diclofenac allant jusqu'à plus de 90%. Par contre, l'extraction de chromate à partir de la phase aqueuse est moins significative. Nous attribuons ces résultats à la haute affinité des anions organiques vers la phase IL hydrophobe. Ces résultats sont corroborés par le fait que le decylguanidinium IL $C_{10}$Gua $NTf_2$ a donné de meilleurs résultats qu'octyl- ou hexyl-guanidinium. En revanche, les composés minéraux ou les anions métalliques montrent une affinité moins prononcée vers la phase liquide ionique guanidinium. Il est à signaler que dans tous les cas, les ILs à base de guanidinium ont donné des résultats nettement meilleurs par rapport à leurs homologues imidazolium.

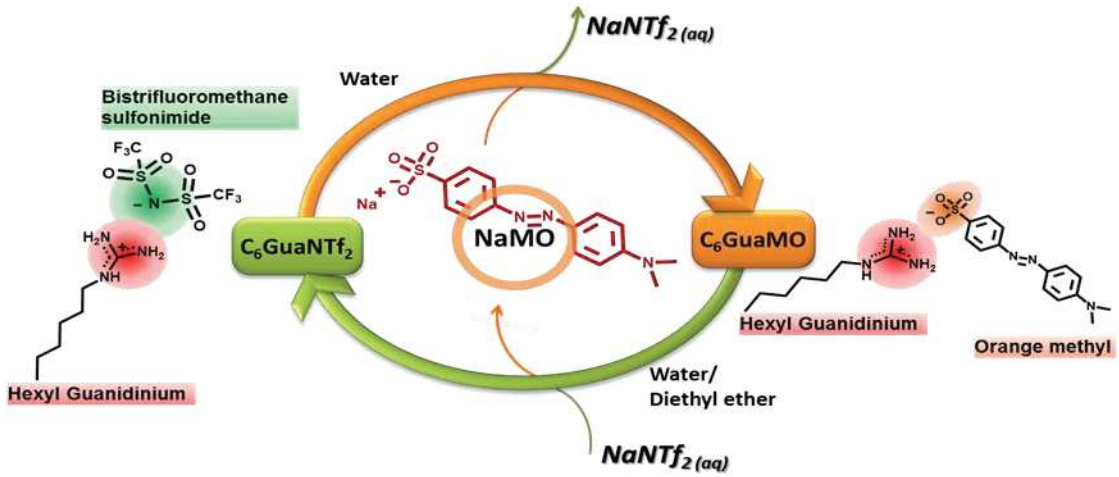


**Figure 3: cycle de extraction / régénération de $C_6$Gua $NTf_2$ dans la séparation de MO.**

Enfin, pour une chimie verte et durable, la régénération des extractants est d'un intérêt particulier. Ici, cette question est d'une haute importance. En effet, outre sa toxicité notable, l'anion bis-trifluorométhane sulfonimide n'est pas biodégradable et a tendance à s'accumuler dans la biosphère. Nous avons donc étudié le recyclage des ILs guanidinium en vue de l'élaboration d'un cycle extraction / régénération. Une autre caractéristique intéressante des ILs guanidinium est leur miscibilité atypique avec certains solvants organiques. Nous avons observé que les ILs guanidinium sont complètement miscibles dans l'éther diéthylique. Ainsi, notre travail démontre la possibilité de ré-utiliser le cation et l'anion des liquides ioniques à base de guanidinium et de mettre en place un cycle d'extraction-régénération fermé (Figure 3).

## Les matériaux d'ionosilices

Dans cette section on mettra en évidence les différentes mises en forme d'ionosilice en nanoparticules, poudres et monolithes émergeant des fonctionnalités supplémentaires et des propriétés exceptionnelles dans les domaines de la séparation et de la vectorisation.

Les matériaux d'ionosilices sont définis comme des matériaux de silice mésoporeuse contenant des groupements ioniques incorporés de façon covalente et sont situés à l'interface de silice mésoporeuse et de liquide ionique. Les ionosilices combinent à la fois une porosité élevée, une architecture régulière au niveau mésoscopique avec une polyvalence chimique incomparable induite par la forte variabilité et le nombre élevé d'espèces ioniques incorporés. Ces matériaux sont obtenus par réaction d'hydrolyse polycondensation de précurseurs ioniques silylés. Cette approche est particulièrement intéressante puisque le groupement

organo-ionique du précurseur silylé favorise le processus de structuration au cours de la réaction d'hydrolyse-polycondensation. Cette stratégie a permis l'accès à une grande variété de matériaux hybrides de silice poreuse contenant différents types de groupes ioniques et présentant des textures différentes.
Dans cette section nous présenterons trois parties : les ionosilices sous forme de poudres, nanoparticules et monolithes.

### *Ionosilices sous forme de poudre*

*Pour étudier le potentiel d'ionosilices pour le traitement des eaux usées, l'adsorption des principes actifs dans une solution aqueuse a été effectuée sur l'ionosilice sous forme de poudre. Différentes molécules ont été utilisées, telles que le diclofénac de sodium et sulindac sous forme neutre et ionique. Dans cette partie, nous avons étudié la sélectivité des matériaux d'ionosilice et les forces motrices de leur potentiel d'adsorption.*

Les matériaux à base de silice sont bien établis et largement utilisés dans les procédés de séparation et de la séquestration des polluants. Les silices mésoporeuses telles que HMS et SBA-15 ont déjà été utilisées pour l'adsorption des produits pharmaceutiques tels que la carbamazépine, diclofénac et ibuprofène. La fonctionnalisation de surface de silice mésoporeuse permet l'accès à une grande variété de matériaux pour la séparation des polluants organiques et inorganiques. Par exemple, les matériaux de silice poreuse fonctionnalisée avec triméthylsilyle, aminopropyl et mercaptopropyl améliorent la capacité d'adsorption des produits pharmaceutiques. Dans le domaine des matériaux hybrides, l'échange d'ions impliquant des matériaux à base de silice contenant des groupements ioniques apparait comme un moyen intéressant pour la séquestration des espèces chargées. Ici nous avons étudié les matériaux d'ionosilices sous forme de poudre pour l'adsorption des principes actifs anioniques tout en comparant avec un matériau de silice de type MCM-41.

Dans ce qui suit, nous avons évalué le potentiel d'un matériau d'ionosilice hybride contenant une sous structure ammonium (A) pour l'adsorption de principes actifs anioniques : le diclofénac et le sulindac. Le diclofénac est habituellement utilisé dans les formulations pharmaceutiques en tant que sel de potassium ou de sodium tandis que le sulindac est habituellement commercialisé sous sa forme acide donc neutre (pKa = 4,7). Nous avons utilisé le sel commercial diclofénac de sodium (DCF-Na) et le sulindac (SUL) et nous avons

préparé le sel de sodium de sulindac (SUL-Na) par traitement de la forme acide de sulindac dans une solution d'hydroxyde de sodium.

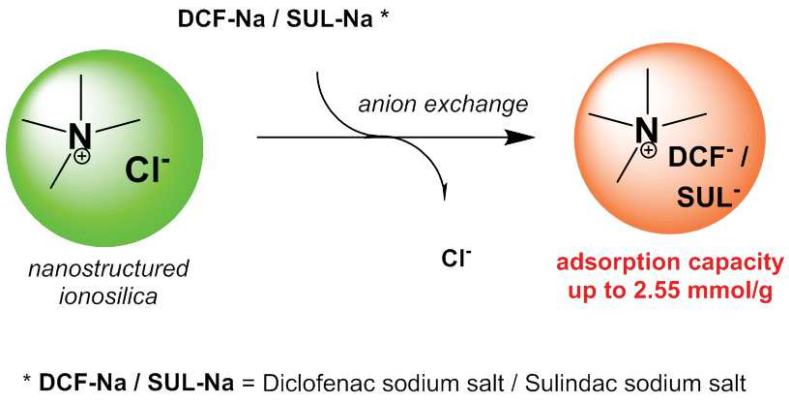


**Figure 4. Représentation schématique de l'adsorption d'ionosilice des pricipes actifs anionique par échange anioniques.**

La capacité d'adsorption du matériau d'ionosilice A a été contrôlée envers DCF-Na, Na et SUL-SUL. Tous les principes actifs ont été utilisés pour tester leur adsorption à partir de solutions à haute concentration. Ensuite nous avons testé la capacité du matériau à absorber une très faible concentration pour se rapprocher des faits réels.

Les résultats montrent que ce matériau présente des capacités d'absorption élevées jusqu'à 2,55 mmol / g. Cependant, la capacité d'adsorption dépend de la nature de l'adsorbant étudié. Le diclofénac et le sulindac de sodium sont absorbée en grande quantité (Figure 4) alors qu'aucune absorption n'a été observée en utilisant le principe actif sous la forme neutre acide (sulindac neutre). Outre la sélectivité du matériau ionosilice vis-à-vis des molécules anioniques, le diclofénac de sodium plus petit et plus hydrophile DCF-Na est adsorbé en une quantité supérieure par rapport au sulindac de sodium SUL-Na qui est plus grand et plus hydrophobe. L'ionosilice est un adsorbant très efficace même pour des traces de principes actifs anioniques, mettant ainsi en évidence la forte affinité de ces composés avec le matériau. Cette affinité a été également suivie par des tests de libération de principes actifs. Aucune libération significative de la drogue n'a été observée après la mise en contact de l'échantillon pendant 32 h à la fois dans de l'eau ou dans une solution d'acide chlorhydrique (pH = 3). Toutefois, il convient de mentionner que ces traitements conduisent à un effondrement complet de la structure poreuse du matériau.

## *Nanoparticules ionosiliciques*

*La mise en forme de matériaux d'ionosilice en nanoparticules permet l'extension des applications dans le domaine de la nanomédecine. Au cours de cette thèse, les nanoparticules contenant des entités ioniques essentiellement ammonium ont été synthétisées. La non-toxicité et la biocompatibilité de ces nanoparticules sont ensuite vérifiées par des études in- vitro et in-vivo. Les nanoparticules sont synthétisées afin de les utiliser comme nano-vecteur pour la vectorisation de principes actifs. A cet effet, le diclofénac de sodium, un anti-inflammatoire non stéroïdien, a été utilisé comme modèle.*

Le développement de méthodes originales efficaces et ciblées pour l'administration de médicaments demeure un défi majeur dans la nanomédecine. L'élaboration de différents types de nano-vecteurs de médicament est actuellement un champ d'activité de recherches intenses.
Dans le domaine de matériaux de silice hybride, les nanoparticules périodiques mésoporeuses organosilylées (PMO) apparaissent récemment comme des nanoobjets originaux avec des propriétés de surface accordables qui offrent de nouvelles perspectives dans la catalyse et la nanomédecine. Cependant leur synthèse est encore un défi majeur. Les exemples de nanoparticules PMO sont rares. En 2006, Lu *et al.* ont rapporté pour la première fois des nanosphères PMO creuses avec 100-400 nm de diamètre. En 2012, Guan *et al.* ont rapporté les premières nanoparticules PMO monodisperses et mésostructurées. L'approche consistant à combiner une dispersion homogène des groupements organiques au sein de nanoparticules avec une taille et une propriété texturale contrôlées offre la possibilité d'ajuster les propriétés interfaciales chimiques et physico-chimiques de ces nanoobjets.
Les matériaux d'ionosilices présentent des propriétés hydrophiles particulières, avec une forte affinité vis-à-vis de l'eau conduisant à un transfert accru de masse et à une accessibilité élevée de sites ioniques. Les ionosilices apparaissent comme des matériaux efficaces pour l'adsorption des anions métalliques tels que le chromate, le perrhénate et le pertechnetate. Comme présenté dans la partie ci-dessus, nous avons démontré que les ionosilices adsorbent efficacement les principes actifs anioniques tels que le diclofenac et le sulindac de sodium.

Cependant les ionosilices sont seulement disponibles en poudre à l'échelle macroscopique. Au cours de cette thèse nous avons réalisé la synthèse de nanoparticules ionosiliciques avec une granulométrie uniforme et homogène. Cette nouvelle forme d'ionosilice est essentiellement intéressante pour l'application dans plusieurs domaines tels que la nanocatalyse, l'imagerie et

la nanomédecine. Dans cette partie, l'objectif est la synthèse de nanoparticules d'ionosilice portant des sous-structures ammonium avec le contrôle de la morphologie et des propriétés texturales. Pour l'application à usage biomédical, la synthèse de particules de taille inférieure à 200 nm est fortement souhaitée. Afin de les tester pour la délivrance de médicaments, un principe actif anti-inflammatoire non stéroïdien a été mobilisé à l'intérieur des nanoparticules.

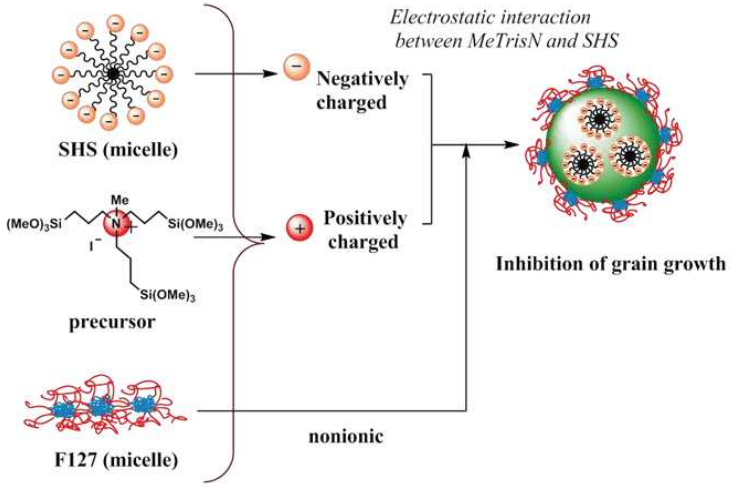


**Figure 5. Synthèse de nanoparticules d'ionosilices en utilisant le système tensio-actif binaire.**

L'obtention de nanoparticules ionosiliciques contenant des groupements ammonium est réalisée en utilisant un système de tensio-actif binaire (Figure 5). Nous avons effectué une étude complète sur l'influence des différentes conditions de synthèse tels que: la quantité du précurseur et de l'agent tensio-actif, la température, le catalyseur et le contrôle des réactions d'hydrolyse / condensation. Cette étude nous a permis de synthétiser des nanoparticules avec une taille de diamètre de l'ordre de 100 nm avec une propriété de surface importante.

Afin d'améliorer la biocompatibilité des nanoparticules, un polyéthylène glycol silylé (PEG) a été ajouté à la fin de la synthèse. Une étude complète sur les différentes caractérisations de ces nanoparticules a été réalisée. Des études in-vitro et in-vivo ont été effectuées pour déterminer la bio-distribution, la cytotoxicité afin d'évaluer la biocompatibilité de ces nanoparticules. Enfin, nous les avons chargées avec du diclofenac (DCF), un médicament anti-inflammatoire non stéroïdien anionique (AINS) qui a été choisi comme modèle de principes actifs pour évaluer le potentiel des nanoparticules ionosilices en tant que nanocarriers pour la vectorisation et la délivrance de principes actifs. Les nanoparticules chargées avec le diclofenac sont obtenues par simple réaction d'échange d'ion.

En résumé, nous avons synthétisé des nanoparticules d'ionosilices originales de sous structures ammonium qui sont obtenues avec succès en utilisant un système de tensioactif binaire. Les différentes conditions de synthèse ont été étudiées pour contrôler leurs propriétés texturales et morphologiques. Ces nanoobjets originaux ont été synthétisés exclusivement à partir d'un précurseur ammonium silylé et montrent des diamètres de taille uniforme inférieure à 100 nm, avec une surface spécifique élevée allant jusqu'à 1000 $m^2.g^{-1}$ et un arrangement de pores régulier. Les études in vitro et in vivo montrent une biocompatibilité élevée. Cette caractéristique est due en partie à la stratégie de synthèse des nanoparticules impliquant des agents tensio-actifs anioniques à la place d'agents tensio-actifs cationiques plus toxiques. Finalement, il a été démontré que les nanoparticules peuvent être chargées avec un principe actif anionique (diclofénac de sodium) par réaction d'échange d'anions. Nous avons également observé que la libération de diclofénac dépend de la composition du milieu de libération. Nos résultats indiquent le potentiel élevé de ces nanoparticules d'ionosilices hydrophiles et fonctionnelles dans le domaine de la vectorisation et de la délivrance de médicaments.

### *Ionosilices sous forme de monolithe*

*Dans le but d'extraction ionique en écoulement continu, des matériaux contenant des fonctions ioniques ont été synthétisés sous forme de monolithes. Ces monolithes hybrides contiennent des sous structures amine et ammonium obtenus par procédé de co-condensation à partir du tetraethoxysilane (TEOS) et avec un précurseur organosilylé (amine et ammonium). Ensuite, un monolithe PMO de sous structure ammonium a également été synthétisés exclusivement à partir d'un précurseur ionique silylé. Dans cette étude, différents paramètres ont été optimisés afin de synthétiser des monolithes bien définis à porosité hiérarchisée.*

La fabrication de nouveaux systèmes multifonctionnels et complexes est souvent dictée par l'émergence de matériaux poreux de construction proches aux matériaux présents dans la nature. Les matériaux portant une organisation hiérarchique (comme dans tous les biominéraux) sont très recherchés pour une large variété d'applications comme dans les techniques classiques de séparation, l'absorption et la catalyse hétérogène, etc.
La préparation des matériaux avec adaptation simultanée de la morphologie (monolithes, fibres, etc.) et des structures de pores sur différentes longueur d'échelles a émergé comme un

domaine prometteur avec un vaste champ d'application. Récemment, les monolithes ont attiré l'attention des chercheurs dans divers domaines, en particulier dans celui de la séparation. L'utilisation d'une émulsion directe concentrée et d'une phase lyotropique permet la fabrication de matériaux monolithiques hiérarchiquement structurés avec une porosité contrôlée et accessible et avec de bonne propriétés mécaniques.

Dans cette thèse, nous avons synthétisé des monolithes hybrides à base d'organo-silice contenant une sous structure amine et ammonium avec une structure poreuse hiérarchique trimodale (micro, méso et macroporosité).

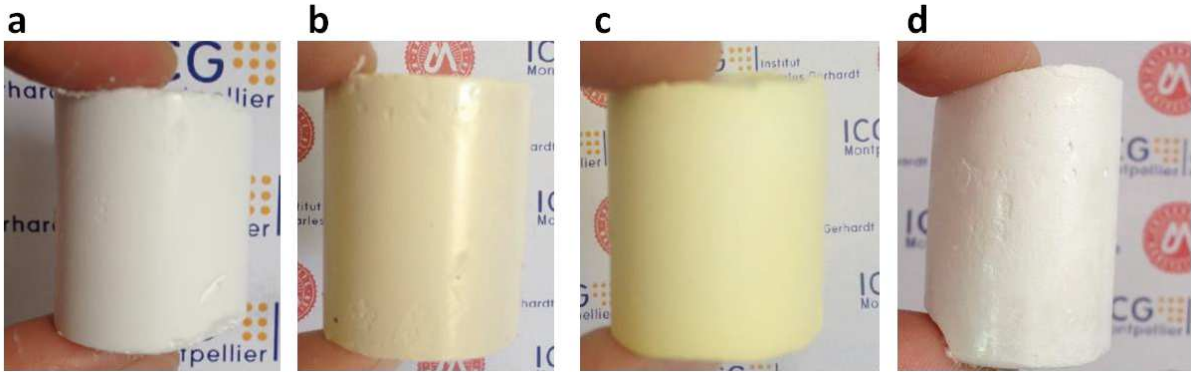


**Figure 6. Photographie des monolithes obtenus pour chaque condition de synthèse : a et b** monolithe synthétisé par voie acide contenant des entités amines et ammonium respectivement, **c)** monolithe synthétisé par voie basique avec des sous structures ammonium et **d)** PMO monolithe obtenue à partir d'un précurseur ammonium uniquement.

Ici, nous avons utilisé deux procédés pour synthétiser des monolithes de silice hybrides avec des fonctionnalités amines et ammoniums; Tout d'abord par l'intermédiaire de processus de co-condensation par réaction simultanée de TEOS et d'un précurseur organique silylé (amine et ammonium) incorporé dans le milieu réactionnel. Deuxièmement, à partir uniquement d'hydrolyse et condensation d'un précurseur ammonium nous sommes arrivés à l'obtention d'un monolithe PMO. Différentes conditions de synthèse ont été étudiées en vue d'optimiser la synthèse du monolithe de silice hybride contenant des sous-structures ioniques.

La synthèse des monolithes est réalisée par un double processus faisant usage de l'émulsion directe et de la mésophase lyotrope. L'émulsion directe a été utilisée pour créer la macroporosité. La phase lyotrope agit à la fois pour stabiliser l'interface eau / huile et créer une phase micellaire qui induit une porosité mésoscopique.

Des monolithes bien définis ont été obtenus via le procédé de co-condensation dans des conditions acides avec un tensio-actif cationique et dans des conditions basiques avec un tensio-actif anionique (Figure 6- a, b et c). La synthèse a été très sensible à plusieurs paramètres: la charge du groupe organique du précurseur organo-silane, l'agent tensio-actif et le choix du catalyseur. L'étude montre que l'interaction du tensio-actif / précurseur est un paramètre clé pour la formation de monolithes. En général, les monolithes obtenus montrent une structure de pores avec une hiérarchie trimodale. En utilisant la catalyse basique, la formation des monolithes a été observée uniquement avec le précurseur ionique (ammonium). Dans ces conditions, nous avons pu incorporer une plus grande quantité de groupement ammonium. Pour finir nous avons rapporté la synthèse des monolithes PMO portant des fonctionnalités ammonium répartis de façon homogène sur l'ensemble du réseau silicique (Figure 6-d). Cependant, l'optimisation des paramètres est fortement recommandée afin d'améliorer la surface spécifique mésoporeuse.

Ces monolithes portant des sous-structures amines et ammoniums sont particulièrement intéressants dans le domaine de la séparation et de l'adsorption de molécules. La forte concentration de groupements organiques ioniques situés dans le réseau des matériaux permet l'immobilisation des molécules ioniques via des réactions d'échange d'ions. Ces matériaux favorisent une utilisation ultérieure pour le procédé d'extraction continue.

## Conclusion

Dans cette thèse, nous avons démontré que la présence d'entités cationiques dans les systèmes ioniques fonctionnels étudiés engendre des propriétés et des applications différentes. Les systèmes sont : *i)* l'auto-assemblage des tensio-actifs guanidiniums, *ii)* les liquides ioniques contenant des sous-structures guanidiniums pour la chimie verte et *iii)* les matériaux ionosiliciques mésoporeux contenant des sous-structures à base d'entité ammonium.

*i)* Considérant le premier système, nous avons étudié les tensio-actifs guanidinium en chlorure à longues chaines alkyle. Différentes techniques physico-chimiques ont été utilisées pour étudier leurs caractères d'auto-assemblages. Les résultats montrent un rapport clair entre la longueur de la chaîne alkyle et le comportement d'auto-agrégation. Par rapport aux chlorures d'alkyltriméthylammonium, les tensio-actifs alkylguanidinium présentent une activité de surface différente alors que la formation de micelles est beaucoup plus exothermique.
*ii)* Dans le deuxième système, nous avons rapporté la synthèse des liquides ioniques en bis-trifluoromethane sulfonimide à courte chaîne alkyle avec sous-structure guanidinium. Ces nouveaux composés montrent de façon significative l'efficacité d'extraction des espèces organiques et inorganiques anioniques par rapport aux liquides ioniques à base d'imidazolium classique.

*iii)* Dans le troisième système, l'étude est menée sur des matériaux ionosiliciques de trois différentes formes : poudre, nanoparticule et monolithe.
Les poudres ont été utilisées pour l'adsorption des principes actifs. Ces matériaux présentent une importante propriété d'extraction vis-à-vis des molécules anioniques qui les rend intéressants dans le domaine du traitement des eaux.
La mise en forme des ionosilices en nanoparticules permet l'extension des applications d'ionosilice au domaine de la nanomedecine. Ainsi, des nanoparticules contenant des sous-structures ioniques (ammonium) sont synthétisées pour la première fois. Des tests in vitro et in-vivo ont montré la non toxicité et la biocompatibilité de ces nanoparticules. La vectorisation d'un principe actif anti-inflammatoire diclofenac est ensuite étudié.
Dans l'objectif d'une extraction ionique en flux continu, des matériaux contenant des fonctions ioniques sous forme de monolithe sont synthétisés par voie de co-condensation et à partir uniquement d'un précurseur ionique silylé. Les monoltihes ainsi obtenus montrent une

bonne teneur mécanique avec une structure poreuse hiérachique trimodal à différentes échelles (micro, méso et macropores).

Pour chacune des parties de cette thèse des améliorations peuvent être envisagées :

1. L'utilisation des liquides ioniques guanidiniums pour la séquestration des molécules anioniques se trouvant en quantités infimes à partir d'une phase aqueuse pour se rapprocher des concentrations réelles des polluants dans les eaux usées.

2. Les nanoparticules contenant des entités ammonium synthétisées peuvent être utilisées dans le domaine du traitement anti-cancéreux par l'incorporation de médicaments anticancéreux anioniques par l'intermédiaire de simple échange ionique. Ainsi la synthèse de nanoparticules avec d'autre groupement ionique tel que le guanidinium et le phosphonium constitue une excellente perspective dans les domaines de l'imagerie, la nanomédecine et la nanocatalyse.
3. Concernant les monolithes ioniques ammoniums, l'optimisation de la synthèse doit être effectuée afin d'augmenter la surface des mésopores. Toutefois des caractérisations complémentaires comme l'analyse thermogravimétrique et la spectroscopie $^{13}C$ RMN du solide sont nécessaires afin de quantifier les groupements amine et ammonium au sein des monolithes. La forte concentration de groupement organique ionique située dans ces matériaux monolithiques permet l'immobilisation de molécules ioniques via des réactions d'échange d'ions favorisant ainsi une utilisation future dans le procédé d'extraction continue.

*« C'est à tort que les hommes se plaignent de la fuite du temps, en l'accusant d'être trop rapide, sans savoir qu'il s'écoule à la bonne vitesse »*

*Léonard de Vinci*

## Surfactants, Ionic liquids and Ionosilicas: Functional ionic systems for supramolecular chemistry and elaboration of materials by design (ion exchange and vectorization)


### Abstract

This dissertation deals with innovative synthetic materials bearing cationic entities that are guanidinium and ammonium. These cationic entities give interesting and functional properties for each ionic system studied: surfactant, ionic liquid and ionosilica. For this purpose, we investigated two families groups composed of: guanidiniums salts and ionosilica. Regarding guanidiniums salts, we studied the formation and self-assembly behavior of guanidinium surfactants using different measurement techniques (conductivity, surface tension and calorimetry). This remarkable molecular synthon that represents guanidinium was also highlighted as an ionic liquid for the extraction of methyl orange, diclofenac and chromate. As for ionosilicas, although they also have advantageous properties for ion extraction and adsorption of the active ingredients, however their shaping remains a key parameter for targeting their application. In fact, the design of ionosilica material as nanoparticle allows applications extension in the field of nanomedicine. So during this thesis, nanoparticles containing ammonium substructures were synthesized for the first time and used as a nano-vector to deliver an anti-inflammatory drug (diclofenac). Furthermore, with the aim of ionic extraction in continuous flow, materials containing ionic functions as monolith were synthesized from ammonium precursor via sol gel route. This thesis allowed us to find the theoretical, experimental and illustrative elements of the different aspects of materials formation based on cationic entities with remarkable properties that are guanidiniums and ammonium salts.



**Keywords:** guanidinium, ammonium, surfactant, ionic liquid and ionosilica.


## Tensio-actifs, Liquides Ioniques et Ionosilices : Systèmes ioniques fonctionnels pour la chimie supramoléculaire et l'élaboration de matériaux par design (échange ionique et vectorisation)


### Résumé

Cette thèse s'inscrit dans le cadre de synthèses de matériaux innovants contenant des entités cationiques que sont le guanidinium et l'ammonium. Ces entités cationiques confèrent des propriétés intéressantes et fonctionnelles pour chacun des systèmes ioniques suivants : tensio-actifs, liquides ioniques et ionosilices. A cet effet, nous avons procédé à l'étude de deux familles de composés : les sels de guanidiniums et les ionosilices. Pour les sels de guanidiniums, nous avons étudié la formation et les propriétés d'auto-assemblage de tensio-actifs en utilisant différentes techniques de mesures (conductivité, tension de surface et calorimétrie). Ce remarquable synthon moléculaire qu'est le guanidinium a été aussi mis en avant comme liquide ionique pour l'extraction du méthyl orange, du diclofenac et du chromate. Quant aux ionosilices, bien qu'ils présentent aussi des propriétés intéressantes pour l'extraction ionique et l'adsorption de principes actifs, leur mise en forme reste cependant un paramètre clef pour cibler leur application. En effet, la mise en forme des ionosilices en nanoparticules permet l'extension des applications dans le domaine de la nanomedecine. Ainsi, durant cette thèse, des nanoparticules avec des sous-structures ioniques ammoniums sont synthétisées pour la première fois et utilisées comme nano-vecteur pour le relarguage d'un anti-inflammatoire (diclofenac). Par ailleurs, dans le but d'une extraction ionique en flux continu, des matériaux contenant des fonctions ioniques sous forme de monolithe ont été synthétisés à partir de précurseur ammonium par voie sol gel. Ainsi cette thèse nous a permis de trouver les éléments théoriques, illustratifs et expérimentaux des différentes facettes de la formation de matières à base d'unités cationiques aux propriétés remarquables que sont les sels de guanidiniums et les sels d'ammoniums.



**Mots clés :** guanidinium, ammonium, tension actif, liquide ionique et ionosilice.